Available online at www.sciencedirect.com
SCIENCE DIRECT®
Physics Reports 386 (2003) 29–222
PHYSICS REPORTS
www.elsevier.com/locate/physrep

Front propagation into unstable states

Wim van Saarloos*

Instituut-Lorentz, Universiteit Leiden, Postbus 9506, 2300 RA Leiden, The Netherlands

Accepted 12 August 2003
editor: C.W.J. Beenakker

Abstract

This paper is an introductory review of the problem of front propagation into unstable states. Our presentation is centered around the concept of the asymptotic linear spreading velocity v^*, the asymptotic rate with which initially localized perturbations spread into an unstable state according to the linear dynamical equations obtained by linearizing the fully nonlinear equations about the unstable state. This allows us to give a precise definition of pulled fronts, nonlinear fronts whose asymptotic propagation speed equals v^*, and pushed fronts, nonlinear fronts whose asymptotic speed $v^\dagger$ is larger than v^*. In addition, this approach allows us to clarify many aspects of the front selection problem, the question whether for a given dynamical equation the front is pulled or pushed. It also is the basis for the universal expressions for the power law rate of approach of the transient velocity $v(t)$ of a pulled front as it converges toward its asymptotic value v^*. Almost half of the paper is devoted to reviewing many experimental and theoretical examples of front propagation into unstable states from this unified perspective. The paper also includes short sections on the derivation of the universal power law relaxation behavior of $v(t)$, on the absence of a moving boundary approximation for pulled fronts, on the relation between so-called global modes and front propagation, and on stochastic fronts.

PACS: 47.54.+r; 47.20.−k; 02.30.Jr; 82.40.Ck; 47.20.Ky; 87.18.Hf

Contents

* Tel.: +31-71-5275501; fax: +31-71-5275511.
E-mail address: saarloos@lorentz.leidenuniv.nl (W. van Saarloos).

0370-1573/$ - see front matter
doi:10.1016/j.physrep.2003.08.001

1. Introduction

1.1. Scope and aim of the article

The aim of this article is to introduce, discuss and review the main aspects of front propagation into an unstable state. By this we mean that we will consider situations in spatio-temporally extended systems where the (transient) dynamics is dominated by a well-defined front which invades a domain

in which the system is in an unstable state. With the statement that the system in the domain into which the front propagates is in an unstable state, we mean that the state of the system in the region far ahead of the front is *linearly unstable*. In the prototypical case in which this unstable state is a stationary *homogeneous* state of the system, this simply means that if one takes an arbitrarily large domain of the system in this state and analyzes its linear stability in terms of Fourier modes, a continuous set of these modes is unstable, i.e., grows in time.

At first sight, the subject of *front propagation into unstable states* might seem to be an esoteric one. After all, one might think that examples of such behavior would hardly ever occur cleanly in nature, as they appear to require that the system is first prepared carefully in an unstable state, either by using special initial conditions in a numerical simulation or by preparing an experimental system in a state it does not naturally stay in. In reality, however, the subject is not at all of purely academic interest, as there are many examples where either front propagation into an unstable state is an essential element of the dynamics, or where it plays an important role in the transient behavior. There are several reasons for this. First of all, there are important experimental examples where the system is essentially quenched rapidly into an unstable state. Secondly, fronts naturally arise in convectively unstable systems, systems in which a state is unstable, but where in the relevant frame of reference perturbations are convected away faster than they grow out—it is as if in such systems the unstable state is actually dynamically produced since the convective effects naturally sweep the system clean. Even if this is the case in an infinite system, fronts do play an important role when the system is finite. For example, noise or a perturbation or special boundary condition near a fixed inlet can then create patterns dominated by fronts. Moreover, important changes in the dynamics usually occur when the strength of the instability increases, and the analysis of the point where the instability changes over from convectively unstable to absolutely unstable (in which case perturbations in the relevant frame do grow faster than they are convected away) is intimately connected with the theory of front propagation into unstable states. Thirdly, as we shall explain in more detail later, close to an instability threshold front propagation always wins over the growth of bulk modes.

The general goal of our discussion of front propagation into unstable states is to investigate the following *front propagation problem:*

> *If initially a spatially extended system is in an unstable state everywhere except in some spatially localized region, what will be the large-time dynamical properties and speed of the nonlinear front which will propagate into the unstable state? Are there classes of initial conditions for which the front dynamics converges to some unique asymptotic front state? If so, what characterizes these initial conditions, and what can we say about the asymptotic front properties and the convergence to them?*

Additional questions that may arise concern the sensitivity of the fronts to noise or a fixed perturbation modeling an experimental boundary condition or an inlet, or the question under what conditions the fronts can be mapped onto an effective interface model when they are weakly curved.

Our approach to introducing and reviewing front propagation into unstable states will be based on the insight that there is a single unifying concept that allows one to approach essentially all these questions for a large variety of fronts. This concept is actually very simple and intuitively appealing, and allows one to understand the majority of examples one encounters with just a few

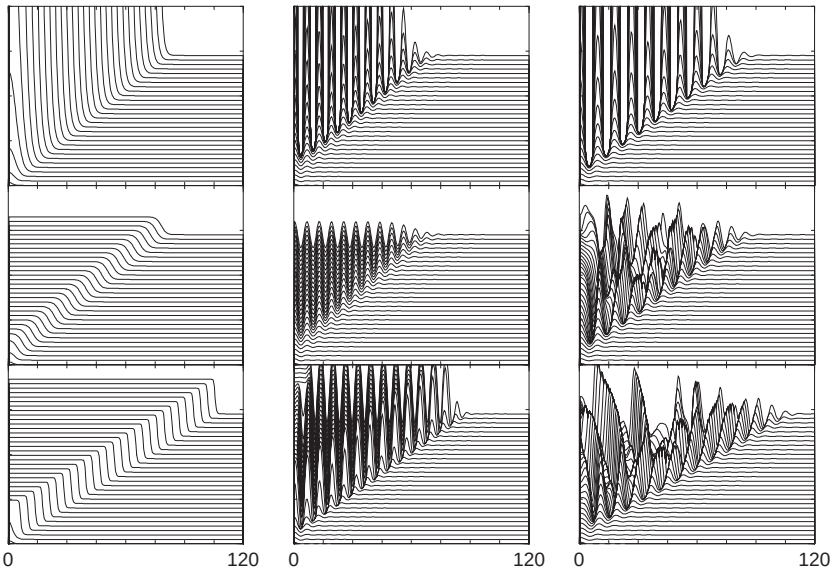

Fig. 1. Graphical summary of one of the major themes of this paper. From top to bottom: *linear spreading*, *pulled fronts* and *pushed fronts*. From left to right: *uniformly translating fronts, coherent pattern forming fronts and incoherent pattern forming fronts*. The plots are based on numerical simulations of three different types of dynamical equations discussed in this paper. In all cases, the initial condition was a Gaussian of height 0.1, and the state to the right is linearly unstable. To make the dynamics visible in these space-time plots, successive traces of the fronts have been moved upward. Thicks along the vertical axes are placed a distance 2.5 apart. Left column: F-KPP equation (1) with a pulled front with $f(u) = u - u^3$ (middle) and a pushed one for $f(u) = u + 2\sqrt{3}u^3 - u^5$ in the lower row, for times up to 42. Middle column: the Swift–Hohenberg equation of Section 2.11.2 (middle) and an extension of it as in Fig. 14(b) (bottom). Right column: Kuramoto–Sivashinsky equation discussed in Section 2.11.4 (middle) and an extension of it, as in Fig. 16, but with $c = 0.17$ (bottom).

related theoretical tools. Its essence can actually be stated in one single sentence:

> *Associated with any given unstable state is a well-defined and easily calculated so-called "linear" spreading velocity v^*, the velocity with which arbitrarily small linear perturbations about the unstable state grow out and spread according to the dynamical equations obtained by linearizing the full model about the unstable state; nonlinear fronts can either have their asymptotic speed $v_{\rm as}$ equal to v^* (a so-called pulled front) or larger than v^* (a pushed front).*

The name pulled front stems from the fact that such a front is, as it were, being "pulled along" by the *leading edge* of the front, the region where the dynamics of the front is to good approximation governed by the equations obtained by linearizing about the unstable state. The natural propagation speed of the leading edge is hence the asymptotic linear spreading speed v^*. In this way of thinking, a pushed front is being pushed from behind by the nonlinear growth in the nonlinear front region itself [333,334,384].

The fact that the linear spreading velocity is the organizing principle for the problem of front propagation is illustrated in Fig. 1 for all three classes of fronts, simple *uniformly translating fronts*, and *coherent* and *incoherent pattern forming fronts*. In the upper panels, we show simulations of the spreading of an initial perturbation into the unstable state according to the linear equations, obtained

by linearizing the model equation about the unstable state. This illustrates the linear spreading problem associated with the linear dynamics. The asymptotic linear spreading speed v^* can be calculated explicitly for any given dynamical equation. Note that since the dynamical equations have been linearized, there is no saturation: The dynamical fields in the upper panels continue to grow and grow (in the plots in the middle and on the right, the field values also grow to negative values, but this is masked in such a hidden-line plot). The middle panels show examples of pulled fronts: These are seen to advance asymptotically with the *same* speed v^* as the linear spreading problem of the upper panel. The lower panels illustrate pushed fronts, whose asymptotic speed is larger than the linear spreading speed v^*. The fronts in the left column are *uniformly translating*, those in the middle column are *coherent pattern forming fronts*, and those in the right *incoherent pattern forming fronts*. We will define these front classifications more precisely later in Section 2.7—for now it suffices to become aware of the remarkable fact that in spite of the difference in appearance and structure of these fronts, it is useful to divide fronts into two classes, those which propagate with asymptotic speed v^* and those whose asymptotic speed $v^\dagger$ is larger. Explaining and exploring the origin and ramifications of this basic fact is one of the main goals of this article.

In line with our philosophy to convey the power of this simple concept, we will first only present the essential ingredients that we think a typical non-expert reader should know, and then discuss a large variety of experimental and theoretical examples of front propagation that can indeed be understood to a large extent with the amount of theoretical baggage that we equip the reader with in Section 2. Only then will we turn to a more detailed exposition of some of the more technical issues underlying the presentation of Section 2, and to a number of advanced topics. Nevertheless, throughout the paper our philosophy will be to focus on the essential ideas and to refer for the details to the literature—we will try not to mask the common and unifying features with too many details and special cases, even though making some caveats along the lines will be unavoidable. In fact, even in these later chapters, we will see that the above simple insight is the main idea that also brings together various important recent theoretical developments: the derivation of an exact results for the universal power law convergence of pulled fronts to their asymptotic speed, the realization that many of these results extend without major modification to fronts in difference equations or fronts with temporal or spatial kernels, the realization that curved pulled fronts in more than one dimension cannot be described by a moving boundary approximation or effective interface description, as well as the effects of a particle cutoff on fronts, and the effects of fluctuations.

A word about referencing: when referring to several papers in one citation, we will do so in the numerical order imposed by the alphabetic reference list, not in order of importance of the references. If we want to distinguish papers, we will reference them separately.

1.2. Motivation: a personal historical perspective

My choice to present the theory this way is admittedly very personal and unconventional, but is made deliberately. The theory of front propagation has had a long and twisted but interesting history, with essential contributions coming from different directions. I feel it is time to take stock. The field started essentially some 65 years ago [1] with the work of Fisher [163] and Kolmogoroff, Petrovsky,

[1] As mentioned by Murray [311, p. 277], the Fisher equation was apparently already considered in 1906 by Luther, who obtained the same analytical form as Fisher for the wave front.

and Piscounoff [234] on fronts in nonlinear diffusion type equations motivated by population dynamics issues. The subject seems to have remained mainly in mathematics initially, culminating in the classic work of Aronson and Weinberger [15,16] which contains a rather complete set of results for the nonlinear diffusion equation (a diffusion equation for a single variable with a nonlinear growth term, Eq. (1) below). The special feature of the nonlinear diffusion equation that makes most of the rigorous work on this equation possible is the existence of a so-called comparison theorem, which allows one to *bound* the actual solution of the nonlinear diffusion equation by suitably chosen simpler ones with known properties. Such an approach is mathematically powerful, but is essentially limited by its nature to the nonlinear diffusion equation and its extensions: A comparison theorem basically only holds for the nonlinear diffusion equation or variants thereof, not for the typical types of equations that we encounter in practice and that exhibit front propagation into an unstable state in a pattern forming system.

In the early 1980s of the last century, the problem of front propagation was brought to the attention of physicists by Langer and coworkers [38,111,248], who noted that there are some similarities between what we will call the regime of pulled front propagation and the (then popular) conjecture that the natural operating point of dendritic growth was the "marginally stable" front solution [247,248], i.e., the particular front solution for which the least stable stability eigenmode changes from stable to unstable (for dendrites, this conjecture was later abandoned). In addition, they re-interpreted the two modes of operation[2] of front dynamics in terms of the stability of front solutions [38]. This point of view also brought to the foreground the idea that front propagation into unstable states should be thought of as an example of *pattern selection*: since there generally exists a continuum of front solutions, the question becomes which one of these is "selected" dynamically for a large class of initial conditions. For this reason, much of the work in the physics community following this observation was focused on understanding this apparent connection between the stability of front profiles and the dynamical selection mechanism [83,333,334,354,380,420,421]. Also in my own work along these lines [420,421] I pushed various of the arguments for the connection between stability and selection. This line of approach showed indeed that the two regimes of front propagation that were already apparent from the work on the nonlinear diffusion equation do in fact have their counterparts for pattern forming fronts, fronts which leave a well-defined finite-wavelength pattern behind. In addition, it showed that the power law convergence to the asymptotic speed known for the nonlinear diffusion equation [54] is just a specific example of a generic property of fronts in the "linear marginal stability" [420,421] regime—the "pulled" regime as we will call it here. Nevertheless, although some of these arguments have actually made it into a review [105] and into textbooks [189,320], they remain at best a plausible set of arguments, not a real theoretical framework; this is illustrated by the fact that the term "marginal stability conjecture" is still often used in the literature, especially when the author seems to want to underline its somewhat mysterious character.

Quite naturally, the starting point of the above line of research was the *nonlinear* evolution of fronts solutions. From this perspective it is understandable that many researchers were intrigued but also surprised to see that in the pulled (or linear marginal stability) front regime almost all the essential properties of the fronts are determined by the dispersion relation of the *linearized* dynamics of arbitrarily small perturbations about the unstable state. Perhaps this also explains, on hindsight, why for over 30 years there was a *virtually independent* line of research that originated in plasma

[2] Their "case I" and "case II" [38] are examples of what we refer to here as pulled and pushed front solutions.

physics and fluid dynamics. In these fields, it is very common that even though a system is linearly unstable (in other words, that when linearized about a homogeneous state, there is a continuous range of unstable Fourier modes), it is only *convectively unstable*. As mentioned before, this means that in the relevant frame a localized perturbation is convected away faster than it is growing out. To determine whether a system is either convectively unstable or absolutely unstable mathematically translates into studying the long-time asymptotics of the Green's function of the dynamical equations, linearized about the unstable state.[3] The technique to do so was developed in the 1950s [62] and is even treated in one of the volumes of the Landau and Lifshitz course on theoretical physics [264], but appears to have gone unnoticed in the mathematics literature. It usually goes by the name of "pinch point analysis" [49,204,205]. As we will discuss, for simple systems it amounts to a saddle point analysis of the asymptotics of the Green's function. In 1989 I pointed out [421] that the equations for the linear spreading velocity of perturbations, according to this analysis, the velocity we will refer to as v^*, are actually the *same* as the expressions for the speed in the "linear marginal stability" regime of nonlinear front propagation [38,111,421]. Clearly, this cannot be a coincidence, but the general implications of this observation appear not to have been explored for several more years. One immediate simple but powerful consequence of this connection is that it shows that the concept of the linear spreading velocity v^* applies equally well to difference equations in space and time—after all in Fourier language, in which the asymptotic analysis of the Green's function analysis is most easily done, putting a system on a lattice just means that the Fourier integrals are restricted to a finite range (a physicist would say: restricted to the Brillouin zone). The concept of linear spreading velocity also allows one to connect front propagation with work in recent years on the concept of global modes in weakly inhomogeneous unstable systems [98,99].

Most of the work summarized above was confined to fronts in one dimension. The natural approach to analyze nontrivial patterns in more dimensions on scales much larger than the typical front width is, of course, to view the front on the large pattern scale as a sharp moving interface—in technical terms, this means that one would like to apply singular perturbation theory to derive a moving boundary approximation or an effective interface approximation (much like what is often done for the so-called phase-field models that have recently become popular [29,71,219]). When this was attempted for discharge patterns whose dynamics is governed by "pulled" fronts [141,142], the standard derivation of a moving boundary approximation was found to break down. Mathematically, this traced back to the fact that for pulled fronts the dynamically important region is *ahead* of the nonlinear transition zone which one normally associates with the front itself. This was another important sign that *one really has to take the dynamics in the region ahead of the front seriously!*

My view that the linear spreading velocity is the proper starting point for understanding the two regimes of front propagation into unstable states, and for tying together the various theoretical developments and experiments—and hence that an introductory review should be organized around it—is colored by the developments sketched above and in particular the fact that Ebert and I have recently

[3] Some readers may be amused to note that there are traces of such arguments in the original paper of Kolmogorov et al. [234]: although hidden, the Green's function of the diffusion equation plays an important role in their convergence proofs. This makes me believe that it is likely that it will be possible to prove results concerning front propagation into unstable states for more complicated equations like higher order partial differential equations, by putting bounds on the Green's function.

been able to derive from it important *new and exact* results for the power law convergence of the velocity and shape of a pulled front to its asymptotic value [143,144]. The fact that starting from this concept one can set up a fully explicit calculational scheme to study the long time power law convergence or relaxation and that this yields new universal terms which are exact (and which even for the nonlinear diffusion equation [15,16] go beyond those which were previously known [54]), shows more than anything else that we have moved from the stage of speculations and intuitive concepts to what has essentially become a well-defined and powerful theoretical framework. My whole presentation builds on the picture coming out of this work [143–147].

As mentioned before, the subject of front propagation also has a long history in the mathematics literature; moreover, especially in the last 10–15 years a lot of work has been done on coherent structure type solutions like traveling fronts, pulses etc. With such a diverse field, spread throughout many disciplines, one cannot hope to do justice to all these developments. My choice to approach the subject from the point of view of a physicist just reflects that I only feel competent to review the developments in this part of the field, and that I do want to open up the many advances that have been made recently to researchers with different backgrounds who typically will not scan the physics literature. I will try to give a fair assessment of some of the more mathematical developments but there is absolutely no claim to be exhaustive in that regard. Luckily, authoritative reviews of the more recent mathematical literature are available [170,172,434,442]. The second reason for my choice is indeed that most of the mathematics literature is focused on equations that admit uniformly translating front solutions. For many pattern forming systems, the relevant front solutions are not of this type, they are either coherent or incoherent pattern forming fronts of the type we already encountered in Fig. 1 (these concepts are defined precisely in Section 2.7). Even though not much is known rigorously about these more general pattern forming fronts, our presentation will allow us to approach all types of fronts in a unified way that illuminates what is and is not known. We hope this will also stimulate the more mathematically inclined reader to take up the challenge of entering an area where we do know most answers but lack almost any proof. I am convinced a gold mine is waiting for those who dare.

As explained above, we will first introduce in Section 2 the key ingredients of front propagation into unstable states that provide the basic working knowledge for the non-expert physicist. The introduction along this line also allows us to identify most clearly the open problems. We then turn right away to a discussion of a large number of examples of front propagation. After this, we will give a more detailed discussion of the slow convergence of pulled fronts to their asymptotic velocity and shape. We are then in a position to discuss what patterns, whose dynamics is dominated by fronts propagating into an unstable state, can be analyzed in terms of a moving boundary approximation, in the limit that the front is thin compared to the pattern scale. This is followed by a discussion of the relation with the existence of "global modes" and of some of the issues related to stochastic fronts.

2. Front propagation into unstable states: the basics

The central theme of this paper is to study fronts in spatio-temporally extended systems which propagate into a linearly unstable state. The special character and, to a large extent, simplicity of such fronts arises from the fact that arbitrarily small perturbations about the unstable state already grow and spread by themselves, and thus have a nontrivial—and, as we shall see, rather universal—dynamics by themselves. The "linear spreading speed" v^* with which small perturbations spread out

is then automatically an important reference point. This is different from fronts which separate two linearly stable states—in that case the perturbations about each individual stable state just damp out and there is not much to be gained from studying precisely how this happens; instead, the motion of such fronts is inherently nonlinear.[4]

It will often be instructive to illustrate our analysis and arguments with a simple explicit example; to this end we will use the famous nonlinear diffusion equation with which the field started,

$$\partial_t u(x,t) = \partial_x^2 u(x,t) + f(u), \quad \text{with} \quad \begin{array}{l} f(0)=0,\ \ f(1)=0\ , \\ f'(0)=1,\ \ f'(1)<0\ . \end{array} \tag{1}$$

This is the equation studied by Fisher [163] and Kolmogorov et al. [234] back in 1937, and we shall therefore follow the convention to refer to it as the F-KPP equation. As we mentioned already in the introduction, this equation and its extensions have been the main focus of (rigorous) mathematical studies of front propagation into unstable states, but these are not the main focus of this review—rather, we will use the F-KPP equation only as the simplest equation to *illustrate* the points which are generic to the front propagation problem, and will not rely on comparison-type methods or bounds which are special to this equation.[5] At this point it simply suffices to note that the state $u=0$ of the real field u is an unstable state: when u is positive but small, $f(u) \approx f'(0)u = u$, so the second term on the right-hand side of the F-KPP equation drives u away from zero. The front propagation problem we are interested in was already illustrated in Fig. 1: We want to determine the long time asymptotic behavior of the front which propagates to the right into the unstable state $u=0$, given initial conditions for which $u(x \to \infty, t=0) = 0$. A simple analysis based on constructing the uniformly translating front solutions $u(x-vt)$ does not suffice, as there is a continuous family of such front solutions. Since the argument can be found at many places in the literature [15,38,105,144,249,268,421,428], we will not repeat it here.

2.1. The linear dynamics: the linear spreading speed v^*

Our approach to the problem via the introduction of the linear spreading speed v^* is a slight reformulation of the analysis developed over 40 years ago in plasma physics [49,62,264]. We first formulate the essential concept having in mind a simple partial differential equation or a set of partial differential equations, and then briefly discuss the minor complications that more general classes of dynamical equations entail. We postpone the discussion of fronts in higher dimensions to Section 5, so we limit the discussion here to fronts in one dimension.

Suppose we have a dynamical problem for some field, which we will generically denote by $\phi(x,t)$, whose dynamical equation is translation invariant and has a homogeneous stationary state $\phi=0$ which is *linearly unstable*. With this we mean that if we linearize the dynamical equation in ϕ about the unstable state, then Fourier modes grow for some range of spatial wavenumbers k. More concretely,

[4] Technically, determining the asymptotic fronts speed then usually amounts to a nonlinear eigenvalue problem. The spreading of the precursors of such fronts is studied in [227].

[5] A physicist's introduction to comparison type arguments can be found in the appendix of [38]; for recent work on bounds on the asymptotic speed of fronts in the F-KPP equation see in particular [33–37]. A new look at the global variational structure was recently given in [310]. A recent example of a convergence proof in coupled equations can be found in [323].

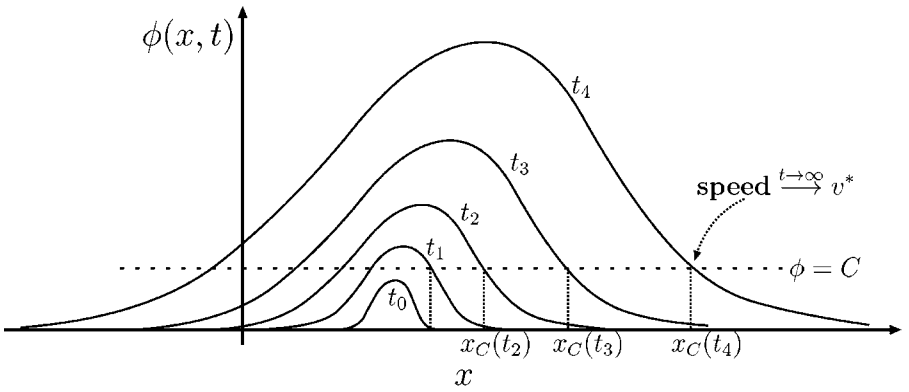

Fig. 2. Qualitative sketch of the growth and spreading of the field $\phi(x,t)$ according to the dynamical evolution equation linearized about the unstable state $\phi = 0$. The successive curves illustrate the initial condition $\phi(x,t_0)$ and the field $\phi(x,t)$ at successive times $t_1 < t_2 < t_3 < t_4$. Note that there is obviously no saturation of the field in the linearized dynamics: The asymptotic spreading velocity v^* to the right is the asymptotic speed of the positions $x_C(t)$ where $\phi(x,t)$ reaches the level line $\phi = C$: $\phi(x_C(t),t) = C$. The asymptotic spreading velocity to the left is defined analogously.

if we take a spatial Fourier transform and write

$$\tilde{\phi}(k,t) = \int_{-\infty}^{\infty} \mathrm{d}x\, \phi(x,t) \mathrm{e}^{-\mathrm{i}kx} \ , \tag{2}$$

substitution of the Ansatz

$$\tilde{\phi}(k,t) = \bar{\phi}(k) \mathrm{e}^{-\mathrm{i}\omega(k)t} \tag{3}$$

yields the *dispersion relation* $\omega(k)$ of Fourier modes of the linearized equation. We will discuss the situation in which the dispersion relation has more than one branch of solutions later, and for now assume that it just has a single branch. Then the statement that the state $\phi = 0$ is linearly unstable simply means that

$$\phi = 0 \ \textit{linearly unstable} : \ \mathrm{Im}\,\omega(k) > 0 \ \text{for some range of} \ k\text{-values} \ . \tag{4}$$

At this stage, the particular equation we are studying is simply encoded in the dispersion relation $\omega(k)$.[6] This dispersion relation can be quite general—we will come back to the conditions on $\omega(k)$ in Section 2.4 below, and for now will simply assume that $\omega(k)$ is an analytic function of k in the complex k-plane.

We are interested in studying the long-time dynamics emerging from some generic initial condition which is sufficiently localized in space (we will make the term "sufficiently localized" more precise in Section 2.3 below). Because there is a range of unstable modes which grow exponentially in time as $\mathrm{e}^{\mathrm{Im}\,\omega(k)t}$, a typical localized initial condition will grow out and spread in time under the linear dynamics as sketched in Fig. 2. If we now trace the level curve $x_C(t)$ where $\phi(x_C(t),t) = C$ in space-time, as indicated in the figure, the *linear spreading speed* v^* is defined as the *asymptotic*

[6] The reader who may prefer to see an example of a dispersion relation is invited to check the dispersion relation (86) for Eq. (85).

speed of the point $x_C(t)$:

$$v^* \equiv \lim_{t\to\infty} \frac{\mathrm{d}x_C(t)}{\mathrm{d}t} \ . \tag{5}$$

Note that v^* is independent of the value of C because of the linearity of the evolution equation. However, for systems whose dynamical equations are not reflection symmetric, as happens quite often in fluid dynamics and plasmas, one does have to distinguish between a spreading speed to the left and one to the right. In order not to overburden our notation, *we will in this paper by convention always focus on the spreading velocity of the right flank* of ϕ; this velocity is counted positive if this flank spreads to the right, and negative when it recedes to the left.

Given $\omega(k)$ and $\bar{\phi}(k)$, which according to (3) is just the Fourier transform of the initial condition $\phi(x, t=0)$, one can write $\phi(x,t)$ for $t>0$ simply as the inverse Fourier transform

$$\phi(x,t) = \frac{1}{2\pi} \int_{-\infty}^{\infty} \mathrm{d}k\, \bar{\phi}(k) \mathrm{e}^{\mathrm{i}kx - \mathrm{i}\omega(k)t} \ . \tag{6}$$

The more general Green's function formulation will be discussed later in Section 2.4. Our definition of the linear spreading speed v^* to the right is illustrated in Fig. 2. We will work under the assumption that the asymptotic spreading speed v^* is finite; whether this is true can always be verified self-consistently at the end of the calculation. The existence of a finite v^* implies that if we look in frame

$$\xi = x - v^* t \tag{7}$$

moving with this speed, we neither see the right flank grow nor decay exponentially. To determine v^*, we therefore first write the inverse Fourier formula (6) for ϕ in this frame,

$$\begin{aligned} \phi(\xi,t) &= \frac{1}{2\pi} \int_{-\infty}^{\infty} \mathrm{d}k\, \bar{\phi}(k) \mathrm{e}^{\mathrm{i}k(x-v^*t) - \mathrm{i}[\omega(k) - v^*k]t} \ , \\ &= \frac{1}{2\pi} \int_{-\infty}^{\infty} \mathrm{d}k\, \bar{\phi}(k) \mathrm{e}^{\mathrm{i}k\xi - \mathrm{i}[\omega(k) - v^*k]t} \ , \end{aligned} \tag{8}$$

and then determine v^* self-consistently by analyzing when this expression neither leads to exponential growth nor to decay *in the limit* ξ *finite,* $t\to\infty$. We cannot simply evaluate the integral by closing the contour in the upper half of the k-plane, since the large-k behavior of the exponent is normally dominated by the large-k behavior of $\omega(k)$. However, the large-time limit clearly calls for a saddle-point approximation [32] (also known as stationary phase or steepest descent approximation): Since t becomes arbitrarily large, we deform the k-contour to go through the point in the complex k plane where the term between square brackets varies least with k, and the integral is then dominated by the contribution from the region near this point. This so-called saddle point k^* is given by

$$\left.\frac{\mathrm{d}[\omega(k) - v^*k]}{\mathrm{d}k}\right|_{k^*} = 0 \ \Rightarrow \ v^* = \left.\frac{\mathrm{d}\omega(k)}{\mathrm{d}k}\right|_{k^*} \ . \tag{9}$$

These saddle point equations will in general have solutions in both the upper and the lower half of the complex k-plane; the ones in the upper half correspond to the asymptotic decay towards large x in the Fourier decomposition (8) associated with the right flank of the perturbation sketched in Fig. 2, and those in the lower half to an exponentially growing solution for increasing x and thus to the behavior on the left flank. By convention, we will focus on the right flank, which may invade the unstable state to the right. If we deform the k-contour into the complex plane to go through the

saddle point in the upper half plane, *and assume for the moment that* $\bar{\phi}(k)$, the Fourier transform of the initial condition, *is an entire function* (one that is analytic in every finite region of the complex k-plane), the dominant term to the integral is nothing but the exponential factor in (8) evaluated at the saddle-point, i.e., $e^{i[\omega(k^*)-v^*k^*]t}$. The self-consistency requirement that this term neither grows nor decays exponentially thus simply leads to

$$\mathrm{Im}\,\omega(k^*) - v^*\,\mathrm{Im}\,k^* = 0 \;\;\Rightarrow\;\; v^* = \frac{\mathrm{Im}\,\omega(k^*)}{\mathrm{Im}\,k^*} = \frac{\omega_i}{k_i}\ . \tag{10}$$

The notation ω_i which we have introduced here for the imaginary part of ω will be used interchangeably from now on with $\mathrm{Im}\,\omega$; likewise, we will introduce the subindex r to denote the real part of a complex quantity. Upon expanding the factor in the exponent in (8) around the saddle point value given by Eqs. (9) and (10), we then get from the resulting Gaussian integral

$$\begin{aligned}\phi(\xi,t) &\simeq \frac{1}{2\pi}\int_{-\infty}^{\infty} \mathrm{d}k\,\bar{\phi}(k) e^{-i\omega_r^* t + i(k^*+\Delta k)\xi - \mathscr{D}t(\Delta k)^2} \quad (\Delta k = k - k^*)\ ,\\ &\simeq \frac{1}{2\pi}\, e^{ik^*\xi - (\omega_r^* - k_r v)t}\int_{-\infty}^{\infty} \mathrm{d}k\,\bar{\phi}(k) e^{-\mathscr{D}t[\Delta k - i\xi/2\mathscr{D}t]^2 - \xi^2/4\mathscr{D}t}\ ,\\ &\simeq \frac{1}{\sqrt{4\pi\mathscr{D}t}}\, e^{ik^*\xi - i\omega_r^* t} e^{-\xi^2/4\mathscr{D}t}\bar{\phi}(k^*) \quad (\xi \text{ fixed},\ t\to\infty)\ ,\end{aligned} \tag{11}$$

where all parameters are determined by the dispersion relation through the saddle point values,

$$\left.\frac{\mathrm{d}\omega(k)}{\mathrm{d}k}\right|_{k^*} = \frac{\omega_i(k^*)}{k_i^*},\quad v^* = \frac{\omega_i(k^*)}{k_i^*},\quad \mathscr{D} = \frac{i}{2}\left.\frac{\mathrm{d}^2\omega(k)}{\mathrm{d}k^2}\right|_{k^*}\ . \tag{12}$$

Since ω and k are in general complex, the first equation can actually be thought of as two equations for the real and imaginary parts, which can be used to solve for k^*. The second and third equation then give v^* and $\mathscr{D}$.

The exponential factor $e^{ik^*\xi}$ gives the dominant spatial behavior of ϕ in the co-moving frame ξ on the right flank in Fig. 2: if we define the asymptotic spatial decay rate λ^* and the effective *diffusion coefficient*[7] D by

$$\lambda^* \equiv \mathrm{Im}\,k^*,\quad \frac{1}{D} \equiv \mathrm{Re}\,\frac{1}{\mathscr{D}}\ , \tag{13}$$

then we see that the modulus of ϕ falls off as

$$|\phi(\xi,t)| \sim \frac{1}{\sqrt{t}}\, e^{-\lambda^*\xi} e^{-\xi^2/4Dt} \quad (\xi \text{ fixed},\ t\to\infty)\ , \tag{14}$$

i.e., essentially as $e^{-\lambda^*\xi}$ with a Gaussian correction that is reminiscent of diffusion-like behavior.

We will prefer not to name the point k^* after the way it arises mathematically (e.g., saddle point or "pinch point", following the formulation discussed in Section 2.4). Instead, we will usually refer to k^* as the *linear spreading point*; likewise, expressions (11) and (14) for ϕ will be referred to as the linear spreading profiles.

[7] We stress that D is the effective diffusion coefficient associated with the saddle point governing the linear spreading behavior of the *deterministic* equation. In Section 7 we will also encounter a front diffusion coefficient D_{front} which is a measure for the stochastic front wandering, but this is an entirely different quantity.

For an ordinary diffusion process to be stable, the diffusion coefficient has to be positive. Thus we expect that in the present case D should be positive. Indeed, the requirement that the linear spreading point corresponds to a maximum of the exponential term in (8) translates into the condition, $\mathrm{Re}\,\mathscr{D} > 0$, and this entails $D > 0$. We will come back to this and other conditions in Section 2.4 below.

In spite of the simplicity of their derivation and form, Eqs. (11) and (12) express the crucial result that as we shall see permeates the field of front propagation into unstable states:

associated with any linearly unstable state is a linear spreading speed v^* given by (12); this is the natural asymptotic spreading speed with which small "sufficiently localized" perturbations spread into a domain of the unstable state according to the linearized dynamics.

Before turning to the implications for front propagation, we will in the next sections discuss various aspects and generalizations of these concepts, including the precise condition under which "sufficiently localized" initial conditions do lead to an asymptotic spreading velocity v^* (the so-called steep initial conditions given in (37) below).

Example. Application to the linear F-KPP equation.

Let us close this section by applying the above formalism to the F-KPP equation (1). Upon linearizing the equation in u, we obtain

$$\text{linearized F-KPP:} \quad \partial_t u(x,t) = \partial_x^2 u(x,t) + u \ . \tag{15}$$

Substitution of a Fourier mode $\mathrm{e}^{-\mathrm{i}\omega t + \mathrm{i}kx}$ gives the dispersion relation

$$\text{F-KPP:} \quad \omega(k) = \mathrm{i}(1 - k^2) \ , \tag{16}$$

and from this we immediately obtain from (12) and (13)

$$\text{F-KPP:} \quad v^*_{\mathrm{FKPP}} = 2, \quad \lambda^* = 1, \quad \mathrm{Re}\,k^* = 0, \quad D = \mathscr{D} = 1 \ . \tag{17}$$

The special simplicity of the F-KPP equation lies in the fact that $\omega(k)$ is quadratic in k. This not only implies that the effective diffusion coefficient D is nothing but the diffusion coefficient entering the F-KPP equation, but also that the exponent in (8) is in fact a Gaussian form without higher order corrections. Thus, the above evaluation of the integral is actually exact in this case. Another instructive way to see this is to note that the transformation $u = \mathrm{e}^t n$ transforms the linearized F-KPP equation (15) into the diffusion equation $\partial_t n = \partial_x^2 n$ for n. The fundamental solution corresponding to delta-function initial condition is the well-known Gaussian; in terms of u this yields

$$\text{F-KPP:} \ u(x,t) = \frac{1}{\sqrt{4\pi t}}\, \mathrm{e}^{t - x^2/4t} \quad \text{(delta function initial conditions)} \ . \tag{18}$$

2.2. The linear dynamics: characterization of exponential solutions

In the above analysis, we focused immediately on the importance of the linear spreading point k^* of the dispersion relation $\omega(k)$ in determining the spreading velocity v^*. Let us now pay more attention to the precise initial conditions for which this concept is important.

In the derivation of the linear spreading velocity v^*, we took the Fourier transform of the initial conditions to be an entire function, i.e., a function which is analytic in any finite region of the

complex plane. Thus, the analysis applies to the case in which $\phi(x,t=0)$ is a delta function ($\bar{\phi}(k)$ is then k-independent[8]), has compact support (meaning that $\phi(x,t=0)=0$ outside some finite interval of x), or falls off faster than any exponential for large enough x (like, e.g., a Gaussian).

For all practical purposes, the only really relevant case in which $\bar{\phi}(k)$ is not an entire function is when it has poles off the real axis in the complex plane.[9] This corresponds to an initial condition $\phi(x,t=0)$ which falls off exponentially for large x. To be concrete, let us consider the case in which $\bar{\phi}(k)$ has a pole in the upper half plane at $k=k'$. If we deform the k-integral to also go around this pole, $\phi(x,t)$ also picks up a contribution whose modulus is proportional to[10]

$$|\mathrm{e}^{-\mathrm{i}\omega(k')t+\mathrm{i}k'x}| = \mathrm{e}^{-\lambda(x-v(k')t)}, \quad \text{with } \lambda \equiv \operatorname{Im} k' \ , \tag{19}$$

and whose *envelope velocity* $v(k')$ is given by

$$v(k') = \frac{\operatorname{Im}\omega(k')}{\operatorname{Im} k'} \ . \tag{20}$$

We first characterize these solutions in some detail, and then investigate their relevance for the full dynamics.

Following [144], we will refer to the exponential decay rate λ of our dynamical field as the *steepness*. For a *given* steepness λ, $\omega(k')$ of course still depends on the real part of k'. We choose to introduce a *unique* envelope velocity $v_{\mathrm{env}}(\lambda)$ by taking for $\operatorname{Re} k'$ the value that maximizes $\operatorname{Im}\omega$ and hence $v(k')$,

$$v_{\mathrm{env}}(\lambda \equiv k_{\mathrm{i}}') = \left.\frac{\omega_{\mathrm{i}}(k)}{k_{\mathrm{i}}}\right|_{k=k'} \quad \text{with} \quad \left.\frac{\partial\omega_{\mathrm{i}}(k)}{\partial k_{\mathrm{r}}}\right|_{k=k'} = \operatorname{Im}\left.\frac{\mathrm{d}\omega}{\mathrm{d}k}\right|_{k=k'} = 0 \ , \tag{21}$$

where the second condition determines k_{r} implicitly as a function of $\lambda = k_{\mathrm{i}}'$. The rationale to focus on this particular velocity as a function of λ is twofold: First of all, if we consider for the fully linear problem under investigation here an initial condition whose modulus falls of as $\mathrm{e}^{-\lambda x}$ but in whose spectral decomposition a whole range of values of k_{r} are present, this maximal growth value will dominate the large time dynamics. Secondly, in line with this, when we consider nonlinear front solutions corresponding to different values of k_{r}, the one not corresponding to the maximum of ω_{i} are unstable and therefore dynamically irrelevant—see Section 2.8.2. Thus, for all practical purposes the branch of velocities $v_{\mathrm{env}}(\lambda)$ is the real important one.

The generic behavior of $v_{\mathrm{env}}(\lambda)$ as a function of λ is sketched in Fig. 3(a). In this figure, the dotted lines indicate branches not corresponding to the envelope velocity given by (21): For a given value of λ, the other branches correspond to a smaller value of ω_{i} and hence to a smaller value of

[8] Most of the original literature [49,62,204,264] in which the asymptotic large-time spreading behavior of a perturbation is obtained through a similar analysis or the more general "pinch point" analysis, is implicitly focused on this case of delta-function initial conditions, since the analysis is based on a large-time asymptotic analysis of the Greens function of the dynamical equations. Note in this connection that (18) is indeed the Green's function solution of the linearized F-KPP equation.

[9] Of course, one may consider other examples of non-analytic behavior, such as power law singularities at $k=0$. This would correspond to a power law initial conditions $\phi(x,t=0) \sim x^{-\delta}$ as $x \to \infty$. Such initial conditions are so slowly decaying that they give an infinite spreading speed, as $\phi(x,t) \sim \mathrm{e}^{\operatorname{Im}\omega(0)t}x^{-\delta}$. Also the full nonlinear front solutions have a divergent speed in this case [256].

[10] We are admittedly somewhat cavalier here; a more precise analysis of the crossover between the various contributions is given in the next subsection below Eq. (31).

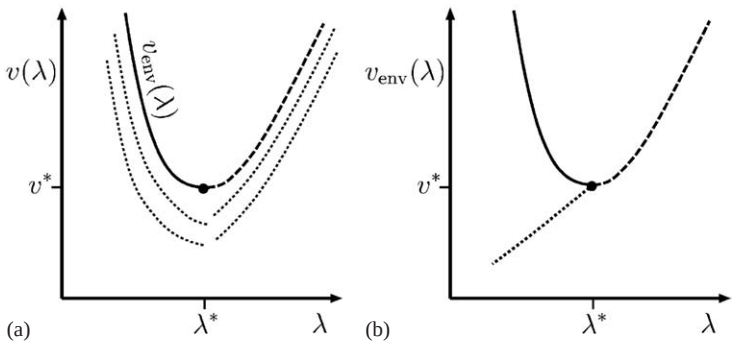

Fig. 3. (a) Generic behavior of the velocity $v(\lambda)$ as a function of the spatial decay rate λ. The thick full line and the thick dashed line indicate the envelope velocity defined in (21): for a given λ this corresponds to the largest value of $\omega_{\rm i}$ and hence to the largest velocity on these branches. The minimum of $v_{\rm env}$ is equal to the linear spreading speed v^*. (b) The situation in the special case of uniformly translating solutions which obey $\omega/k = v$. The dotted line marks the branch of solutions with velocity less than v^* given in (27).

$v(\lambda)$. Furthermore, since we are considering the spreading and propagation dynamics at a linearly unstable state, the maximal growth rate $\omega_{\rm i}(\lambda) > 0$ as $\lambda \downarrow 0$. Hence $v_{\rm env}(\lambda)$ diverges as $1/\lambda$ for $\lambda \to 0$. When we follow this branch for increasing values of λ, at some point this branch of solutions will have a minimum. This minimum is nothing but the value v^*: Since along this branch of solutions $\partial\omega_{\rm i}/\partial k_{\rm r} = 0$, we simply have

$$\frac{{\rm d}v_{\rm env}}{{\rm d}\lambda} = \frac{1}{\lambda}\left(\frac{\partial\omega_{\rm i}}{\partial\lambda} + \frac{\partial\omega_i}{\partial k_{\rm r}}\frac{{\rm d}k_{\rm r}}{{\rm d}\lambda} - \frac{\omega_{\rm i}}{\lambda}\right) = \frac{1}{\lambda}\left(\frac{\partial\omega_{\rm i}}{\partial\lambda} - \frac{\omega_{\rm i}}{\lambda}\right) \ , \tag{22}$$

and so at the linear spreading point k^*

$$\left.\frac{{\rm d}v_{\rm env}}{{\rm d}\lambda}\right|_{k^*} = \frac{1}{\lambda^*}\left(\left.\frac{\partial\omega_{\rm i}}{\partial\lambda}\right|_{k^*} - \frac{\omega_{\rm i}^*}{\lambda^*}\right) = 0 \ , \tag{23}$$

since at the point k^* the term between brackets precisely vanishes, see Eq. (12). By differentiating once more, we see that the curvature of $v_{\rm env}(\lambda)$ at the minimum can be related to the effective diffusion coefficient[11] D introduced in (13),

$$\left.\frac{{\rm d}^2 v_{\rm env}(\lambda)}{{\rm d}\lambda^2}\right|_{\lambda^*} = \frac{1}{\lambda^*}\left[\left.\frac{\partial^2\omega_{\rm i}}{\partial\lambda^2}\right|_{k^*} + 2\left.\frac{\partial^2\omega_{\rm i}}{\partial\lambda\partial k_{\rm r}}\right|_{k^*}\left.\frac{{\rm d}k_{\rm r}}{{\rm d}\lambda}\right|_{k^*} + \left.\frac{\partial^2\omega_{\rm i}}{\partial k_{\rm r}^2}\right|_{k^*}\left(\frac{{\rm d}k_{\rm r}}{{\rm d}\lambda}\right)^2_{k^*}\right]$$

[11] Aside for the reader familiar with amplitude equations [105,155,189]: The relation between the curvature of $v_{\rm env}(\lambda)$ at the minimum and the diffusion coefficient D bears some intriguing similarities to the relation between the curvature of the growth rate as a function of k of the pattern forming mode near the bifurcation to a finite-wavelength pattern and the parameters in the amplitude equation [105,189,193,316,320]. That curvature is also essentially the diffusion constant that enters the amplitude equation. Nevertheless, one should keep in mind that the minimum of $v_{\rm env}(\lambda)$ is associated with the saddle point of an invasion mode which falls off in space, *not* with the maximum growth rate of a Fourier mode. Moreover, while the amplitude equations only describe pattern formation near the instability threshold, the pulled front propagation mechanism can be operative far above an instability threshold as well as in pattern forming problems which have no obvious threshold.

$$= \frac{2}{\lambda^*}\left[\mathscr{D}_r + 2\mathscr{D}_i\left(\frac{\mathscr{D}_i}{\mathscr{D}_r}\right) - \mathscr{D}_r\left(\frac{\mathscr{D}_i}{\mathscr{D}_r}\right)^2\right] = \frac{2}{\lambda^*}\left[\mathscr{D}_r + \frac{\mathscr{D}_i^2}{\mathscr{D}_r}\right] ,$$

$$= \frac{2D}{\lambda^*} , \tag{24}$$

where $\mathscr{D}$ was defined in (12) and where we used the fact that according to the definition (13) of D, we can write $D = \mathscr{D}_r + \mathscr{D}_i^2/\mathscr{D}_r$. Furthermore, in deriving these results, we have repeatedly used the Cauchy–Riemann relations for complex analytic functions that relate the various derivatives of the real and imaginary part, and the fact that along the branch of solutions v_{env}, the relation $\partial\omega_i/\partial k_r = 0$ implies $\mathscr{D}_i - \mathscr{D}_r(dk_r/d\lambda) = 0$.

If we investigate a dynamical equation which admits a uniformly translating front solution of the form $\phi(x - vt)$, the previous results need to be consistent which this special type of asymptotic behavior. Now, the exponential leading edge behavior $e^{ikx - i\omega t}$ we found above only corresponds to uniformly translating behavior provided

$$\text{uniformly translating solutions}: \quad v(\lambda) = \frac{\omega(k)}{k} \quad (\lambda = k_i) . \tag{25}$$

The real part of this equation is consistent with the earlier condition $v = \omega_i/k_i$ that holds for all fronts, but for uniformly translating fronts it implies that in addition $\mathrm{Im}(\omega/k) = 0$.

Hence, the above discussion is only self-consistent for uniformly translating solutions if the branch $v_{env}(\lambda)$ where the growth rate ω_i is maximal for a given λ coincides with the condition (25). In all the cases that I know of,[12] the branch of envelope solutions for $v > v^*$ coincides with uniformly translating solutions because the dispersion relation is such that the growth rate ω_i is maximized for $k_r = 0$:

$$\text{uniformly translating solutions with } v > v^*: \quad k_r = \omega_r = 0, \quad \mathscr{D}_i = 0 . \tag{26}$$

Obviously, in this case the branch $v_{env}(\lambda)$ corresponds to the simple exponential behavior $\exp(-\lambda x + \omega_i t)$ which is neither temporally nor spatially oscillatory.[13]

We had already seen that there generally are also solutions with velocity $v < v^*$, as the branches with velocity $v_{env} > v^*$ shown in Fig. 3(a) are only those corresponding to the maximum growth condition $\partial\omega_i/\partial k_r = 0$, see Eq. (21). It is important to realize that if an equation admits uniformly translating solutions, there is in general also a branch of uniformly translating solutions with $v < v^*$. Indeed, by expanding the curve $v_{env}(\lambda)$ around the minimum v^* and looking for solutions with $v < v^*$, one finds that these are given by[14]

$$\lambda - \lambda^* \approx \frac{v'''}{3(v'')^2}(v - v^*), \quad k_r - k_r^* \approx \sqrt{2|v - v^*|/v''} \quad (v < v^*) . \tag{27}$$

---

[12] As we shall see in Section 2.11.1, the EFK equation illustrates that when the linear spreading point ceases to obey (26), the pulled fronts change from uniformly translating to coherent pattern forming solutions.

[13] For uniformly translating fronts, it would be more appropriate to use in the case of uniformly translating fronts the usual Laplace transform variables $s = -i\omega$ and $\lambda = -ik$ as these then take real values. We will refrain from doing so since most of the literature on the asymptotic analysis of the Green's function on which the distinction between convectively and absolutely unstable states is built, employs the ω-k convention.

[14] Note that the formula given on p. 53 of [144] is slightly in error.

The situation in the special case of uniformly translating solutions is sketched in Fig. 3(b); in this figure, the dotted line shows the branch of solutions with $v < v^*$. Since solutions for $v < v^*$ are always spatially oscillatory ($k_r \neq 0$), they are sometimes disregarded in the analysis of fronts for which the dynamical variable, e.g. a particle density, is by definition non-negative. It is important to keep in mind, however, that they do actually have relevance as intermediate asymptotic solutions during the transient dynamics: as we shall see in Section 2.9, the asymptotic velocity v^* is always approached slowly from below, and as a result the transient dynamics follows front solutions with $v < v^*$ adiabatically. Secondly, this branch of solutions also pops up in the analysis of fronts in the case that there is a small cutoff in the growth function—see Section 7.1.

The importance of this simple connection between the minimum of the curve $v_{\rm env}(\lambda)$ and the linear spreading speed v^* can hardly be overemphasized:

For equations of F-KPP type, the special significance of the minimum of the $v_{\rm env}(\lambda)$ branch as the selected asymptotic velocity in the pulled regime is well known, and it plays a crucial role in more rigorous comparison-type arguments for front selection in such types of equations. The line of argument that we follow here emphasizes that v^* is the asymptotic speed that naturally arises from the linearized dynamical problem, and that this is the proper starting point both to understand the selection problem, and to analyze the rate of convergence to v^* quantitatively.

Example. Application to the linear F-KPP equation.

We already gave the dispersion relation of the F-KPP equation in (16); using this in Eq. (21) immediately gives for the upper branches with $v_{\rm env} \geqslant v^* = 2$

$$\text{F-KPP}: \quad \lambda = \frac{v_{\rm env} \pm \sqrt{v_{\rm env}^2 - 4}}{2} \quad \Leftrightarrow \quad v_{\rm env} = \lambda + \lambda^{-1} \ , \tag{28}$$

and for the branches below v^*

$$\text{F-KPP}: \quad \lambda = v/2, \quad k_r = \pm\frac{1}{2}\sqrt{4 - v^2} \quad (v < v^* = 2) \ , \tag{29}$$

in agreement with the above discussion and with (27).

2.3. The linear dynamics: importance of initial conditions and transients

We now study the dependence on initial conditions and the transient behavior. This question is obviously relevant: The discussion in the previous section shows that simple exponentially decaying solutions can propagate faster than v^*—at first sight, one might wonder how a profile spreading with velocity v^* can ever emerge from the dynamics if solutions exist which tend to propagate faster. Moreover, as we shall see, initial conditions which fall with an exponential decay rate $\lambda < \lambda^*$ do give rise to a propagation speed $v_{\rm env}(\lambda)$ which is larger than v^*.

If the initial condition is a delta function, or, more generally, if the initial condition has compact support (i.e. vanishes identically outside some finite range of x), then the Fourier transform $\bar{\phi}(k)$ is an entire function. This means that $\bar{\phi}(k)$ is analytic everywhere in the complex k-plane. The earlier analysis shows that whatever the precise initial conditions, the asymptotic spreading speed is always simply v^*, determined by the saddle point of the exponential term.

The only relevant initial conditions which can give rise to spreading with a constant finite speed are the exponential initial conditions already discussed in some detail in the previous subsection. Let us assume that $\bar{\phi}(k)$ has a pole in the complex k-plane at k', with spatial decay rate $k'_{\rm i} = \lambda$. In our first round of the discussion, we analyzed the limit ξ fixed, $t \to \infty$, but it is important to keep in mind that the limits ξ fixed, $t \to \infty$ and t fixed, $\xi \to \infty$ do not commute. Indeed, it follows directly from the inverse Fourier formula that the spatial asymptotic behavior as $x \to \infty$ is the same as that of the initial conditions, [15]

$$\phi(x \to \infty, t = 0) \sim {\rm e}^{-\lambda x} \;\; \Rightarrow \;\; \phi(x \to \infty, t) \sim {\rm e}^{-\lambda x} \; . \tag{30}$$

In order to understand the competition and crossover between such exponential parts and the contribution from the saddle point, let us return to the intermediate expression (11) that arises in analyzing the large-time asymptotics,

$$\phi(\xi, t) \simeq \frac{1}{2\pi}\, {\rm e}^{{\rm i}k^*\xi - {\rm i}\omega_{\rm r}^* t} \int_{-\infty}^{\infty} {\rm d}k\; \bar{\phi}(k) {\rm e}^{-\mathscr{D}t[\Delta k - {\rm i}\xi/2\mathscr{D}t]^2 - \xi^2/4\mathscr{D}t} \; , \tag{31}$$

and analyze this integral more carefully in a case in which $\bar{\phi}(k)$ has a pole whose strength is small. The term $-{\rm i}\xi/2\mathscr{D}t$ in the above expression gives a shift in the value of the k where the quadratic term vanishes. For fixed ξ, this shift is very small for large t, and the Gaussian integration yields the asymptotic result (11). However, when ξ is large enough that the point where the growth rate is maximal moves close to the pole, the saddle point approximation to the integral breaks down. This clearly happens when the term between brackets in the exponential in (31) is small at the pole, i.e., at the *c*ross*o*ver point $\xi_{\rm co}$ for which

$$\xi_{\rm co}\, {\rm Re}\left(\frac{1}{2\mathscr{D}t}\right) \sim (\lambda - \lambda^*) \;\; \Rightarrow \;\; \xi_{\rm co} \sim 2D(\lambda - \lambda^*)t \; , \tag{32}$$

where we used the effective diffusion coefficient D defined in (13). This rough argument relates the velocity and direction of motion of the crossover point to the difference in steepness λ of the initial condition and the steepness λ^*, and gives insight into how the contributions from the initial condition and the saddle point dominate in different regions. Before we will discuss this, it is instructive to give a more direct derivation of a formula for the velocity of the crossover region by matching the expressions for the field ϕ in the two regions. Indeed, the expression for ϕ in the region dominated by the saddle point is the one given in (14),

$$|\phi(\xi, t)| \simeq \frac{1}{\sqrt{4\pi D t}}\, {\rm e}^{-\lambda^*\xi} {\rm e}^{-\xi^2/4Dt} |\bar{\phi}(k^*)| \; , \tag{33}$$

while in the large ξ region the profile is simply exponential: in the frame ξ moving with the linear spreading speed v^* the profile is according to (19)

$$|\phi(\xi, t)| \simeq A {\rm e}^{-\lambda[\xi - (v_{\rm env}(\lambda) - v^*)t]} \; , \tag{34}$$

where A is the pole strength of the initial condition. The crossover point is simply the point where the two above expression match; by equating the two exponential factors and writing $\xi_{\rm co} = v_{\rm co} t$, we obtain from the dominant terms linear in t

$$-\lambda^* v_{\rm co} - v_{\rm co}^2/4D = -\lambda v_{\rm co} + \lambda[v_{\rm env}(\lambda) - v^*] \; , \tag{35}$$

[15] For the F-KPP equation, this is discussed in more detail in Section 2.5 of [144], where this property is referred to as "conservation of steepness".

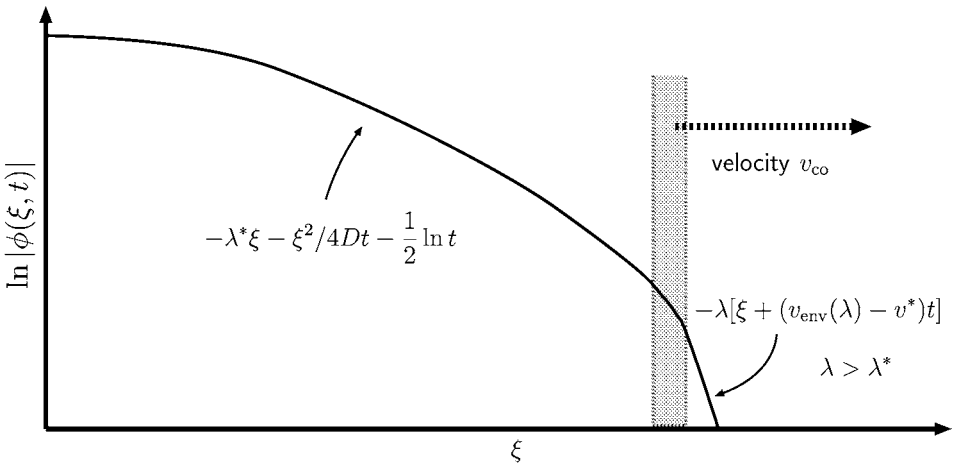

Fig. 4. Illustration of the crossover in the case of an initial condition which falls of exponentially with steepness $\lambda > \lambda^*$, viewed in the frame $\xi = x - v^* t$ moving with the asymptotic spreading speed. Along the vertical axis we plot the logarithm of the amplitude of the transient profile. The dashed region marks the crossover region between the region where the linear spreading point contribution dominates and which spreads asymptotically with speed v^* in the lab frame, and the exponential tail which moves with a speed $v_{env} > v^*$. As indicated, the crossover region moves to the right, so the steep fast-moving exponential tail disappears from the scene. The speed of the crossover region is obtained by matching the two regions, and is given by (36).

and hence

$$v_{co} = 2D(\lambda - \lambda^*) \pm 2D\sqrt{(\lambda - \lambda^*)^2 - \lambda[v_{env}(\lambda) - v^*]/D}\ . \tag{36}$$

It is easy to check that for equations where $\omega(k)$ is quadratic in k, the F-KPP equation as well as the Complex Ginzburg Landau equation discussed in Section 2.11.5, the square root vanishes in view of relation (24) between D and the curvature of $v_{env}(\lambda)$ at the minimum. Hence, (36) then reduces to (32). This is simply because when $\omega(k)$ is quadratic, the Gaussian integral in the first argument is actually exact. Since the square root term in (36) is always smaller than the first term in the expression, we see that the sign of v_{co}, the velocity of the crossover point, is the same as the sign of $\lambda - \lambda^*$. Thus, the upshot of the analysis is that the crossover point to a tail with steepness λ *larger* than λ^* moves to the *right*, and the crossover point to a tail which is *less steep*, to the *left*.[16]

The picture that emerges from this analysis is illustrated in Figs. 4 and 5. When $\lambda > \lambda^*$, i.e. for initial conditions which are steeper than the asymptotic linear spreading profile, to the right for large enough ξ the profile always falls of fast, with the steepness of the initial conditions. However, as illustrated in Fig. 4 the crossover region between this exponential tail and the region spreading with

[16] Note that when the velocity is expanded in the term under the square root sign, the terms of order $(\lambda - \lambda^*)^2$ always cancel in view of Eq. (24). Thus the argument of the square root term generally grows as $(\lambda - \lambda^*)^3$, and depending on $v'''_{env}(\lambda^*)$ the roots of Eq. (36) are complex either for $\lambda > \lambda^*$ or for $\lambda < \lambda^*$. This indicates that the detailed matching in the regime where the roots of (36) are complex is more complicated than we have assumed in the analysis, but the general conclusion that the direction of the motion of the crossover point is determined by the sign of $\lambda - \lambda^*$ is unaffected.

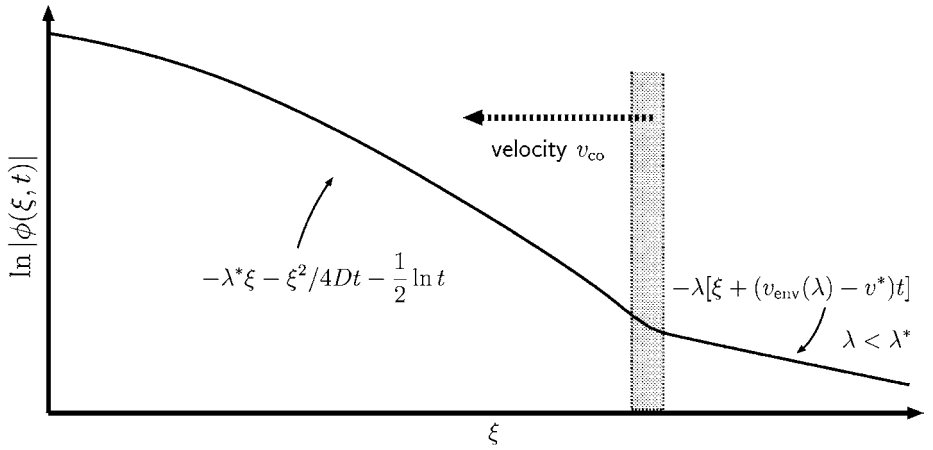

Fig. 5. As Fig. 4 but now for the case of an initial condition which falls of exponentially with steepness $\lambda < \lambda^*$. In this case, the dashed crossover region moves to the left, so the slowly decaying exponential tail gradually overtakes the region spreading with velocity v^* in the lab frame. In other words, the asymptotic rate of propagation for initial conditions which decay slower than $\exp(-\lambda^* x)$ is $v_{env} > v^*$.

velocity v^* moves to the right in the frame moving with v^*, i.e. moves out of sight! Thus, as time increases larger and larger portions of the profile spread with v^*.[17]

Just the opposite happens when the steepness λ of the initial conditions is less than λ^*. In this case $v_{co} < 0$, so as Fig. 5 shows, in this case the exponential tail expands into the region spreading with velocity v^*. In this case, therefore, as time goes on, larger and larger portions of the profile are given by the exponential profile (34) which moves with a velocity larger than v^*.

Because of the importance of initial conditions whose steepness λ is larger than λ^*, we will henceforth refer to these as *steep initial conditions*:

$$\textit{steep} \text{ initial conditions:} \quad \lim_{x\to\infty} \phi(x,0)e^{\lambda^* x} = 0 \ . \tag{37}$$

We will specify the term "localized initial conditions" more precisely when we will discuss the nonlinear front problem in Section 2.7.6.

In conclusion, in this section we have seen that

According to the linear dynamics, initial conditions whose exponential decay rate ("steepness") λ is larger than λ^* lead to profiles which asymptotically spread with the linear spreading velocity v^*. Initial conditions which are less steep than λ^* evolve into profiles that advance with a velocity $v_{env} > v^*$.

As we shall see, these simple observations also have strong implications for the nonlinear behavior: according to the linear dynamics, the fast-moving exponential tail moves out of sight. Thus, with steep initial conditions we can only get fronts which move faster than v^* *if this exponential tail*

[17] There is an amusing analogy with crystal growth: the shape of a growing faceted crystal is dominated by the slowing growing facets, as the fast ones eliminate themselves [420].

matches up with a nonlinear front, i.e. if there are nonlinear front solutions whose asymptotic spatial decay rate $\lambda > \lambda^*$. These will turn out to be the pushed front solutions.

Example. Crossover in the linear F-KPP equation.

The above general analysis can be nicely illustrated by the initial value problem $u(x,0) = \theta(x)e^{-\lambda x}$ for the linearized F-KPP equation (15), taken from Section 2.5.1 of [144]. Here θ is the unit step function. The solution of the linear problem is

$$u(x,t) = \exp[-\lambda x - v_{\rm env}(\lambda)t]\,\frac{1+\mathrm{erf}\left[(x-2\lambda t)/\sqrt{4t}\right]}{2}\ , \tag{38}$$

where $\mathrm{erf}(x) = 2\pi^{-1/2}\int_0^x e^{-t^2}$ is the error function and where $v_{\rm env}(\lambda)$ is given in (28). The position of the crossover region is clearly $x \approx 2\lambda t$, which corresponds to a speed $2(\lambda - \lambda^*)$ in the $\xi = x - 2t$ frame, in accord with (32) and (36) with $D = 1$, $\lambda^* = 1$ and $v^* = 2$ [Cf. (17)]. Moreover, this crossover region separates the two regions where the asymptotic behavior is given by

$$\begin{aligned} u(x,t) &\approx \exp[-\lambda[x - v_{\rm env}(\lambda)t]]\ , \\ &= \exp[-\lambda[\xi - (v_{\rm env}(\lambda) - v^*)t]] \quad \text{for } \xi \gg 2(v_{\rm env} - 2)t\ , \end{aligned} \tag{39}$$

and

$$\begin{aligned} u(x,t) &\approx \frac{1}{\sqrt{4\pi t}\lambda(1 - x/(2\lambda t)}\exp[-(x-2t) - (x-2t)^2/4t]\ , \\ &\approx \frac{1}{\sqrt{4\pi t}\lambda}\exp[-\xi - \xi^2/4t] \quad \text{for } \xi \ll 2(v_{\rm env} - 2)t\ , \end{aligned} \tag{40}$$

in full agreement with the general expressions (34) and (33). Finally, note that according to (38) the width of the crossover region grows diffusively, as $\sqrt{t}$. We expect this width $\sim \sqrt{t}$ behavior of the crossover region to hold more generally.

2.4. The linear dynamics: generalization to more complicated types of equations

So far, we have had in the back of our minds the simple case of a partial differential equation whose dispersion relation $\omega(k)$ is a unique function of k. We now briefly discuss the generalization of our results to more general classes of dynamical equations, following [144].

First, consider difference equations. The only difference with the previous analysis is that in this case the k-space that we introduce in writing a Fourier transform, is periodic—in the language of a physicist, the k space can be limited to a finite Brillouin zone. Within this zone, k is a continuous variable and $\omega(k)$ has the same meaning as before. So, if $\omega(k)$ has a saddle point in the first Brillouin zone, this saddle point is given by the *same* saddle point equations (12) as before, and the asymptotic expression (14) for the dynamical field ϕ is then valid as well! [18]

[18] When $\omega(k)$ is periodic in k space, there will generally also be saddle points at the boundary of the Brillouin zone. These will usually not correspond to the unstable modes—they correspond to a an oscillatory dependence of the dynamical field (like in antiferromagnetism)—but there is no problem in principle with the linear spreading being determined by a saddle point associated with the edges of the Brillouin zone.

In passing, we note that although the above conclusion is simple but compelling, one may at first sight be surprised by it. For, many coherent solutions like fronts and kinks are susceptible to "locking" to the underlying lattice when one passes from a partial differential equation to a difference equation [154,222]. Mathematically this is because perturbations to solutions which on both sides approach a stable state are usually governed by a solvability condition. The linear spreading dynamics into an unstable state, on the other hand, is simply governed by the balance of spreading and growth, and this is virtually independent of the details of the underlying dynamics.

The concept of linear spreading into an unstable state can be generalized to sets of equations whose linear dynamics about the unstable state can, after spatial Fourier transformation and temporal Laplace transform, be written in the form

$$\sum_{m=1}^{N} \hat{S}_{nm}(k,\omega)\hat{\phi}_m(k,\omega) = \sum_{m=1}^{N} \hat{H}_{nm}(k,\omega)\tilde{\phi}_m(k,t=0), \quad n=1,\ldots,N \ . \tag{41}$$

Here n is an index which labels the fields. The above formulation is the one appropriate when we use a temporal Laplace transform,

$$\hat{\phi}_n(k,\omega) = \int_0^\infty \mathrm{d}t \int_{-\infty}^{\infty} \mathrm{d}x\, \phi_n(x,t)\mathrm{e}^{-\mathrm{i}kx+\mathrm{i}\omega t} \ . \tag{42}$$

In the Laplace transform language, terms on the right-hand side arise from the partial integration of temporal derivative terms $\partial_t^k \phi_m(x,t)$ in the dynamical equation; the coefficients H_{nm} therefore have no poles in the complex ω plane but poles in the k plane can arise from exponentially decaying initial conditions.

It is important to realize that the class of equations where the linearized dynamics about the unstable state can be brought to the form (41) is extremely wide: in includes sets of partial differential equations, difference equations, equations with a spatial and temporal kernels of the form $\int \mathrm{d}x' \int^t \mathrm{d}t' K(x-x',t-t')\phi(x',t')$, as well as equations with a mixture of such terms.[19] In addition, we conjecture that much of the analysis in this section can quite straightforwardly be extended to front propagation into periodic media (see Section 3.18). We will give a few simple examples based on extensions of he F-KPP equation below.

The Green's function $\underline{\underline{\hat{G}}}$ associated with the equations is the inverse of the matrix $\underline{\underline{\hat{S}}}$,

$$\underline{\underline{\hat{G}}}(k,\omega) \equiv \underline{\underline{\hat{S}}}^{-1}(k,\omega) \tag{43}$$

and the formal solution of (41) can be written simply in terms of $\underline{\underline{\hat{G}}}$ as

$$\underline{\hat{\phi}}(k,\omega) = \underline{\underline{\hat{G}}}(k,\omega)\cdot\underline{\underline{\hat{H}}}(k,\omega)\cdot\underline{\bar{\phi}}(k,t=0) \ . \tag{44}$$

When we invert the Fourier-Laplace transform, the term on the right-hand side has, in view of (43), poles at the points where the determinant $|\underline{\underline{\hat{S}}}|$ of $\underline{\underline{\hat{S}}}$ vanishes. There may generally be various

[19] I have the impression that population dynamicists [124,295] realized most clearly first that the front speed of what we refer to as pulled fronts can be calculated explicitly also for equations with a memory kernel. Within the physics community, this was realized of course from the start by the plasma physicists when they developed the "pinch point formulation" discussed below. Quite surprisingly, it appears that many of these early developments have never become standard knowledge in the mathematics literature. The "new method" proposed in [164] is essentially a reinvention of parts of the work half a century before in plasma physics and fluid dynamics referenced below, and this paper contains no references to these earlier developments. Even in this paper, the analysis is presented as a method that applies to partial differential equations only.

branches of solutions of the equation $|\underline{\underline{\hat{S}}}|=0$. In discussing the large-time behavior, one first assumes that the initial conditions have compact support, so that their spatial Fourier transform is again an entire function of k. The analysis then amounts to extracting the long-time behavior of the Green's function $\underline{\underline{G}}$.

The poles given by the zeroes of $|\underline{\underline{\hat{S}}}|$ determine the dispersion relations $\omega_\alpha(k)$ of the various branches α. The branches on which all modes are damped do not play any significant role for the long-time asymptotics. For each of the branches on which some of the modes are unstable, the analysis of the previous sections applies, and for the linear problem *the* linear spreading velocity v^* is simply the largest of the linear spreading speeds v^*_α of these branches.

In fact, the long time asymptotics of $\phi_n(x,t)$ can be extracted in two ways from (44), depending on whether one first evaluates the ω-integral or the k-integral. The first method essentially reproduces the formulation of the previous sections, the second one leads to the so-called pinch-point formulation [49,62,204,264] developed in plasma physics in the 1950s. We discuss their differences, as well as their advantages and disadvantages in Appendix A, and proceed here keeping in mind that the two methods invariably give the same expressions for the linear spreading velocity v^* and associated parameters.

In order to keep our notation simple, we will from now on drop the branch index α, assuming that the right linear spreading point has been selected if there is more than one, and we will usually also drop the index n or the vector notation for the dynamical field ϕ.

Example. Finite difference version of the F-KPP equation.

As a simple example of the implications of the above discussion, imagine we integrate the F-KPP equation with a cubic nonlinearity with a simple Euler scheme.[20] This amounts to replacing the F-KPP equation by the following finite difference approximation:

$$\frac{u_j(t+\Delta t)-u_j(t)}{\Delta t}=\frac{u_{j+1}(t)-2u_j(t)+u_{j-1}(t)}{(\Delta x)^2}+u_j(t)-u_j^3(t)\ . \tag{45}$$

If we linearize the equation by ignoring the last term and substitute a linear mode $u_j\sim\exp(st-\lambda j\Delta x)$ (this amounts to writing $\omega=is$ with s real) we obtain the dispersion relation

$$\frac{\exp[s\Delta t]-1}{\Delta t}=1+\left(\frac{\sinh\frac{1}{2}\lambda\Delta x}{\frac{1}{2}\Delta x}\right)^2\ . \tag{46}$$

The saddle point equations or, what amounts to the same, the minimum of the curve $v_{\rm env}(\lambda)=s/\lambda$ is easy to determine numerically. For small Δt and Δx one can also solve the equation analytically by expanding about the values for the continuum case given in (17), and one finds [144]

$$\text{Euler approximation to F-KPP}\quad\begin{cases} v^*=2-2\Delta t+\frac{1}{12}(\Delta x)^2+\cdots\ , \\ \lambda^*=1+\Delta t-\frac{1}{8}(\Delta x)^2+\cdots\ , \\ D=1-4\Delta t+\frac{1}{2}(\Delta x)^2+\cdots\ , \end{cases} \tag{47}$$

[20] The equivalent expressions for the second-order implicit ("Crank–Nicholson") integration scheme are given in Section 5.6.4 of [144].

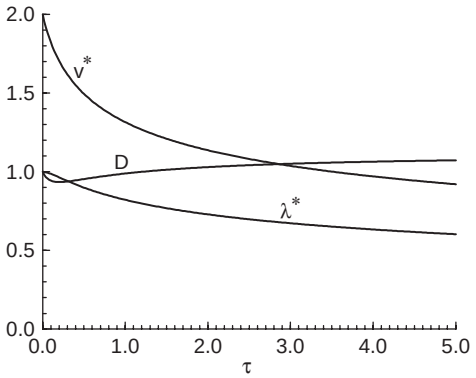

Fig. 6. Plot of v^*, λ^* and D as a function of τ for the extension (48) of the F-KPP equation with memory kernel (49). From [144].

Although these expressions look simply like error estimates for the finite difference approximation of the F-KPP partial differential equation, they are actually more than that: they give the *exact* parameters v^*, λ^* and D of the finite difference approximation. So when the precise values of these parameters are not so important, e.g., if one want to study the emergence of patterns or the power law relaxation discussed below in Section 2.9, one can take advantage of this by doing numerical simulations with relatively large values of Δt and Δx using the above properties as the reference values, rather than those obtained in the continuum limit $\Delta t, \Delta x \to 0$.

Example. F-KPP equation with a memory kernel.

The extension of the F-KPP equation in which the linear growth term is replaced by a term with a memory kernel,

$$\partial_t u(x,t) = \partial_x^2 u + \int_0^t \mathrm{d}t'\, K(t-t')u(x,t') - u^k(x,t) \quad (k>1)\ , \tag{48}$$

is an example of a dynamical equation which can still be treated along the lines laid out above, as its Fourier transform is of form (41). If we take for instance [144]

$$K(t-t') = \frac{1}{\sqrt{\pi}\tau}\exp\left[\frac{-(t-t')^2}{4\tau^2}\right]\ , \tag{49}$$

the implicit equation for $s(\lambda) = \omega_{\mathrm{i}}(\lambda)$ becomes

$$\lambda^2 - s + \exp[\tau^2 s^2]\,\mathrm{erfc}(\tau s)\ , \tag{50}$$

where erfc is the complementary error function. The result for v^*, λ^* and D obtained by solving numerically for the minimum of $v_{\mathrm{env}} = s(\lambda)/\lambda$, are shown in Fig. 6.

Note that when $\tau \ll 1$ we can to a good approximation expand $u(x,t')$ in the memory term in (48) around $u(x,t)$ to second order. In this approximation, we then arrive at a second order version of the

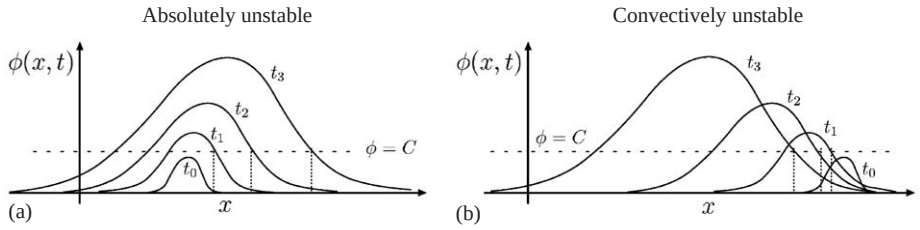

Fig. 7. Illustration of the distinction between an absolute instability and a convective instability, according to the linearized dynamics. In the first case, sketched on the left in (a), the perturbation about the unstable state grows for sufficiently long times at any position x. In the convectively unstable case sketched on the right in (b), the perturbation grows but is at the same time advected away so fast that it eventually dies at any fixed position x. Note that as a result of it, the point on the right where ϕ reaches the level line $\phi = C$ retracts to the left. The transition from convective to absolute instability occurs when this point does not move for long times, i.e. when the left spreading velocity v_L^* equals zero [49,62,204,205,264]. Note that the distinction between absolutely and convectively unstable depends on the frame of reference. The case sketched on the left which is absolutely unstable in the x frame is convectively unstable in a frame moving with a sufficiently large speed to the right, while the case sketched on the right in the x-frame becomes absolutely unstable in a frame moving with speed larger than v^* to the left.

F-KPP equation. Such extensions have often been used as a simple way to model delay effects, as will be discussed briefly in Section 3.19. From the point of view of determining the linear spreading speed, however, there is no real advantage in using a second order equation rather than an equation with a kernel.

2.5. The linear dynamics: convective versus absolute instability

The case that we will typically have in mind is the one in which the growth rate of the unstable modes is so strong that the amplitude of a generic localized perturbation grows for long times at any fixed position, as sketched in Fig. 7(a). It thus spreads into the unstable state on both flanks of the perturbation.

However, even when a state is linearly unstable, so that according to (4) a range of modes has a positive growth rate ω_i, if there are symmetry breaking convective terms in the dispersion relation a localized perturbation may be convected away faster than it grows out. Fig. 7(b) illustrates how in this case the amplitude of the perturbation for any fixed position on the right actually decreases in time, even though the overall amplitude grows. Even for any position on the left of the figure, if we wait sufficiently long the amplitude of the perturbation eventually decays. This regime is usually referred to as the *convectively unstable regime*, while the other regime is referred to as the *absolutely unstable regime* [49,62,204,205,264].

Clearly, these concepts are intimately connected with the linear spreading speed discussed above. Indeed, given our convention to focus on the right flank of a perturbation, the two regimes are distinguished according to whether v^* is positive or negative:

$$v^* > 0 : \text{linearly absolutely unstable regime} ,$$

$$v^* < 0 : \text{linearly convectively unstable regime} . \tag{51}$$

It is important to keep in mind that the two regimes are defined in relation to a particular frame of reference: if $v^* > 0$ in the lab frame, so that the instability is absolute in that frame, the instability becomes convectively unstable for an observer moving to the right with velocity larger than v^*. Furthermore, a convectively unstable system ideally remains in or will return to the unstable state according to the linear deterministic dynamics. Nevertheless, small perturbations or fluctuations are amplified while they are advected away. This makes convectively unstable systems particularly sensitive to fluctuations and to small but fixed perturbations at a particular point. The latter could arise in real experiments due to imperfections in experimental setup or due to local perturbations at an inlet in systems with a throughflow. We will encounter a nice experimental illustration of the sensitivity to noise near the convective to absolute transition in Section 3.11.

We finally note that we have followed here the standard practice to distinguish the two regimes according to the fully linear dynamics. The generalization of these concepts to the nonlinear regime will be given later in Section 2.10.

Example. The F-KPP equation with a convective term.

Consider the F-KPP equation with a convective term,

$$\partial_t u(x,t) + s\partial_x u(x,t) = \partial_x^2 u(x,t) + f(u) \ , \tag{52}$$

where, as in the standard form (1), $f(0)=0$ and $f'(0)=1$. Since this equation simply becomes the standard F-KPP equation (1) upon transforming to the moving frame $x' = x - st$, the linear spreading velocity associated with (52) is $v^* = s + v^*_{\mathrm{FKPP}} = s+2$. Thus the linear instability changes from absolute to convective at $s=-2$. Whether nonlinearly the transition also happens at this point depends on the function $f(u)$: when f is such that fronts are pulled, the nonlinear transition remains at $s=-2$, but when the fronts become pushed, the transition shifts to more negative values of s—see Section 2.10. In the Taylor–Couette experiments reviewed in Section 3.11 the velocity s in the closely related amplitude equation is controlled with a flow through the cell.

2.6. *The two-fold way of front propagation into linearly unstable states: pulled and pushed fronts*

In the previous sections, we have analyzed the *linear* spreading dynamics into a linearly unstable state. We concluded that starting from sufficiently localized initial conditions—the precise condition being given in (37)—the perturbations spread into the unstable state with asymptotic speed v^*. This asymptotic spreading speed and associated parameters are determined through the dispersion relation $\omega(k)$ via Eqs. (12).

We now turn to the genuine *nonlinear front propagation problem* already stated in the introduction, questions like: *If initially a spatially extended system is in a linearly unstable state everywhere except in some spatially localized region, what will be the large-time dynamical properties and speed of the nonlinear front which will propagate into the unstable state? Are there classes of initial conditions for which the front dynamics converges to some unique asymptotic front state? If so, what characterizes these initial conditions, and what can we say about the asymptotic front properties and the convergence to them?*

As before, our discussion is aimed to be as general as is possible. The only restriction we will make, barring pathological cases, is that the nonlinear dynamical equations of the system under investigation have a sufficient degree of "locality": they can involve partial derivative terms and nonlocal terms with a kernel whose range is essentially finite, but the dynamics of the dynamical variables at a given position should not depend crucially on the nonlinear state of the system infinitely far away.[21,22]

A characteristic feature of front propagation into unstable states which carries over from the linear dynamics that we discussed above, is that initial conditions which decay very slowly spatially lead to a large front speed whose value depends on the spatial decay rate. We will come back to this later. Hence, in order to make precise statements we need to limit the class of initial conditions we consider. Now, for any given set of deterministic dynamical evolution equations with an unstable state, the linear spreading speed v^* and associated steepness λ^* are explicitly and uniquely calculable according to the discussion of the previous sections. This motivates us to distinguish the front propagation properties of dynamical equations according to the long-time evolution starting from steep initial conditions:

Whenever we associate a particular front propagation mechanism with a given dynamical equation, this is a statement about the dynamical evolution of fronts that evolve from localized initial conditions. These include all initial conditions which are steep", i.e., which as defined in (37) fall off faster than $\exp[-\lambda^* x]$.[23]

Let $v_{\rm front}(t)$ be some suitably defined instantaneous front velocity. The crucial insight on which our presentation will be based is the following simple insight: *For front propagation into a linearly unstable state, there are only two possibilities if we start from steep initial conditions*,

I. $v_{\rm as} \equiv \lim_{t\to\infty} v_{\rm front}(t) = v^* \Leftrightarrow$ "*pulled*" front,
II. $v_{\rm as} \equiv \lim_{t\to\infty} v_{\rm front}(t) = v^\dagger > v^* \Leftrightarrow$ "*pushed*" front.

This statement amounts to the claim that nonlinear fronts propagating into a linearly unstable state can asymptotically not propagate with speed slower than v^* for equations of the type we consider, in which the dynamics is "local" in the sense that the linear dynamics is not suppressed by nonlinear behavior arbitrarily far away. To see this, suppose we start with a front solution which propagates with speed less than v^*. Any sufficiently small perturbation ahead of it will then grow out and spread, asymptotically with the linear spreading speed v^*. Eventually these perturbations will grow large enough that nonlinear behavior kicks in, *but the crossover region where this happens must*

[21] This requirement is comparable to the fact that in statistical physics the standard universality classes of equilibrium phase transitions only apply to Hamiltonians in which the interactions are sufficiently short-ranged. This does include Hamiltonians where the interactions decay as a power $r^{-\sigma}$ provided σ is large enough.

[22] A simple example that illustrates this is the following extension of the F-KPP equation: $\partial_t u = \partial_x^2 u + u(1 - m\tanh[\int_{-\infty}^{\infty} {\rm d}x\, u^2]) - u^3$. For $m < 1$ fronts in this equation are still pulled, albeit with a spreading speed renormalized down from the value obtained by linearizing the equation in u about $u = 0$. For $m > 1$ there is no finite asymptotic front speed. This example illustrates that although it is difficult to specify the general conditions under which our analysis applies precisely, in practice common sense gets one quite far for any given problem.

[23] We will later in Section 2.7.6 enlarge the class of initial conditions which lead to pushed front solutions.

asymptotically advance at least with the speed v^*. In other words, since the nonlinearities cannot suppress the linear growth arbitrarily far ahead of the front, they cannot prevent the linear spreading to asymptotically move ahead with asymptotic speed v^* and thus create a front with at least this speed. Consequently, nonlinearities can only drive front speeds up, i.e., to $v^\dagger > v^*$.

Admittedly, while the above conclusion that fronts can asymptotically not move slower than v^* may be dynamically "obvious", I know of no general mathematical proof of it. For some of the fourth order equations reviewed in Section 2.11, this conclusion is either implicit or explicit in a formulation in which one proves that in any frame moving with velocity less than v^* one sees perturbations grow [93,144].

At this point, the names "*pulled*" and "*pushed*" front fall fully into place.[24] With a pulled front we literally mean one which is pulled along by the linear spreading of small perturbations into the linearly unstable state. Any front which asymptotically moves with speed $v^\dagger$ faster than v^* is somehow "pushed" into the unstable state by the nonlinear behavior in the front region itself or the region behind it—if there were no nonlinear behavior, one would find spreading with velocity v^*. We will thus refer to $v^\dagger$ as the pushed front speed.

The present line of argument, where one takes the classical linear spreading of perturbations into an unstable state as the starting point, has several important advantages and ramifications. First of all, it allows one to make statements irrespective of the nature of the nonlinear state behind the front: Quite literally the picture that underlies it and that both the analytical and numerical results presented later confirm, is that a pulled front spreads in the way the linear spreading point conditions (12) *force it to do*. In other words, the nonlinear dynamics in the region behind the leading edge just has to adapt to whatever is forced by the linear spreading. Depending on the existence, stability and nature of nonlinear front solutions, this behavior can be coherent or incoherent, but this by itself does not really feed back onto the linear spreading.[25] This simple idea can be made explicit and quantitative: it lies at the basis of the exact results for the universal relaxation behavior of pulled fronts discussed in Sections 2.9 and 4.

The second advantage is that the present line of argument focuses on the fact that the most clear and relevant issue is to understand the mechanism through which we can get fronts to propagate at speeds larger than v^*, i.e., to be pushed.

We finally note that the concept of a pulled front is only well-defined for propagation into a linearly unstable state: A small perturbation around a linearly stable state dies out and does not spread. As a result, the propagation of a front into a linearly stable state is always driven by the nonlinearities and the nonlinear or dynamical competition between this state and a different one. From this perspective, especially near subcritical bifurcation points, it is sometimes useful to think of a front which propagates into a stable state as being "pushed".

---

[24] The names *pulled* and *pushed* were introduced back in 1976 by Stokes [384] and revived in the physics literature in the mid-90s by Paquette et al. [333,334]. Ben-Jacob et al. [38] referred to them as *Case I* and *Case II* marginal stability and I initially used the words *linear* and *nonlinear marginal stability* [421]. The great advantage of the nomenclature of Stokes is that the notions of "pulled" and "pushed" tie in nicely with the general concept of linear spreading velocity, and hence that they can be defined independently of whether or not a uniformly translating or coherent front solution exists.

[25] Actually, we can make this quite precise: As we shall see, the first consequence of the feedback of the nonlinear behavior onto front propagation is the change of the prefactor of the $1/t$ relaxation term by a factor 3. See Section 2.9.

2.7. Front selection for uniformly translating fronts and coherent and incoherent pattern forming fronts

In order to discuss the selection of a particular type of front and its propagation mechanism, it is useful to distinguish three different classes of nonlinear front dynamics: [26]

- *Uniformly translating fronts* are nonlinear front solutions for the dynamical variable ϕ of form

$$\phi(x,t) = \Phi_v(\zeta) \ , \tag{53}$$

where ζ is the co-moving coordinate

$$\zeta \equiv x - vt \ , \tag{54}$$

which we will use for general velocity v, to distinguish it from the coordinate $\xi = x - v^* t$ moving with velocity v^*. We remind the reader that, unless noted otherwise, we do not distinguish notationally between a single dynamical variable or a set (vector) of them. Eq. (53) expresses that in a frame moving with velocity v, the front solution is stationary, i.e., invariant in time. Uniformly translating solutions are normally only appropriate solutions for problems in which the front leaves behind a homogeneous state, i.e., does not generate a pattern. The overwhelming majority of asymptotic front solutions which have been analyzed in the mathematics literature are of this type. An example of a pushed front in the F-KPP equation is shown in the lower left panel of Fig. 1.
- *Coherent pattern forming fronts* are the generalization of uniformly translating solutions to systems where the front leaves behind a pattern with a well-defined wavenumber. As the middle panel of Fig. 1 and the examples discussed in Sections 2.11 and 3 illustrate, usually the pattern behind the front is stationary or moves with a velocity different from the front speed. In other words, when viewed in the frame moving with the front, the pattern behind the front is *not* stationary. Hence the front solution cannot be of form (53). However, we may generalize the concept by introducing a *coherent pattern forming front solution* as a front solution which is periodic in the frame $\zeta = x - vt$ moving with speed v, i.e.,

$$\phi(x,t) = \Phi(\zeta,t) \quad \text{with } \Phi(\zeta, t+T) = \Phi(\zeta,t) \ . \tag{55}$$

We can equivalently write this as

$$\phi(x,t) = \sum_{n=0,\pm 1,\ldots} \mathrm{e}^{-\mathrm{i}n\Omega t} \Phi_v^n(\zeta) \quad (\Omega = 2\pi/T) \ , \tag{56}$$

---

[26] With our classification we have in mind fronts which propagate in a homogeneous background medium. If the medium itself is periodic, fronts which are uniformly translating in a homogeneous medium become automatically periodic; likewise if the parameters of the dynamical equation are randomly varying the fronts will always be incoherent. Strictly speaking, fronts in a periodic medium, which are sometimes referred to as "periodically pulsating fronts", are of the type (55) below but as stated, we will always have in mind that the medium itself is homogeneous, and when considering periodic front solutions concentrate on fronts which then generate a nontrivial pattern. For the linear dynamics of small perturbations about the unstable state of a homogeneous system, the dispersion relation can be obtained from a simple Fourier transformation. As we shall discuss below in Section 3.18, the analysis of pulled fronts can be extended to the case of periodic media by recognizing that one simply has to do a Floquet analysis to determine $\omega(k)$.

where for real dynamical fields ϕ the complex functions Φ_v^n obey the symmetry

$$\Phi_v^{-n}(\zeta) = \Phi_v^n(\zeta) \ . \tag{57}$$

Clearly, Eq. (55) expresses that in the co-moving frame the front solution is periodic.[27] Hence, in representation (56) the functions $\Phi_v^n(\zeta)$ can at every position be viewed as the Fourier coefficients of the time-periodic function $\Phi(\zeta, t)$.

These *time-periodic coherent front solutions* of form (55) or (56) are relevant for e.g. the Swift–Hohenberg equation discussed in Section 2.11.2 and were to my knowledge for the first time introduced for the analysis of fronts in this equation by Collet and Eckmann [92]. Moreover, they can also be viewed as an extension of the "coherent structure solutions" [424] introduced in the context of the Complex Ginzburg Landau equations of Sections 2.11.5 and 2.11.6—because of the fact that the Complex Ginzburg Landau equation arises as the lowest order amplitude equation for traveling wave patterns, only one term in the sum (56) is nonzero in this case. As we shall see, both pulled and pushed coherent fronts solutions are found in certain parameter ranges.

- *Incoherent pattern forming fronts* is the name we will use for all the incoherent fronts like those of the right column of Fig. 1 which do not fit into one of the two previous classes. We will encounter other pulled and pushed examples of them later, but they are the least understood of all.

We now proceed to discuss the dynamical mechanism that distinguishes pushed and pulled fronts for these various classes of equations. The essential ingredient will be to maximally exploit the constraints imposed by the linear dynamics about the unstable state.

2.7.1. Uniformly translating front solutions

When a dynamical equation also admits a homogeneous stable stationary state $\phi_{ss} = const.$ in addition to the unstable state $\phi = 0$, then usually this dynamical equation also admits uniformly translating front solutions of form (53), $\phi(x,t) = \Phi_v(\zeta)$ with $\zeta = x - vt$. To investigate whether it does, one substitutes this Ansatz into the dynamical equation and analyzes its behavior. The simplicity of uniformly translating fronts lies in the fact that the function $\Phi_v(\zeta)$ depend on the single variable ζ only, so that the function Φ_v then obeys an ordinary differential equation rather than a partial differential equation. The existence of front solutions can from there on be analyzed using standard methods [13,14,191]: the homogeneous stationary states $\phi = 0$ and $\phi = \phi_{ss}$ are fixed points of this ordinary differential equation. By linearizing about these fixed points and studying the dimensions of the stable and unstable manifolds (i.e. the dimensions of the manifolds flowing into and out of each fixed point), one can then study the multiplicity of front solutions (see e.g. [424] for an extensive use of such "counting arguments" in the context of CGL equations). For the F-KPP equation the analysis, which is summarized below, is relatively trivial; one finds that there is a one-parameter family of front solutions that connect the stable homogeneous state with the unstable state $\phi = 0$. For the F-KPP equation, one can easily go beyond a simple counting argument based on the analysis

[27] We prefer to use the general name "coherent pattern forming front solution" instead of periodic front solutions for two reasons. First of all, this name is consistent with the name "coherent structure solutions" for special type of solutions of the CGL equation (see Eq. (101) in Section 2.11.6). Secondly, we wish to stress the fact that we aim at pattern forming solutions and so want to distinguish them from the simpler periodic or "pulsating" types of fronts that arise in equations like the F-KPP equation when the medium itself is periodic—see Section 3.18.

near the fixed points to prove more rigorously when there is such a family of solutions. These front solutions can be parametrized by their velocity v. We stress that for an arbitrary dynamical equation that admits a stable homogeneous state and a homogeneous unstable state, there is not necessarily always a one-parameter family of front solutions connecting the two. However, this *is* what is typically found and what is intuitively most reasonable based on the fact that a special feature of the linear dynamics about an unstable state is that any exponential tail with steepness λ less than λ^* can propagate into the unstable state with speed $v_{\rm env}(\lambda)$—see Section 2.2.[28]

Let us first proceed by assuming the equations do admit a one-parameter family of front solutions, parametrized by their velocity. Then this family generically will include a uniformly translating front solution $\Phi_{v^*}(\xi)$ moving with velocity v^*, to which the front will asymptotically converge in the pulled regime, i.e., starting from steep initial conditions.

The behavior near the fixed points of the ordinary differential equation for $\Phi_v(\zeta)$, obtained by linearizing the flow equations around the fixed point, corresponds to an exponential ζ-dependence. Thus, for an arbitrary velocity v, the solutions $\Phi_v(\zeta)$ will decay to zero exponentially for large ζ,

$$\Phi_v(\zeta) \approx a_1 \mathrm{e}^{-\lambda_1\zeta} + a_2 \mathrm{e}^{-\lambda_2\zeta} + \cdots \quad (\zeta \to \infty)\ , \tag{58}$$

where all roots λ_i are positive and where the real coefficients a_1, a_2, etc. can only be determined by solving the equations for the fully nonlinear front solution.[29] We take these roots ordered, $0 < \lambda_1 < \lambda_2 \cdots$. The relation between the velocity v and the two smallest roots in the generic case[30] is shown in Fig. 3: For $v > v^*$ the root $\lambda_1 < \lambda^*$ while $\lambda_2 > \lambda^*$. In passing we note that at $v{=}v^*$ two roots coincide; general results [13,14,191] for the flow behavior in the presence of degenerate eigenvalues then imply

$$\Phi_{v^*}(\xi) \approx (a_1\xi + a_2)\mathrm{e}^{-\lambda^*\xi} + a_3\mathrm{e}^{-\lambda_3\xi} + \cdots\ . \tag{59}$$

When do we expect the equation to be pushed, i.e., when do we expect that a pushed front solutions with velocity $v^\dagger > v^*$ will emerge starting from steep initial conditions? The answer lies hidden in Fig. 4: *according to the fully linear dynamics* an exponential tail which is steeper than λ^* and which corresponds to the dashed branch λ_2 in Fig. 3, *does run faster than* v^* *but disappears from the scene* because the crossover point to the linear spreading profile moves to the right. According to

[28] An explicit counting argument for partial differential equations that are symmetric under spatial reflection confirms that for such equations one typically expects a one-parameter family of front solutions (see Appendix A of [420]). There are two intimately related ways to understand why this is so often the case: (i) Suppose we first change the dynamical equation so as to make the unstable state stable. One then expects there to be at least one front solution (or maybe a discrete set of them) connecting the two stable states. Now when we change the equation back to its original form, at the moment when the $\phi = 0$ state becomes unstable again, the dimension of the stable manifold flowing into the $\phi = 0$ fixed point increases by one, because a new root appears which is related to the left branch in Fig. 3; (ii) According to the linear dynamics discussed in Section 2.2, any exponential tail with $\lambda < \lambda^*$ can propagate into the unstable state with envelope velocity $v_{\rm env}(\lambda)$. When the dynamical equation admits a stable homogeneous state as well, it is not unreasonable that every exponential tail propagating with some velocity v in the leading edge can match up smoothly with a saturating behavior behind the front.

[29] In (58) we want to bring out that there are contributions from the various roots, or, in more technical language, from the various directions that span the stable many-fold of the fixed point corresponding to $\phi{=}$. If $\lambda_1 < \lambda_2/2$ then of course terms $\exp[-2\lambda_1\zeta]$ dominate over terms $\exp[-\lambda_2\zeta]$, but this is all hidden in the dots.

[30] We assume here for simplicity that there are no other branches at even smaller λ; this is usually the case, as the branch which in Fig. 3 diverges as $\lambda \downarrow 0$ is associated with the instability, the fact that $\omega_{\rm i}(\lambda = 0) > 0$. We will briefly come back to the case where other branches intervene in Section 2.7.7.

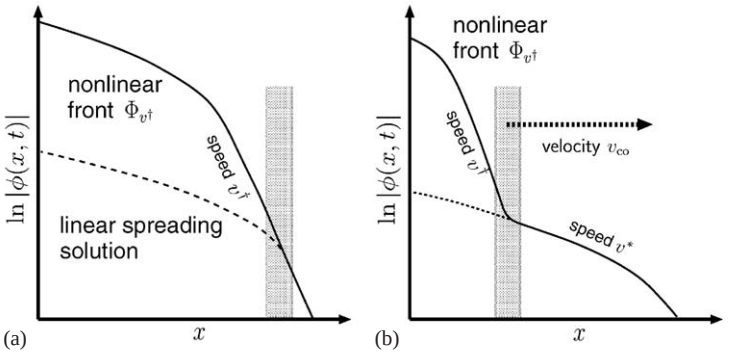

Fig. 8. Illustration of the fact that when a nonlinear front solution $\Phi_{v^\dagger}$ exists, whose asymptotic steepness is according to (60) larger than λ^*, then this front will generically emerge: it is the selected pushed front solution. Figure (a) should be compared to Fig. 4: If the equation would be fully linear, the steep tail on the right, which moves at velocity larger than v^*, would cross over in the dashed region to the dashed profile moving with asymptotic speed v^*. However, this does not happen. When the steep profile matches up arbitrarily well with a fully nonlinear front profile $\Phi_{v^\dagger}$ this steep region does not disappear from the scene: Instead a fully nonlinear profile with speed $v^\dagger$ emerges. While (a) shows how only the pushed front solution $\Phi_{v^\dagger}$ can asymptotically emerge, (b) illustrates how a pushed front solution invades a region where the profile is close to that given by the linear spreading analysis. The dashed line indicates the continuation of the profile as given by the linear spreading analysis of previous sections, but in the dashed region the profile crosses over to the steep tail of the nonlinear pushed profile. The fact that the crossover region moves to the right with the speed v_{co} determined earlier, confirms that the pushed front solution invades the leading edge.

our "locality" assumption for the dynamics, the same holds arbitrarily far into the leading edge of a front, *unless the nonlinearities in the dynamical equation allow the fast exponential tail to match up perfectly with a nonlinear front solution!* This is illustrated in Fig. 8: if a uniformly translating front solution with $v = v^\dagger > v^*$ exists for which $a_1 = 0$ so that its asymptotic behavior is given by the root λ_2,

$$\Phi_{v^\dagger}(\zeta) \approx a_2 e^{-\lambda_2 \zeta} + a_3 e^{-\lambda_3 \zeta} + \cdots \quad (\lambda_2 > \lambda^*, \zeta = x - v^\dagger t \to \infty) \,, \tag{60}$$

then this front solution *can and will overtake* any transient dynamical tail in the leading edge. In other words, such a solution is the asymptotic pushed front solution sought for, and *if it exists it is the dynamically relevant front solution emerging from steep initial conditions*.

As we noted before, front solutions $\Phi_v(\zeta)$ obey an ordinary differential equation or a set thereof; such a differential equations can be formulated as a flow in phase space [13,14,191]. In such an interpretation, a front solution corresponds to a so-called heteroclinic orbit, an orbit which goes from one point (the asymptotic state behind the front) to another (the state $\phi = 0$). For general v, the orbit approaches the fixed point corresponding to the state $\phi = 0$ asymptotically along the eigendirection whose rate of attraction, given by λ_1, is slowest. The pushed front solution $\Phi_{v^\dagger}(\zeta)$, however, approaches it along the slowest but one eigendirection, the one with eigenvalue λ_2. For this reason, a uniformly translating pushed front solution is sometimes referred to as a *strongly heteroclinic orbit* [354].

Let us illustrate the above considerations briefly for two equations, the F-KPP equation and an extension of it, the EFK equation. Uniformly translating solutions $U(x - vt) = U(\zeta)$ of the F-KPP

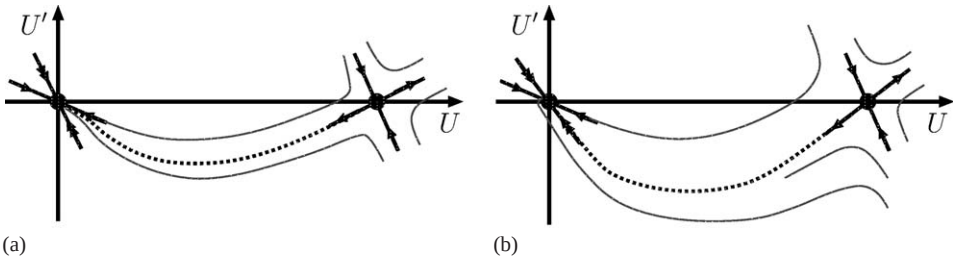

Fig. 9. Sketch of the flow in the phase space (U, U') of the flow equations (62) and (63) that govern the uniformly translating solutions of the F-KPP equation. The solid lines at the two fixed points indicate the shape of the stable and unstable manifolds near each fixed point, obtained by linearizing the flow around each fixed point. The arrows indicate the direction of the flow, and the double arrow at the $(0,0)$ fixed point indicates that the contraction along this eigendirection is stronger than along the other one ($\lambda_2 > \lambda_1$). The dashed trajectory is the heteroclinic orbit connecting the two fixed points; it corresponds to the front solution connecting the stable and the unstable state. (a) Flow in the case $v \geqslant \max(v^\dagger, v^*)$. The trajectory approaches the $(0,0)$ fixed point along the slowest contracting direction. (b) If for some velocity $v = v^\dagger$ the dashed trajectory becomes a "strongly heteroclinic orbit" which approaches the $(0,0)$ fixed point along the more strongly contracting direction, the equation admits a pushed front solution.

equation (1) obey the ordinary differential equation

$$-v\frac{\mathrm{d}U}{\mathrm{d}\zeta} = \frac{\mathrm{d}^2U}{\mathrm{d}\zeta^2} + f(U)\ . \tag{61}$$

It is convenient to use the standard trick of writing this second order equation as a set of first order equation: by introducing the variable $U' = \mathrm{d}U/\mathrm{d}\zeta$ we can write (61) as

$$\frac{\mathrm{d}U}{\mathrm{d}\zeta} = U'\ , \tag{62}$$

$$\frac{\mathrm{d}U'}{\mathrm{d}\zeta} = -vU' - f(U)\ . \tag{63}$$

These equations describe the flow in the two-dimensional phase space (U, U'), with ζ playing the role of time. Because $f(0) = f(1) = 0$ according to (1), the points $(0,0)$ and $(1,0)$ are fixed points of these flow equations; the first one corresponds to the stable state and the second one to the unstable state. With our convention that fronts move into the unstable state on the right, a uniformly translating front solution corresponds to a trajectory flowing from the $(1,0)$ fixed point to the $(0,0)$ fixed point. Such a "heteroclinic orbit" is sketched for large arbitrary v in Fig. 9(a).[31] The solid lines near the two fixed points in this figure denote the directions of the stable and unstable manifolds flowing into and out of each fixed point. These are easily determined by linearizing equations (62), (63) about the fixed point solutions and solving for the eigenvalues of the linearized flow. The arrows in Fig. 9 indicate the directions of the flow for increasing ζ ("time"). As is indicated in the figure, there is one stable and one unstable stable direction at the $(1,0)$ fixed point. For any fixed velocity v, there is hence a unique trajectory coming out of this fixed point in the direction of decreasing u. At the $(0,0)$ fixed point, however, both eigendirections are attracting; we have indicated the direction along which the contraction is largest with a double arrow. Now, because there is

[31] For $v < v^*$ the eigenvalues at the fixed point $(0,0)$ are complex so trajectories spiral into this fixed point.

a two-dimensional manifold flowing into the $(0,0)$ fixed point, the unique dashed trajectory that flows out of the $(1,0)$ fixed point will flow into the $(0,0)$ fixed point, and it will asymptotically flow in along the slowest contracting eigendirection—these observations correspond to the statements that there is a front solution for a any v and that the asymptotic large-ζ behavior in (58) is dominated by the smallest eigenvalue λ_1.

Depending on the form of the nonlinearity $f(u)$, the situation as sketched in Fig. 9 may occur: for a particular value $v^\dagger$ of the velocity, it may happen that the unique dashed trajectory that flows out of the $(1,0)$ fixed point flows into the stable $(0,0)$ fixed point along the most rapidly contracting direction which is indicated in the figure with the double arrow. In other words, for this trajectory the asymptotic behavior of $U(\zeta)$ goes as $e^{-\lambda_2\zeta}$, i.e., has $a_1=0$ in (58). This "strongly heteroclinic orbit" thus corresponds to a pushed front solution—if it exists, the selected front in the F-KPP equation is a pushed front. Clearly, *whether such a pushed front solution exists depends on the global nonlinear properties of the equation*, the full nonlinear behavior of $f(u)$ in this case—determining or proving whether for a given equation the selected front is pushed, requires a fully nonlinear global analysis of the flow. All the details of the nonlinear behavior count. In the example at the end of this section we will show that for certain classes of nonlinearities $f(u)$, the pushed front solution of the F-KPP equation can be obtained analytically.

To give an idea of the complications that one immediately encounters when one goes beyond the F-KPP equation, let us briefly consider the equation

$$\partial_t u = \partial_x^2 u - \gamma\partial_x^4 u + f(u)\ , \tag{64}$$

which can be thought of as an extension of the F-KPP equation. Indeed, with $f(u)=u-u^3$ this equation is the EFK ("Extended Fisher–Kolmogorov") equation which we will discuss in more detail in Section 2.11.1. As we shall see there, the pulled fronts in this equation exhibit a transition from uniformly translating fronts to coherent pattern forming fronts at $\gamma=1/12$, but we focus for now on the uniformly translating fronts for $\gamma<1/12$. If we substitute the Ansatz $=U(\zeta)$ into the equation and write the resulting ordinary differential equation as a set of first order equations, we get in analogy with (62) and (63)

$$\frac{dU}{d\zeta} = U'\ , \tag{65}$$

$$\frac{dU'}{d\zeta} = U''\ , \tag{66}$$

$$\frac{dU''}{d\zeta} = U'''\ , \tag{67}$$

$$\frac{dU'''}{d\zeta} = \gamma^{-1}[U''+vU'+f(U)]\ . \tag{68}$$

Since the flow is now in a four-dimensional phase space, it is clear that the question of existence of such uniformly translating front solutions is much more subtle than for the F-KPP equation: all the

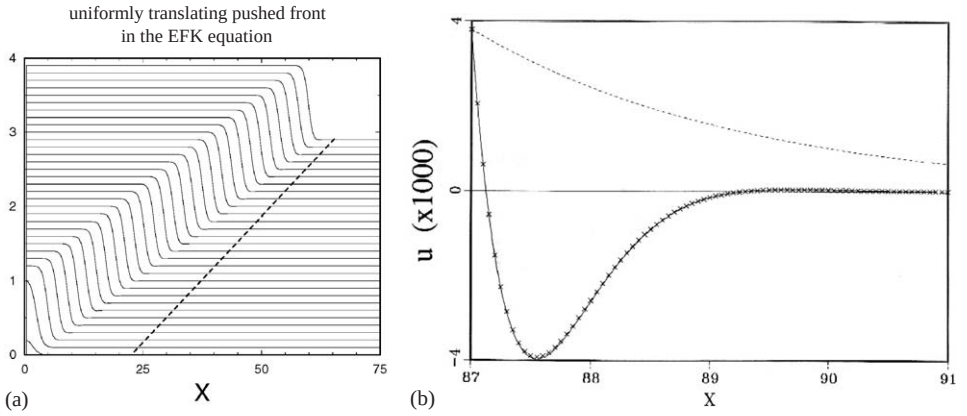

Fig. 10. (a) Space time of a numerical solution of Eq. (64) with nonlinearity $f(u)=u+9u^2-10u^3$. This is an extension of the EFK equation discussed in Section 2.11.1. For this nonlinearity, the selected front is a pushed front propagating with speed $v^\dagger = 2.751$ [421]. The time increment between successive time-slices is 0.75; the initial condition is a small Gaussian peak centered at the origin, and the total simulation time is 22.5. The dashed line indicates a position moving with the speed $v^* = 1.8934$. Although the front might appear to be monotonically decaying to the right, close inspection of this pushed front in the tip shows that it is actually non-monotonic; the enlargement in panel (b) shows this more clearly. (b) Blow up of the asymptotic front profile in the leading edge. The symbols denote the actual front values at the grid points in the simulations, while the full line is the profile in the leading edge given by the three terms in (60). The dashed line denotes the mode $\exp(-\lambda_1\zeta)$. Clearly, for the pushed front solution, a_1=0 indeed, in accordance with the mechanism of pushed front propagation set forth in the main text. From [421].

simplifications of flow in a two-dimensional plane, special to the F-KPP equation, are lost.[32] Let us here simply illustrate that one important simplifying property of the F-KPP equation is immediately lost. From the phase space arguments sketched above for the F-KPP equation, it immediately follows that the selected front is the front solution with the smallest speed for which the front solution is monotonically decaying with ζ. Therefore, this idea has sometimes been proposed in the literature as a general principle for front selection. However, it is simply a property of the F-KPP equation and a limited class of extensions of it—it is a property that does not really have anything to do with front selection and just does not hold generally. The simulations of Fig. 10 illustrate this for the above Eq. (64) with $f(u) = u + 9u^2 - 10u^3$. As the left panel illustrates, the selected front is a uniformly translating pushed front in this case. Although this is hardly visible in the space-time plot on the left, this pushed front solution is not monotonically decaying towards the right. The enlargement of the leading edge in the right panel shows how U first goes through zero and then has a local maximum at negative U. This plot also confirms fully the mechanism for pushed fronts that we have identified above: the selected profile fits the form (58) with $a_1 = 0$.

[32] If one again linearizes the flow near the two fixed points $(0,0,0,0)$ and $(1,0,0,0)$, the multiplicity of the stable and unstable manifolds is such that one would indeed expect the existence of a one-parameter family of front solutions [421]. A more rigorous study of such front solutions and of the flow in this four-dimensional phase space has been taken up only recently in the mathematics literature. See in particular [371] for a proof of the existence of front solutions of the above flow equations and [340,410] for other types of solutions.

Let us return to our general formulation of the mechanism through which pushed fronts arise for uniformly translating fronts. While this scenario is arrived at simply by exploiting our insight into the leading edge where the dynamics is essentially given by the linear dynamics, it is in complete agreement with (i) what is known rigorously for the second order F-KPP equation, (ii) the (marginal) stability arguments for front selection (Section 2.8) which show that if a strongly heteroclinic front solution $\Phi_{v^\dagger}$ exists, all front solutions with lower speed are unstable to invasion by this front, and (iii) all numerical results known to me. Furthermore, the extension of the argument to coherent pattern forming fronts is fully consistent with the analytical and numerical results for the quintic CGL equation discussed in Section 2.11.6).

We finally return to the question what happens if the front solutions do not admit a one-parameter family of front solutions. If this happens, then we generically expect that the equations will not admit a uniformly translating pulled front solution moving with velocity v^*. A pulled front can then not be uniformly translating—the pulled front solution must then show nontrivial dynamics in the front region. Presumably, the dynamics is then either that of a coherent or incoherent pattern forming front, even if the state it finally leaves behind is structureless. Furthermore, the absence of a one-parameter family of uniformly translating front solutions makes it also very unlikely that there will be uniformly translating pushed front solutions, as these have to obey one additional constraint $a_1 = 0$.

Example. Pushed front solutions of the F-KPP equation and the reduction of order method.

For the F-KPP equation, for which the dispersion relation $\omega(k)$ is quadratic, a general uniformly translating front solution $u(x - vt) = U(\zeta)$ falls off to $u = 0$ with two exponentials—in other words, for a front solution with arbitrary velocity v there are two terms in expression (58) for the large ζ behavior. However, as we already discussed above, a pushed front solution of the F-KPP equation approaches $u = 0$ with a single exponent, as $a_1 = 0$. A good strategy to look for exact pushed front solutions of the F-KPP equation is therefore [421] to investigate when front solutions of the first order equation

$$\frac{\mathrm{d}U_v}{\mathrm{d}\zeta} = h(U_v) \tag{69}$$

are also front solutions of the full ordinary differential equation for front solutions $U_v(\zeta)$ of the F-KPP equation. This is the case if they satisfy Eq. (61),

$$-v\frac{\mathrm{d}U_v(\zeta)}{\mathrm{d}\zeta} = \frac{\mathrm{d}^2U_v(\zeta)}{\mathrm{d}\zeta^2} + f(U_v(\zeta)) \ . \tag{70}$$

Searching for solutions of the type (69) is very easy; to see this, note that upon substitution of (69) into (70) we get

$$-vh(U_v) = h'(U_v)\,h(U_v) + f(U_v) \ , \tag{71}$$

so that we just need to look for combinations of functions h and f which obey this last equation (for any given h one can trivially find a function f but the converse is not true). This is especially simple for polynomial functions. Indeed, it is straightforward to check that the functions [144]

$$h(u) = -\lambda u(1 - u^n), \quad f(u) = \tilde{\varepsilon}u + u^{n+1} - (1 + \tilde{\varepsilon})u^{2n+1} \tag{72}$$

solve (71) provided we take

$$\lambda^2 = \frac{\tilde{\varepsilon}+1}{n+1}, \quad v = (n+2)\lambda - 1/\lambda \ . \tag{73}$$

In order that the front solution of these equations corresponds to a pushed front solution of the F-KPP equation, the decay rate λ given by (73) needs to be bigger than $\lambda^* = \sqrt{\tilde{\varepsilon}}$; this is easily found to be the case for $\tilde{\varepsilon} < 1/n$. Thus, the F-KPP equation with a nonlinearity $f(u)$ given by[33] (72) has the pushed to pulled transition at $\tilde{\varepsilon} = 1/n$, and for $\tilde{\varepsilon} < 1/n$ the pushed front velocity $v^\dagger$ is given by (73).

For further discussion of these results for the most common cases $n = 1$ (f a cubic polynomial in u) and $n = 2$ (f a function of u, u^3 and u^5), we refer to [38,421]. Other examples are discussed in [34,144,198,212,326,355,436,447] and Section 3.15, where we will discuss a nontrivial case relevant to liquid crystals. Quite surprisingly this "reduction of order method", as it is sometimes called, also allows one to find the pushed front solutions of the quintic CGL equation (see Section 2.11.6) and to construct other types of exact solutions of the CGL equation [95,312,322,424]. Deep down, the method is related to the construction of exact solutions of nonlinear equations using Painlevé analysis [95,96,360]. Also symmetry reduction methods have been used to search for exact solutions of the nonlinear diffusion equation [89,325].

2.7.2. *Coherent pattern forming front solutions*

Let us now turn to coherent pattern forming front solutions of form (56). Every function $\Phi_v^n(\zeta)$ in this expression also depends only on the co-moving coordinate ζ. Hence if we substitute the expansion (56) into the dynamical equation under investigation, the functions $\Phi_v^n(\zeta)$ will in general obey a set of coupled ordinary differential equations. In general, this infinite set of ordinary differential equations is quite cumbersome; however, for fronts we need to have $\Phi_v^n(\zeta) \to 0$ as $\zeta \to \infty$, and to linear order all the Φ_v^m obey essentially the same equation obtained by linearizing the dynamical equation about the unstable state. We then have the freedom to take the term with $n = 1$ to correspond to asymptotic decay $\exp[-\lambda_1\zeta]$ associated with the smallest root λ_1; in analogy with (58) we then have

$$\Phi_v^1(\zeta) \approx A_1 e^{ik_{r,1}\zeta - \lambda_1\zeta} + A_2 e^{ik_{r2}\zeta - \lambda_2\zeta} + \cdots \ , \tag{74}$$

where now the coefficients A_1, A_2, etc. are complex. Again it follows from the general arguments underlying Fig. 3 that for any $v > v^*$, we generally have $\lambda_1 < \lambda^*$, $\lambda_2 > \lambda^*$.

One may, like in the case of uniformly translating fronts, wonder about the multiplicity of coherent pattern forming fronts. There are even fewer results in this case, but indications are that for front propagation into unstable states the typical case is that there is a two-parameter family of front solutions. That this is the case has been proved for the Swift–Hohenberg equation [92] and is also found [424] for the quintic CGL equation of Section 2.11.6. Moreover, counting-type arguments for the pattern-forming regime of the EFK equation (Section 2.11.1) are consistent with this—we expect that the methods developed by Sandstede and Scheel [375] will allow one to establish this more generally and cleanly. Intuitively, the existence of a two-parameter family of front solutions is the

[33] The prefactor of the term u^{n+1} looks special, but the analysis covers all cases with $f(u)$ of form (72) since all other cases can be brought to this form by a proper scaling of space, time and u—see [355] and Appendix C of [144].

natural extension of the existence of a one-parameter family of uniformly translating front solutions, since the leading edge of pattern forming fronts generically is characterized by a wavenumber k_r in addition to the steepness λ. In other words, our conjecture that the generic situation is that there is a two-parameter family of coherent pattern forming fronts, means that for every velocity v, there is a one-parameter family of fronts parametrized e.g. by the wavenumber k_r in the leading edge or by the wavenumber of the coherent pattern behind the front. The front solutions whose wavenumber leads to maximal growth in the leading edge for given steepness ($\partial\omega_i/\partial k_r = 0$), then correspond to the left branch in Fig. 3.

Let us proceed first by assuming that indeed the equations for the coherent pattern forming front solutions admit a two-parameter family of front solutions. The above considerations then imply that there will in general exist a coherent pulled front solution, i.e., a solution whose asymptotic behavior to the right matches the linear spreading point behavior,

$$\Phi^1_{v^*}(\xi) \sim (A_1\xi + A_2)e^{-\lambda^*\xi + i(k_r^*\xi - (\omega_r^* - k_r v)t)} \quad (\xi = x - v^*t \to \infty)\ , \tag{75}$$

where in analogy with (59) the term linear in ξ arises because two roots coincide at v^*. The coherent pulled front solutions determined this way will be the ones that one will observe in the regime of pulled front propagation.

The mechanism to get coherent pushed solutions moving at a speed $v^\dagger > v^*$ is completely analogous to the one we discussed above for uniformly translating solutions with the aid of Fig. 8: starting from steep initial conditions an arbitrary front solution with speed $v > v^*$ cannot emerge, since that would be incompatible with the dynamics in the leading edge, but any special coherent front solution whose asymptotic spatial decay is steeper in that

$$\Phi^1_{v^\dagger}(\zeta) \sim A_2 e^{-\lambda_2\zeta + ik_{r2}\zeta} + \cdots\ , \tag{76}$$

can and will invade the leading edge. In other words, if a solution for which $A_1 = 0$ in (74) exists, *this is the pushed front solution that will be selected by the dynamics*. Note that since the coefficients A_1, A_2, etc. in (74) are complex coefficients, the condition that $A_1 = 0$ amounts to *two* conditions. Whether there are front solutions which obey this condition depends on the equation under investigation, but since we assume that there is a *two*-parameter family of front solutions, if they exist, pushed front solutions are expected to be isolated solutions.

This selection mechanism for coherent pattern forming front solutions is clearly quite analogous to the one we discussed for uniformly translating fronts, but for coherent fronts I am not aware of any rigorous work on the pulled to pushed transition of coherent fronts. The numerical and analytical work on a modified version of the Swift–Hohenberg equation and on the quintic CGL equation, summarized briefly in Sections 2.11.2 and 2.11.6 are in full accord with the above scenario.

It is important to keep in mind that our discussion has been based on the idea that coherent front solutions come as a two-parameter family *if they exist.* For a particular equation, it is not guaranteed that they do exist, of course. Indeed, the quintic CGL equation discussed in Section 2.11.6 illustrates this: In some parameter ranges one can show that the equation does not admit any coherent pulled front solution. In the parameter range where this happens, the pulled fronts become incoherent—see Fig. 17. Likewise, if the coherent front solutions do not come as a two-parameter family, then neither coherent pulled front solutions nor coherent pushed front solutions are expected to exist: the dynamics is then expected to be incoherent.

We finally note an important point. We already noted above that the condition $A_1 = 0$ is equivalent to *two* conditions, and that this implies that pushed fronts solutions, if they exist, generically come as isolated (discrete) solutions. Moreover, this simple counting argument also shows that the dominant spatial decay rate λ_2 of this isolated solution (76) *generally does not lie* on the thick dashed branch in Fig. 3.[34] By the same token, this implies that at the pulled to pushed transition, i.e. when $v^\dagger \downarrow v^*$, $\lambda_2 \neq \lambda^*$ in (76). So, while for uniformly translating profiles the pulled to pushed transition corresponds to a continuous transition in the front shape, for coherent pattern forming fronts the transition is discontinuous in the front shape! Such discontinuous behavior, which was first discovered for the quintic CGL equation of Section 2.11.6, imply that "structural stability" conjectures do not apply to pattern forming fronts. We will come back to this in Section 2.8.3.

Examples of pushed coherent fronts will be encountered later in Sections 2.11.1, 2.11.2, 2.11.6, 3.8, and 3.17; we also conjecture that pushed coherent fronts can arise in the models of Sections 3.2 and 3.3, for which so far only pulled fronts have been found.

2.7.3. *Incoherent pattern forming front solutions*

Incoherent pattern forming fronts are those fronts which do not leave behind a coherent pattern. Hence they cannot be of form (56). From the numerical simulations of the cubic and quintic CGL equation discussed in Sections 2.11.5 and 2.11.6 and the full-blown numerical simulations of turbulence fronts discussed in Section 3.9 we know that both pulled and pushed incoherent fronts can exist. Of course, as always we can calculate the speed of incoherent pulled fronts, but to my knowledge there is essentially no good understanding of what drives an incoherent front to be pushed. Thus I cannot give a precise mathematical formulation, analogous to (60) or (76), that identifies what property will give rise to a pushed incoherent front. My conjecture is that in analogy with what we found for uniformly translating and coherent pattern forming fronts, incoherent pulled fronts are solutions which in some average sense do fall off with a well-defined steepness larger than λ^*. The simulations of turbulence fronts discussed in Section 3.9 confirm this idea, but I do not know how to give *predictive power* to this statement. Unfortunately, the problem of the transition from pulled to pushed incoherent fronts appears to be as hard as the spatio-temporal chaos and turbulence problem itself!

Examples of pushed incoherent fronts will be encountered in Sections 2.11.4, 2.11.6, 3.9 and 3.22.

2.7.4. *Effects of the stability of the state generated by the front*

In our discussion of how pushed fronts can arise in the various modes of front propagation, a central role is played by the *existence* of the special type of uniformly translating or coherent pattern forming solutions which for $\zeta \to \infty$ decay with steepness larger than λ^*—these become the pushed front solutions. To what extent does the stability of fronts play a role? As we will discuss in Section 2.8 below, one can relate the above selection mechanism of pushed fronts to the stability properties of front solutions with $v < v^\dagger$, but it is more appropriate to think of this as a *consequence* rather than a *cause* of front selection.

The stability or instability of the state generated by the front does have important consequences for the dynamics, however. The examples discussed in Section 2.11 will illustrate this most clearly: it is quite possible that the state which emerges behind the front is itself unstable. When the selected

[34] In [421], we suggested that the combinations $v^\dagger, \lambda_2$ of pushed fronts of the Swift–Hohenberg equation should lie on the dashed branch. This suggestion is wrong.

state is nonlinearly convectively unstable in the frame moving with the front, the state behind the first front is invaded by a second front which moves slower than the first. If, however, the state generated by the first front is absolutely unstable in the frame moving with the first front, then the second one will catch up with the first and alter its properties. In the examples we will discuss the second front is usually an incoherent front, and when the one with which it catches up is a coherent front, this induces a transition from coherent to incoherent front dynamics in the leading front. In practice, therefore, what type of front dynamics one will get is *determined both by the existence of front solutions and by the stability of the state these solutions generate.*

2.7.5. When to expect pushed fronts?

The requirement for existence of a pushed front solution, $a_1 = 0$ according to Eq. (60) for a uniformly translating front solution to exist, or $A_1 = 0$ according to Eq. (76) for a coherent pattern forming solution, is a condition on the global properties of the solution of a nonlinear ordinary differential equation. Hence whether a pushed front solution exists depends on the full nonlinear properties of the dynamical equation we wish to investigate. There does not appear to be a general mathematical framework that allows us to predict from the appearance or the global structure of an equation whether a strongly heteroclinic front solution does exist, and hence whether fronts will be pulled or pushed. For the F-KPP equation one can derive general conditions on the nonlinear function $f(u)$ such that the selected fronts in the equation are pulled [35,37]. One of the simple results is that when $f(u)/u \leqslant f'(0)$ the fronts are pulled, which confirms our intuitive understanding that for a front to become pushed one needs the nonlinearities to enhance the growth. For (sets of) equations that admit uniformly translating fronts one typically finds the same trend, namely that the enhancement of the growth by the nonlinear terms in the dynamical equations tends to favor the occurrence of pushed fronts.

It is important to realize, however, that for coherent and incoherent pattern forming fronts, these intuitive ideas do not necessarily apply. Several of the examples to be discussed in Section 2.11 will illustrate this: in the quintic CGL equation the cubic term enhances the growth, but there are large regions of parameter space where nonlinear dispersion effects completely suppress the occurrence of pushed fronts. Likewise, fronts in the Kuramoto–Sivashinsky equation of Section 2.11.4 are pulled, but if one adds a linear term to the equation, a pulled to pushed transition is found. However, in dynamical pattern forming equations which derive from a Lyapunov functional and for which one has an reasonable understanding of whether the nonlinearities enhance or suppress the growth about the unstable state, one's intuition of what to expect is usually correct. Our discussion of front dynamics in the Swift–Hohenberg and Cahn–Hilliard equation will illustrate this.

As the example discussed at the end of Section 2.7.1 illustrated, for the second order partial F-KPP equation, the pushed front solutions can in a number of cases be explicitly constructed analytically. The reason is the following. While for an arbitrary v the large-ζ asymptotics (58) is characterized by two different exponentials, the pushed front solutions (60) of the F-KPP equation are characterized by one root. It is therefore possible (but not necessary) that the pushed solutions obey a first order equation. The "reduction of order method" briefly reviewed in Section 2.7.1 is based on substituting a first order Ansatz into the second order ordinary differential equation for the uniformly translating solutions. The most remarkable success of this method is that the pushed solutions of the quintic CGL equation have been found this way—see Section 2.11.6.

2.7.6. Precise determination of localized initial conditions which give rise to pulled and pushed fronts, and leading edge dominated dynamics for non-localized initial conditions

So far, we have focused on the front dynamics emerging from initial conditions which are "steep", in the sense that they fall off faster than $\exp[-\lambda^* x]$. This is because only for such initial conditions does the front selection problem have a sharp and unique answer—whether fronts are pushed or pulled is an *inherent* property of the dynamical equations. Indeed, the values of the corresponding velocities v^* and $v^\dagger$ are determined completely by the equation itself.

What happens if the initial conditions are not steep, i.e., fall of slower than $\exp[-\lambda^* x]$? Given our assumption of locality of our dynamical equations (no influence off from points arbitrarily far away) the answer lies hidden again in our analysis of the linear dynamics illustrated in Fig. 5. If initial conditions fall off with steepness $\lambda < \lambda^*$, the spatially slowly decaying leading edge on the right, which moves with velocity $v_{\rm env}(\lambda)$, expands in time. In other words, in the frame moving along with this leading edge, the crossover region to the slower part of the profile recedes to the left and larger and larger parts of the profile move with asymptotic velocity $v_{\rm env}$. Whatever the nonlinear dynamics is, it must be compatible with this dynamical constraint in the leading edge of the profile. Indeed, such initial conditions which are not steep necessarily lead to a front moving with speed $v_{\rm env}(\lambda)$ with $\lambda < \lambda^*$, unless a pushed front solution exists whose speed $v^\dagger$ is larger than $v_{\rm env}$. For, if such a pushed front solution with $v^\dagger > v_{\rm env}(\lambda)$ exists, this solution will invade the leading edge according the mechanism sketched in Fig. 8(b). Thus we conclude:

For an equation whose fronts are pulled, all initial conditions with steepness $\lambda < \lambda^*$ lead to fronts moving with speed $v_{\rm env}(\lambda) > v^*$. In other words, in the pulled regime we can identify "localized" initial conditions which lead to pulled fronts with initial conditions which are steep, i.e., which fall off faster than $\exp[-\lambda^* x]$.

For an equation whose fronts are pushed, only initial conditions with steepness $\lambda < \lambda_1$ lead to fronts moving with speed $v_{\rm env}(\lambda) > v^\dagger$, where λ_1 is the smallest root for which $v_{\rm env}(\lambda_1) = v^\dagger$. In other words, localized initial conditions which lead to pushed fronts are initial conditions which fall off faster than $\exp[-\lambda_1 x]$*, where λ_1 is determined implicitly by the pushed front solution through the requirement $v_{\rm env}(\lambda_1) = v^\dagger$.*

Intuitively the mechanism through which non-localized initial conditions lead to fronts that move faster than the naturally selected pulled or pushed speed, is very much like "pulling along" the nonlinear front. However, in order to distinguish them from the pulled front solutions which naturally emerge from all localized initial conditions, we refer to this type of dynamics more generally as "leading edge dominated" dynamics [144].

2.7.7. Complications when there is more than one linear spreading point

In our discussion of the pushed fronts, we have so far assumed that the linear dispersion is such that the $v_{\rm env}(\lambda)$ versus λ diagram is of the type sketched in Fig. 3, i.e., that there is only one branch which in the limit $\lambda \downarrow 0$ corresponds to a positive growth rate $\omega_{\rm i}$ and hence to a divergent $v_{\rm env}(\lambda)$. This is the normal situation for problems where there is essentially one branch of linear modes which is unstable. We now briefly discuss the subtleties associated with having more than one unstable branch of the dispersion relation.

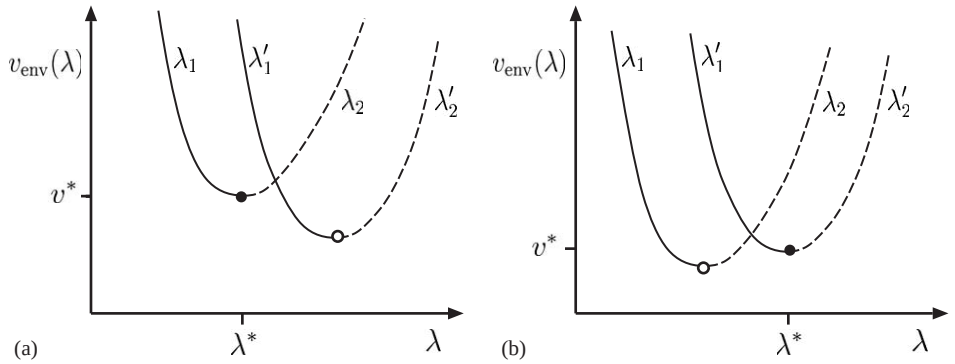

Fig. 11. Illustration of possible $v_{\rm env}(\lambda)$ versus λ diagrams in the case in which there is more than one unstable branch of modes. The relevant linear spreading velocity in each case is indicated with a filled circle. As explained in the text, the asymptotic steepness of a pushed front has to be associated with one of the two dashed branches.

Two examples of possible $v_{\rm env}(\lambda)$ diagrams for the case of two unstable branches are sketched qualitatively in Fig. 11. As we discussed before, according to the fully linear spreading analysis, the relevant linear spreading velocity v^* is the largest spreading velocity of the two branches. The crucial point to understand for the proper extension of the concept of a pushed front in such cases is that the linear dynamics associated with the two individual branches is completely independent—we can repeat the earlier discussion of how pushed fronts can emerge for each branch individually, and this leads to the conclusion that a pushed front is again a front whose asymptotic exponential decay is faster than $e^{-\lambda^*\zeta}$. However, in addition the exponential steepness $\lambda^\dagger$ of the pushed front should be larger than the value λ_1^* or λ_2^* associated with the minimum of the branch to which it belongs [86].[35] In other words, the leading steepness of a pushed front should correspond to[36] one of the two dashed branches in the figure. In the case of Fig. 11(a), a uniformly translating pushed front solution is a solutions whose asymptotic decay is as $e^{-\lambda_2\zeta}$, not as $e^{-\lambda_1'\zeta}$. Likewise, for the case sketched in Fig. 11(b) a transition from the pulled front with velocity v^* to a pushed one, whose asymptotic behavior is as $e^{-\lambda_2\zeta}$, could occur.

Like before, the possibility of such situations to occur is intimately related with counting arguments for the multiplicity of front solutions. E.g., for uniformly translating fronts with a dispersion relation consistent with one of the cases sketched in Fig. 11, one in general expects there to be a two-parameter family of front solutions. For the case of Fig. 11(a) pushed front solutions with the required asymptotic behavior are then expected to come as isolated front solutions, just as before.

[35] Another way to arrive at the same conclusion, stressed in particular by Chomaz and Couairon [86], is to note that asymptotic behavior with steepness given by one of the two left branches λ_1 or λ_2 can only emerge dynamically from non-localized initial conditions falling off with this steepness: Chomaz and Couairon [86] call these branches non-causal. In the language of [421] one can understand this from the fact that on these branches the group velocity is less than the envelope velocity—perturbations cannot work their way up towards the far tip.

[36] In the case of coherent pattern forming front solutions, "correspond to" should be read as "analytically connected to", since as we explained in Section 2.7.2 the asymptotic decay of a pushed front does not correspond to a value on the dashed branch of $v_{\rm env}$.

2.8. Relation with existence and stability of front stability and relation with previously proposed selection mechanisms

In this section, we briefly discuss the relation between front selection and stability, and the relation with some of the older proposed selection mechanisms.

2.8.1. Stability versus selection

The main difference in perspective with the "marginal stability" selection mechanism of the 1980s [38,111,420,421] is that we here emphasize that by starting from the classical linear spreading analysis [49,62,264] the concept of a linear spreading velocity v^* naturally arises. This concept holds irrespective of whether or not there are well-defined front solutions, and applies equally well to partial differential equations, difference equations and integro-differential equations. From this perspective, the possibility of having pulled fronts arises most naturally and independently of whether they are coherent or incoherent. In addition, the saddle point integration immediately shows that the intermediate asymptotic dynamics giving the approach to the asymptotic spreading speed is that of a diffusion equation, even if the equation itself is not at all a simple diffusion equation. This latter fact lies at the basis of the universal relaxation behavior discussed in the next section. Moreover, by exploring the constraints imposed by the linear dynamics, the essential properties of pulled fronts follow.

The drawback of the "marginal stability" formulation of [420,421] is that when one wants to relate selection with the stability properties of fronts, one can at best only understand the selection once one is already close to an asymptotic front solution.[37] Why the intermediate asymptotics bring one there is less clear—even though the two are quite consistent the attempt in the marginal stability approach to treat selection and linear spreading in one fell swoop makes the problem unnecessarily cumbersome and masks the generality of the linear spreading concept. Likewise, the universal relaxation behavior of pulled fronts that we will discuss in the next section is virtually impossible to get from a stability analysis (for uniformly translating or coherent pulled fronts, the spectrum of the stability operator is continuous with arbitrarily small eigenvalues), whereas it naturally emerges from the linear spreading concept.

Our simple observation that *whenever a solution* (60) *or* (76) *with* $v^\dagger > v^*$ *exists whose asymptotic steepness is larger than* λ^*, this solution *can and will* invade the leading edge and lead to pushed front propagation, is actually a general formulation which encompasses the "nonlinear marginal stability" scenario that when one considers fronts as a function of there velocity, front solutions with speed $v < v^\dagger$ are unstable [38,421]. One can see this as follows [144, Appendix I]. For dynamical equations which are translation invariant, the translation mode is always a mode with zero eigenvalue of the stability operator. At $v = v^\dagger$ the front solution is a strongly heteroclinic orbit, and hence the zero eigenmode of the stability operator corresponds to a strongly heteroclinic orbit. Continuity and counting arguments then imply that for v close to but different from $v^\dagger$, there is a strongly heteroclinic solution of the stability operator whose eigenvalue crosses zero at $v = v^\dagger$. In other words, when the stability of the front solutions is studied for varying velocity v, the stability

[37] Booty et al. [53] have also analyzed the dynamics in the leading edge of the F-KPP equation. Conceptually, their approach has much in common with that of [420,421].

changes at $v^\dagger$—front solutions with velocity $v < v^\dagger$ are unstable due to the invasion of the pushed front solution into the leading edge.

Another reason for separating front stability from front selection is that the simulations discussed in Section 2.11 will show that the state generated by the front becomes absolutely unstable in the frame moving with the front, this entails a transition from a coherent pattern forming front to an incoherent pattern forming front, not necessarily a change from pulled to pushed dynamics.

2.8.2. *Relation between the multiplicity of front solutions and their stability spectrum*

The above discussion of the implication of the existence of a pushed front solution for the stability of fronts also illustrates that there generically is an intimate connection between the multiplicity of uniformly translating and coherent front solutions and the stability properties. We can illustrate this for the other stability modes as follows. As we discussed in the previous section, a uniformly translating or coherent front solution corresponds to an orbit in the phase space of the ordinary differential equations that govern these solutions, and the multiplicity of these solutions is determined by "counting arguments" for the dimension of the manifolds that flow into and out of the fixed points that correspond to the asymptotic states. Consider now the case in which the dynamical equations admit a one-parameter family of front solutions, parametrized by their speed v—we argued that this is the usual case for front propagation into unstable states. If we now pick an arbitrary front solution from this family and write down the stability operator for perturbations about the front solution, then the counting arguments for the stability modes is essentially unchanged because the linearization about the asymptotic states before and after the front is unchanged. Hence the existence of a one-parameter family of fronts, parametrized by v, generically implies that if we fix v and consider the stability modes, then we expect there to be in general a one-parameter family of stability modes, parametrized by their growth/decay rate. Together with the fact that translation invariance of the dynamical equation implies that there is a zero mode of the stability operator, this also implies that there generically is a continuous spectrum of the stability operator near zero. A general analysis of the asymptotic behavior of these modes about the unstable state shows that the modes from this spectrum which decay faster than the front solution are stable, and that those which decay less fast than the front solution are unstable [421]. This line of analysis in combination with the one above for the possible presence of a localized stability mode if a pushed front solution exists, gives a quite complete generic picture of the stability of the front solutions in the generic case. In short: if no pushed front solution exists, so that the selected fronts are pulled, then the front solutions with $v > v^*$ are stable to perturbations which decay faster than the front itself, and unstable to those which spatially decay less fast than the front itself. If a pushed front solution exists, then the generic picture is that front solutions with $v < v^\dagger$ are unstable to the localized mode, and those with speed $v > v^\dagger$ are stable to this mode and to perturbations whose spatial decay to the right is faster than that of the front solution itself.

For coherent pattern forming fronts, similar arguments apply. Let us again focus on the generic case (see Section 2.7.2) that these front solutions come into a two parameter family. If we consider a particular front solution at a fixed velocity v, then the generic scenario that results from similar continuity arguments is that any arbitrary front solution which in the tail does not match up with the maximal growth rate ω_i in the leading edge, or, in other words, whose asymptotic behavior does not correspond with the left branch drawn with a full line in Fig. 3(a), is unstable. This is the reason we

focused on the analysis of $v_{\rm env}$ defined in Eq. (21) in Section 2.2: only that branch matches up with asymptotic coherent front solutions which are stable to perturbation that decay spatially faster to the right than the front solutions themselves. The discussion of stability of a possible localized stability mode, associated with the existence of a pushed front solution, is analogous to the one given above.

The explicit stability calculation for the uniformly translating fronts in the F-KPP equation or extensions of it can be found in a number of papers [60,72,144,149,216,230,252,317,371] and will not be repeated here. The results are completely in accord with the above general discussion.

2.8.3. Structural stability

We finally comment briefly on the proposal to connect propagating front selection with "structural stability" ideas. According to this conjecture [83,334], the pulled front is the natural front speed as it is the only front solution which is "structurally stable" to small changes in the dynamical equations (like those which would suppress the instability or make the state $\phi = 0$ even linearly stable). It is easy to convince oneself that uniformly translating pulled solutions do have this property, as the dynamically relevant front solutions are characterized by a *real* spatial decay rate only, but that as we discussed at the end of Section 2.7.2 coherent pattern forming front solutions which are characterized by a decay rate and wavenumber in the leading edge, generically do *not* have this property. Indeed, the quintic CGL equation provides an explicit counterexample to the "structural stability" postulate: As we shall see under (iii) in Section 2.11.6, for the quintic CGL equation the selected wavenumber can jump at the pulled to pushed transition.

2.8.4. Other observations and conjectures

The issue of front selection issue has intrigued many authors, so various other observations and conjectures have been made. In Appendix B we briefly discuss some of these: a (wrong) conjecture concerning the analytic structure of pushed front solutions, an observation about obtaining the selected uniformly translating front by studying the front solutions on a finite interval, and the connection with Hamilton-Jacobi theory and renormalization group ideas.

2.9. Universal power law relaxation of pulled fronts

Up to now, we have focused on the asymptotic front velocity. Let us now assume we study an equation whose fronts are pulled, and ask how the asymptotic front velocity is approached. To do so, we first have to state how we define a time-dependent velocity of a front during the transient regime when it approaches its asymptotic value. We will be quite pragmatic in our discussion: the asymptotic convergence to v^* will turn out to be very slow, so slow that the differences between various conventions do not really matter. We will therefore focus simply on the most natural definition.

In this section, we will simply state the results for the convergence to v^*; the essential ingredients of the derivation are reviewed in Section 4.

It is good to stress that the universal relaxation only holds for pulled fronts. The discussion of Section 2.8 implies that the stability spectrum of a pushed front solution is gapped, and hence that a pushed front relaxes exponentially fast to its asymptotic velocity and shape [144,227,421]. This is in line with the intuitive idea illustrated in Fig. 8 that a pushed front invades the region ahead of it with a finite speed.

2.9.1. Universal relaxation towards a uniformly translating pulled front

If a pulled front is asymptotically uniformly translating, we can simply follow the same idea as in our discussion of the linear spreading problem in Section 2.1: In essence our convention will always be to determine a front speed $v_C(t)$ by tracking the position $x_C(t)$ of the level line where the dynamical field ϕ reaches a level C; the velocity is then the speed of this point

$$\phi(x_C,t)=C \quad \Leftrightarrow \quad v_C(t)=\frac{\mathrm{d}x_C}{\mathrm{d}t} \ . \tag{77}$$

Of course, for dynamical fields with more than one component, the transient velocity could in principle depend on which component we track, but we will not distinguish this possibility notationally, as we will focus on those aspects which are independent of those details.

The analysis [144] of the convergence of the nonlinear pulled front speed to v^* is based on matching the behavior in the leading edge, where corrections to the asymptotic exponential behavior $\mathrm{e}^{-\lambda^*\xi}$ are governed by an equation which in dominant order is a diffusion-type equation, to the behavior in the fully nonlinear region. In this step, the fact that the asymptotic front solution $\Phi_{v^*}(\xi)$ has according to (59) a $\xi\mathrm{e}^{-\lambda^*\xi}$ behavior plays a crucial role—see Section 4. The final result of the matching analysis [144] is the following *exact* expression for the velocity $v(t)$ of an asymptotically uniformly translating front,

$$v(t)=v^*-\frac{3}{2\lambda^* t}+\frac{3\sqrt{\pi}}{2\sqrt{D}(\lambda^*)^2 t^{3/2}}+\mathcal{O}\left(\frac{1}{t^2}\right) \ , \tag{78}$$

which holds provided one starts from steep initial conditions which fall off faster than $\mathrm{e}^{-\lambda^* x}$.[38] This slow power-law like relaxation of the velocity to its asymptotic value v^* entails a slow relaxation of the front profile to its asymptotic shape. Indeed, if we define $X(t)$ as the shift of the front position in the frame moving with speed v^*,

$$X(t)=\int^t \mathrm{d}t'\,(v(t')-v^*) \quad \Leftrightarrow \quad X(t)\simeq -\frac{3}{2\lambda^*}\ln t+\mathcal{O}(t^{-1/2}) \ , \tag{79}$$

then one finds for the relaxation of the front profile to its asymptotic shape

$$\phi(x,t)\simeq \Phi_{v(t)}(\xi_X)+\mathcal{O}\left(\frac{1}{t^2}\right), \quad \xi_X \ll \sqrt{Dt} \ , \tag{80}$$

where ξ_X is the frame

$$\xi_X \equiv \xi - X(t) = x - v^* t - X(t) \tag{81}$$

which includes the logarithmically increasing shift $X(t)$.

There are many points to note about these universal relaxation results for pulled fronts and the physical picture underlying their derivation:

(i) While the above results are exact for all pulled fronts which asymptotically are uniformly translating, for the special case of the F-KPP equation, the $1/t$ term was known for over

[38] To be more precise, the result holds provided the initial conditions fall off exponentially faster than $\exp[-\lambda^* x]$, i.e., provided there is some $\delta>0$ such that $\phi(x,t=0)\mathrm{e}^{\lambda^* x}<\mathrm{e}^{-\delta x}$ as $x\to\infty$. The special case in which $\phi(x,t=0)\sim x^{\nu}\mathrm{e}^{-\lambda^* x}$ is discussed in [54,144,255,256,314].

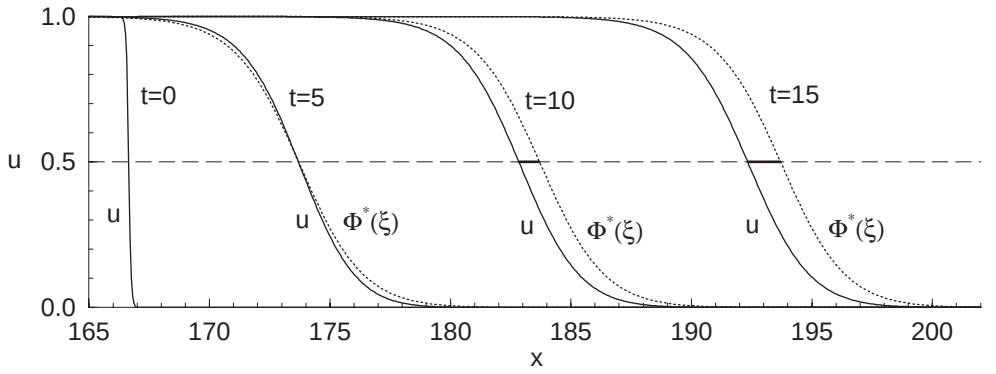

Fig. 12. Illustration of the logarithmic shift of the transient profile relative to the asymptotic profile Φ_{v^*} moving with constant speed v^*, for the case of the F-KPP equation with $f(u) = u - u^3$. The solid line shows the actual shape and position of the front emerging from an initial condition at time $t = 0$ at three successive times. The dotted line shows the uniformly translating solution Φ_{v^*} (labeled Φ^* in the figure) at three successive times; at $t = 5$ this solution was placed such that it intersects the actual solution at $u = 0.5$. The thick solid line indicates that the transient solution and the asymptotic solution separate more and more as time goes on, even though the shape of the transient front is always close to the asymptotic one. From [144].

20 years [138,139,291] and was derived rigorously in 1983 by Bramson [54]. Since then it has been re-derived by various methods (including a matching analysis of [64] similar to ours), but to my knowledge even for the F-KPP equation the universal $1/t^{3/2}$ term was not known before the matching analysis [144] described in more detail in Section 4.

(ii) The dominant logarithmic shift in $X(t)$ which is driven by the diffusive dynamics in the leading edge implies that when viewed in the frame moving with the asymptotic velocity v^*, the front moves back while it is relaxing. This is illustrated in Fig. 12 for a simulation of the F-KPP equation starting from a localized initial condition. The plot shows the actual front profile at times $t = 5$, 10 and 15 (full line), and compares these with the uniformly translating asymptotic profile Φ_{v^*} (dotted line) which has been placed so that it intersects the transient profile at $\phi = 1/2$ at time $t = 5$. The increase of the length of the thick line with time illustrates that the actual transient profile and the asymptotic profile Φ_{v^*} separate more and more in time.

(iii) The results which are illustrated in Fig. 12 show quite clearly that any method based on linearizing about the asymptotic front solution Φ_{v^*} will not work: the differences between the actual front solution and this asymptotic one grow arbitrarily large! This is why the insight to use the logarithmically shifted frame ξ_X is crucial for any theoretical analysis.

(iv) Nevertheless, the figure does confirm that already quite soon the transient front *shape* is close to the asymptotic shape Φ_{v^*}. This fact is expressed in precise mathematical terms by (80): to order t^{-2} *the front shape is given by the expression for the uniformly translating front solution* Φ_v, *provided we use the instantaneous value* $v(t)$ *given by* (78) *for the velocity, and put the front at the appropriately shifted position* ξ_X. In other words, to $\mathcal{O}(t^{-2})$ the transient front shape follows the uniformly translating solutions adiabatically. This fact was first noted empirically in simulations by Powell et al. [354].

(v) The above results are valid for any pulled front which asymptotically is uniformly translating: *it is independent on the precise nonlinearities and applies to all pulled fronts in equations for which the linear spreading speed v^* can be determined according to our discussion of Section* 2.4. The fact that these results apply equally well to difference equations like the finite difference version (45) of the F-KPP equation or the difference-differential equation discussed in Section 3.23, is that the saddle point expression for v^* ensures that the corrections to the asymptotic exponential $e^{-\lambda^* x}$ behavior are governed by a diffusion-type equation. In other words, as these corrections become arbitrarily smooth for long times, the lattice effects only give higher order corrections [144,146]. See Section 4 for further details.

(vi) Since the above results are independent of the precise form of the nonlinearities in the dynamical equation as long as the fronts are pulled, one may wonder where the nonlinearities are hidden. Comparison with the result for the convergence to v^* according to the fully linear dynamics discussed in Section 4.1 shows that the prefactor 3/2 of the $1/t$ term and the subdominant $t^{-3/2}$ term both reflect the nonlinear behavior. [39]

(vii) In line with the earlier conclusion of Section 2.3 that the limits $t \to \infty$, ξ fixed and $\xi \to \infty$, t fixed do not commute, we stress that the expression (80) is the correct asymptotic expression for $t \to \infty$, ξ_X fixed. At $\xi_X \simeq \sqrt{Dt}$, there is a crossover to a different asymptotics that governs the large ξ_X limit [144].

(viii) Note that the above result for the universal velocity relaxation holds independent of the initial conditions and of the level line which is used to track the position of the front, provided one is not at the pulled to pushed transition. [40] In fact, the correction to the velocity relaxation associated with the shape relaxation is according to (80) of order $[\delta\Phi_v(\zeta)/\delta v]\,\mathrm{d}v(t)/\mathrm{d}t \sim t^{-2}$.

(ix) The terms displayed in (78) for $v(t)$ and in (80) for the relaxation of the front profile are also the *only* universal terms. This can easily be seen as follows. Suppose we compare the velocity formula for two cases, one starting from some steep initial condition at time $t = 0$ and the other one by viewing the dynamical state at time $t = \Delta t$ as the initial condition. For large times the $1/t$ terms for the two cases differ of order $\Delta t/t^2$. Thus the term of order $1/t^2$ depends on the initial conditions, i.e., is non-universal.

(x) Formula (78) shows that the asymptotic velocity is always approached *from below*. This explains why in many finite time simulations of pulled fronts the published velocity data are slightly below v^* (we will encounter several examples of this later). This fact together with Eq. (80) for the shape relaxation of the front imply that for the transient dynamics the front solutions with speed $v < v^*$ are important. This is the reason for our cautionary note in Section 2.2 about using the phrase "the minimum velocity".

(xi) Extensive numerical investigations and illustrations of the universal relaxation behavior of uniformly pulled fronts can be found in [144,146]. An example of such tests will be discussed in Section 4.2.

---

[39] As we will show in Section 4.1, Eq. (203), according to the fully *linear* dynamics a level line asymptotically recedes as $-(\ln t)/2\lambda^*$ in the frame moving with v^*, rather than as the $-3(\ln t)/2\lambda^*$ term of the nonlinear front profile. Hence if we would also draw in Fig. 12 the profile as it evolves according to the linearized equation, it would for large times and not too large u lie in between the asymptotic front profile Φ_{v^*} and the actual transient profile.

[40] At the pulled to pushed transition the prefactors of the $1/t$ and $1/t^{3/2}$ term are different—see Appendix G of [144].

2.9.2. Universal relaxation towards a coherent pattern forming pulled front

How to define the instantaneous front velocity for a coherent pattern forming fronts is subtle issue. If one traces the position of the foremost point where a dynamical field which develops oscillations reaches a given value, this position will make finite jumps when a new oscillatory part in the leading edge grows large enough that it reaches the predetermined level C. Since the time between successive jumps will be finite, averaging over some finite time then already gives a crude idea of the slow long-time convergence. A better way is to determine numerically an envelope of the front profile from traces of e.g. the maxima of the oscillations during one period, and to then determine the velocity from the positions of a level line of this empirical envelope of the front [388,383]. The advantage of this method is that it also works well when one wants to trace level lines in the range where the nonlinearities in the dynamical equation are clearly important. If, on the other hand, one decides to track the front velocity in the leading edge only, then a good method is to fit a decaying oscillatory exponential to the front profile, and to determine the position of a given level from that fit. We will not dwell on the advantages and disadvantages of the these methods further, as they are of little relevance when one wants to probe the universal slow long-time relaxation.

Under the same assumptions as before for the uniformly translating fronts (see footnotes 38 and 40), the front velocity of a coherent pulled front relaxes to its asymptotic value v^* as [147,383,388]

$$v(t) \equiv v^* + \dot{X}(t) = v^* - \frac{3}{2\lambda^* t} + \frac{3\sqrt{\pi}}{2(\lambda^*)^2 t^{3/2}} \operatorname{Re} \frac{1}{\sqrt{\mathscr{D}}} + \mathcal{O}\left(\frac{1}{t^2}\right) , \tag{82}$$

which reduces to the result (78) for uniformly translating fronts when $\operatorname{Im} \mathscr{D} = 0$. The relaxation of the front profile to its asymptotic behavior (56) is characterized by the relaxation of the velocity and a global phase $\Gamma(t)$: it is found that in this case one can write for the long-time asymptotics

$$\phi(x,t) \approx \sum_{n=0,\pm 1,\ldots} \mathrm{e}^{-in[\Omega t + \Gamma(t)]} \Phi^n_{v(t)}(\xi_X) + \mathcal{O}\left(\frac{1}{t^2}\right) , \tag{83}$$

where $\Gamma(t)$ is given by [147,383,388]

$$\dot{\Gamma}(t) = -k_{\mathrm{r}}^* \dot{X}(t) - \frac{3\sqrt{\pi}}{2\lambda^* t^{3/2}} \operatorname{Im} \frac{1}{\sqrt{\mathscr{D}}} + \mathcal{O}\left(\frac{1}{t^2}\right) . \tag{84}$$

These equations simply express that to $\mathcal{O}(t^{-2})$ also the pattern forming fronts follow adiabatically a family of coherent front solutions.

Essentially all the remarks made about the slow relaxation behavior of uniformly translating fronts apply equally well to the relaxation behavior of the pattern forming fronts—the only additional feature is the analogous slow convergence of the frequency $\dot{\Gamma}(t)$: it implies a slow convergence of the wavelength of the pattern generated by the front. To our knowledge, this behavior has been verified both qualitatively as well as quantitatively only for the Swift–Hohenberg equation—see Section 2.11.2 and Fig. 19 below. It does not appear to have been studied experimentally in a systematic way, although the slow velocity relaxation of pattern forming fronts does appear to play a role in some pattern forming experiments—see Section 3.1.

2.9.3. Universal relaxation towards an incoherent pattern forming pulled front

Quite remarkably, though we cannot make a prediction for the front shape relaxation for an incoherent pulled front, we will argue in Section 4 that the *same* velocity relaxation formula (82)

applies to an incoherent pattern forming pulled front. The reason for this is that even when a pulled front is nonlinearly incoherent, the behavior in the leading edge is still very smooth and coherent, as it is governed by the *same* linear dynamical equation for the expansion about the linear spreading point. This latter observation also implies that the velocity of an incoherent front is in practice most easily measured in the leading edge. Even the phase correction $\Gamma(t)$ is well-defined there and follows (84)—the results for the quintic CGL equation shown in Fig. 19 provide evidence in support of this claim.

2.10. Nonlinear generalization of convective and absolute instability on the basis of the results for front propagation

In Section 2.5 we discussed the difference between convective and absolute instabilities in the case that the evolution of a perturbation around the unstable state evolves *according to the linearized equations*. As Fig. 7 illustrated, if we focus on the right flank of the local perturbation, the linear instability is absolute if $v^* > 0$ and convective if $v^* < 0$—in the latter case the perturbation "retreats" so that it eventually dies out at any fixed position. If perturbations have enough time to grow that the nonlinearities become important and that a nonlinear front develops, it is straightforward to extend the distinction between the two regimes to the nonlinear case [85,99,412]. Clearly, in the pulled regime the criterion is the same since the nonlinearities do not affect the asymptotic front speed, so the instability is nonlinearly convectively unstable for $v^* < 0$ and nonlinearly absolutely unstable for $v^* > 0$. When the fronts are pushed in the dynamical equation under consideration, the criterion becomes simply that the instability is nonlinearly convectively unstable if $v^\dagger < 0$ and nonlinearly absolutely unstable when $v^\dagger > 0$. That's all there is to it. A recent nice experiment on the Kelvin–Helmholtz instability in which the transition from a nonlinearly convective to a nonlinearly absolute instability was observed, can be found in [186].

2.11. Uniformly translating fronts and coherent and incoherent pattern forming fronts in fourth order equations and CGL amplitude equations

In this section we illustrate many of the basic issues of front propagation into unstable states by reviewing the diversity of such fronts in Complex Ginzburg Landau (CGL) equations and in a number of well known fourth order partial differential equations which have been introduced in the literature as model problems for a variety of physical phenomena.[41] In fact, we encounter all three different modes of front propagation dynamics both for pushed and for pulled fronts in these equations, so taken together the examples discussed below give a good idea of the richness of front propagation into unstable state as well as of the power of the concepts of a pulled and pushed fronts.

We will limit our discussion completely to the dynamics of fronts which propagate into an unstable state, so it is important to keep in mind that such behavior constitutes just a small fraction of the wide

[41] We focus in the section on rather well known model equations. From a historical perspective, it is interesting to note that pulled propagating fronts were also found back in 1983 in a fourth order caricature model aimed at describing sidebranching in dendrites [248]. The dispersion relation for the sidebranch instability in this model is of the same form as the general form we consider here, Eq. (86) below.

range of dynamical behavior that is found in these equations. The books by Greenside and Cross [189] and by Nishiura [320] provide nice complementary introductions to these model equations.

While the nonlinear front dynamics will be found to be different for all of the fourth order equations we will discuss, the linear dynamics obtained by linearizing the equations about the unstable state will always be a special case of

$$\partial_t \phi = a\phi - b\partial_x^2 \phi - \partial_x^4 \phi \ . \tag{85}$$

The negative prefactor of the fourth order derivative term is required to ensure stable behavior of the equations at the short length scales. Indeed, the dispersion relation corresponding to this equation is

$$\omega = \mathrm{i}(a + bk^2 - k^4) \ , \tag{86}$$

so for any value of a and b the short wavelength modes at large k are always damped ($\omega_{\mathrm{i}} < 0$). The requirement that the state about which we linearize is unstable for a range of modes implies that the coefficients should obey $a + b^2/4 > 0$. It is simply a matter of some straightforward algebra to work out the linear spreading point equations (12) and (13) explicitly. We find that there are two regimes: for $a > 0$ and $b < -\sqrt{12\,a}$ we get

$$\begin{aligned}
v^*_{4\text{th ord}}(a,b) &= \frac{2}{3\sqrt{6}}(-2b + \sqrt{b^2 - 12a})(-b - \sqrt{b^2 - 12a})^{1/2} \ , \\
\lambda^*_{4\text{th ord}}(a,b) &= \frac{1}{\sqrt{6}}(-b - \sqrt{b^2 - 12a})^{1/2} \ , \\
k^*_{\mathrm{r},4\text{th ord}}(a,b) &= 0 \ , \\
D_{4\text{th ord}}(a,b) &= \sqrt{b^2 - 12a} \ ,
\end{aligned} \tag{87}$$

while for $a > 0$ and $b > -\sqrt{12\,a}$ as well as for $a < 0$ but $b > 2\sqrt{-a}$

$$\begin{aligned}
v^*_{4\text{th ord}}(a,b) &= \frac{2}{3\sqrt{6}}(2b + \sqrt{7b^2 + 24a})(-b + \sqrt{7b^2 + 24a})^{1/2} \ , \\
\lambda^*_{4\text{th ord}}(a,b) &= \frac{1}{2\sqrt{6}}(-b + \sqrt{7b^2 + 24a})^{1/2} \ , \\
k^*_{\mathrm{r},4\text{th ord}}(a,b) &= \pm\frac{1}{2\sqrt{2}}(3b + \sqrt{7b^2 + 24a}) \ , \\
D_{4\text{th ord}}(a,b) &= 2\sqrt{7b^2 + 24a} \ ,
\end{aligned} \tag{88}$$

As we shall see below, in the first regime $a > 0$, $b < -\sqrt{12\,a}$, fronts are uniformly translating, while in the other regime they are pattern forming.

2.11.1. The extended Fisher–Kolmogorov equation

While the relevant asymptotic front solutions of the F-KPP equation are uniformly translating and monotonically decaying in space to the right, if one includes a fourth order derivative term in the equation, the front dynamics becomes much more rich. If we consider the case in which

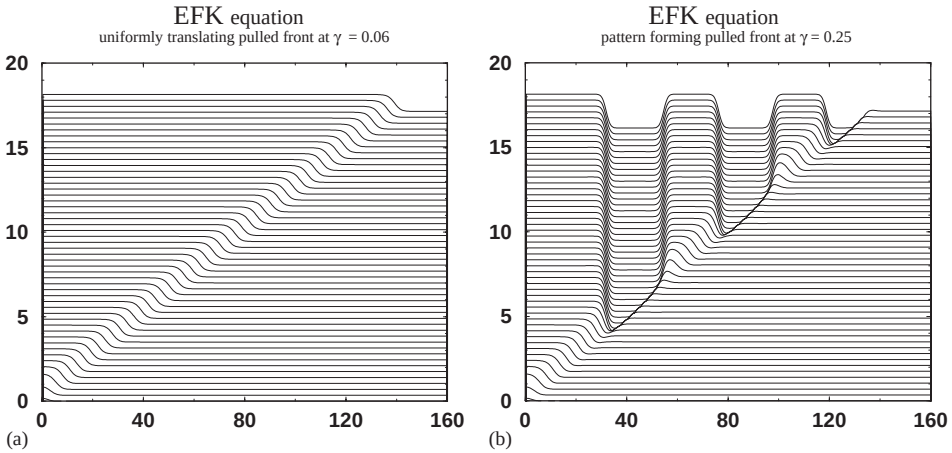

Fig. 13. Space–time plot of simulations results for pulled fronts in the EFK equation (89). The lines denote the front position at successive time intervals of 1.5, and are shifted upward relative to each-other for clarity. The initial condition is a Gaussian of amplitude 0.1 centered at the origin and the total simulation time is 75. (a) Illustration of the front dynamics in the regime $\gamma < 1/12$. The plot, made for $\gamma = 0.06$ illustrates that the fronts converge to uniformly translating solutions propagating with velocity $v^*_{\rm EFK}$. (b) The simulation for $\gamma = 0.25$ illustrates that in the regime $\gamma > 1/12$ the pulled fronts generate patterns: they leave behind an array of kinks. As can be seen from the graph, nodes are conserved under the dynamics, and as a result the wavelength of the pattern is given by the node conservation formula (91). Note also the smooth uniform propagation of the leading edge, in spite of the complicated nonlinear dynamics in the front region itself.

the nonlinear term is a simple cubic nonlinearity so as to study pulled fronts, we arrive at what is usually referred to as the Extended Fisher–Kolmogorov or EFK equation [113,421]

$$\partial_t u = \partial_x^2 u - \gamma \partial_x^4 u + u - u^3 \quad (\gamma > 0) \ . \tag{89}$$

This form of the equation is the most suitable for studying the behavior in the F-KPP limit $\gamma \to 0$. For any nonzero γ, however, upon transforming to the scaled coordinate $x' = x/\gamma^{1/4}$ the linear terms in this equation are precisely of form (85) with $a = 1$ and $b = -1/\sqrt{\gamma}$. Thus we can use the above expressions provided we rescale all lengths by a factor $\gamma^{1/4}$; e.g., the linear spreading speed of the EFK equation is simply

$$v^*_{\rm EFK} = \gamma^{1/4}\, v^*_{\rm 4th\ ord}(1, -1/\sqrt{\gamma}) \ . \tag{90}$$

The most interesting aspect of the EFK equation as far as front propagation is concerned is the bifurcation that occurs in the pulled front behavior at $\gamma = 1/12$: For $\gamma < 1/12$, we are in the regime where the pulled front parameters are given by (87) as $b < -\sqrt{12}$, and hence where we have $k^*_{\rm r} = 0$. This means that the asymptotic front profile falls off monotonically, just like in the F-KPP equation. Fig. 13(a) shows an example of the front dynamics in this regime. For $\gamma > 1/12$, however, $k^*_{\rm r} \neq 0$, and the leading edge of the pulled front falls off in an oscillatory manner. The dynamics that results from this oscillatory behavior is illustrated in Fig. 13(b): the oscillations in the leading edge periodically grow in size and "peel off" from the leading edge to generate an array of kinks between the two stable states $u = \pm 1$ [113].

In the numerical simulation one empirically observes that, in this process, nodes in the profile where u goes through zero, never disappear nor are generated spontaneously: They are formed in the

far leading edge, and then just gradually drift through the leading edge until they detach and come to rest as a kink. To our knowledge, there is no real theory which shows under what conditions or for what type of equations nodes are "conserved" under the dynamics. However, given that we empirically observe it, we can calculate the wavelength of the stationary nonlinear kink pattern behind the front [111,113]! In the frame ξ moving with the asymptotic speed v^*, the oscillatory part of the profile is for long times given by $\exp[-\mathrm{i}(\omega_r^* - k_r^* v^*)t]$, so the angular frequency with which nodes pass any fixed position in the leading edge is $|\omega_r^* - k_r^* v^*|$. Far behind the front, the kinks come to rest in the x frame. If the wavenumber of the kink profile is q_{stat}, then the angular frequency with which nodes pass a fixed position ξ far behind the front in the moving frame is simply $v^* q_{\mathrm{stat}}$. Node conservation together with expressions (88) therefore implies that

$$q_{\mathrm{stat}} = |\omega_r^*/v^* - k_r^*| = \frac{3}{8\sqrt{2}} \frac{(3b + \sqrt{7b^2 + 24a})^{3/2}}{2b + \sqrt{7b^2 + 24a}} \ . \tag{91}$$

The expression for the front speed in both regimes, as well as this one for the pattern wavenumber in the regime $\gamma > 1/12$, was found to be fully consistent with the results of numerical simulations.[42] In fact, an ideal periodic kink pattern of the type generated behind the front is not necessarily stable, so the emerging near-periodic state is usually only an intermediate asymptotic state: For $1/12 < \gamma < 1/8$, successive kinks and antikinks attract each other. This attraction is very weak for widely spaced kinks, and so the bunching instability that it gives rise to is virtually unnoticeable in the simulations. For $\gamma > 1/8$, the spatially oscillatory tail of a single kink gives rise to an oscillatory interaction between kinks [113,340]. This is just one example of the rich type of behavior that the EFK displays—see [340,410] for further details or [370,371] for work on the existence and stability of the front solutions.

Just like the F-KPP equation exhibits a transition to pushed fronts if the cubic nonlinearity u^3 is changed into a nonlinear function $f(u)$ whose growth is enhanced over the linear term at intermediate values (e.g. by a quadratic nonlinearity u^2), so does the EFK equation [421]—we already illustrated this in Fig. 10. Even for $\gamma < 1/12$, when pulled fronts in the EFK equation are spatially monotonic, pushed fronts in this regime can be non-monotonic even though they remain uniformly translating, see Fig. 10 and [421]. So, as we already stressed before, unlike fronts in the F-KPP equation, both pulled and pushed fronts in the EFK equation can be non-monotonic—monotonicity has nothing to do with front selection.

What else does the EFK equation teach us? Well, this equation with its bifurcation from uniformly translating fronts for $\gamma < 1/12$ to pattern forming fronts for $\gamma > 12$ is probably the simplest equation that illustrates the essence of pulled dynamics: the dynamics in the leading edge just does what the linear spreading point conditions impose, while the rest of the front where the nonlinear saturation term becomes important just cannot do anything but adjust to the dynamics enforced by the leading edge dynamics. In the present case, where essentially the only basic coherent structures admitted by the equation are kinks, the state behind the front is in first approximation an array of such kinks or domain walls. This state itself may be unstable or have other nontrivial dynamics, but this does not really affect the propagation of the pulled front.

[42] Inspection of the data points for the velocity in [113] shows that they fall slightly below the predictions for v^*_{EFK}. This is due to the fact that in a finite time simulation one always observes a velocity slightly less than v^* due to the power law convergence to v^* from below discussed in Section 2.9. Similar effects can be observed in virtually all published data of studies of pulled fronts, some of which are reviewed in Section 3.

As we discussed in Section 2.7, the coherent pattern forming front solutions (56) are coherent in that they are temporally periodic in the frame ξ moving with velocity v^*. The node-conservation argument is one immediate implication of this. Hence the empirical observation of node-conservation in the EFK equation for $\gamma > 0$ strongly suggests that the pattern forming solutions are coherent, i.e., of the form (56). Indeed one can convince oneself [429] term by term in the expansion that the EFK equation for $\gamma > 1/12$ should admit a two-parameter family of front solutions, parametrized by their velocity v and the wavelength of the kink pattern behind the front.

We finally note that while the EFK equation has been introduced mainly as a model equation to illustrate the transition from uniformly translating fronts to coherent pattern forming fronts as the spreading points parameters change when γ is increased beyond 1/12. Zimmermann [450] has shown that the equation can arise as a type of amplitude equation in electro-hydrodynamic convection in liquid crystals. In this interpretation the point $\gamma = 1/12$ can be viewed as a dynamical Lifshitz point. [43]

2.11.2. The Swift–Hohenberg equation

The Swift–Hohenberg equation

$$\partial_t u = \varepsilon u - (\partial_x^2 + 1)^2 u - u^3 = (\varepsilon - 1)u - 2\partial_x^2 u - \partial_x^4 u - u^3 \tag{92}$$

was introduced as a simple model equation for the dynamics just above a supercritical finite-wavelength instability [389]. [44] In the Swift–Hohenberg equation, the $u = 0$ state is linearly unstable for $\varepsilon > 0$; for $0 < \varepsilon \ll 1$ the equation gives rise to patterns of wavenumber about 1 whose dynamics can be analyzed in terms of an amplitude equation. The dispersion relation for small perturbations about the unstable state is given by (86) with $a = \varepsilon - 1$ and $b = 2$.

For $\varepsilon > 0$ the Swift–Hohenberg equation admits a band of stable periodic states, and this has made the Swift–Hohenberg equation an attractive model equation for front propagation in the past, as fronts propagating into the unstable state $u = 0$ are found to generate one of these regular and stable periodic patterns behind them—see Fig. 14(a). For this reason the Swift–Hohenberg equation has played an important role both from a historical and from a practical point of view:

(i) The first numerical study of a pulled pattern forming front was done for this equation and expression (88) for v^* was confirmed in detail [111,421].

(ii) The node conservation that we discussed in the previous subsection on the EFK equation was first observed empirically for this equation by Dee and Langer [111] and this lead these authors to derive Eq. (91) with $a = \varepsilon - 1$ and $b = 2$ for the wave number $q_{\rm stat}$ of the stationary periodic profile generated behind the front. Numerical results were found to be in full accord with this expression [111,421], indicating, as for the EFK equation, that these front solutions appear to be of the coherent pattern forming type (56).

(iii) It was the first pattern forming equation for which the transition from pushed to pulled fronts was studied in detail both numerically and analytically by including either a symmetry breaking quadratic term u^2 or by changing the sign of the cubic term and adding a stabilizing quintic term [421]. Simulations of a pushed front in the presence of a quadratic term are shown in Fig. 14(b).

[43] A Lifshitz point is a point in parameter space where a phase transition from a homogeneous to a modulated state occurs.

[44] It also arises in the context of laser physics [258] or as an amplitude equation near a particular type of co-dimension 2 bifurcation point [369].

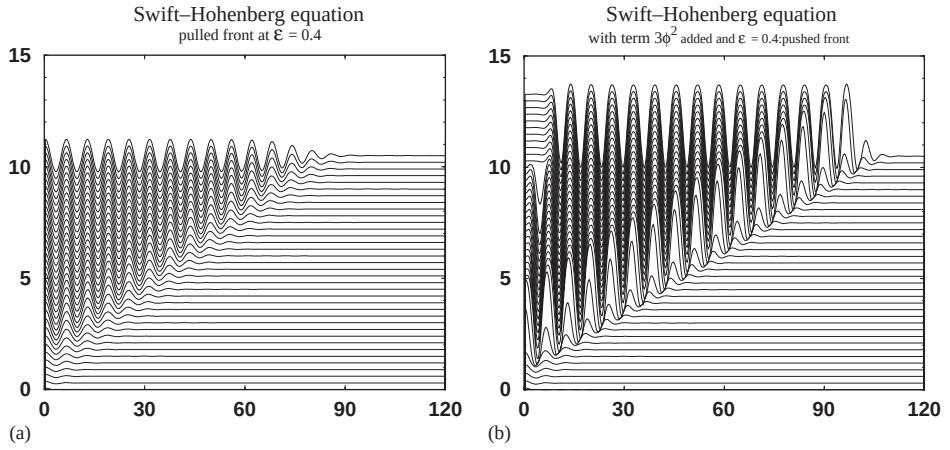

Fig. 14. Space–time plot similar to Fig. 13, but now for the Swift–Hohenberg equation. Total run time is 35, and the time difference between successive lines is 1; the simulations started from a Gaussian initial condition. The plots in this figure are more detailed version of those in the middle column of Fig. 1. (a) A pulled front at $\varepsilon = 0.4$. (b) Simulation of the Swift–Hohenberg equation with a symmetry breaking term bu^2 added to the right-hand side. For $b > b_c(\varepsilon)$ fronts in this equation are pushed, where $b_c(\varepsilon \downarrow 0) = \sqrt{27/38}$ [421]. The simulation shown is for $b = 3$ and $\varepsilon = 0.4$, while $b_c(0.4) \approx 1.85$ [421]. Note that after a while, a second front develops; at later times this moves into the periodic state generated by the first front. This front generates a stable homogeneous state $u = const$.

The dynamics of the pushed fronts generated this way was confirmed to be associated with the existence of nonlinear front solutions with steepness larger than λ^*, in agreement with the arguments presented in Section 2.7.

(iv) The Swift–Hohenberg equation is to our knowledge essentially the only pattern forming equation for which the *existence* of pattern forming fronts has been proved rigorously and for which the pulled front selection has been established with some rigor [91–93]. In fact, the first formulation of what we refer to as coherent pattern forming front solutions appears to have been made for this equation by Collet and Eckmann [92].

(v) The Swift–Hohenberg equation has recently also been used in extensive numerical tests of the power law convergence discussed in Section 2.7 of the wavenumber of the pattern generated behind a pulled front [388]. The results which are reported in Fig. 19 below are found to be in excellent agreement with the theoretical predictions.

2.11.3. The Cahn–Hilliard equation

The Cahn–Hilliard equation is a simple model equation for the problem of phase separation and dynamic coarsening [56,192], which we will briefly review in the context of polymer phase separation in Section 3.7. The dynamical equation is based on the idea that in the phase separation regime the coarse grained free energy functional $\mathscr{F} = \int \mathrm{d}x\, \frac{1}{2}(\partial_x u)^2 - u^2/2 + u^4/4$ for the composition field u has two minima, at $u = \pm 1$, and on the idea that this composition field is a "conserved order parameter". This means that mass is neither created nor destroyed, but that it can exchange due to diffusion in response to a free energy gradient. These ingredients lead to the Cahn–Hilliard equation

$$\partial_t u = \partial_x^2 \left(\frac{\delta \mathscr{F}}{\delta u} \right) = -\partial_x^2 (u - u^3) - \partial_x^4 u \ . \tag{93}$$

Note that this gradient structure of the equation implies the conservation of composition in the following form: if we imagine taking a large system of size L with zero flux boundary conditions, then it follows immediately that

$$\frac{\mathrm{d}}{\mathrm{d}t}\int_0^L \mathrm{d}x\, u(x,t) = 0 \ . \tag{94}$$

Thus the spatially averaged composition is conserved under the dynamics.[45] The long-time dynamical behavior implied by (93) is that the system is driven towards a phase consisting of domains where u is close to one of the two minimal values ± 1, separated by domain walls or kinks. In higher dimensions the dynamics of these domains is driven by the curvature of the domains ("droplets"), while in one dimension the coarsening is driven by the interaction between the domain walls. This interaction is exponentially small for large separations, and the coarsening dynamics in one dimension is therefore quite slow.

Consider now a homogeneous state $u = u_c = constant$. If we linearize the Cahn–Hilliard equation about u_c, the resulting equation for $u - u_c$ is of the form (85) with $a=0$ and $b=1-3u_c^2$. For $u_c < 1/\sqrt{3}$ the homogeneous state is thus unstable and one can consider the following front propagation problem [266,21]: we consider an initial condition where $u \approx u_c < 1/\sqrt{3}$ everywhere except in a small localized region near the left edge, where we impose the boundary conditions $u = 1$, $\partial_x u = 0$, and investigate the front which propagates into the linearly unstable state, whose linear spreading point values are given by (88) with $a = 0$ and $b = 1 - 3u_c^2$.

An interesting aspect of the Cahn–Hilliard equation (and of similar equations with conserved dynamics) is that one can immediately see that even if uniformly translating front solutions of the type $u(x - vt)$ obeying the boundary conditions exist, they cannot be relevant for the dynamics. To see this, suppose such a solution exists; for such a solution, we would then have

$$\frac{\mathrm{d}}{\mathrm{d}t}\int_0^L \mathrm{d}x\, u(x-vt) = -v\int_0^L \mathrm{d}x\, \partial_x u(x-vt) = -v(u_c - 1) \neq 0 \ , \tag{95}$$

in contradiction with (94). A more intuitive way to understand this is as follows: because of mass conservation, the phase separation in the front region can only occur through the formation of domains of the two preferred phases. An isolated wall between two domains has no intrinsic motion. So, the region behind the front is a modulated phase with only a slow coarsening dynamics associated with the slow motion of domain walls in either direction, and a coherent solution moving with the front speed is dynamically impossible.[46]

The simulations of the Cahn–Hilliard equation of [21,267] and those shown in Fig. 15 confirm that fronts in the Cahn–Hilliard equation are pulled in agreement with intuitive notion that the nonlinearities slow down the growth. Beyond this, not much is known with certainty, as the fronts in this equation do not appear to have been investigated in any detail. The most likely scenario, it appears to us, is that the relevant front solutions are incoherent ones, since the coarsening of the pattern sets in as soon as it is formed. However, it is not excluded that the equation does admit coherent pattern forming front solutions, and that the state generated by the front is unstable to

[45] Moreover, form (93) implies that $\mathscr{F}$ is also a Lyapunov function for the dynamics: $\mathrm{d}\mathscr{F}/\mathrm{d}t = -\int \mathrm{d}x\,[\partial(\delta\mathscr{F}/\delta u)/\partial x]^2 \leqslant 0$.

[46] Such arguments apply of course more generally to conserved equations. As an example of this, the complex dynamics of bacterial flagella traces back partially to the conserved nature of the underlying dynamical equations [97].

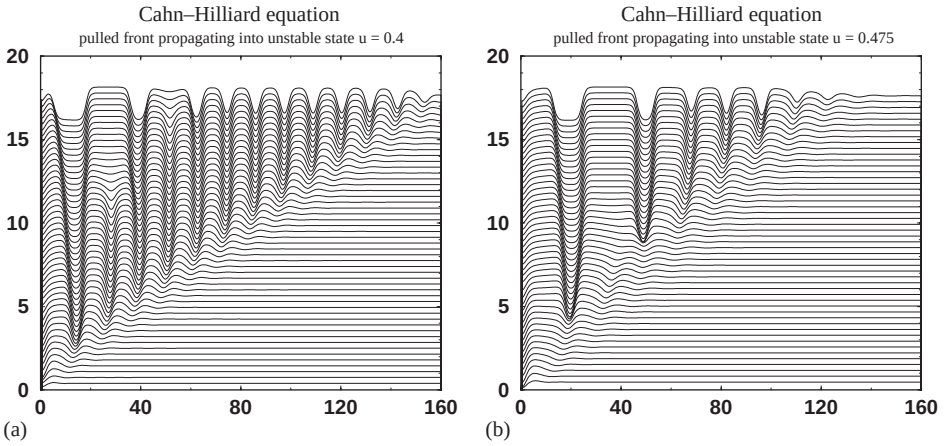

Fig. 15. Space–time plot similar to Fig. 13, but now for the Cahn–Hilliard equation, starting from a Gaussian initial condition. (a) A pulled front propagating into the unstable state $u = 0.4$. Total run time is 300, and the time difference between successive lines is 6. Note the slow coarsening (domain merging) behind the profile at later times. (b) The same for an homogeneous initial state $u = 0.475$. The total run time is 500, time difference between successive lines is 10. Note that the front propagates slower than in the case shown in (a), due to the fact that the homogeneous state on the right is less unstable.

coarsening. Indeed, since during the coarsening process domains can merge, a simple node counting argument can not be applied to predict the final state pattern. Nevertheless, it does appear from the plots that such an analysis might give a reasonable estimate of the transient domain size in the regime where the front propagation speed is rather high.[47] Whether there might possibly be a transition from coherent to incoherent pattern forming fronts as u_c is increased, has to my knowledge not been investigated.

Thus, while the linear spreading dynamics of the Cahn–Hillard equation is just a special case of that of the Swift–Hohenberg equation, the dynamical nonlinear behavior of the patterns that the front gives rise to is very different. This confirms the picture that a pulled front just propagates as is dictated in essence by the linear spreading point conditions, while the nonlinear dynamics behind it just follows in whatever way is allowed or imposed by the dynamics in the nonlinear region.

2.11.4. The Kuramoto–Sivashinsky equation

The Kuramoto–Sivashinsky equation [244,386]

$$\partial_t u = -\partial_x^2 u - \partial_x^4 u + u\partial_x u \tag{96}$$

has played an important role in the study of nonlinear chaotic dynamics. Even though the equation admits periodic solutions, it has nearby weakly turbulent states. Even though the latter states may be transient, they usually dominate the dynamics, as their survival time grows exponentially fast with the size of the system [381,448]. The scaling properties of these turbulent states, in particular the

[47] If so, the picture is somewhat similar to the one shown in Fig. 17(a) for the cubic CGL equation: the first pulled front generates a state which is unstable, and which hence is invaded by a second front.

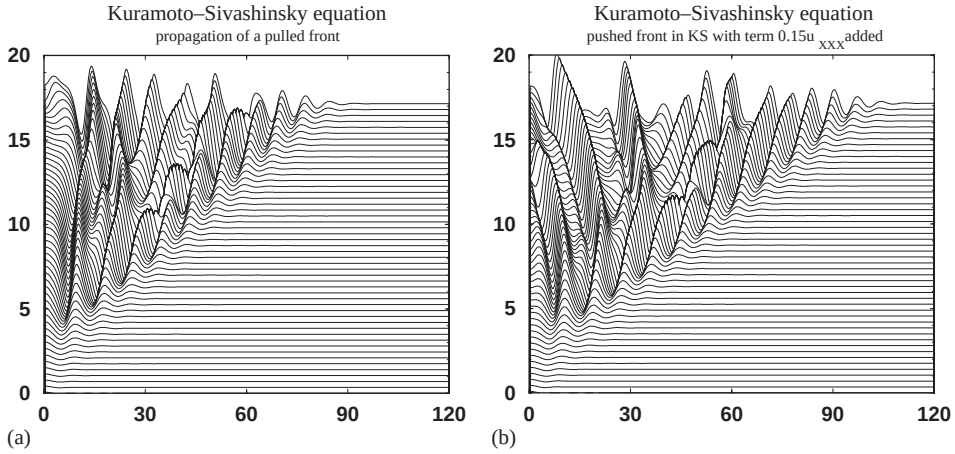

Fig. 16. Space–time plot similar to Fig. 13, but now for the Kuramoto–Sivashinsky equation, starting from a Gaussian initial condition. Total run time is 60, and the time difference between successive lines is 1.2. (a) A pulled front propagating into the unstable state $u = 0$. The state generated by the front is a weakly chaotic state of the type typically found for this equation. (b) The same but now for an extension of the Kuramoto–Sivashinsky equation, obtained by adding a term $c\partial_x^3 u$ to the right-hand side. The results of [79,196] imply that upon increasing c, a transition from pushed to pulled fronts occurs at $c \approx 0.14$. The simulations shown in the plot are for $c = 0.15$ as in [196], i.e., just above the transition, which itself is not understood in detail. Note that in this case the transition is tuned by changing a linear term in the equation, not a nonlinear term! The plots in this figure are more detailed versions of those in the right column of Fig. 1, except that there $c = 0.17$ in the lower panel.

question whether they are in the so-called KPZ universality class, has also been a subject of intense research [52,273,367,445].

Clearly, the state $u = 0$ is unstable due to the negative prefactor of the diffusion-like term, and the dispersion relation is again of the standard form (86) with $b = 1$ and $a = 0$; substitution of these values into (88) gives the linear spreading parameters for this equation for fronts propagating into the state $u = 0$.

Several authors [94] have studied the front propagation problem in this equation both numerically and analytically. Some representative simulation results are shown in Fig. 16, where starting from a localized initial condition one obtains two pulled fronts which propagate out with velocity $v^*_{4\text{th ord}}(0, 1)$ in opposite directions. Although this has to my knowledge not been investigated explicitly, it is quite clear from such simulations that these front solutions are inherently incoherent. Whether the Kuramoto–Sivashinsky admits (unstable) coherent pattern forming front solutions is not known to me; in any case this issue is probably not very relevant for the dynamics.

Another interesting feature is that when the Kuramoto–Sivashinsky equation is modified by adding a cubic term $c\partial_x^3 u$ to the right-hand side of (96), then one of the two fronts becomes pushed for a critical value of c of about 0.14 [79,196]. The pushed fronts appear to be driven by a pulse-type structure which propagates faster than $v^*_{4\text{th ord}}$, and which leaves behind a series of pulse-type structures as well. It is an understatement to say that these empirical observations are not very well understood theoretically. Possibly, in some limit it is more appropriate to think of the pushed dynamics in terms of the splitting and birth of pulse-type solutions [131,120] than in terms of a propagating front.

2.11.5. The cubic complex Ginzburg–Landau equation

The cubic Complex Ginzburg–Landau (CGL) equation

$$\partial_t A = (1 + \mathrm{i}c_1)\partial_x^2 A + \varepsilon A - (1 - \mathrm{i}c_3)|A|^2 A \tag{97}$$

with $\varepsilon > 0$ is the appropriate amplitude equation just above the onset to finite wavelength traveling wave patterns. The amplitude A is a complex quantity, and describes the slow space and time modulation of the finite wavelength mode that goes unstable [9,105,155,189,316,320,413,426,435]. The phase diagram of the dynamics behavior of this equation as a function of the real parameters c_1 and c_3 is extremely rich, and includes chaotic phases as well as coherent dynamics phases [9,81,105,382,418,419].

An important simple set of solutions of the CGL equation are the periodic or *phase winding solutions*

$$A = a\mathrm{e}^{\mathrm{i}qx - \mathrm{i}\Omega t} , \tag{98}$$

with a a constant. Upon substitution of this expression in to the cubic CGL, it is easy to check that these solutions form a one-parameter family parametrized by q, as we can express a and Ω in terms of q as

$$a^2 = \varepsilon - q^2, \quad \Omega = (c_1 + c_3)q^2 - c_3\varepsilon, \quad -\sqrt{\varepsilon} < q < \sqrt{\varepsilon} . \tag{99}$$

In an amplitude description, the phase winding solutions represent periodic traveling patterns whose wavenumber differs by q from the critical mode at the bifurcation. Because the CGL equation admits a family of these pattern-type solutions, fronts typically generate a pattern and hence are pattern forming fronts—although the CGL equation looks superficially like the F-KPP equation, the fact that the dynamical field is complex makes its dynamical behavior much more intricate (One might even say the pulled front propagation mechanism is virtually the only element they have in common!).

Not all the phase winding solutions are stable. Those near the edge of the band are always linearly unstable (the so-called Benjamin–Feir instability), while the stability of those near the center of the band depends strongly on c_1 and c_3. In fact, for $c_1 c_3 > 1$ none of the phase winding solutions is stable [105,278,279,315]. Chaotic behavior is typically found in this region of the phase diagram.

The state $A = 0$ in the cubic CGL (97) is linearly unstable; since the dispersion equation is quadratic in k, it is easy to obtain the spreading point parameters

$$v^*_{\mathrm{CGL}} = 2\sqrt{\varepsilon(1 + c_1^2)}, \quad \lambda^* = \sqrt{\frac{\varepsilon}{1 + c_1^2}}, \quad k^*_{\mathrm{r}} = c_1\sqrt{\frac{\varepsilon}{1 + c_1^2}}, \quad D = 1 + c_1^2 . \tag{100}$$

CGL equations generally admit an important class of so-called *coherent structure solutions* of the form

$$A(x,t) = \mathrm{e}^{-\mathrm{i}\hat{\Omega}t}\hat{A}(x - vt) , \tag{101}$$

which is a special case of the general form (56) of coherent pattern forming fronts. Coherent structure solutions of this type—fronts, sources, sinks, pulses [424] and other types of localized solutions [418,419]—turn out to be the crucial building blocks of the dynamics of the CGL, but we limit our discussion here exclusively to fronts. The simplicity of the coherent fronts in the CGL equation lies in the fact that they are of the coherent pattern forming type (56), but that there

is *only one* nonzero term in this sum (we can think of the function $\hat{A}$ as the term Φ_1 in this expression). Since $\hat{A}$ depend only on a single co-moving coordinate $\zeta = x - vt$, $\hat{A}$ obeys an ordinary differential equation. The multiplicity of coherent structure solutions (do they come in discrete sets, one- or two parameter families?) can therefore be studied from the number of stable and unstable manifolds near the fixed points that describe the asymptotic behavior of these solutions (so-called "counting arguments"). For fronts, these counting arguments show [424] that there generically is a two-parameter family of front solutions which to the right decay exponentially and on the back side approach a phase winding solution. Since k^* is a complex quantity, this implies that there generally will be a unique coherent front solution (101) with velocity v^* and which smoothly connects the linear spreading point behavior $e^{ik^*(x-v^*t)}$ on the right with a phase winding solution like (98) on the left.

Since the temporal phase factor is a global (x-independent) factor, one can use an argument reminiscent of the conservation of nodes argument discussed in Section 2.11.1 to calculate the wavenumber of the coherent pulled front solution. Indeed, if we compare in the frame moving with velocity v^* two points a fixed distance apart, this *phase difference is fixed* since $\hat{A}(\xi)$ is time-independent in this frame while the prefactor $e^{-i\hat{\Omega}t}$ is common to both points. By equating the temporal phase winding in this frame at the two points we then get the wavenumber q behind the front: In the leading edge to the right, $\hat{\Omega}$ simply needs to be equal to the temporal phase winding in the moving frame, $\hat{\Omega} = \omega_r^* - v^* k_r^* = -c_1$. Likewise, let us write the asymptotic phase-winding behavior behind the front for $\xi \to -\infty$ as $\hat{A}(\xi) = a e^{iq\xi}$; the amplitude a, wavenumber q and frequency Ω are then related by $\hat{\Omega} = (c_1 + c_3)q^2 - c_3\,\varepsilon + v^* q$, which is the analog of Eq. (99) in the moving frame. Equating the two expressions for $\hat{\Omega}$ and solving for the root $-\sqrt{\varepsilon} < q < \sqrt{\varepsilon}$ simply yields for the wavenumber $q_{\rm sel}$ selected by the coherent pulled front solution [321]

$$q_{\rm sel} = \frac{\sqrt{1 + c_1^2} - \sqrt{1 + c_3^2}}{c_1 + c_3}\,\sqrt{\varepsilon}\ . \tag{102}$$

Soon after the broader applicability of what we now refer to as the pulled front concept started to emerge [38,111], Nozaki and Bekki [321] studied the front propagation problem in the CGL numerically. Their results can be understood simply in combination with the results of the stability analysis of the phase winding solution $q_{\rm sel}$:

(i) In large parts of the phase diagram, the first front propagating into the unstable state $A = 0$ is a coherent pulled front of the type (101), with velocity $v^*_{\rm CGL}$ given by (100) and selected wavenumber $q_{\rm sel}$ given by (102).
(ii) If the selected mode $\sim \exp(iq_{\rm sel}x)$ is stable, a domain with this state remains behind the front.[48]
(iii) As Fig. 17 illustrates, if the $q_{\rm sel}$ is unstable due to the Benjamin–Feir instability, the domain behind the first coherent front is invaded by a second front. This front is again a pulled front [112,321], whose speed $v^*_{\rm BF}$ can be calculated explicitly in terms of $q_{\rm sel}$ and c_1 and c_3.[49] Depending on the parameters c_1 and c_3 this front can give rise either to a more stable phase winding solution, or a chaotic state. An example of the latter case is shown in Fig. 17(a).

[48] Depending on the initial conditions, this domain can subsequently be invaded by a front connecting to another phase winding solution.

[49] Since the Kuramoto–Sivashinsky equation is the amplitude equation for the Benjamin–Feir instability in the limit when the instability is weak [105], the second front is essentially a pulled Kuramoto–Sivashinsky front.

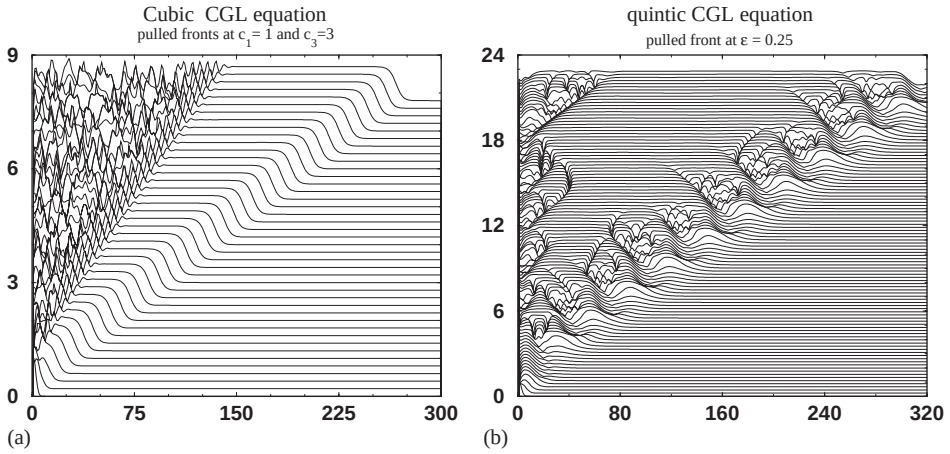

Fig. 17. (a) Space–time plot of the amplitude A in a simulation of the cubic GL equation (97) with $\varepsilon = 1$, $c_1 = 1$ and $c_3 = 3$. Time difference between successive lines is 2 and the total simulation time is 80. The plot illustrates how the first front is a pulled coherent pattern forming front of the type (101), but that the state behind the front is unstable, so that the domain with the state selected by the first front is invaded by a second front. This second front is also a pulled one. Note the similarity between the leading part of the second front and the pulled front found in the Kuramoto–Sivashinsky equation—see Fig. 16(a). This is no accident, as the Kuramoto–Sivashinsky equation is the lowest order amplitude equation just above the Benjamin–Feir instability [105,189]. (b) Space–time plot of a propagating pulled front in the quintic CGL equation with $\varepsilon = 0.25$, $c_1 = 1$, $c_3 = -1$ and $c_5 = -1$. For these parameter values, no coherent nonlinear front solution of the type (101) exists [424]. The first front is followed by a region with phase slips (points where A vanishes), before giving rise to a state close to a phase-winding solution. At the later stage, this region is invaded by another front.

Clearly, this regime can only exist if the first coherent front outruns the second one, hence in the parameter range where $v^*_{\mathrm{CGL}} > v^*_{\mathrm{BF}}$. In the frame moving with the first front, the state generated by the first front is nonlinearly convectively unstable to the Benjamin–Feir instability.

(iv) In the parameter range where the Benjamin–Feir instability becomes nonlinearly absolutely unstable in the frame moving with the first front, i.e., in the range where $v^*_{\mathrm{CGL}} < v^*_{\mathrm{BF}}$ (which is most easily entered by tuning c_3 as v^*_{CGL} does not depend on c_3) the coherent pulled front solution is irrelevant. Instead, one observes a pulled incoherent front:[50] the chaotic behavior sets in right at the front region front. The dynamical behavior in this regime is similar to that shown in Fig. 19(a) below for the pulled chaotic behavior of the quintic CGL.

In conclusion, the cubic CGL equation admits a two-parameter family of coherent front solutions. This family includes the pulled front solution, for which the selected wavenumber can be determined explicitly. The dynamics behind the first front depends on the stability of this state. When $v^*_{\mathrm{BF}} < v^*_{\mathrm{CGL}}$ the first front is a coherent pulled front, while in the opposite regime an incoherent pulled front emerges.

[50] Actually, it is conceivable that in some parameter ranges the Benjamin–Feir instability of the nonlinear region is so strong, that the very first front becomes a pushed incoherent front. To my knowledge this issue has not been studied systematically.

2.11.6. The quintic complex Ginzburg–Landau equation

Unlike the cubic CGL equation, which arises as the lowest order amplitude equation near a supercritical (forward) bifurcation to traveling wave patterns, the quintic CGL equation

$$\partial_t A = (1 + \mathrm{i}c_1)\partial_x^2 A + \varepsilon A + (1 + \mathrm{i}c_3)|A|^2 A - (1 - \mathrm{i}c_5)|A|^4 A \tag{103}$$

is a model equation for the case in which such a bifurcation is subcritical (backward). Because of the different sign of the cubic term, this term now enhances the growth of amplitude, while saturation is only caused by the quintic term. Indeed, the destabilizing cubic term implies that the only stable phase winding solutions have a finite amplitude for any ε. So an expansion based on assuming that the amplitude is small is not really justified. In other words, the quintic CGL is not a consistent lowest order amplitude equation. Nevertheless, the equation has played an important role in identifying the main coherent structures and dynamical regimes near a subcritical bifurcation. Note that the terms linear in A are the same in the quintic and cubic CGL, so the linear spreading point expressions (100) apply to the quintic CGL equation for $\varepsilon > 0$ as well.

In the subcritical range, $\varepsilon < 0$, the state $A=0$ is linearly stable, and hence a small perturbation does not spread with a finite speed: instead it will die out. However, nonlinear states, in particular phase winding solutions, can perfectly well be stable. In analogy with thermodynamic systems, where one is used to interface-type solutions between two stable phases separated by a first order transition, one expects there to be front solutions in the subcritical range $\varepsilon < 0$. When ε is increased towards small but positive values, these front solutions would then be expected to remain dynamically relevant as they have nonzero speed larger than the linear spreading speed $v^*_{\mathrm{CGL}} \sim \sqrt{\varepsilon}$. In other words, one would naively expect that for small ε fronts in the quintic CGL are pushed.

The remarkable feature of the quintic CGL is that the front solutions corresponding to the pushed fronts can be obtained *analytically* [423,424] by a generalization of the "reduction of order method" reviewed briefly in the example at the end of Section 2.7.1: When $\hat{A}(\zeta)$ with $\zeta = x - v^\dagger t$ is written in the form $\hat{A} = a(\zeta)\mathrm{e}^{\mathrm{i}\phi(\zeta)}$ and the Ansatz

$$\frac{\mathrm{d}a}{\mathrm{d}\zeta} = \sqrt{e_1(a^2 - a_N^2)}, \quad \frac{\mathrm{d}\phi}{\mathrm{d}\zeta} = q_N + e_0(a^2 - a_N^2)\ , \tag{104}$$

is substituted into the equations, one arrives at algebraic equations for the coefficients e_0 and e_1 and the wavenumber q_N and amplitude a_N of the phase winding solution behind this front solution. These coherent pattern forming pushed front solutions, which are unique for a fixed set of parameters, only exist in parts of the $\varepsilon, c_1, c_3, c_5$ parameter space: Effectively they exist only in a band around the line $c_3 = -c_5$ where the nonlinear dispersion terms almost cancel and especially in the subcritical range $\varepsilon < 0$.

The main findings of a detailed study of the existence of these solutions and of their competition with pulled front solutions are:

(i) Just like we discussed for the pulled front solutions of the cubic CGL equation, the phase winding solution with wavenumber q_N behind the pushed front can be unstable to the Benjamin–Feir instability. If it is, and if the propagation velocity v^*_{BF} is smaller than $v^\dagger$, then the size of the domain behind the first front grows as $(v^\dagger - v^*_{\mathrm{BF}})t$ in time. If $v^*_{\mathrm{BF}} > v^\dagger$, however, an incoherent pattern forming pushed front results (see Figs. 13 and 14 of [424]).

(ii) Even though the quintic Ginzburg–Landau equation always admits phase winding solutions in a subcritical range $\varepsilon_c < \varepsilon < 0$, outside a band where $c_3 \approx -c_5$ there are no pushed front solutions. This means that the "thermodynamic" intuition formulated above, according to which one always expects a pushed to pulled transition at some *finite* positive value of ε, does not apply to the quintic CGL equation (in line with the fact that there is no standard Lyapunov function for this equation). In other words, in some parameter ranges, the dynamically relevant fronts for *any* positive ε are pulled fronts! This is quite remarkable, as it means that in the parameter ranges where this happens, from the point of view of the front propagation problem the dynamical behavior is more like that found near a supercritical bifurcation.[51] This also illustrates that while for the F-KPP equation the nonlinear behavior of the growth function $f(\phi)$ determines whether fronts are pushed or pulled, the distinction between the two regimes is generally more subtle—in the quintic CGL it is determined by the strength of the nonlinear dispersion, in the extension of the Kuramoto–Sivashinsky equation it is tuned by a symmetry-breaking linear third order derivative term.

(iii) In equations where the relevant front solutions are uniformly translating ones, the pushed solutions normally bifurcate off the pulled ones continuously. In the quintic CGL equation, this is generically not the case for pattern forming fronts—see the discussion in Section 2.8. As a result, the selected wavenumber can *jump* as one goes from a coherent pulled front solution to a coherent pushed front solution (see Fig. 1(c) of [423] or 23 of [105]). Thus, the coherent pattern forming front solutions found in the quintic CGL provide a counterexample to the "structural stability" postulate [333,334] that pulled front solutions are smoothly connected to the pushed front solutions, as one tunes one of the parameters in the dynamical equation.

(iv) As we discussed, for the cubic CGL equation, so-called "counting arguments" for the multiplicity of front solutions indicate that there generally is a two-parameter family of front solutions. Although this has not been checked explicitly, we believe that for any value of the parameters there is indeed a unique pulled front solution, in line with the fact that (102) fixes q_{sel} uniquely. For pulled fronts in the quintic CGL equation, a new feature is encountered: an extension of the earlier analysis to the quintic case shows that in some parameter ranges the equations for q_{sel} behind the front do *not* admit a solution. This implies that in these parameter ranges no coherent front solutions (101) can exist [424]. Fig. 17(b) shows an example of the type of dynamical behavior that is found in this regime: in the front region the dynamics is very incoherent and associated with the occurrence of "phase slips" (points in space-time where $A = 0$). The fact that the incoherent front region is followed by a zone where A is close to a stable phase-winding solution illustrates that the incoherent front dynamics in this case is not due to an instability of the selected state, but *to the absence of a coherent pulled front solution*.

(v) Because of the subcritical nature of the transition, the quintic CGL equation also has parameter ranges at $\varepsilon < 0$ where a chaotic phase is statistically stable. If one puts such a chaotic phase next to a domain of the stable $A = 0$ phase, the front between them can move. Upon increasing ε one can then observe a pushed to pulled transition of an incoherent front—see Fig. 18.

(vi) As we discussed in Section 2.9, the universal $1/t$ power law relaxation even applies to the coherent and incoherent pattern forming fronts. This was checked numerically for the simulations

[51] For $\varepsilon < 0$, a new class of retracting fronts ($v < 0$) was recently found [103]; these solutions determine much of the dynamical behavior in the subcritical regime, especially outside the band where the pushed front solutions exist.

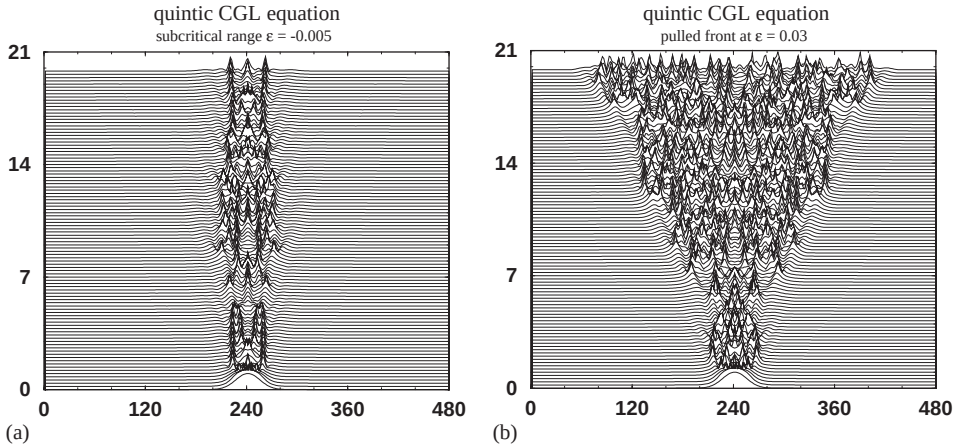

Fig. 18. Space–time plot of A illustrating the pushed to pulled transition for incoherently propagating fronts in the quintic CGL equation (103) [119]. In each plot, the total simulation time is 100, and the time difference between successive lines is 2. (a) Simulation for $c_1 = -2.2$, $c_3 = -0.5$, $c_5 = -2$ in the weakly subcritical range $\varepsilon = -0.005$. According to Fig. 15 of [424], in this range the incoherent domain in the center slowly spreads, corresponding with a pushed incoherent front with velocity ≈ 0.15, although this may be a finite-size effect. (b) The same for $\varepsilon = 0.03$.

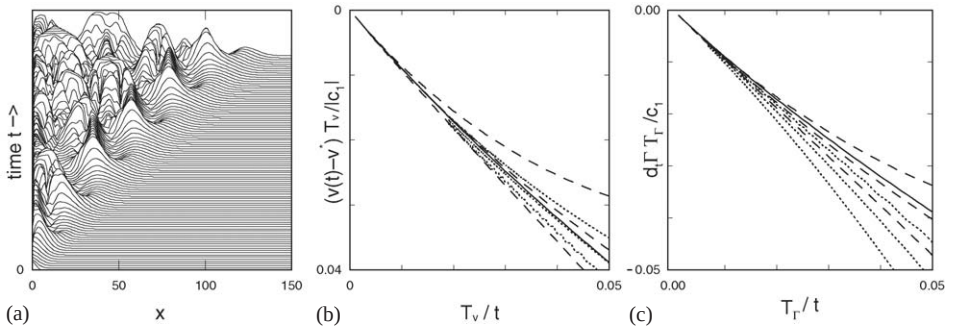

Fig. 19. (a) Space–time plot of the amplitude $|A|$ of a pulled incoherent front in the quintic CGL at $\varepsilon = 0.25$, $c_1 = 1$, $c_3 = c_5 = -3$. Note that in the leading edge, where $|A|$ is small, the dynamics is actually quite coherent, in agreement with the fact that the linear spreading dynamics is always coherent. The front only becomes incoherent once the nonlinear behavior sets in. (b) Scaling plot of the scaled velocity relaxation $[v(t) - v^*]T/C_1$ versus T/t for simulations of coherent fronts in the Swift–Hohenberg equation and the quintic CGL simulations shown in (a). Here T is a properly defined time scale introduced so that both equations fall on the same asymptotic curve, and C_1 is an appropriate combination of the linear spreading point parameters [388]. From left to right, the first three lines are Swift–Hohenberg data with $\varepsilon = 5$, at heights $u = \sqrt{\varepsilon}, 0.01\sqrt{\varepsilon}$ and $0.0001\sqrt{\varepsilon}$, and the next three lines show the CGL data traced at amplitudes 0.002, 0.0002 and 0.00002. The solid line is the universal asymptote predicted by the analytic theory. (c) The same for the appropriately scaled $\dot{\Gamma}(t)$ relaxation (84). From [388].

of the incoherent fronts of the CGL equation shown in Fig. 19(a). The other panels confirm that after scaling the velocity and time with the predicted values, both the velocity [panel (b)] and wavenumber [panel (c)] relaxation data of the incoherent quintic CGL fronts and the coherent fronts in the Swift–Hohenberg equation are in accord with the universal predictions.

2.12. Epilogue

The insight we have attempted to bring across in Section 2 is that the special nature and generality of front propagation into unstable states lies in the fact that there is a well-defined linear spreading speed v^* associated with any linear instability. The linear spreading point is the organizing center for all subsequent developments: We can make a large number of general predictions because the linear dynamics puts a strong constraint on any possible nonlinear dynamics. On the one hand, it forces us to focus on the question "how can a front faster than v^* emerge?" and this naturally leads to the concepts of pulled and pushed front. On the other hand it shows that the approach to the asymptotic velocity and state of a pulled front is governed by an equation which in lowest order is of diffusion-type, and this allows one to derive the universal asymptotic relaxation of a pulled front.

For uniformly translating fronts and coherent pattern forming fronts, the regime of pushed front propagation is essentially governed by the *existence* of special solutions which we can think of as "strongly heteroclinic orbits". For incoherent pushed fronts we are at present unable to formulate the pushed front propagation mechanism sharply, although intuitively we expect it to be very similar to that of the other two types of fronts.

The various examples in the previous section illustrate that a pulled front essentially does what it should do, namely propagate with asymptotic speed and shape dictated by the linear spreading point, while the rest of the front just follows in whatever way is allowed by the global nonlinear properties of the dynamical equation: (i) a bifurcation in the structure of the linear spreading point is responsible for the transition to coherent pattern forming fronts in the EFK equation; (ii) the quintic CGL equation illustrates that the limited range of existence of coherent pattern forming fronts can lead to a transition from coherent pulled fronts to incoherent pulled fronts; (iii) if the state generated by a front in the cubic or quintic CGL equation is unstable, the first front remains a coherent front if the spreading speed of the secondary instability is less than v^* of the first front, while the first front becomes incoherent if the pulled speed of the secondary front is larger than v^* of the first front.

The difficulty in making generic statements about pushed fronts is that apart from the fact that their convergence to the asymptotic speed $v^\dagger$ is exponential, there are few generic features. Because of the strong heteroclinicity requirements (60) or (76) that the slowest decaying exponential mode is absent, pushed front solutions are technically determined by an analysis which has all the properties of a nonlinear eigenvalue problem for an isolated solution. Because of this structure, the relaxation towards the asymptotic pushed front speed and shape is generally exponential, and singular perturbation theory can be applied to pushed fronts (Section 5). Moreover, because of this structure, whether a pushed front solution exists depends on the full *global* and hence *nonlinear* properties of the equations. As a result, virtually every example is special, and there are few nontrivial examples which one has been able to obtain analytically. The quintic CGL equation is a remarkable exception in this regard.

As we discussed, with few exceptions, most mathematical investigations of front propagation into unstable states have focused on uniformly translating fronts and in particular on systems of equations which are closely related to the F-KPP equation. It appears to us that many of the ingredients of the theoretical framework that we have discussed here are ready for more rigorous analysis: rigorous developments that I expect are around the corner are (i) rigorous bounds for the Green's function of whole classes of linearized equations and, in relation with this, rigorous proofs of the pulled

front mechanism of new classes of equations, (ii) proofs of the universal relaxation of pulled fronts, (iii) the development of a mathematical framework for the pulled to pushed transition of coherent pattern forming fronts, and (iv) extension of the approach of Sandstede and Scheel [374,375] to analyze the interaction between front dynamics and the dynamics of the state behind the front, or to classify defects.

3. Experimental and theoretical examples of front propagation into unstable states

In this section we discuss a number of examples of front propagation into unstable states. We first review experiments on fronts or in which front propagation plays an important role, and then move on to discuss examples of fronts in theoretical models. The examples concern mostly fronts in one dimension. The difficulty of analyzing patterns whose dynamics is governed by the propagation of pulled fronts is discussed later in Section 5.

At first sight, one might well wonder why front propagation into unstable states is a relevant problem anyway. After all, it seems counterintuitive that a physical system would naturally end up in an *unstable* steady state and wait for a nice front to develop! On closer inspection, however, there are many reasons why front propagation into unstable states is not an esoteric problem:

(i) A natural way in which a system can stay in a self-sustained unstable state is when an overall flow or motion makes the instability convective (see Sections 2.5 and 2.10). This happens in particular in many fluid dynamic systems. Likewise, in plasma physics the strong asymmetry between the mobility of electrons and ions usually makes plasma instabilities convective. Examples where these considerations apply are discussed in Sections 3.5, 3.9, 3.10, 3.11, 3.12, and 3.17.

(ii) Sometimes a natural way to probe a system is to quench it into an unstable state with a laser pulse, ramping or flipping a voltage, flipping a plate, dropping a temperature, scraping a skin tissue, etc. In all these cases, the relevant question is whether we can change the system on a timescale shorter than the natural time scale of the evolution of the state into which we quench it. Examples are encountered in Sections 3.1, 3.2, 3.3, 3.5, 3.6, 3.7, 3.14, 3.15, and 3.20.

(iii) We sometimes encounter intrinsically chaotic systems where the dynamics itself continuously generates states which are transient because they themselves are unstable. We discuss a clear example of this in Section 3.4.

(iv) In thermodynamic systems with first order transitions, interfaces play a predominant role because the bulk nucleation rate is exponentially small near the transition, while interface velocities usually vary linearly with the distance from the transition. Although fluctuations near a second order thermodynamic transition are usually too large to allow clear fronts to develop, this is not necessarily true for polymer systems (Section 3.7). Moreover, near supercritical ("second order like") bifurcations in pattern forming systems, where fluctuation effects are usually small [105], a similar argument holds as well: as we shall discuss more explicitly in the next subsection, if ε is the dimensionless control parameter measuring the distance from the instability threshold, the front speed scales as $\sqrt{\varepsilon}$ while the growth rate of bulk modes scales as ε. Hence, front propagation in principle always dominates for sufficiently small ε [161]. Of course, the range over which fronts do dominate the dynamics depends on the prefactors, i.e. on the time and

length scales of the problem under investigation. Such considerations play a role in the examples of Sections 3.1, 3.2, 3.3, 3.5, 3.7, 3.8, and 3.14.

(v) Front propagation into an unstable state sometimes emerges theoretically from an unexpected angle through mapping a seemingly unrelated problem onto a front propagation problem—see Sections 3.21, 3.23, 3.25, 3.26.1 and 3.26.5.

3.1. Fronts in Taylor–Couette and Rayleigh–Bénard experiments

Soon after Dee and Langer [111] and Ben-Jacob and co-workers [38] drew the attention of the physics community to the special simplicity of what we now refer to as pulled fronts, two experiments on pattern forming systems were done that are still very illuminating: One by Ahlers and Cannell [4] on vortex fronts in a Taylor–Couette cell, and one by Fineberg and Steinberg [161] on front propagation in a Rayleigh–Bénard cell.

A Taylor–Couette cell consists of two concentric cylinders which can rotate independently. The gap between the two cylinders is filled with a normal Newtonian fluid. When the inner and outer cylinder rotate slowly, the flow between the two cylinders is laminar and in the azimuthal direction. At higher rotation rates, one finds an amazing number of fluid dynamics instabilities when both the inner and the outer cylinder are rotating with sufficiently high frequencies [105,125]. The experiments that are of interest to us probed fronts that lead to the first nontrivial patterned state that emerges if the rotation rate of the inner cylinder is increased while the outer cylinder does not rotate [4]. At some critical rotation rate, there is a bifurcation to a state with so-called Taylor vortices: a pattern which is periodic in the direction along the axis of the cylinders emerges. This flow is referred to as Taylor vortex flow, since the velocity in the r,z plane has the appearance of alternating clockwise and counterclockwise rotating vortices that span the whole gap between the two cylinders.

A Rayleigh–Bénard cell consists of a fluid sandwiched between two parallel plates at a fixed but different temperature. When the bottom plate is hotter than the top plate, the fluid density is largest at the top. For small enough temperature differences, there is no convection—there is just heat conduction through a quiescent fluid. However, when the temperature difference and hence the density difference becomes larger than some threshold value, this simple state is unstable and convection sets in spontaneously [105,155,189,282]. The convection patterns that emerge just above threshold are often referred to as rolls, but if we look at the velocity pattern in a vertical cross section, they look like the vortex-type patterns in the r,z cross-section of the Taylor–Couette cell.

The transition to Taylor vortex patterns and to convection patterns in the Rayleigh–Bénard case are both examples of forward (supercritical) bifurcations to a stationary finite wavelength patterns. Just above onset, the patterns can be described by a so-called amplitude expansion by writing the physical fields in terms of the complex amplitude as [105,189,193,316,320]

$$\text{physical fields} \;\propto A\mathrm{e}^{\mathrm{i}k_c x} + A^*\mathrm{e}^{-\mathrm{i}k_c x}\ . \tag{105}$$

For simplicity, we restrict the analysis to one-dimensional patterns as this is the relevant case for the front experiments; k_c is the wavenumber of the pattern at onset, and x is the coordinate along which the patterns develop. The amplitude expansion simply implements the observation that just above onset the amplitude of the patterns is small, and that the amplitude A varies on slow space and

time scales. In lowest order, A then obeys the so-called real Ginzburg–Landau amplitude equation [52] [105,155,189,316,320,413,435]

$$\tau_0 \partial_t A = \varepsilon A + \xi_0^2 \partial_x^2 A - g|A|^2 A \ . \tag{106}$$

Here ε is the dimensionless control parameter, which for $\varepsilon > 0$ is a measure for how far one is above the instability threshold. The time scale τ_0 and length scale ξ_0 depend on the particular system, and can be calculated explicitly from the linear dispersion relation of the system under study. This has been done both for the transition to Taylor vortices and for the transition to Rayleigh–Bénard convection patterns. The nonlinear parameter g, which follows from the amplitude expansion, is also known for both systems, but it, of course, does not play a role for the pulled fronts of interest here.

The real amplitude or Ginzburg–Landau equation should in general not be thought of as just a simple straightforward generalization of the F-KPP equation to a complex field—while the F-KPP equation only allows for stable homogeneous solutions $u = \pm 1$, the amplitude equation admits stable phase winding solutions of the form $A = a e^{iqx}$ with a and q constant [105,155,189,320,435]. As (105) illustrates, these describe physical patterns with a wavenumber $k_c + q$ different from the critical wavenumber. The interaction and competition between the various modes in general makes the dynamics of the amplitude A much more interesting and complicated than that of the F-KPP equation. Nevertheless, since the dynamics of pulled fronts is dominated by the linear terms in A, and since these are the same for the two equations, both the asymptotic pulled front solutions and the convergence to them are the same for the two equations.

The attractive feature of the experiments is that because ξ_0 and τ_0 are known explicitly, they offer the possibility to study front propagation *quantitatively*. Indeed, for the amplitude equation in form (106) we get for the pulled front speed

$$v^*_{\text{ampeq}} = 2\frac{\xi_0}{\tau_0}\sqrt{\varepsilon} \ . \tag{107}$$

This result explicitly confirms the assertion made already in point (iv) at the beginning of Section 3 that near a supercritical bifurcation, the front speed increases as $\sqrt{\varepsilon}$, while the growth rate of bulk modes according to (106) increases linearly in ε. As stressed by Fineberg and Steinberg [161], front propagation into unstable states can therefore generally be observed at small enough ε, i.e. just above the onset of the transition.

In order to compare the measured front velocities to the F-KPP equation in the standard form in which the prefactors of the linear terms are equal to 1, the experimental results have been reported in terms of the scaled velocity

$$\tilde{v} = v\frac{\tau_0}{\xi_0\sqrt{\varepsilon}} \ . \tag{108}$$

Of course, front speeds should only converge to v^*_{ampeq} if the initial condition is sufficiently localized, as explained in Section 2.7.6. In both experiments, the system was initially below the instability threshold, corresponding to $\varepsilon < 0$ in the amplitude equation (106), and then brought above threshold ($\varepsilon > 0$) at time $t = 0$. In the Taylor–Couette experiment, even below threshold, when the bulk of

[52] The equation—used as the amplitude equation (106) in the discussion of fronts in Rayleigh–Bénard and Taylor–Couette experiments in Section 3.1 below—is called the real Ginzburg–Landau equation because the prefactors of all the terms are real. The amplitude equation for traveling wave patterns is the CGL equation; as discussed in Section 2.11.5, in principle all its terms have complex prefactors [105,189,435].

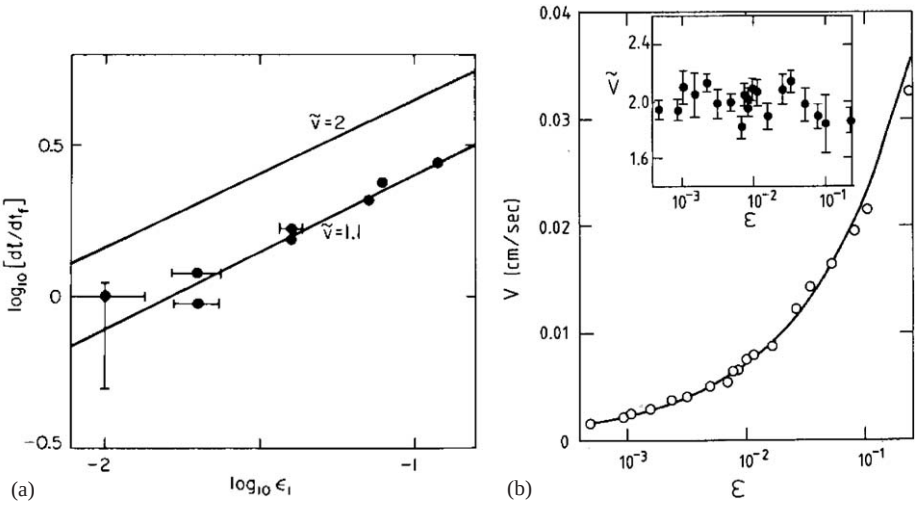

Fig. 20. (a) Velocity data of fronts in the Taylor vortex experiments of Ahlers and Cannell [4]. Data are plotted on a log–log scale as a function of ε. The solid lines have slope $\frac{1}{2}$ and hence illustrate the $\sqrt{\varepsilon}$ scaling of the velocity. The lower line shows that the data are consistent with a scaled velocity $\tilde{v} \approx 1.1$ instead of the asymptotic values $\tilde{v}^{\mathrm{as}} = 2$. (b) Experimental data of Fineberg and Steinberg [161] on fronts in the Rayleigh–Bénard system on a log-linear scale. The solid line is the theoretical prediction (107). The inset shows the scaled velocity $\tilde{v}$ which is consistent with the theoretical asymptotic value 2, within the error bars.

the cell is in the stable laminar flow state, there are so-called Ekman vortices at the ends of the cylinders. These play the role of localized nonzero initial conditions for the amplitude A when the system is brought above threshold at time $t = 0$. For the Rayleigh–Bénard experiment, Fineberg and Steinberg used a long cell, so as to get one-dimensional fronts, and they turned on an extra heater at the cell ends as well, when they brought the system to $\varepsilon > 0$. This made the convection patterns nucleate at the ends and then propagate into the bulk of the cell.

Fig. 20(a) shows the velocity of the Taylor vortex fronts as they propagate into the Taylor–Couette cell over a distance of up to 10 to 15 vortex diameters [4], plotted on a log-log scale. As the two solid lines indicate, the $\sqrt{\varepsilon}$-scaling of the vortex velocity is confirmed, but the prefactor is only about 55% of the predicted asymptotic values $\tilde{v}^{*}_{\mathrm{ampeq}} = 2$: the data are consistent with $\tilde{v} \approx 1.1$ instead of 2.

The fact that the measured front velocity was significantly below the asymptotic value in this 1983 Taylor–Couette experiment made many researchers wonder whether there was something crucially wrong,[53] and stimulated Fineberg and Steinberg a few years later to perform experiments on fronts in Rayleigh–Bénard convection. Actual space–time plots of their convection front profiles as they propagate to the right along their cell, are shown in Fig. 21(a). These traces illustrate how these fronts (as well as those in the Taylor–Couette cell) are examples of true *pattern forming fronts* propagating

[53] It was realized that if the measured velocity had been too high, a possible candidate for the discrepancy could have been that the initial convection profile associated with the Ekman end vortices was not sufficiently localized, i.e., that at $t = 0$ the amplitude did not fall off to the right faster than $\mathrm{e}^{-\lambda^* x} = \mathrm{e}^{-\sqrt{\varepsilon} x/\xi_0}$. However, as we discussed in Section 2.6, asymptotic front speeds below v^* are impossible.

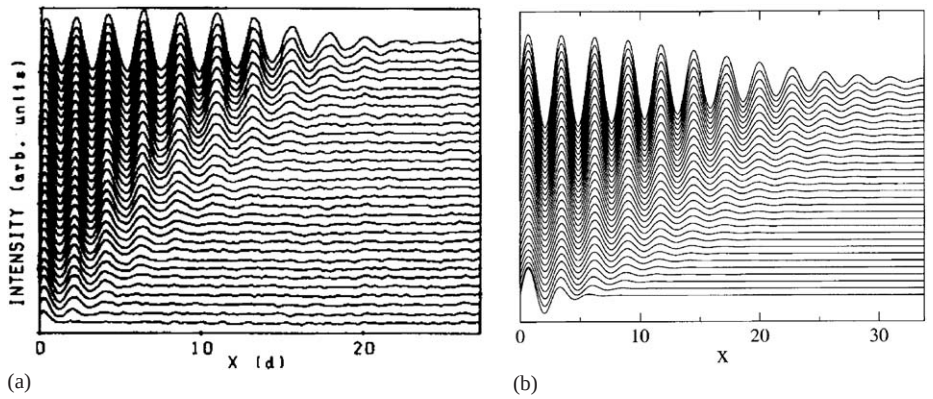

Fig. 21. (a) Space–time plot of a propagating front in the Rayleigh–Bénard experiment of Fineberg and Steinberg [161] for $\varepsilon = 0.012$, made using the shadowgraph technique. The time between successive traces is 0.42 t_v, where t_v is the vertical diffusion time in the experiments, and distances are measured in units of the cell height d. (b) A space-time plot obtained from a numerical simulation of the Swift–Hohenberg equation at the same value $\varepsilon = 0.012$ and length and time scales adjusted to correspond to those in the experiments of (a). After Kockelkoren et al. [233].

into an unstable state, like those observed in simulations of the Swift–Hohenberg equation (92), see the central panel of Fig. 1, and Figs. 14(b) and 21(b).

The data of Fig. 20(b) for the scaled front velocity $\tilde{v}$, calculated from the actual data by using the theoretical values for ξ_0 and τ_0 in (108) were found to be consistent to within a few percent with the asymptotic value $\tilde{v}^{\rm as} = 2$. At the time, this was considered to be an important experimental confirmation of the quantitative prediction of the pulled front speed, and of the idea that the concept of a pulled front applies more generally to pattern forming systems. But, as we shall see, there is a new twist to the story.

The reason for the apparent discrepancy between theory and experiment on the Taylor vortex fronts remained unresolved till Niklas et al. [319] performed an explicit numerical simulation of such fronts which showed that the front speed had not yet relaxed to its asymptotic value, in contrast to what was found in numerical studies of the propagating fronts in the Rayleigh–Bénard cell [271]. Indeed, over the range of times probed experimentally, the transient speeds they found for the Taylor vortex fronts were quite consistent with the experimental data. Instead of showing these results, we will approach this issue by extrapolating back from the asymptotic formula (78) as this allows us to discuss both experiments in a unified way.

When (78) is applied to the amplitude equation, one finds for the long time rate of approach to the asymptotic speed $\tilde{v}^* = 2$

$$\tilde{v}(t) = 2 - \frac{3}{2\varepsilon t/\tau_0} + \frac{3\sqrt{\pi}}{2(\varepsilon t/\tau_0)^{3/2}} + \cdots \ . \tag{109}$$

This formula shows that in any experiments on fronts just above the onset of a finite-wavelength supercritical bifurcation, one can a priori only hope to observe front speeds very close to the asymptotic value at times

$$t \gg t_{\rm co} \equiv \tau_0 \pi/\varepsilon \ . \tag{110}$$

Note that we have defined the crossover time t_{co} as the time at which the third correction term is equal in magnitude to the first correction term in (109). Although this asymptotic formula is only valid in the long-time regime when the third term is much smaller than the second one, and although for times of $\mathcal{O}(t_{co})$ one is in the non-universal crossover regime, the important message is that the velocity always approaches the asymptotic value *from below* and that transient effects are very significant, even for times of order several t_{co}. For example, even at times of $\mathcal{O}(3t_{co})$ when the formula becomes reasonably accurate [144], the velocity is still some 8% below its asymptotic value, and at t_{co} both corrections terms, though of opposite sign, are about 24% of the asymptotic value in magnitude.

When an actual experiment is suddenly brought into the unstable parameter range $\varepsilon > 0$, bulk modes also start to grow at a rate proportional to ε. Since one can only study fronts properly as long as bulk fluctuations have not grown enough that bulk "nucleation" starts to become visible, in practice experiments like those we consider here can only be done up to a time which scales as ε^{-1} [4,161]. In other words, *experiments can in practice only be done up to a time which is a finite multiple of* t_{co}!

In the Taylor vortex front experiments, most measurements for $\varepsilon = 0.02$ were done in the time interval of 1–2 t_{co}. It is therefore not surprising that transient effects did play an important role in these experiments [319,422] and that the measured velocity was significantly below the asymptotic value. However, from our present perspective, it *is* important to turn the question around and ask whether the fronts observed in the Rayleigh–Bénard experiments were indeed propagating with approximately the asymptotic speed, and if so, why so [233].

As it turns out, in the experiments of Fineberg and Steinberg, growth of bulk modes also limited the observation of fronts to times of order t_{co} [161]. Kockelkoren et al. [233] therefore reanalyzed the experiment from this perspective, and concluded that most likely the actual measured front speed *was* some 15% below the asymptotic one. In their interpretation, the theoretical value for ξ_0 used in converting the observed front speeds to dimensionless front speeds $\tilde{v}$ may have been about 15% smaller than the actual one.[54] If so, the velocity had been overestimated by about this amount in the interpretation of the experiments, thus hiding a possible transient effect.

We stress that only new experiments can settle whether this interpretation is the correct one. However, there are also indications in the actual traces of the fronts in Fig. 21(a) that the velocity in this run was slowly increasing in time. The solid line in Fig. 22(a) shows the experimental velocity as a function of time, extracted by measuring successive front positions with a ruler and using a value of ξ_0 which is 15% larger than the theoretical value [233]. For comparison, a plot of the velocity as function of time in a simulation of the real Ginzburg–Landau equation (106) is shown with a dashed line.

One important point has not been included in the theoretical analysis so far. When growth of bulk modes in practice becomes important for times of order t_{co}, then at the latest times the growth of the bulk fluctuations may become important. This will have the effect of *increasing* the velocity above the one studied analytically and numerically with localized initial conditions and in the absence of fluctuations. With this caveat, we nevertheless tentatively conclude that both experiments on fronts

[54] Indications that this may be the case come from fact that the observed wavelength at onset was also about 13% bigger than the theoretical one. See [233] for further discussion of this.

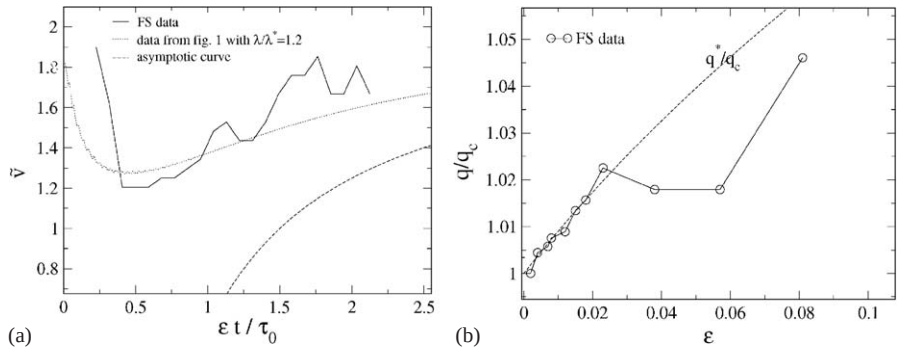

Fig. 22. (a) Full line: scaled velocity versus time in the Rayleigh–Bénard front [161] whose space-time plot is shown in Fig. 21(a). The velocity is obtained by interpolating the maxima of the traces. As explained in the text, a value of ξ_0 which is 15% bigger than used by Fineberg and Steinberg to convert the data. A different value would not change the shape of the curve, only the absolute numbers on the vertical axis. The dashed line shows the measured velocity in a simulation of Eq. (106) with an exponential initial condition $A(x,0) \sim e^{-1.2\lambda^* x}$ and the dotted line the asymptotic result (109) with the $t^{-3/2}$ term excluded. Note that the curves are not fitted, as only the absolute vertical scale is affected by our choice of ξ_0. (b) Open circles: data-points for the wavenumber selected by the front in the experiments of Fineberg and Steinberg. Dashed curve: q^*/q_c for the Swift–Hohenberg equation with parameters corresponding to the Rayleigh–Bénard experiment. The fact that the data follow the line q^*/q_c for small ε, indicates that just above threshold the experiments probe the leading edge of the front. After Kockelkoren et al. [233].

in pattern forming systems illustrate that such fronts are prone to transient behavior associated with the slow power law relaxation of pulled fronts from below to v^*.

As a final note, we point out that both experiments also addressed the *wavelength selection* by the front. Wavelength selection goes beyond the lowest order amplitude equation (106), since the real F-KPP-type fronts in this equation simply yield a wavenumber equal to the critical wavenumber k_c throughout the front, to order $\sqrt{\varepsilon}$. For the changes in order ε, one needs to start from the linear dispersion relation of the problem, correct to order ε. In the original paper on the Rayleigh–Bénard experiment, the data were compared to the results for the selected wavelength in the Swift–Hohenberg equation (92). Strong deviations were found in this case. The most likely explanation for this is the following [233]: for small ε, the full front whose width scales as $1/\sqrt{\varepsilon}$ is too wide to even fit in the experimental cell; hence one then cannot measure the selected wavenumber *behind* a fully developed pulled front, but instead only an effective wavenumber in the leading edge of the front which is close to the local wavenumber k_r^* given in (88). Fig. 22(b) shows that indeed the Rayleigh–Bénard data for small ε are consistent with this.

More recently, the problem of fronts in the Rayleigh–Bénard and Taylor–Couette system has been analyzed in great detail by Lücke and co-workers [68–70,210,269–271,349,361], both in the case discussed here and in the presence of a throughflow (see Section 3.11). In these approaches, the front predictions based on the lowest order amplitude equation are compared in detail with those for pulled fronts obtained by determining the linear spreading point of the full Navier–Stokes equations for this system, and with full numerical simulations. We refer to these papers for a detailed discussion of how the full result starts to differ from the lowest order amplitude result as ε increases. In particular, the effect that the nodes of the fields drift in the front region before coming to rest behind the front is a characteristic effect that goes beyond the amplitude equation (the Swift–Hohenberg equation also shows this, of course).

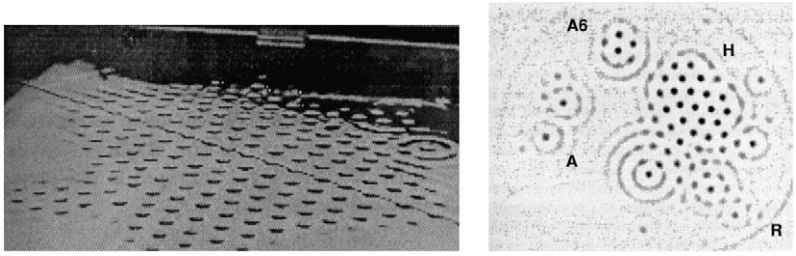

(a) (b)

Fig. 23. (a) Photograph of a well-developed array of pendant drops at the end of the experiments of Fermigier, Limat, Wesfreid et al. [158,159,265]. The drops are seen from above through the glass plate across which the film was spread before the system was made unstable by flipping the plate. From [265]. (b) Two-dimensional patterns observed in the Rayleigh–Taylor instability of a thin layer in the same experiments [159,265]. Note that a "roll" or "stripe" type pattern generally appears near the boundary of the regions. The two structures labeled *A* and *A*6 were initiated by small dust particles on the interface. When they grow, they usually develop into a six-field symmetric hexagonal pattern like in H. The pattern near R was initiated by the thickness gradient close to the edge of the fluid layer.

3.2. The propagating Rayleigh–Taylor instability in thin films

The name Rayleigh–Taylor instability refers to gravitational instabilities of the interface between two fluids or of stratified fluids [78]. A simple example is when one has two immiscible fluids separated by a planar interface, in which the heavier fluid is on top of the lighter one. More generally the instability arises in density-stratified fluids, when the acceleration is directed from the heavier to the lighter fluid. The instability is important in a variety of practical situations, ranging from explosives to the spreading of paint or coating on a solid surface.

About a decade ago, Fermigier, Limat, Wesfreid and co-workers [158,159,265] performed a series of experiments on the Rayleigh–Taylor instability of thin films. They studied pattern selection by first spreading thin films of silicon oil on a flat solid plate, and then making the system unstable by flipping this plate upside down. For films of suitable thickness, the instability develops slowly enough that it can easily be studied. The photo of Fig. 23(a) illustrates that the typical hexagonal patterns that one often observes after the instability is well-developed. The experiments illustrate several basic issues in pattern formation,[55] but we will focus here on the propagating fronts. Right

[55] For example, the generic appearance of hexagonal patterns is associated with the fact that the thin film equations (112) below for the deviation ζ of the film thickness from the uniform value, are not invariant under a change of sign of ζ (see [51] and references therein). In the Rayleigh–Bénard instability hexagonal patterns generically arise for the same reason very close to threshold, since very small non-Boussinesq effects break the symmetry that the Boussinesq equations happen to exhibit. Furthermore, the fact that the pattern looks stripe-like near the edge, even though the pattern is hexagonal in the bulk—see Fig. 23(b)—is a generic phenomenon (also known in convection, see e.g. [51]) which can be understood simply from symmetry considerations [350]: When one considers a front or domain wall solution in the amplitude equations for the three modes necessary to describe a hexagonal pattern, symmetry considerations dictate that the prefactor of the spatial second derivative term of the modes whose wavevector is normal to the front is a factor two larger than those of the other two modes whose wavevector makes an angle of 60° with the front normal. This means that the "coherence length" or correlation length of this first mode is larger than that of the other two modes, and that the pattern in the front region looks stripe-like [350] (see also [106,126]).

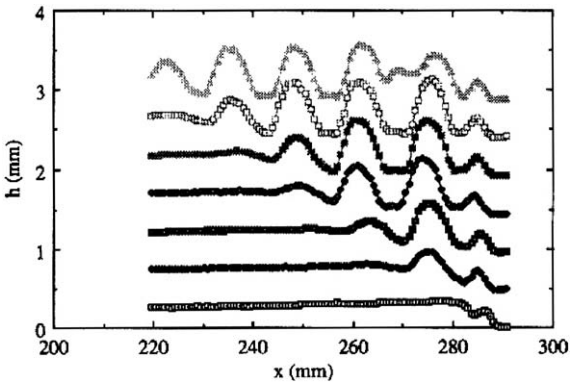

Fig. 24. Time evolution of the thickness profile as a Rayleigh–Taylor front propagates into an unstable state in the experiments of Fermigier, Limat, Wesfreid and co-workers [158,265]. The profiles have been shifted up for clarity and are separated by time intervals of 30 s. x designates the coordinate perpendicular to the stripe-type pattern in the front region.

after the plate has been flipped, a film of uniform thickness is linearly unstable. In many cases, the instability first developed near the boundary of the sample and then propagated into the bulk of the sample. Fig. 24 shows experimental traces of such a front as it propagates into the unstable state [265].

The equations that describe the evolution of a thin liquid film are well known: the separation of length scales allows one to simply integrate out the coordinates perpendicular to the film layer ("lubrication approximation") [324]. If we denote for the experimental case of the free film flow the film height h as the thickness of the film measured from the plane, the dynamical equation for h becomes [324,158]

$$\partial_t h + \frac{1}{3\eta}\nabla_\perp \cdot [h^3 \nabla_\perp (\rho g h + \gamma \nabla_\perp^2 h)] = 0 \ , \tag{111}$$

where η is the viscosity, ρ the density of the liquid, g the gravity, γ the surface tension, and $\nabla_\perp$ the gradient operator in the direction along the surface. To study the stability of a film of uniform thickness h_0, we note that if we substitute $h = h_0 + \zeta$ into (111), the equation can be writted in the form

$$\partial_t \zeta + \frac{h_0^3}{3\eta}(\rho g \nabla_\perp^2 \zeta + \gamma \nabla_\perp^4 \zeta) = N(\zeta, \nabla_\perp \zeta, \nabla_\perp^2 \zeta) \ . \tag{112}$$

Here N denotes all terms which are nonlinear in ζ and its derivatives. As noted in [158], the linear terms in (112) are exactly the same as the linear terms appearing in the various model equations discussed in Section 2.11 (the Kuramoto–Sivashinsky equation, the Cahn–Hilliard equation or the Swift–Hohenberg equation at $\varepsilon = 1$). After a proper rescaling of space and time units, the pulled front velocity v^* for the Rayleigh–Taylor fronts in the thin film experiments is therefore just given by Eq. (88).

The experimentally observed front speed was indeed found to be consistent with the pulled speed v^* within the uncertainty of the experimental measurements and the theoretical estimate (which was of order 30%). In addition, there seemed to be a clear trend for the front patterns to have

a wavelength some 5% smaller than the wavelength corresponding to the most unstable mode. This is also what would be expected from the results for pulled fronts with the above linear dispersion relation.

Although the results of the experiments thus seem to indicate that the Rayleigh–Taylor fronts in the experiment are examples of pulled fronts, we do want to express an important caveat: just like the bifurcation to hexagonal convection patterns is generally subcritical (except when a symmetry imposes the equations to be invariant under a change of sign of the dynamical fields), the bifurcation to hexagonal Rayleigh–Taylor patterns should be expected to have a subcritical character too; indeed this is indicated by the weakly nonlinear results in [158]. This suggests that when the instability is weak, one will actually get pushed rather than pulled fronts. However, to my knowledge this possibility has neither been explored theoretically nor experimentally.

3.3. Pearling, pinching and the propagating Rayleigh instability

Another instability with which Rayleigh's name is associated is the instability of a cylindrical body of fluid [78]. In daily life, we encounter this phenomenon when a stream of water from a tap breaks up into drops or when the paint on a thin wire or hair of a brush breaks up into droplets. The instability is caused by the surface tension: for a "peristaltic" perturbation of the radius of the cylindrical fluid, the capillary pressure due to surface tension is enhanced in the narrower region and reduced in the wider regions; this pressure difference tends to enhance the perturbation even more.

In tubular membranes, the instability normally does not arise, since membranes generally have a small surface tension but a high bending rigidity, which measures the resistance of the membrane against changes in the curvature. However, Bar-Ziv and Moses [26] observed that when they applied laser tweezers to their tubular membranes, a sinusoidal instability developed, see Fig. 25(a). This instability propagated out at a constant velocity in both directions from the point of application of the tweezers. Presumably, the instability is due to the fact that the tweezers pull some lipid molecules into the trap, and that as a result the surface tension increases, rendering the cylindrical geometry unstable. Indeed, as pointed out in [26], for a tube with surface tension Σ and bending modulus κ, the free energy $\mathscr{F}$ can be written as

$$\mathscr{F} = \int \mathrm{d}S[\Sigma + 2\kappa H^2] \ . \tag{113}$$

Here H is the mean curvature and the integral is over the surface S. For a tube with cylindrical symmetry and the z-coordinate along the axis, we can write the terms in $\mathscr{F}$ in terms of $r(z)$ as

$$\mathrm{d}S = \mathrm{d}z\, 2\pi r\sqrt{1+r_z^2}, \quad H = \frac{r_{zz}}{(1+r_z^2)^{3/2}} - \frac{1}{r(1+r_z^2)^{1/2}} \ . \tag{114}$$

As pointed out by Bar-Ziv and Moses a tube of constant radius R exhibits the Rayleigh instability when the surface tension is above a critical value $\Sigma_c \approx 3\kappa/R^2$. Above this value the free energy is lower for a periodically modulated tube than for a tube of constant radius. As $\kappa \to 0$ one recovers the pure Rayleigh instability. Thus, the experimental scenario is that the laser tweezers pull in the lipid molecules, and that the increase in surface tension that this entails is large enough for the membrane to become unstable.

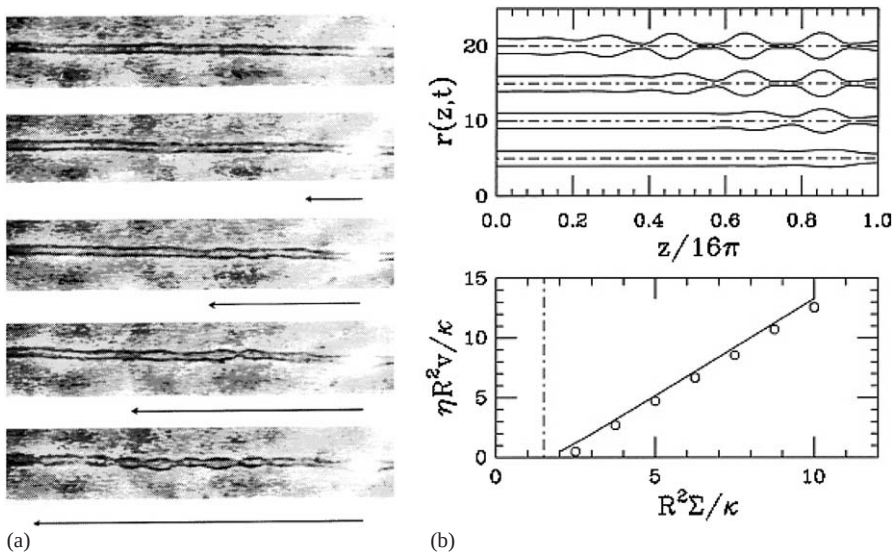

Fig. 25. (a) Photographs showing the pearling front along a tubular membrane formed by lipid bilayers in the experiments of Bar-Ziv et al. [26,27], as it propagates out from the bright laser spot on the right. In this experiment the dimensionless control parameter $\varepsilon = (\Sigma - \Sigma_c)/\Sigma_c = 6.5$. From top to bottom the times are 0.14, 0.68, 0.86, 1.04 and 1.22 s after the laser was turned on. The arrow indicates the leading edge as it was determined by the authors. The height of each photographs corresponds to a distance of about 10 μm. (b) Results by Powers and Goldstein [356] for the simplified model (115) for the pearling instability. The top panel shows four snapshots of the pearling obtained from numerical simulation of the model. The higher snapshots are obtained at later times, so the front is traveling to the left. Bottom panel: dimensionless front velocity as a function of the ratio of surface tension and bending modulus. The solid line denotes the pulled front velocity v^*, the dots the data obtained in the numerical simulations. Note that the data points lie slightly below the curve for v^*. Undoubtedly, this is due to the slow convergence of the front speed to the asymptotic speed v^*.

The pearling instability through propagation of the Rayleigh fronts that the experiments suggest have been studied theoretically by Powers and Goldstein and co-workers [356,185], who pointed out that in the approximation that the flow profile through the tube remains a parabolic Poiseuille profile,[56] the dynamical equation for the tubular interface becomes

$$\partial_t r^2 = \frac{1}{4\eta}\,\partial_z\left(r^4\partial_z\left[\frac{\delta\mathscr{F}}{\delta r}\right]\right)\ , \tag{115}$$

where $\mathscr{F}$ is the interfacial free energy given in Eq. (113) above. The numerical results from [356] for this equation are shown in Fig. 25(b). The top panel shows four snapshots as the Rayleigh front propagates along the tube, generating strongly nonlinear bead-like undulations behind it. In the lower panel the velocity of these fronts is compared to the pulled front velocity v^* for this model

[56] This approximation, which is in the spirit of the the thin-film equations described in the previous section, is justified in the limit in which distortion of the tube diameter happens on length scales much longer than the tube diameter. This is not really true for the Rayleigh instability. Nevertheless, the equation is expected to capture the essentials of the pearling instability.

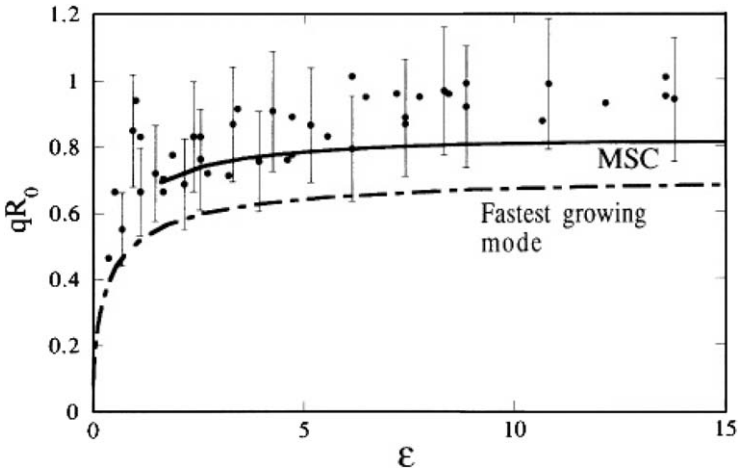

Fig. 26. Experimentally measured values of the wavenumber of the pearling instability as a function of the dimensionless control parameter $\varepsilon = (\Sigma - \Sigma_c)/\Sigma_c$ in the experiments of Bar-Ziv et al. [27]. The line labeled MSC is the wavenumber selected by the pulled front in the model discussed in the text.

(full line) as a function of the dimensionless parameter $R^2\Sigma/\kappa$. Note that this velocity vanishes at a critical value—as already noted above, below this value the cylindrical tube is stable. Note that the data points fall slightly below the pulled speed v^*. Although not enough data are provided in [356] to check this explicitly, this is undoubtedly due to the slow convergence of the front speed to the asymptotic value v^*—as mentioned before, numerical data at long but finite times will alway approach v^* very slowly from below, and indeed a discrepancy like the one in this plot is what one often encounters if a careful extrapolation of the speed to its asymptotic value is not made.

It is instructive to realize that although the nonlinear behavior of this pearling model is quite different from those encountered before, the dispersion relation for small linear perturbations of the radius is not! Note that when $\mathscr{F}$ is expanded to quadratic order in the deviations from a cylinder shape, the highest derivative terms it contains are of order r_{zz}^2. Upon taking the functional derivative in (115), we immediately see that the dispersion relation $\omega(k)$ is a polynomial in k of sixth degree [185,27]. Thus, from the perspective of the linear dispersion relation and the calculation of v^*, the equation can be viewed as an interesting generalization to sixth order of the fourth order models equations of Section 2.11!

In more recent experiments, Bar-Ziv et al. [27] have tested the predictions from the above theory in detail, both for the propagation velocity and for the wavelength of the pattern selected by the front. Their data for the pattern wavenumber as a function of the dimensionless control parameter $\varepsilon = (\Sigma - \Sigma_c)/\Sigma_c$ are reproduced in Fig. 26. The full line in this plot (labeled MSC for "Marginal Stability Criterion") shows that the wavenumber of the pattern selected by a pulled front in this model is slightly larger than the wavenumber corresponding to the fastest growing mode. The experimental data are consistent with this trend although they lie somewhat above the predicted values. Whether this slight discrepancy is real is not clear. In any case, however, the experiment illustrates an important point: the data shown in Fig. 26 cover a large range of values of ε: if one knows the

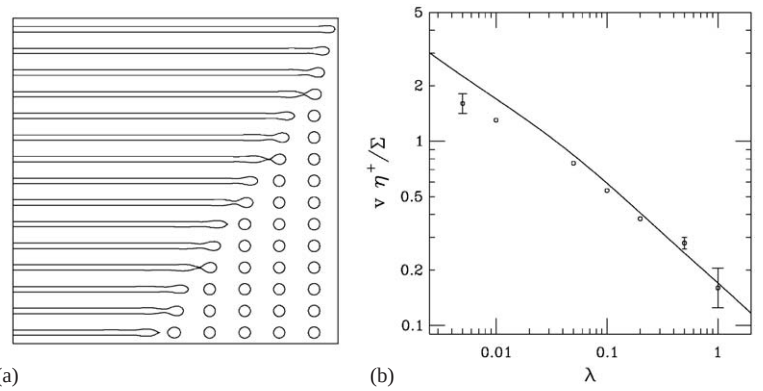

Fig. 27. Results from the full hydrodynamical simulations of Powers et al. [357] of the propagating Rayleigh instability in the absence of a bending modulus. (a) Sequence of drop shapes for viscosity ratio $\lambda \equiv \eta^{\text{inner}}/\eta^{\text{outer}} = 0.05$ at times $t_n = 6.67n\eta^{\text{outer}}R/\Sigma$, $n = 1, 2, 3, \ldots, 15$ from top to bottom. The evolution of each connected component was computed independently of the others. (b) The dimensionless Rayleigh front velocity as a function of the viscosity ratio λ. For $\lambda > 1$ the smoothly propagating front behavior is lost.

dispersion relation for a given problem, predictions for the properties of a pulled front can be made for any value of the parameters, not just close to threshold ($\varepsilon \ll 1$) where an amplitude equation description with F-KPP-type fronts might be appropriate.

Although the driving force is different—gravity in one case, surface tension in the other—there are some clear similarities between these propagating Rayleigh fronts and the Rayleigh–Taylor fronts in the thin film equations discussed in the previous section. The analogy even extends to the following issue: as we remarked at the end of our discussion of the Rayleigh–Taylor fronts, that instability is expected to be (weakly?) subcritical; therefore when the linear instability is weak, one expects there to be a transition to pushed fronts. The same might happen here: as pointed out by Bar-Ziv and Moses [26], there is a small regime where the transition to modulated states of the tube is subcritical. In this regime, one might therefore also expect pushed front solutions, but to my knowledge this issue has not been studied here either.

Powers and co-workers [357] have also studied the pure Rayleigh instability (without bending rigidity for the interface) numerically using the full hydrodynamic equations using a boundary integral technique. As their calculations reproduced in Fig. 27(a) illustrate, in this case droplets pinch off when the viscosity η^{inner} of the fluid inside the tube is smaller than η^{outer} of the outer fluid.

Fig. 27(b) shows their data for the front velocity as a function of the viscosity contrast $\lambda = \eta^{\text{inner}}/\eta^{\text{outer}}$. The full line is again the pulled front speed v^* for the full problem, while the symbols mark the numerical data. At the smallest values of λ these are some 30% lower than v^*, but there is every reason to believe that this is again due to finite simulation time and system size. Provided this is true, these simulations are one of the most convincing ones that illustrate that pulled fronts have no other choice than to propagate for large times with the linear spreading speed, even if the dynamics behind them is highly nonlinear—what could be more nonlinear and nontrivial than the pinching off of a droplet?

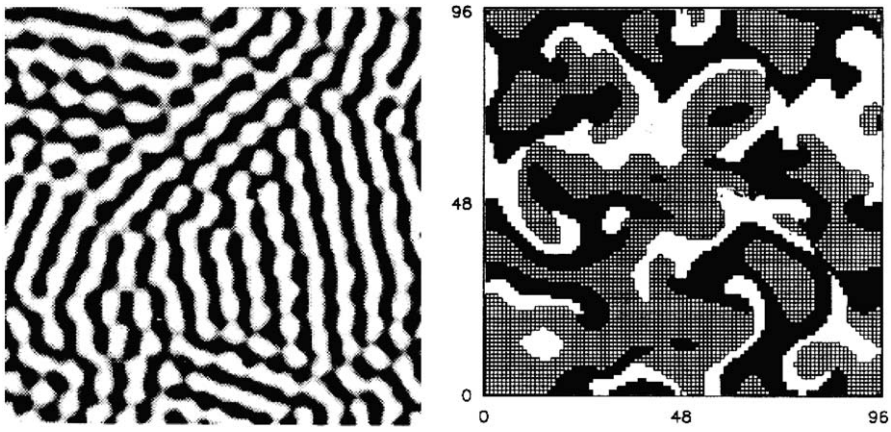

Fig. 28. (a) Snapshot of a convection pattern in a rotating Rayleigh–Bénard cell in the Kuppers–Lorz unstable regime, made with the shadowgraph technique. One identifies domains with essentially three orientations of rolls. From Bodenschatz et al. [51]. (b) A snapshot of the spatial pattern in the statistically steady state in simulations of Tu and Cross [407] of Eq. (116) with $g_+ = 2$ and $g_- = 0.5$. The dark, grey and light regions represent the domains occupied by A_1, A_2 and A_3, respectively. The occupancy is determined by which one of the three amplitudes is largest.

3.4. Spontaneous front formation and chaotic domain structures in rotating Rayleigh–Bénard convection

In Section 3.1 we already encountered a Rayleigh–Bénard experiment: a fluid heated from below exhibits a transition to convection patterns beyond some critical value of the temperature difference between the top and bottom plate. When a Rayleigh–Bénard cell is rotated as well, the interplay between the thermal buoyancy and the rotation-induced Coriolis force gives rise to a whole plethora of new effects, including traveling wave patterns [148,240,415]. One of the novel phenomena is the so-called Kuppers–Lorz instability [242]: above a critical rotation rate Ω_c, a standard stripe pattern of straight rolls looses stability to a stripe patterns which make an angle of about $2\pi/3$ with the original ones. However, the new pattern that emerges is in turn unstable to stripes which make again an angle of about $2\pi/3$ with it, and so on: no homogeneous stationary stable pattern exists. In practice, the systems settles into a statistical steady state of domains of stripes of roughly three orientations, separated by domains walls or fronts invading these domains: new domains are created and invaded incessantly. A snapshot from an experiment is shown in Fig. 28(a).

The interpretation of this statistical state was put forward by Tu and Cross [407]. They analyzed the amplitude equations for the three roll amplitudes A_1, A_2 and A_3 in this system,

$$\begin{aligned}
\partial_t A_1 &= \partial^2_{x_1} A_1 + A_1(1 - A_1^2 - g_- A_2^2 - g_+ A_3^2) \,, \\
\partial_t A_2 &= \partial^2_{x_2} A_2 + A_2(1 - A_2^2 - g_- A_3^2 - g_+ A_1^2) \,, \\
\partial_t A_3 &= \partial^2_{x_3} A_2 + A_3(1 - A_3^2 - g_- A_1^2 - g_+ A_2^2) \,,
\end{aligned} \tag{116}$$

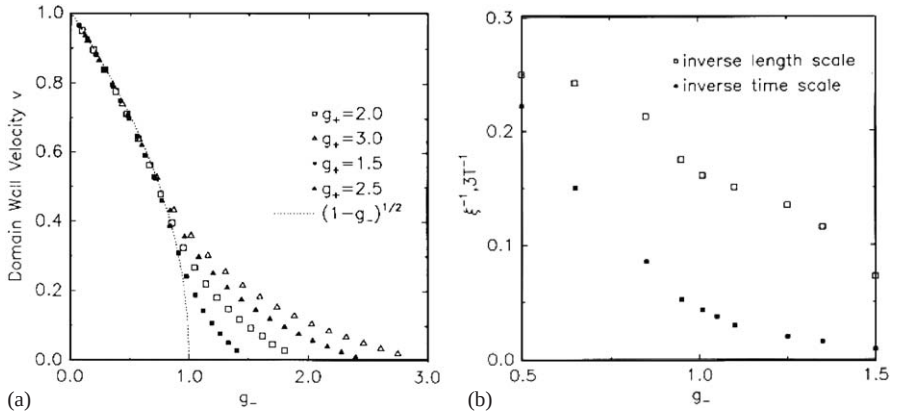

Fig. 29. (a) The front velocity v versus g_- for various values of g_+ as determined numerically by Tu and Cross [407] from the one-dimensional equations (120). The dotted line indicates the pulled front velocity v^*_{KL} given in (117). For sufficiently small g_- the fronts are pulled. From [407]. (b) The inverse correlation length ξ and inverse correlation time T (defined in terms of the amplitude correlation functions) as a function of g_- in the numerical simulations for $g_+ = 2$.

Here 1, 2 and 3 label the three orientations whose normals $\hat{\mathbf{e}}_1$, $\hat{\mathbf{e}}_2$ and $\hat{\mathbf{e}}_3$ make an angle of $2\pi/3$ with each other, and x_i are the spatial coordinates projected along these directions,[57] $x_i = \hat{\mathbf{e}}_i \cdot \mathbf{r}$. The amplitudes in Eq. (116) are taken to be real; this means that we can study the competition between domains but not the variations of the wavelength of the convection patterns in each domain.

For $g_- = g_+$ this system of equations is symmetric in all the amplitudes A_i, and can be derived from a Lyapunov function. This implies that the dynamics is then relaxational, the dynamics tends to drive the system to the minimum of the Lyapunov function.[58] However, for $g_- \neq g_+$ (without loss of generality one can take $g_- < g_+$) the system has a cyclic permutation symmetry only and it is non-potential: it *cannot* be derived from a Lyaponov functional. For g_+ large and g_- small, the A_2 amplitude is strongly suppressed by the A_1 amplitude but not vice versa, so it is intuitively clear that an A_1 domain will invade an A_2 domain, etc.

The snapshot of the simulation of the above equations [407] shown in Fig. 28(b) illustrates that at any given time, the pattern consists of domains of three roll-orientations, separated by domain walls or fronts: the dark domains invade the grey ones, the grey ones the light ones, and the light ones the dark ones. Note also the similarity with the experimental picture of Fig. 28(a).

When Tu and Cross [407] analyzed the statistical properties of these steady states, a surprising feature was found: while the Kuppers–Lorz instability sets in when g_- decreases below 1, the correlation length ξ and correlation time T did *not* diverge as $g_- \uparrow 1$—see Fig. 29(b). The clue to understanding this was identified [407] to be the behavior of the fronts. For $g_- < 1$ a homogeneous state is linearly unstable to the growth of one of the other two amplitudes; indeed, it is easy to see

[57] The geometrical projection factors in $\partial_{x_i} = \hat{\mathbf{e}}_i \cdot \partial_{\mathbf{r}}$ in the gradient terms in (116)–(117) are precisely those which are responsible for the stripe-type appearance of fronts or domain walls at the edge of a hexagonal pattern—see footnote 55.

[58] By saying that a system has a Lyaponov function $\mathscr{F}$, we mean that it can be written in the form $\partial_t A = -\delta\mathscr{F}/\delta A$, where the term on the right-hand side is a functional derivative. An example is given in Eq. (120) below, and we also briefly encountered a Lyapunov function in the discussion of the the Cahn–Hilliard equation in Section 2.11.3. The derivative form implies that $\mathrm{d}\mathscr{F}/\mathrm{d}t = -\int(\delta\mathscr{F}/\delta A)^2 \leqslant 0$ so that $\mathscr{F}$ either decreases under the dynamics or stays constant.

from Eq. (116) that the linear spreading speed of an A_1 perturbation into a domain where $A_2 = 1$ equals

$$v^*_{\rm KL} = 2\sqrt{1-g_-}\ . \tag{117}$$

On the other hand, even though an A_2 domain is linearly stable to small perturbations in all the amplitudes, for $1 < g_- < g_+$ it is only *metastable*: an A_1 domain will invade an A_2 domain even though it is linearly stable. We can show this by using the curious feature that two-mode subdynamics of these equations *is* actually of potential nature, even though the full three-mode dynamics *is not*. Let us consider the one-dimensional dynamics of two modes only,

$$\partial_t A_1 = \cos^2\theta_1\, \partial_x^2 A_1 + A_1(1 - A_1^2 - g_- A_2^2)\ , \tag{118}$$

$$\partial_t A_2 = \cos^2\theta_2\, \partial_x^2 A_2 + A_2(1 - A_2^2 - g_+ A_1^2)\ . \tag{119}$$

Here θ_1 and θ_2 are the angles between the x-axis and the vectors $\hat{\mathbf{e}}_1$ and $\hat{\mathbf{e}}_2$. Upon transforming to the variables $\bar{A}_1 = \sqrt{g_+}A_1$ and $\bar{A}_2 = \sqrt{g_-}A_2$ we can write the equations in the potential form

$$\frac{\partial \bar{A}_1}{\partial t} = -\frac{\delta \mathscr{F}}{\delta \bar{A}_1}, \quad \frac{\partial \bar{A}_2}{\partial t} = -\frac{\delta \mathscr{F}}{\delta \bar{A}_2}\ , \tag{120}$$

where the "free energy", which plays the role of a Lyapunov functional, is given by

$$\mathscr{F} = \tfrac{1}{2}\int \mathrm{d}x \left[\cos^2\theta_1(\partial_x \bar{A}_1)^2 - \bar{A}_1^2 + \frac{1}{2g_+}\bar{A}_1^4 + \cos^2\theta_2(\partial_x \bar{A}_2)^2 - \bar{A}_2^2 + \frac{1}{2g_-}\bar{A}_2^4 + \bar{A}_1^2\bar{A}_2^2\right]\ . \tag{121}$$

For $g_1 > 1$, this free energy functional has local minima at $\bar{A}_1 = \sqrt{g_+}$, $\bar{A}_2 = 0$ and $\bar{A}_1 = 0$, $\bar{A}_2 = \sqrt{g_-}$. For $g_- < 1$ the second point becomes a saddle, in agreement with the fact that the state A_2 state is unstable to the growth of the A_1-mode. However, even though the free energy has two local minima for $g_- > 1$, for any $g_- < g_+$ the second one corresponding to the nonzero A_2-mode always has a higher free energy than the first one, which corresponds with the A_1-phase. These two minima are separated by a free energy barrier (very much like two stable phases near a first order transition), but the relaxational nature of this subdynamics implies that any initial condition which corresponds with an A_1-domain on the left and an A_2-domain on the right will develop into a coherent front which moves to the right. Such "bistable" fronts which connect two linearly stable states are well known for such types of equations; they are like pushed fronts and their speed approaches an asymptotic value exponentially fast.

Indeed, as Tu and Cross found—see Fig. 29(a)— the scenario which emerges is that for any $g_- < g_+$ the dynamical attractor is a statistically steady chaotic domain state. If g_- is reduced below g_+, the invasion of domains is due to pushed fronts up to some critical value of g_- below which the fronts are pulled.[59] The Kuppers–Lorz instability is therefore not only a nice illustration of how fronts propagating into an unstable state can be generated dynamically, but it is also one of the few realistic examples we know of where the front propagation mechanism changes from pushed

[59] Note that the numerical data-points in the pulled regime in Fig. 29 are slightly below $v^*_{\rm KL}$; as always, this is a sign of the slow power law convergence to the asymptotic pulled front speed.

to pulled upon changing a parameter. In this particular experiment this parameter can even be tuned easily by changing the rotation rate.[60]

We finally note that as as we will discuss in Section 5, pulled fronts are not amenable to the usual sharp interface approximation or moving boundary approximation. Whether this gives rise to any noticeable difference between the transient domains in the pushed regime just above the Kuppers–Lorz instability and those in the pulled regime at higher rotation rates, has apparently not been explored. However, I consider it unlikely that it does, since as Fig. 29(a) shows, there is only a large separation of scales between the front thickness and the domain size in the regime near threshold.

3.5. Propagating discharge fronts: streamers

When the electric field is large enough, free electrons in a gas accumulate sufficient energy inbetween collisions that they can knock out an electron from a neutral gas molecule in a collision. In air, the ionization of nitrogen is dominant, and in this case the ionization reaction can be summarized as $e^- + N_2 \Rightarrow 2e^- + N_2^+$. This type of avalanche phenomenon can naturally lead to to the formation of discharge patterns (sparks!) whose dynamics is dominated by the propagation of fronts into the unstable non-ionized state, as is illustrated in Fig. 30. Figures (a) and (b) show two snapshots of simulations of Vitello et al. [433] of the formation of a discharge pattern in nitrogen between two planar electrodes across which a potential difference of 25 kV is applied. Initially, at time $t = 0$, the gas between the electrodes is non-ionized, except for a small region near the upper electrode. Due to the large field, the electrons immediately get accelerated downward into the non-ionized region, ionizing neutral molecules along the way. Figs. 30(a) and (b) show the electron density level lines 4.75 and 5.5 ns later. The regions inside the finger-like regions of these so-called streamer patterns are weakly ionized plasmas; the regions where the level lines crowd mark the zones where the electron density drops quickly to a very small value, and where most of the ionization takes place. The negative space–charge in this transition zone effectively shields the outer field in the non-ionized region from that in the streamer body where both the space-charge and the field are small.

The propagation of streamer patterns is well described by the following set of equations for the electron density n_e, the ion density n_+ and the electric field $\mathbf{E}$ [142,433],

$$\partial_t n_e = \alpha_0 |n_e \mu_e \mathbf{E}| e^{-E_0/|\mathbf{E}|} - \nabla \cdot (-n_e \mu_e \mathbf{E} - D_e \nabla n_e) \ , \tag{122}$$

$$\partial_t n_+ = \alpha_0 |n_e \mu_e \mathbf{E}| e^{-E_0/|\mathbf{E}|} \ , \tag{123}$$

$$\nabla \cdot \mathbf{E} = \frac{e}{\varepsilon_0}(n_+ - n_e) \ . \tag{124}$$

The first term on the right-hand side of the first two equations is the impact ionization term. As μ_e is the electron mobility, $-\mu_e \mathbf{E}$ is the electron velocity, so the prefactor is just the impact rate of electrons on the ions, while the exponential factor accounts for the ionization rate as a function of

[60] For fronts between two locally stable states the front velocity will behave linearly in $g_+ - g_-$ for $g_- \approx g_+$. Since the domain dynamics is driven by the front motion, we therefore expect the correlation length ξ and time scale T to scale as $\xi/T \sim (g_+ - g_-)$ close to the point $g_- = g_+$. The correlation length ξ in Fig. 29(b) does seem to vanish indeed faster than T, but there are insufficient data to test this hypothesis.

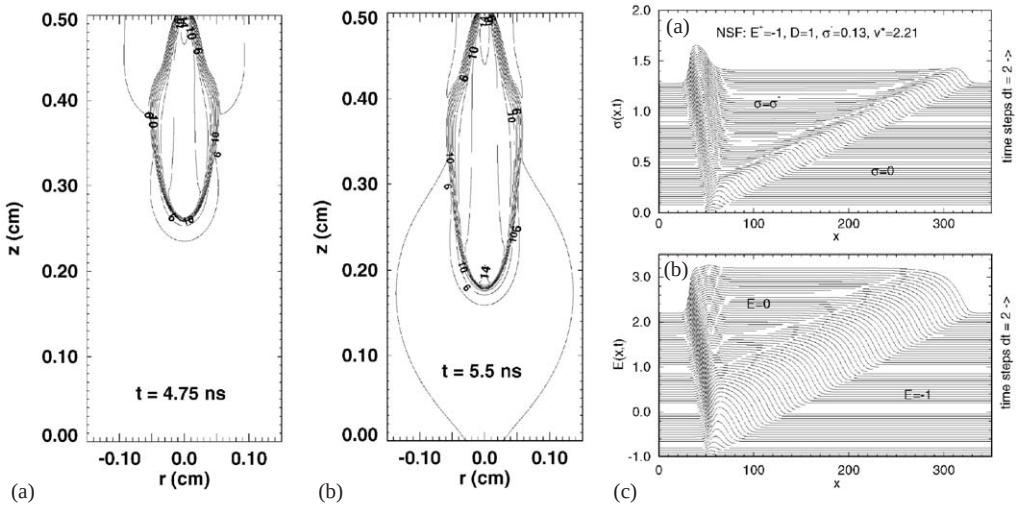

Fig. 30. (a) and (b): results of the numerical simulations of Vitello et al. [433] of the full three-dimensional simulation of Eqs. (122) – (124) for parameters corresponding to nitrogen gas and a potential difference between the planar electrodes of 25 kV. Each line indicates an increase of n_e by a factor of 10. Shown are snapshots of the electron density 4.75 and 5.5 ns after an initial ionization seed was placed at the upper electrode. (c) Space-time plot of a simulation of the equations by Ebert et al. [142] for the case of a planar streamer front in the case $D = D_e\alpha_0/(\mu_e E_0) = 1$ [142]. Upper panel: the dimensionless electron density $\sigma = n_e e/(\varepsilon_0\alpha_0 E_0)$ as a function of time and space. Lower panel: the electric field measured in units of E_0. The initial condition was a homogeneous field $E = -E_0$ and a small, charge-neutral ionized region with Gaussian electron and ion density around $x = 55$. The front propagating to the right in the same direction as the electron drift velocity is called a negative streamer front; it is a pulled front with asymptotic speed v^*_{str} (=2.21 in dimensionless units), given by Eq. (125). The front propagating slowly to the left is a pushed positive streamer front.

the field—small fields give a small ionization rate, as the electron speed at impact is small. The other two terms on the right-hand side of (122) account for the drift and diffusion of the electrons. Similar terms are absent in the equation for the ion density n_+ since on the time scales of interest drift and diffusion of the much heavier ions can be ignored. Finally, Eq. (124) is the Maxwell equation relating the field strength to the charge density.

Clearly the impact ionization term in these equations makes the non-ionized state with $n_e = n_+ = 0$ linearly *unstable*. Moreover, since a nonzero charge density tends to screen the field, the field is largest just ahead of a front. The exponential factor in the impact ionization term is an increasing function of the field strength, hence the growth is gradually decreased from a large value ahead of the front to a small value in the plasma behind the front where the field is screened. At first sight, it may therefore come as no surprise that discharge fronts which propagate in the same direction as the electron drift velocity—so-called negative streamers—are examples of pulled fronts [141,142]. Now, apart from the drift term, Eq. (122) has, to linear order in n_e, the same terms as the F-KPP equation (1), a linear growth term and a diffusion term. We therefore immediately obtain the asymptotic speed of planar streamer fronts

$$v^{as}_{str} = v^*_{str} = -\mu_e E^+ + 2\sqrt{D_e|\mu_e E^+|}e^{-E_0/E^+}\ , \tag{125}$$

where E^+ is the value of the field just ahead of the front. This prediction has been fully confirmed by extensive numerical simulations by Ebert et al. [141,142], an example of which is shown in Fig. 30(c).

The streamer problem is very instructive from a more general point of view. First of all, in the F-KPP equation, it is rigorously known [16,35,37] that one is always in the pulled regime if the growth function $f(\phi)/\phi < f'|_{\phi=0}$. The streamer problem nicely illustrates that such simple results generally do not hold in more complicated cases. As we mentioned above, the ionization term in the streamer equations rapidly decreases when the field strength drops; hence the ionization rate per electron $\alpha_0\mu_e|\mathbf{E}|\exp - E_0/|\mathbf{E}|$, which is the analog of the growth ratio $f(\phi)/\phi$ in the F-KPP equation, decreases monotonically from the front side to the back side of the front. In spite of this, for each set of parameter values, the streamer equations not only admit *pulled* negative streamer front solutions, but also *pushed* positive streamer front solutions which propagate in the opposite direction. Fig. 30(c) illustrates this. The reason for this is that streamer front propagation arises through the interplay of ionization *and* screening of the field. Screening is a nonlocal phenomenon mediated through Eq. (124), and so the monotonic behavior of the field dependence of the local ionization term is just half of the story.

Secondly, the negative streamer patterns like those of Figs. 30(a,b) are nice examples of interface-like growth patterns whose dynamics is associated with propagating pulled fronts. Indeed, if we write the electric field in terms of the electrical potential Φ as $\mathbf{E} = -\nabla\Phi$, we see that outside the streamer body, where the charge density is negligible, the potential obeys to a good approximation the Laplace equation $\nabla^2\Phi = 0$. Moreover, Eq. (125) shows that to a good approximation the normal velocity of a streamer equals $\mu_e\nabla\Phi$. These are precisely the two equations for viscous fingering [44,250,338] or for thermal plumes in two dimensions [451], so if we think of the streamer pattern as a moving interface, we expect their dynamics to have a number of similarities with the dynamics of viscous fingers or plumes [141,428].

However, the story is not that simple! The problem is that pulled fronts cannot straightforwardly be mapped onto a moving boundary problem, even when their width is much smaller than the pattern scale [as is clearly the case for the streamer patterns of Figs. 30(a,b)]. As we will discuss more generally in Section 5, the fact that the dynamically important region of pulled fronts is *ahead* of the front itself entails not only a power law convergence to the asymptotic speed but also a breakdown of the standard moving boundary approximation. The precise implications of this for streamers are still under active investigation—very much like dendrites, they do show a tip-splitting instability [18], but the dispersion relation of small perturbations of a planar discharge front does appear to be different from what one would expect based on the analogy with viscous fingering or dendrites.

3.6. Propagating step fronts during debunching of surface steps

When a crystal is cut with an angle slightly different from one of the principle crystal facets, the resulting "vicinal surface" contains a lot of steps. The predominant mechanism during vapor growth is then that adatoms which have landed on the surface diffuse towards these steps and attach there. The crystal growth is thus accompanied by the propagation of steps along the surface.

It has been known since long that growing mono-atomic steps can "bunch": instead of staying equidistant, on average, they bunch together and form macro-steps. Many of these and other step

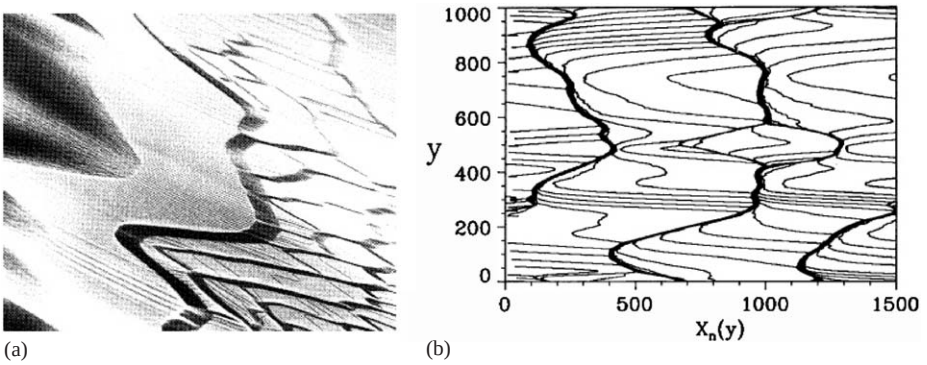

Fig. 31. Reflection electron microscopy image of a vicinal Si(111) surface 10 s after the a change of direction of the current direction; a series of steps "peel off" from a large macro-step in a characteristic pattern: steps "debunch" from the macro-step that is visible as the thick line meandering through the middle of the figure. From Latyshev et al. [253]. (b) Snapshot of a Monte Carlo simulation by Kandel and Weeks [215] of the stochastic version of the step model (127). Note the similarity with the experimental observations shown in panel figure (a).

instabilities can be understood in terms of the following simple model of step flow [42,168,214,411],

$$\partial_t X_n = f_+(W_n) + f_-(W_{n-1}) + \gamma \partial_y^2 X_n \ . \tag{126}$$

Here $X_n(y,t)$ is the position of the nth step measured along y, the coordinate along the step. The terms $f_+(W_n)$ and $f_-(W_{n-1})$ describe the growth due to attachment of atoms from the terrace of width $W_n = X_{n+1} - X_n$ in front of the step and the terrace of width W_{n-1} just behind the step. The last term is a curvature correction analogous to the surface tension type term that occurs in almost all interfacial problems. Note that from a mathematical point of view, Eq. (126) is of mixed character: it is a partial differential equation with respect to the y-variable, but a difference equation with respect to the step index n.

A straightforward stability analysis shows that an equidistant array of steps (all $W_n = W$) is unstable when the attachment kinetics is such that steps predominantly incorporate atoms from the terrace behind it, i.e. if $f'_-(W) > f'_+(W)$. This is in full agreement with the intuitive idea that when a step lags a bit behind, the terrace behind it becomes smaller and hence the step will capture fewer atoms from this terrace.[61] This instability leads to step bunching in the nonlinear regime.

It has been found in various experiments that application of a current along the surface can induce very complex patterns. Indeed, one of the new phenomena that occurs is shown in Fig. 31(a): right after reversal of the current, steps "peel off" from a macro-step in a characteristic pattern.

This experimentally observed "debunching" behavior is not found in the above model for the step dynamics, but Kandel and Weeks [215] have shown that it can be understood in terms of the following extension of it. The shortcoming of model (126) is that the growth functions $f_\pm(W)$ only depend on the terrace width right ahead of and behind the step. However, when steps bunch they

[61] Early work on step bunching by Frank [168] described it on a coarse-grained scale in terms of the Burgers equation. If the step velocity decreases as a function of step density, the well-known formation of shocks in the Burgers equation implies step bunching. From this perspective, the phenomenon is similar to the formation of traffic jams in elementary models for traffic flow.

get so close that this simple approximation breaks down: capture of adatoms by steps in a bunch is strongly suppressed because steps cannot move any closer. Instead, surface diffusion over the entire bunch becomes more probable. Kandel and Weeks [215] therefore replace (126) by

$$\partial_t X_n = f_+(Z_n^{(\mathrm{f})}) + f_-(Z_n^{(\mathrm{b})}) + \gamma \partial_y^2 X_n \ , \tag{127}$$

for $W_n > W_{\min}$, while $\partial_t X_n = 0$ for $W_n < W_{\min}$. Here $Z_n^{(\mathrm{f})}$ ($Z_n^{(\mathrm{b})}$) is the width of the first terrace in front of (behind of) the nth step that is larger than $W_{\min}$. Note that this introduces a dynamically generated non-locality in the model: the terraces from which a step captures atoms depend on the dynamical state of the step configuration itself. As a result, as discussed in detail in [215], these equations also lead to a *debunching instability* near the edge of a step bunch: one or a series of steps can "peel off" in a characteristic fashion from the bunch, while the other steps in the bunch remain virtually immobilized together. A snapshot of a Monte Carlo simulation [215] of a stochastic version of this model with

$$f_-(W) = k_- W, \quad f_+(W) = k_+ W \ , \tag{128}$$

is shown in Fig. 31(b). Clearly, the type of step patterns found in this model is remarkably similar to that seen experimentally.

From our perspective, the interesting aspect is the arrays of steps—the almost parallel lines in the figure—which cross from one step bunch to the other. As we mentioned above, the step configuration near the edge of a bunch is unstable to the peeling off of an array of steps, and so the propagation of the detachment point can be viewed an an example of a front propagation into an unstable state problem. Indeed, by linearizing the dynamical Eqs. (127) and (128) about an array of straight steps separated by a distance $\approx W_{\min}$ and assuming a behavior for perturbations δX_n of the form

$$\delta X_n(y,t) \sim \mathrm{e}^{-\lambda(y-n\Delta)+\sigma t} \tag{129}$$

one obtains a linear dispersion equation of the form

$$\sigma(\lambda) = k_+(\mathrm{e}^{\lambda\Delta} - 1) + k_-(1 - \mathrm{e}^{-\lambda\Delta}) + \gamma\lambda^2 \ . \tag{130}$$

Note that the various terms in this expression do reflect the mixed character of the equation: the exponential terms are characteristic of a finite difference equation, the last term of a partial differential equation. The linear spreading speed v^*_{debunch} can of course be obtained straightforwardly by determining the minimum of the curve $\sigma(\lambda)/\lambda$. The comparison of v^*_{debunch} with the simulation data for various Δ is shown in Fig. 32. The data clearly show that the debunching point propagates along the bunch with the linear spreading velocity, so apparently the debunching process is an example of a pulled fronts. Pulled fronts were also found to describe certain aspects of the initial bunching process in the original model (126) [214].

Recent experiments on this debunching instability [438,393] are consistent with the relation between growth length λ and step spacing Δ found by Kandel and Weeks [215] but do not test the predictions for the front velocity directly. More recent theoretical work [207] shows that a strain-induced step bunching instability can be convective.

3.7. Spinodal decomposition in polymer mixtures

When a homogeneous mixture is quenched within the so-called spinodal region, the homogeneous state is unstable to composition fluctuations. The lowest free energy state towards which the system

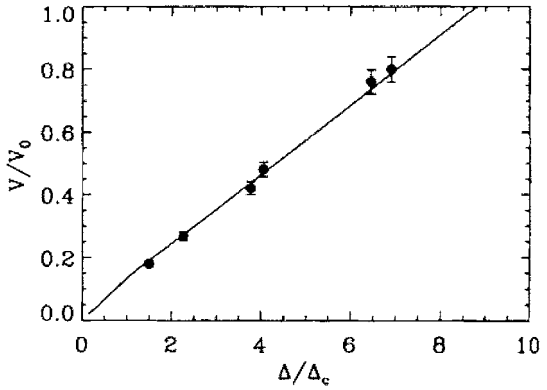

Fig. 32. Comparison of the prediction of $v^*_{\text{debunch}}(\Delta)$ (full line) with the velocity data (symbols) from the simulations shown in Fig. 31(b). V_0 is the initial step velocity $V_0 = (k_+ + k_-)W$ and $\Delta_c = \sqrt{2\gamma/(k_- - k_+)}$. From Kandel and Weeks [215].

evolves at long times is one in which it is demixed into two homogeneous phases of different composition. On the way towards this demixed state the system is spatially inhomogeneous on mesoscopic scales. This spatio-temporal demixing process is called spinodal decomposition [56,192].

At intermediate times the dynamics is normally dominated by motion of interfaces between domains in which the composition is close to one of the equilibrium compositions. The initial phase, however, depend on the system under study. For most systems (like ordinary liquids), the fluctuations are large enough that right after the quench these fluctuations grow out due to the instability of the bulk mode. Moreover, this regime is often difficult to probe experimentally, since it happens on too short time scales. For sufficiently long polymers, however, the dynamics is slow enough that this regime becomes experimentally accessible [440]. Moreover, the longer the polymers the smaller the fluctuations, so that the coarse-grained mean-field like models which have mostly been studied in the literature become more appropriate for polymer systems. It is also conceivable that the short-time dynamics is then sometimes dominated by the propagation of composition modulation fronts into the unstable homogeneous state. If so, it is likely that such fronts typically start at the walls of the sample, since a wall is normally preferentially wetted by one of the compositions [21].

A simple model equation for spinodal decomposition is the Cahn–Hilliard equation which we already introduced in Section 2.11.3. The front propagation problem in this equation in the presence of noise was studied from the above perspective by Liu and Goldenfeld [266] and by Ball and Essery [21] who both found that the composition modulation fronts in this equation are pulled fronts which lead to a incoherent pattern which continues to coarsen.[62] The simulations of Fig. 15 also showed this.

Experimental evidence for the above surface-induced front-dominated spinodal decomposition scenario in polymers was found by Jones et al. [208], but no direct quantitative comparison was made with the predictions from the theory of front propagation.

[62] The data points for the numerical front velocities obtained shown in [266] are as usual slightly below the value v^*: As we remarked already several times, this is true for almost all published data, and reflects the slow convergence of the speed of a pulled front to its asymptotic value.

We finally note that the competition between bulk growth and front propagation in a model with a non-conserved order parameter was also studied in [289,409].

3.8. Dynamics of a superconducting front invading a normal state

The equilibrium and dynamical behavior or vortices in type II superconductors is a vast and active field with many ramifications, which range from fundamental statistical physical studies to applications [50]. Even in the area of vortex dynamics, interesting questions concerning the behavior of propagating fronts separating domains with different vortex properties (e.g. a different density of vortices) come up [137,285], but most of the issues that arise in this area are different from those which are the main focus of this paper. We therefore limit our discussion here to some interesting theoretical findings concerning fronts propagating into an unstable state of a type I superconductor, which also raise some new fundamental questions. Some indirect evidence for such fronts have been found from measurement of the magneto-optical response of thin films [169] but the time-resolution has been insufficient to study the dynamics directly. Recent advances in magneto-optical techniques [202,437] to visualize vortex patterns may open up the possibility to do so in the near future.

It is well known [394] that in so-called type I superconductors the normal state is linearly unstable [63] to the superconducting state when the magnetic field H is reduced below the critical value H_{c2}. For fields $H_{c2} < H < H_c$, the normal state is linearly stable, but has a higher energy than the superconducting state; the superconducting state can then only form through nucleation. The barrier for this nucleation of superconducting domains vanishes as H approaches H_{c2} from above. The dynamical behavior that can result if a type I superconductor is quenched into this unstable state was studied a number of years ago by Liu et al. [267] and by Frahm et al. [132,167], who pointed out the analogy of these two regimes to the spinodal and nucleation regimes of phase separation (see Section 3.7). Moreover, they drew attention to the fact that when the superconducting phase propagates into the normal phase, the effective long-wavelength equations show a strong analogy with the diffusion equations describing diffusion limited growth. As a result, one expects these fronts to have a similar Mullins–Sekerka like long-wavelength instability as crystal growth problems (see [73,220,226,247,251,338,353] and Section 3.17).

In time-dependent Ginzburg–Landau theory the dynamics of a superconductor is governed by the dynamical equation for the complex superconducting wave function $\psi(r,t)$ [132,167,132,394]

$$\frac{\partial\psi}{\partial t} = -\frac{\delta\mathscr{F}}{\delta\psi^*} \ , \tag{131}$$

where the dimensionless free energy functional $\mathscr{F}$ is given by

$$\mathscr{F} = \int \mathrm{d}\mathbf{r}\{-|\psi|^2 + \tfrac{1}{2}|\psi|^4 + |[(\mathrm{i}\kappa)^{-1}\vec{\nabla} - \mathbf{A}]\psi|^2 + (\vec{\nabla}\times\mathbf{A})^2\} \ . \tag{132}$$

The Ginzburg–Landau parameter $\kappa = \lambda(T)/\xi(T)$ in this expression is the ratio of the penetration depth λ and the coherence length ξ; type I superconductors are characterized by $\kappa < 1/\sqrt{2}$. Furthermore,

[63] Tinkham [394] formulates this slightly differently, but if the the problem is formulated as a stability analysis, i.e., as the problem of finding the growth rate $\mathrm{e}^{\sigma t}$ of the linear eigenmodes, one immediately sees that below H_{c2} the normal state is unstable.

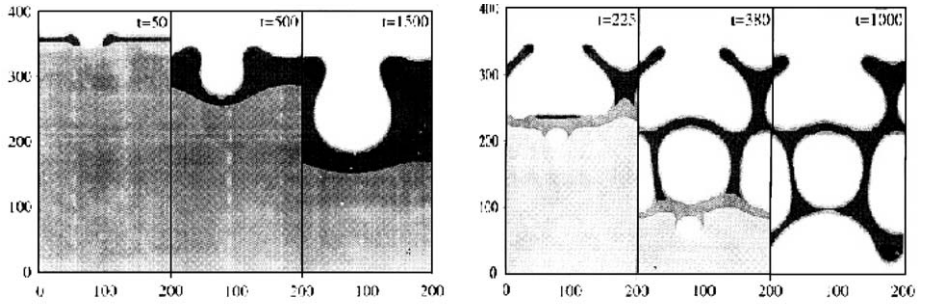

Fig. 33. (a) Penetration of the propagation of a superconducting domain into a normal domain in numerical calculations by Frahm et al. [167]. The penetration is visualized through the strength of the magnetic field shown in greyscale, with black corresponding to $B \approx H_c$ and white corresponding to $B \approx 0$. The field strength in the normal phase corresponds to a value of about 0.57 H_c which corresponds to the nucleation regime where the normal phase is linearly stable, while $\kappa = 0.3$ and $\Sigma = 0.1$. Times are measured in units of the order parameter relaxation time [167,267]. (b) As in (a), but now for a field $H = 0.28H_c$ which corresponds to the spinodal regime where the normal phase is locally unstable.

$\mathbf{A}$ in (132) is the magnetic vector potential which is related to the magnetic field $\mathbf{B}$ through $\mathbf{B}=\vec{\nabla}\times\mathbf{A}$; using Ampère's law and Ohm's law, the dynamics of $\mathbf{A}$ is governed by

$$\Sigma\partial_t\mathbf{A} = [\kappa^{-1}\mathrm{Im}\,(\psi^*\vec{\nabla}\psi) - |\psi|^2\mathbf{A}] - \vec{\nabla}\times(\vec{\nabla}\times\mathbf{A})\ . \tag{133}$$

Here Σ is the dimensionless conductivity [167] and the term between square brackets in this expression is the supercurrent contribution in the Ginzburg–Landau formulation. The gradient term in this term describes the generation of supercurrents in fronts or interfacial zones and near surfaces, while the second term is the Meissner term which is responsible for flux expulsion from the superconductor state where $|\psi|^2 \neq 0$ (note that it acts like a linear damping term for $\boldsymbol{A}$ which drives the field to zero).

Fig. 33 shows two examples of the simulations of Frahm et al. [167] of a superconducting state propagating into the normal state of a two-dimensional sample with the magnetic field $\mathbf{B} = \vec{\nabla}\times\mathbf{A}$ perpendicular to the sample. Since the magnetic field is expelled from the superconductor a good way to represent the dynamics is by plotting the strength of the magnetic field in greyscale. Fig. 33(a) shows an example of a superconducting front penetrating the normal state in the nucleation regime ($H_{c2} < H < H_c$) where the normal state is linearly stable. Due to the flux expulsion, the superconducting region shows up as white in the figure, while the black zones illustrate the field enhancement due to the supercurrents in the interfacial region. Note also that the size of the protrusion increases in time, in agreement with the analogy with diffusion-limited growth problems noted above which suggests that the interface should be unstable on long length scales.

Fig. 33(b) shows that the dynamics is very different when the front propagates into a linearly unstable normal phase (the spinodal regime). In this regime the front itself appears to become very complex, and the dynamics is accompanied by the occurrence of phase slips in the superconductor order parameter ψ (points in space and time where the amplitude $|\psi|$ vanishes so that the phase of ψ can change by a factor 2π).

The scenario that one expects for superconductor fronts propagating into a normal state is somewhat similar to the one discussed for the quintic CGL equation in Section 2.11.6: for fields $H_{c2} < H < H_c$ the behavior is subcritical, and the dynamics of the fronts separating the two phases is like that of a bistable front or a pushed front. When upon reducing the field the value H_{c2} is crossed, the normal state becomes linearly unstable—this corresponds to ε becoming positive in the quintic CGL. The linear spreading speed v^* then becomes nonzero, but clearly for fields just below H_{c2} the dynamically relevant fronts will remain pushed. The question then arises, however, whether upon decreasing the field even more the fronts may become pulled for some range of parameters, just like it happens in the quintic CGL equation. If so, this would be of great advantage, since it might provide a handle at calculating some of the properties of the complex patterns of Fig. 33(b) analytically, just like the propagating Rayleigh instability of Section 3.3 allows one to obtain most essential features of the pattern analytically.

To our knowledge, the question whether the full two-dimensional complex patterns in the spinodal regime are governed in some cases by propagating pulled fronts has not been studied yet. Some indication that a transition to pulled front propagation might be possible comes from the work of Di Bartolo and Dorsey [123]. They studied the propagation of one-dimensional fronts in the absence of the possibility of phase slip generation (as ψ was taken to be real and equal to f below) and in the case that the external field in the normal phase vanishes. In dimensionless units, the equations in this case reduce to

$$\partial_t f = \kappa^{-2}\partial_x^2 f - a^2 f + f - f^3 \ , \tag{134}$$

$$\Sigma\, \partial_t a = \partial_x^2 a - f^2 a \ . \tag{135}$$

The authors studied the case in which the front propagates into the normal state with $f = 0$ and $a = a_\infty$. Since the magnetic field H is this case is simply related to a by $H = \partial_x a$, and since $a = 0$ in the superconductor behind the front, $\int_{-\infty}^{\infty} H = a_\infty$ is simply the amount of magnetic field trapped in the front region and the field in the normal phase far ahead of the front vanishes. Di Bartolo and Dorsey [123] found that fronts in this restricted equation are pulled for small enough values of a_∞ but pushed for larger a_∞. However, because of the possibility of the generation of phase slips was suppressed by taking f real, it is conceivable that fronts at some point are unstable to the splitting off of a localized normal region with some magnetic field trapped and a faster growing growing front with a smaller amount of trapped field. Clearly, various issues regarding these superconductor fronts still remain to be resolved.

We finally note that apart from the practical significance of studying whether fronts might be pulled in the two-dimensional case, this question is also relevant from the following perspective. As we will discuss in Section 5, pulled fronts are not amenable to the usual moving boundary approximation. The full implications of this are not known, so the superconductor front problem might be a good one to explore this issue, if they admit pulled fronts. The only other realistic example known to me where this issue appears to have immediate relevance for the pattern formation are the streamer discharge patterns analyzed in Section 3.5. (See also the remark at the end of Section 3.4 on the Kuppers–Lorz instability.) The recent advance in increasing the time resolution of magneto-optic techniques [437] may open up the possibility that these dynamical issues will become experimentally relevant in the near future.

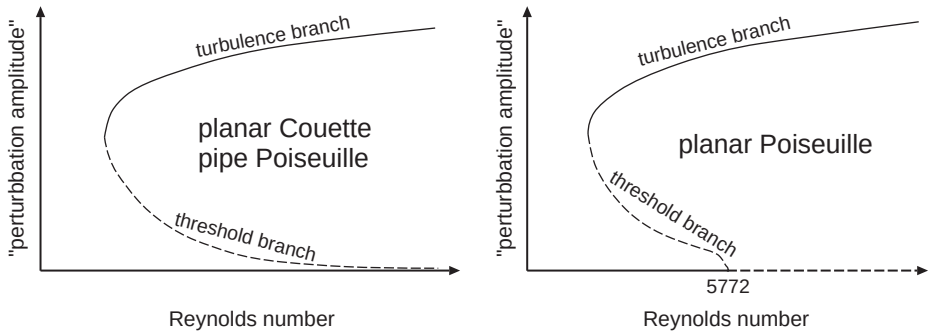

Fig. 34. Schematic illustration of the subcritical bifurcation structure of the transition to turbulence in Couette and Poiseuille flow [205]. For planar Couette flow and pipe Poiseuille flow (left plot), the laminar base flow is linearly stable for *any* finite Reynolds number, but the threshold to turbulence decreases as $Re^{-\gamma}$ with some exponent γ as $Re \to \infty$ [80]. Planar Poiseuille flow is linearly unstable for $Re > 5772$ but the transition is subcritical and the linear instability does not play much of a role in practice for Re of order 2000 or less, where turbulence is often already observed in practice. Note that the drawing is schematic only: although only a single curve is drawn in the left plot, there are important differences between planar Couette flow and pipe Poiseuille flow.

3.9. Fronts separating laminar and turbulent regions in parallel shear flows: Couette and Poiseuille flow

In this and the next three sections we will discuss hydrodynamic instabilities in which both front dynamics and fluctuation effects or turbulence play an important role.

Two of the basic textbook examples of hydrodynamic flow states are Couette flow and Poiseuille flow. We have already encountered Couette flow in Section 3.1 where we considered flow between two concentric cylinders. For that setup, Couette flow refers to the basic laminar flow state. The many instabilities that are found in this system are due to the interplay of the inertial effects and the Coriolis force in a rotating system. In this section, we will be concerned with planar Couette flow, flow between two plates sheared in opposite directions. Experimentally, this setup is realized by moving a transparent plastic band between two glass plates; the fluid in between is then sheared by the plastic band [108,109,283]. In planar Couette flow of a normal Newtonian fluid, the basic flow state for flow in the x-direction between plates separated by a distance $2d$ in the y direction is simply a linear velocity profile $v_x = v_{\text{plates}} y/d$; thus the shear rate $\partial v_x/\partial y$ is constant. The other classic example of a shear flow is flow through a pipe or between plates (the planar case) driven by a pressure gradient: Poiseuille flow. In this case, the basic velocity profile is parabolic, so the shear rate is zero on the center line and increases linearly towards the walls.

The control parameter for Couette flow or Poiseuille flow is the Reynolds number $Re = Ud/\nu$ where U is a typical velocity of the flow (the velocity at the plates in the case of Couette flow), d the half spacing of the plates or the radius of the pipe, and ν the kinematic viscosity of the fluid. For large enough Reynolds numbers, Couette flow and Poiseuille flow become turbulent. However, the transition to turbulence in such systems is not a supercritical bifurcation, in which a nontrivial mode grows gradually in amplitude beyond a threshold at which the basic flow becomes unstable. Instead, the transition is subcritical [80,190,205], as sketched in Fig. 34. This implies that over some

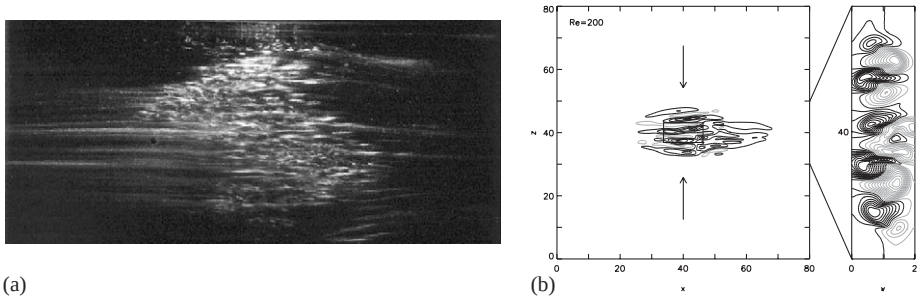

Fig. 35. Example of a turbulent spot in planar Couette flow, taken from the review of Manneville and Dauchot [283]. The seeding of the fluid with small Kalliroscope flakes makes the turbulent regions show up brightly, while laminar regions remain dark (the flakes are lined up by the shear gradient in laminar regions). The spreading of such turbulent spots depends on the Reynolds number of the base flow [108,109,283]. (b) Snapshot of a turbulent spot in the simulations of Schumacher and Eckhardt [378]. The flow is in the x-direction. On the right, a cross-section in the direction normal to the planes is shown. See Fig. 36 for further details.

range of Re linearly stable laminar flow can coexist with turbulent regions[64] (very much like near a first order phase transition). An example of a turbulent spot in a planar Couette experiment is shown in Fig. 35(a). The competition between such turbulent and laminar regions as a function of Reynolds number has been explored in detail only in the last decade [108,109,283].

Actually, as Fig. 34 indicates, although the subcritical behavior is common to all three cases, there is an important conceptual difference as well: planar Poiseuille is *linearly unstable* beyond $Re = 5772$ while planar Couette and pipe Poiseuille flow are *stable* for any finite Reynolds number—the critical amplitude in the latter cases decreases as $Re^{-\gamma}$ for $Re \to \infty$ [80,190] and hence we can think of this case as an instability which has been pushed to infinity. In the latter two cases, the absence of a true instability also implies that there cannot be any pulled fronts: the fronts that separate a turbulent region from a laminar region must always be pushed.

For the case of planar Poiseuille flow, one might wonder whether the propagation of a turbulent region into the laminar flow state could correspond to a pulled front, as the situation is somewhat similar to the one found for the quintic complex Ginzburg–Landau equation discussed in Section 2.11.6.[65] However, a priori this possibility is already unlikely for realistic Reynolds numbers: since the generic behavior of planar Poiseuille flow is so close to that of planar Couette and pipe Poiseuille flow, where fronts definitely have to be pushed, we similarly expect the fronts separating turbulent and laminar domains to be pushed as well. It was indeed found [116] that the linear instability of the planar Poiseuille profile always is always convective, so that pulled fronts could never propagate upstream. As we shall see below, however, the simplified picture based on a straightforward linear stability analysis of the unperturbed flow does not suffice for studying the spreading of a spot, because a coupling with induced cross flow has to be taken into account.

[64] It is interesting to note that also in turbulent superfluid pipe flow, there are strong experimental indications for the coexistence of turbulent and laminar domains [284].

[65] In the quintic complex Ginzburg–Landau equation, expanding chaotic spots were observed in numerical simulations in some parameter ranges [424]. Their behavior is very much like what one would expect intuitively for turbulent spots. See footnote 18.

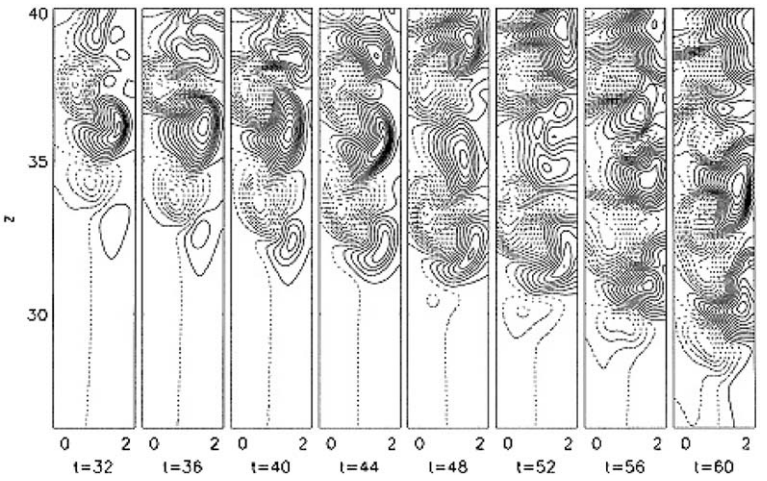

Fig. 36. Snapshots of the stream-wise velocity $v_x(z, y)$ as it spreads downward in the simulations of Schumacher and Eckhardt [378] for $Re = 200$. Dotted lines denote contour lines for positive velocity values, solid lines the contour lines with negative velocity values. Note that the turbulent region propagates downward with a roughly constant speed.

The point at issue here has recently been studied numerically for a closely related situation by Schumacher and Eckhardt [378]. These authors performed direct simulations of the Navier–Stokes equations for the case of shear flow between planes. However, unlike in the case of plane Couette flow, for numerical convenience they imposed free-slip boundary conditions on the bounding plates and drove the bulk flow by bulk force which varies as a cosine in the y-direction normal to the planes, and which forces the flow in opposite directions near the two plates.

Fig. 35(b) shows a snapshot of a turbulent spot in the simulations, which evolved from a localized perturbation of the laminar profile in the center of the simulation cell. Note that qualitative similarity with the turbulent spots observed experimentally: Both spots shows a number of streaks in the stream-wise (horizontal) direction. These streaks can also be recognized in cross-sections in the y-direction perpendicular to the planes shown on the right.

The spreading of the turbulent spot in time in the "span-wise" (vertical) direction in these simulations is shown in Fig. 36. It is immediately obvious that the turbulent region spreads vertically through some kind of front structure which advances with a rather well-defined speed. Moreover, the local turbulent energy $\mathbf{v}^2$ averaged over the normal direction was found to decay *exponentially* into the laminar region, very much as one would expect for a well-defined front solution and as has been found in some incoherent regimes of the quintic CGL equation [424]. Since Schumacher and Eckhardt found that the turbulent spot also gives rise to an overall "span-wise" outflow U_z in the vertical direction, they analyzed the linear spreading velocity v^* by linearizing the flow equations about a laminar state which is the sum of the base flow and this outflow U_z [378], using the so-called Orr–Sommerfeld equation.[66] The measured front speeds in the numerical simulations were about

[66] The Orr–Sommerfeld equation is the linearized equation governing the stability of nearly parallel flows. It is based on linearizing the Navier–Stokes equations in the deviations about a base flow profile U. [135]. In the inviscid limit the equation reduces to the so-called Rayleigh stability equation used in some of the work discussed in Section 3.10 on the formation of Bénard–Von Karman vortices.

a factor 10 larger than the value of v^* obtained this way, leaving no doubt that in the parameter regime studied the span-wise spreading of a turbulent spot is *not* governed by a pulled front: These fronts are pushed. An earlier analysis along the same lines of the spreading of turbulent spots in plane Poiseuille flow lead to the same conclusions [197].

We would like to stress that the above observations are *just empirical*: the simulations do give strong indications that it does make sense to associate the expansion of a turbulent spot with a rather well-defined coherent front, but, as we already pointed out in Section 2.7.3, not much is known about the properties of such fronts. In fact, also in the quintic CGL equation, spreading of chaotic spots was found to proceed with a more or less constant speed larger than v^* (see Fig. 18(a)), but to our knowledge it is a complete mystery why and how this happens, and whether there are still common mechanisms at play.

From this perspective, it is very intriguing that the simulations show that the turbulence front has a spatial decay rate λ which is about twice as large[67] as λ^*: these pushed turbulent fronts apparently also fall off with an exponential decay rate larger than λ^*, just as uniformly translating pushed fronts or coherent pattern forming fronts do!

3.10. The convective instability in the wake of bluff bodies: the Bénard–Von Karman vortex street

Another classic hydrodynamic instability which was analyzed by some of the founding fathers of fluid dynamics, Bénard and Von Karman, is the formation of a "vortex street" behind a cylinder in a flow: for Reynolds numbers Re less than about 4 the fluid flow around a cylinder is laminar. When Re increases past this value, two symmetric eddies form behind the cylinder, but when Re become larger than about 50, vortices are shed from the cylinder in an asymmetric pattern. This well known instability is also of immediate technological interest, since the formation of these vortices can cause serious damage to suspension bridges if they are in resonance with the eigenfrequencies of the bridge. Much of the original work focused on the formation and dynamics of these vortices, their spacing, etc., in other words on the well-developed strongly nonlinear flow regime. In the last two decades, it has become clear from experimental [286] and theoretical work [401,446], however, that the onset of the instability is associated with a linear instability in the wake of the cylinder.

In 1984, Mathis et al. [286] studied the velocity fluctuations in the region behind the cylinder (the "wake" of the cylinder) using laser Doppler velocimetry. It was found that beyond a threshold which for long cylinders approaches a value $Re_c = 47$, the root mean square velocity fluctuations grow as $\sqrt{Re - Re_c}$. This is already a strong indication that the transition to vortex formation is associated with a supercritical ("forward") bifurcation in the wake, and that the behavior there could be modeled by a CGL type of amplitude equation.

Further evidence for this scenario came soon from an analysis of the stability of the flow in the wake [203,300–302,401,446]. In this region, the flow is nearly parallel. It varies rapidly in the y-direction normal to the cylinder and the overall flow direction, but very slowly in the stream-wise direction itself. If one then ignores in a first approximation the variation of the flow in the stream-wise

[67] According to Fig. 8 of [378], in dimensionless units the exponential decay rate $\lambda \approx 1.05$ at $Re = 300$. From the numerical values listed after Eq. (19) in this paper, one finds $\lambda^* = \sqrt{\varepsilon/D} \approx 0.55$ at $Re = 300$.

x-direction,[68] one can then decompose the flow perturbation in this direction in terms of Fourier modes by writing

$$\text{flow field} \sim f(y;k)\mathrm{e}^{\mathrm{i}kx-\mathrm{i}\omega(k)t}\ , \tag{136}$$

where the eigenfunction $f(y;k)$ and the dispersion relation $\omega(k)$ are determined by the Orr–Sommerfeld equation. The latter is based on linearizing the Navier–Stokes equations in v_y and $v_x(x,y)-U(y)$ about a solution for the velocity profile $v_x=U(z)$ in the wake [135]. Once $\omega(k)$ is determined from the eigenvalue problem of the Orr–Sommerfeld equation (or the Rayleigh equation to which it reduces in the inviscid limit), the linear spreading speed v^* can easily be determined numerically. An analysis along these lines shows that the flow becomes linearly convectively unstable for value of Re around 20, and that for Re around 40 the wake becomes linearly absolutely unstable. This means that for Re above this value, a pulled front in the wake will propagate upstream, towards the cylinder. The frequency of the mode at the transition point, $\mathrm{Re}\,\omega(k^*)$, then gives the frequency of vortex shedding.

The above results imply the following scenario for the Bénard–Von Karman vortex instability. At some critical Reynolds number Re_c, which the experiments indicates to be about 47 [286], the region behind the cylinder changes over from convectively unstable to absolutely unstable. The saturation of the velocity fluctuations as $\sqrt{Re-Re_c}$ indicates that one can describe the behavior close to threshold with a cubic CGL equation for the variation of the unstable mode along the stream-wise x-direction. According to the linear dynamics of the flow equations in the wake, the instability is convective below Re_c and absolute above Re_c: in the latter regime a perturbation also spreads upstream towards the cylinder. If a perturbation of the wake flow field grows large enough that nonlinearities become important, then the perturbation develops into a front. This front is pulled (as fronts which propagate into the zero-amplitude state of the cubic CGL equation are always pulled) and hence its velocity v^* behaves just as discussed already above: for $Re>Re_c$ the pulled front moves upstream towards the cylinder. In this picture, the vortices arise as the highly nontrivial and strongly nonlinear structures behind the pulled front! The situation is thus analogous to the one for the propagating Rayleigh instability discussed in Section 3.3, where the propagating Rayleigh front left behind pinching droplets.

For a detailed study and discussion of this scenario of vortex shedding, we refer to the recent work by Pier and coworkers [344,345]. We also note that the ideas have been taken further by Leweke and Provansal and coworkers: they show that secondary transitions in the wake of bluff bodies (like a cylinder) in the regime $180<Re<350$ are both qualitatively as well as quantitatively described by a CGL equation for the behavior in the wake [5,261,262]. Some of the incoherent behavior of the fluctuations is attributed to a Benjamin–Feir instability [105,189] of the nonlinear mode.

[68] At this point, of course, there is a strong connection with the discussion of so-called "global modes" discussed in Section 6. In principle one should take the equation linearized about an overall flow pattern $U(y,x)$ whose spatial x-dependence in the stream-wise direction is kept. Then the linearized equation has spatially dependent coefficients, so one cannot do a Fourier-type analysis. Usually, a WKB-type analysis of the resulting global mode is done instead at this stage. In the limit where the region of instability is large enough, the latter type of analysis reduces to the local one used here [84]. See Section 6 for further discussion of this point.

3.11. Fronts and noise-sustained structures in convective systems I: the Taylor–Couette system with through flow

In almost all hydrodynamic systems with advection due to an overall flow, front propagation is an important ingredient of the dynamics. We already encountered an example in the previous section on the Bénard–von Karman instability in the wake of a cylinder. There are also many pattern-forming systems in which the primary bifurcation is a Hopf-bifurcation to traveling waves. The issue whether the instability is convective or absolute then immediately arises, and if the instability is strong enough that nonlinear saturation effects play a role—as is generally the case near a supercritical (forward) bifurcation—fronts often play an important role in the dynamics and in the emergence of noise-sustained structures. E.g., the so-called "blinking" traveling wave state in binary mixtures can be understood quantitatively in terms of fronts which propagate back and forth in the experimental cell [104,162], and also incoherent pulse dynamics in traveling wave systems has been analyzed in such terms [414]. In this and the next section, we focus on two examples where front dynamics is intimately connected with the transition from coherent to incoherent pattern dynamics. In this section we focus on an example of flow-induced advection, and in the next section we discuss aspects of the role of fronts in systems exhibiting a Hopf bifurcation to traveling wave states.

We already introduced the Taylor–Couette cell in Section 3.1: two concentric cylinders whose "gap" between them is filled with a fluid. When the inner cylinder is rotated, at some critical rotation rate Ω_c a stationary Taylor vortex pattern is formed; this pattern is periodic in the direction along the axis of the cylinders. Babcock et al. [19,20] and Tsameret and Steinberg [404,405] studied the behavior near threshold in the presence of a through flow in the axial direction.[69] Such a through flow has two effects. Firstly, it changes the onset of the instability to Taylor vortex patterns. Secondly, and more importantly, it changes the nature of the instability, as the through flow obviously advects perturbations away from the inlet of the flow at a finite rate. Hence just above the instability threshold, when the growth is small, the system is only convectively unstable. This is illustrated in the space–time diagram of Fig. 37(a), which show the evolution of a perturbation which was initiated near the inlet. Clearly, the initial perturbation grows out and spreads (the pattern widens in time) while being advected away down the axis. The fact that also the left flank of the perturbation is moving to the right—hence is retracting—confirms that the system is convectively unstable in this case.

By studying whether the center of such a wave packet grows or decays in the co-moving frame, both groups have extracted the threshold $\varepsilon_c = [\Omega_c(Re) - \Omega_c(0)]/\Omega_c(0)$ as a function of the Reynolds number Re of the through flow. The results from Tsameret and Steinberg [405] are reproduced in Fig. 37(b). The experimental variation of the threshold is in excellent agreement with the results of a direct stability analysis of the Couette flow with axial through flow. For values of ε above the line in the diagram, the flow in an infinitely long system is unstable to the formation of Taylor vortices.

If there were no noise in the system, one would not observe patterns in a finite system in the convectively unstable regime just above the line in Fig. 38(b). In practice, there is of course always some noise, and the type of patterns this gives rise to as ε is increased above $\varepsilon_c(Re)$ is illustrated in Fig. 38(a) from Babcock et al. [19].

[69] Similar effects will happen in a Rayleigh–Bénard cell with through flow [305], but this system does not appear to have been studied experimentally in as much detail.

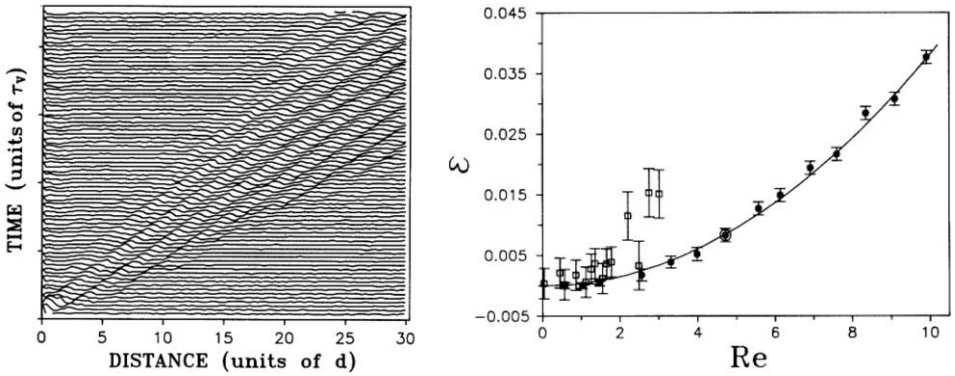

Fig. 37. The growth of a perturbation in the convectively unstable region of the phase diagram for $Re = 6$ and $\varepsilon = 0.0477$ ($\varepsilon - \varepsilon_c(Re) \approx 0.032$) in the experiments by Tsameret and Steinberg [405] on Taylor-Couette flow with though flow. The pulse was generated by a sudden movement of the inlet boundary back and forth. Times are measured in units of the vertical diffusion time τ_v ($=d^2/\nu$ with ν the kinematic viscosity of the fluid) and the distance along the axis is measured in units of the gap spacing d. (b) The threshold to the convective instability $\varepsilon_c(Re)$ as a function of Reynolds number Re in similar experiments by Tsameret and Steinberg [405]. The solid line marks the threshold according to a full theoretical stability calculation, and the solid circles the threshold values determined experimentally by tracing the evolution of a pulse generated near the inlet. The open squares are data obtained by extrapolation from a fit to the CGL equation down from higher ε values. At small enough values of Re, these agree to within experimental error.

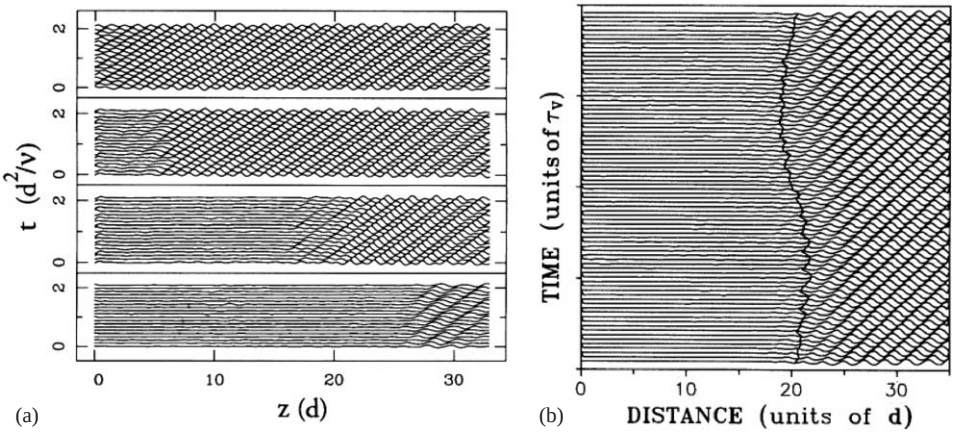

Fig. 38. (a) Space–time plots of the patterns at $Re = 3$ for increasing values of ε in the experiments by Babcock et al. [19], from bottom to top $\varepsilon = 0.0347$, 0.0632, 0.0822 and 0.1020. Only the first quarter of the apparatus behind the inlet is shown. (b) A longer space–time plot in the convectively unstable regime from the experiments of Tsameret and Steinberg [405] at $\varepsilon = 0.04$ and $Re = 3$. The full vertical line marks the position of the front defined by the position where the pattern amplitude reaches a fixed value.

The lower panel corresponds to the case just above threshold ($\varepsilon - \varepsilon_c \approx 0.031$). In this case, incoherent Taylor vortex patterns are found a distance of order 25 down the cylinders away from the inlet—small perturbations and fluctuations near the inlet are amplified while they are advected

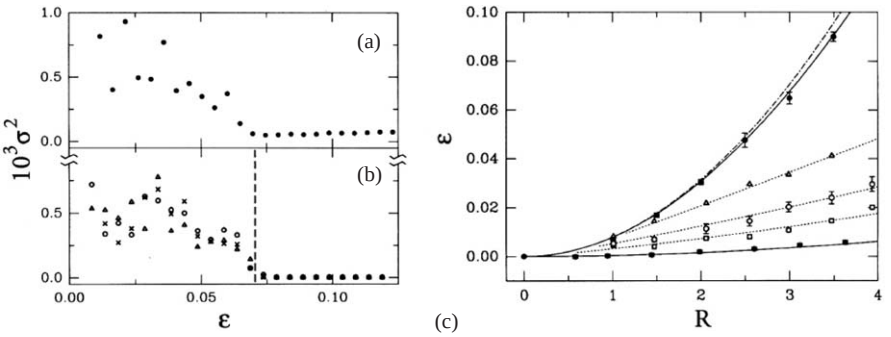

Fig. 39. Various data from the experiments of Babcock et al. [19]. (a) (Upper left panel) Normalized mean squared width σ^2 of the peak in the frequency spectrum as a function of ε at $Re = 3$ obtained from the measurement of the pattern amplitude as a function of time at a position $100d$ behind the inlet (note that this is three times further from the inlet than the region shown in Fig. 38(a)). The sharp transition at $\varepsilon = 0.065$ indicates the change from the small-ε regime where the patterns are incoherent due to phase noise to a coherent large-ε regime where pattern are coherent. This value is therefore associated with the transition from the convectively unstable to the absolutely unstable regime. (b) (Lower left panel) Corresponding results for the CGL equation (137) with three different noise levels, $10^{-6}(\times)$, $10^{-5}(\triangle)$, and $10^{-4}(\bigcirc)$. The dashed line locates the transition $\varepsilon_{ca}^{CGL} = 0.071$ [19]. (c) Stability diagram for axisymmetric Taylor vortex patterns. The lower line and data points mark the line $\varepsilon_c(Re)$ where the instability sets in. The upper data points locate the transition ε_{ca} from the convectively unstable regime to the absolutely unstable regime as determined from the change-over from coherent to incoherent patterns via measurements of the spectrum like those in (a), while the dashed line indicates ε_{ca}^{CGL}. Between the lower line and the upper line, the system is convectively unstable, and noise-sustained structures like those in the one but lowest panel of Fig. 38 occur. Open symbols indicate the boundaries where noise sustained structures occur in simulations, from top to bottom, at $z = 25d$, $50d$, and $100d$. The dotted lines indicate estimates of these boundaries from the deterministic CGL equation (137) with a fixed value of $A(z = 0)$ imposed.

away, and only at this point have they grown large enough in size that they are measurable. Behind this region, they saturate (the plot actually shows only the first quarter of the total cell). In this region, the combination of the fluctuations and perturbations near the inlet and the convective effects give rise to an incoherent front-like state. As Fig. 38(b) from the other group [405] illustrates, the effective front position (defined by tracing the point where the pattern amplitude reaches a certain level) is indeed slowly wandering back and forth on a longer time scale.

As we go up in Fig. 38(a), ε is increased. The pattern fills more and more of the cell, and at the same time become more coherent, while the width of the front separating the two regions decreases. Clearly, in the upper panel for $\varepsilon = 0.102$ the Taylor vortex pattern fills the whole cell, and one is in the absolutely unstable regime. The pattern selection in this regime and near the transition was studied numerically in [68,69,272,390].

The transition from the convectively unstable to the absolutely unstable regime is reflected in the coherence of the pattern. A good way to quantify this is to measure the frequency of the pattern at a fixed position. The more coherent the pattern, the sharper the peak associated with the pattern frequency (the position of the peak is simply fixed by the wavelength and phase velocity of the pattern). The upper panel of Fig. 39(a) shows the mean squared width σ^2 of the measured peak.

The experimental data on this system have been compared in detail [19,405] with the results of numerical studies [318] and with the analytical predictions based on the amplitude equation. Just above the threshold of supercritical (forward) bifurcation to a finite-wavelength pattern, the pattern

dynamics can quite generally be described by an amplitude equation [105,189,193,435]. Because of the advection of the patterns by the through flow, the appropriate amplitude equation in this case is the cubic CGL equation

$$\tau_0\partial_t A + s_0\partial_z A = \xi_0^2(1+\mathrm{i}c_1)\partial_z^2 A + \varepsilon(1+\mathrm{i}c_0)A - g_0(1-\mathrm{i}c_3)|A|^2 A \ , \tag{137}$$

where the second term on the left-hand side is the group velocity term associated with the advection of the pattern, and where z is the fixed coordinate frame along the axis of the cylinders. For an impression of the various types of behavior of the incoherent structures in the CGL equation with an advection term in a finite system with noise we refer to the work by Deissler [115–117,119], Deissler and Kaneko [70] [118] and Proctor et al. [358]. In the present case, all parameters associated with the terms linear in A in this equation were known directly from the stability analysis [318], while c_3 was determined via the standard method of calculating the nonlinear terms in an amplitude expansion [318] (the parameter g_0 only sets the amplitude scale and hence is not of importance in comparing theory and experiment). This therefore allowed a direct comparison between theory and experiment to be made with only one adjustable parameter, the effect of the noise at the inlet. [71] Fig. 39(b) shows the results of simulations of Babcock et al. [19] in which only a random noise term of strength Δ was added to Eq. (137). As can be seen, the behavior of the mean squared width of the spectrum of A in the simulations, sampled at the *same* distance $z = 100d$ as in the experiments, quantitatively reproduces the experimental data of Fig. 39(a)! Moreover, it is seen that the behavior is quite independent of the value of the noise strength Δ, so the comparison between theory and experiment is effectively made without adjusting any crucial parameter!

For the CGL equation (137), the transition from the nonlinearly convectively unstable to the nonlinearly absolutely unstable regime can easily be calculated explicitly since the fronts are pulled. For zero group velocity, $s_0 = 0$, the linear spreading velocity v^* is simply

$$v^*_{\mathrm{CGL}} = 2\,\frac{\xi_0}{\tau_0}\,\sqrt{\varepsilon(1+c_1^2)} \ , \tag{138}$$

compare Eq. (100) for the case $\xi_0 = 1$, $\tau_0 = 1$. In the presence of the advection term with s_0, a pulled front connecting the $A = 0$ state on the left to the saturated state on the right moves with velocity $s_0 - v^*_{\mathrm{CGL}}$. When this velocity is positive, the front is convected away and the system is convectively unstable, while when $s_0 - v^*_{\mathrm{CGL}} < 0$ the front moves upstream to the inlet and the system is absolutely unstable. The transition from the convectively unstable to the absolutely unstable regime therefore occurs when $s_0 - v^*_{\mathrm{CGL}} = 0$, i.e., for

$$\varepsilon_{\mathrm{ca}} = \frac{s_0^2\tau_0^2}{4\xi_0^2(1+c_1^2)} \ . \tag{139}$$

For the parameters corresponding to the experiments of Figs. 39(a) this gives the value marked with the dashed line in panel (b)—the remarkable agreement confirms that the transition from coherent, virtually noiseless patterns at larger values of ε to noise-induced fluctuating structures coincides with the transition from the absolutely unstable to the convectively unstable regime.

---

[70] Deissler and Kaneko [118,213] have introduced in particular the notion of velocity-dependent Lyapunov exponent. This concept will be touched upon briefly in Section 3.22.

[71] Several features of the scaling behavior are actually captured by the deterministic equation if one takes the value of A at the inlet at $z = 0$ fixed at a given value [19,405].

Finally, Fig. 39(c) from [19] shows the full phase diagram of the present system as a function of *Re*. The full symbols along the upper line mark the transition from the coherent patterns to the incoherent noisy patterns determined experimentally from the spectrum, as in panel (a) for $Re = 3$, and the dashed line marks ε_{ca} according to (139). The open symbols denote the values of ε where noise-sustained structures arise for three different downstream values of z.

A detailed theoretical study of the Taylor–Couette system with through flow, which goes beyond the amplitude equation, can be found in [69,349,361]. Also the Rayleigh–Bénard system with through flow has been analyzed along similar lines [70,210].

In conclusion, these experiments on Taylor–Couette patterns in the presence of through flow nicely illustrate several conceptual issues: (i) the distinction between nonlinearly absolutely unstable and convectively unstable regimes; (ii) the change from coherent to incoherent patterns that this transition implies; (iii) the fact that in realistic systems true front structures arise where saturation behind the front is important; (iv) since fronts in the cubic Complex Ginzburg–Landau equation are pulled, all essential properties can still be calculated explicitly from the linear dispersion relation; (v) the importance of noise sustained structures in general for convective systems.

The effect of noise on convective systems has recently been studied systematically for the CGL equation by Proctor et al. [358], who map out the full phase diagram (see also [272,390]). In line with our discussion of the behavior of fronts in the CGL equation in Sections 2.11.5 and 2.11.6, the behavior as a function of the control parameter ε depends strongly on whether or not the state selected by the front is unstable to the Benjamin–Feir instability.

We finally note that recently the effect of through flow on chemical reactions has also been studied experimentally and theoretically [211,290].

3.12. Fronts and noise-sustained structures in convective systems II: coherent and incoherent sources and the heated wire experiment

In the previous section, we discussed the relation between noise-sustained structures in pattern forming system in which an advection of the patterns is induced by externally imposing a flow. In pattern forming systems which exhibit a Hopf-bifurcation to spatially and temporally periodic patterns, the ensuing traveling wave patterns intrinsically have a nonzero group velocity, and close to the threshold the instability to a single mode is always convective. If the transition is supercritical (forward), then close to the threshold in the convectively unstable regime the emergence of noise-sustained patterns is again intimately connected with the dynamics of pulled fronts.

We focus here on the discussion of defects in one-dimensional systems which exhibit a supercritical transition to traveling-wave patterns, as these are most intimately connected with the front propagation issue of interest in this paper. One should note, however, that the motion of defects has experimentally also been studied in great detail in binary mixtures [217,235]. The fact that transition to traveling wave states in this system is subcritical rather than supercritical gives rise to a number of interesting additional effects, like the "locking" of a defect to the underlying period of the pattern [46,352]. We refer to the papers by Kaplan and Steinberg [217] and Kolodner [235] for examples and for an entry into the literature on these issues.

A new feature, in comparison with the discussion of the previous section, is that if the underlying system is spatially reflection symmetric, two types of traveling-wave states will be possible, left-moving waves and right-moving waves. If each mode suppresses the other, the long-time

dynamical state of the system is often dominated by sources and sinks. A source is a solution which sends out left-moving waves to the left, and right-moving waves to the right, while a sink absorbs a right-moving wave from the left and a left-moving wave from the right. Since sources are the active generators of the traveling waves, their behavior is most important for the dynamics of a traveling wave pattern. As we shall see, sources induce a sharp crossover from coherent to incoherent dynamics, which is closely related to the one discussed in Section 3.11 above.

The appropriate amplitude equations for the pattern dynamics just above onset of a Hopf bifurcation to traveling wave patterns are [105]

$$\tau_0(\partial_t A_{\rm R} + s_0\partial_x A_{\rm R}) = \varepsilon A_{\rm R} + \xi_0^2(1+{\rm i}c_1)\partial_x^2 A_{\rm R} - g_0(1-{\rm i}c_3)|A_{\rm R}|^2 A_{\rm R} - g_2(1-{\rm i}c_2)|A_{\rm L}|^2 A_{\rm R}\ , \tag{140}$$

$$\tau_0(\partial_t A_L - s_0\partial_x A_{\rm L}) = \varepsilon A_{\rm L} + \xi_0^2(1+{\rm i}c_1)\partial_x^2 A_{\rm L} - g_0(1-{\rm i}c_3)|A_{\rm L}|^2 A_{\rm L} - g_2(1-{\rm i}c_2)|A_{\rm R}|^2 A_{\rm L}\ . \tag{141}$$

Here $A_{\rm R}$ and $A_{\rm L}$ are the amplitude of the right and left moving waves, and s_0 is the linear group velocity.[72] The terms on the first line of each equation are the same for each individual mode as in the single CGL equation (137) for the advected Taylor vortices. The last term on the second line describes the coupling of the modes. We will be interested in the regime $g_2 > g_0$ where one mode suppresses the other one sufficiently strongly that standing wave patterns do not form [105,417].

To understand how the dynamical behavior or sources is intimately related to that of fronts and to the transition from the convectively unstable to the absolutely unstable regime, consider first the case in which there are no left-moving patterns, $A_{\rm L}=0$. In this case the amplitude equation (140) for $A_{\rm R}$ reduces to the single CGL equation (137) considered in the case of the advected Taylor vortex pattern. As we already mentioned there, fronts in the cubic CGL equation are pulled, and hence the velocity of the rightmost front in the top panel of Fig. 40 (it is sketched with a dashed line and connects the unstable state at $x\to-\infty$ to the saturated finite amplitude state for $x\to\infty$) is simply $s_0 - v^*_{\rm CGL}$, where $v^*_{\rm CGL}$ is the linear spreading velocity of the single CGL equation, given in (138). Furthermore, $\varepsilon_{\rm ca}$ given by (139) marks the transition from the absolutely unstable regime for larger ε to convectively unstable regime for smaller ε. Thus, for $\varepsilon < \varepsilon_{\rm ca}$ the right front actually recedes in the positive x-direction, for $\varepsilon > \varepsilon_{\rm ca}$ the growth is strong enough that it moves upstream. See the top panel of Fig. 40.

The picture of how sources are built from fronts, as it has emerged from theoretical studies [102,417] is the following. Consider two widely separated fronts in $A_{\rm L}$ and $A_{\rm R}$, as sketched in Fig. 40(a). When $\varepsilon > \varepsilon_{\rm ca}$ the two fronts move towards each other; once they get close they form a stationary coherent source solution which sends out waves of the same wavelength and frequency to both sides [417].[73] Very much like what we saw in the previous section, sufficiently deep into

[72] We stress here that the term "right-moving" and "left-moving" refers to the group velocity, in particular also in the definition of a source. In principle, it is possible that the phase velocity of the traveling waves is opposite to the group velocity. If this is the case, to the eye it appears that the pattern runs into the source instead of being sent out by it. See [417] for further discussion of this.

[73] We can thus think of the sources in the absolutely unstable regime $\varepsilon > \varepsilon_{\rm ca}$ as bound states of two pulled fronts. This is somewhat reminiscent of the pulse solutions in the single quintic CGL equation, which can be thought of as a bound state of two pushed front solutions [424].

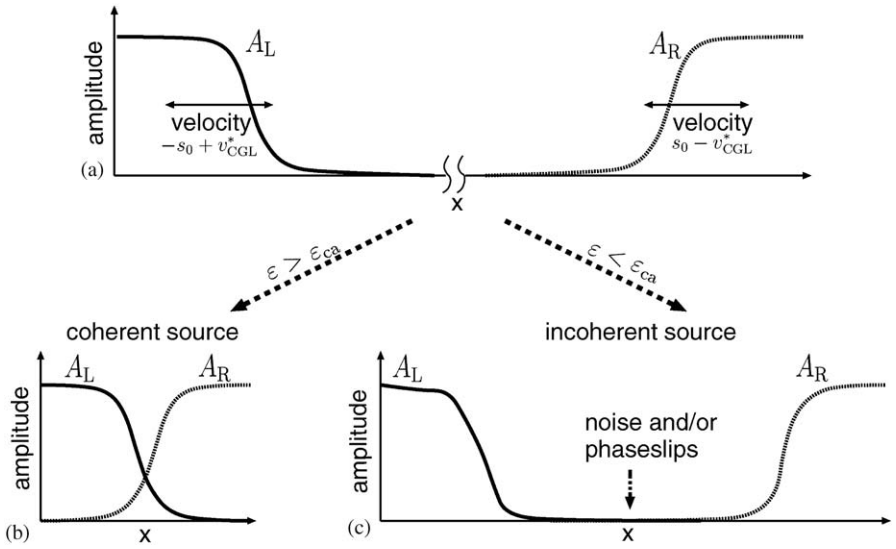

Fig. 40. Schematic illustration of how incoherent and coherent sources in traveling wave systems are built from front solutions. In the upper panel, we start from two isolated front solutions which are so far apart that they are non-interacting. In the absolutely unstable regime, for $\varepsilon > \varepsilon_{ca}$, the two fronts move together. The coherent source solution they then form can be thought of as a bound state of the two fronts (lower left panel). In the convectively unstable regime, $\varepsilon < \varepsilon_{ca}$, the two fronts would move apart in the absence of interactions and of noise. In practice, a wide incoherent fluctuating source results. Whether the average source width is determined by the noise or the interactions, is at present unknown. Possibly, this also depends on the initial separation of the fronts.

the absolutely unstable regime $\varepsilon > \varepsilon_{ca}$ the coherent sources give thus rise to coherent traveling wave patterns with only very small fluctuations.

In the convectively unstable regime $\varepsilon < \varepsilon_{ca}$ the two fronts of Fig. 40(a) would move infinitely far apart if there were no fluctuations and no interactions. The discussion of the previous section would lead one to expect incoherent pattern dynamics in this regime, which originates from the center of the convectively unstable region between the two fronts, as indicated in Fig. 40(c). This *is indeed* what is found in numerical studies [417], but the origin of the fluctuations is not completely understood in this case. Clearly, if a sufficiently large random noise is added to the coupled equations (140) and (141), one will enter a similar incoherent fluctuation-dominated regime like the one we discussed in Section 3.11. The numerical studies give reason to believe, however, that in the small noise limit, another intrinsic incoherent dynamical regime exists where the fluctuations result from the interaction of the two fronts in their tails, presumably via the generation of phase slips which give rise to intrinsically chaotic behavior which in turn is advected away towards the front-like regions.

One way in which the crossover between the two results shows up is in the width of the sources, defined as the distance between the two points where the two amplitudes reach a fixed fraction of the saturated value. In Fig. 41(a) we show the results for the inverse of the (average) source width in numerical simulations of Eqs. (140) and (142). When ε is decreased towards ε_{ca}, the width of the coherent source solutions increases rapidly: the width of the coherent source solutions appears

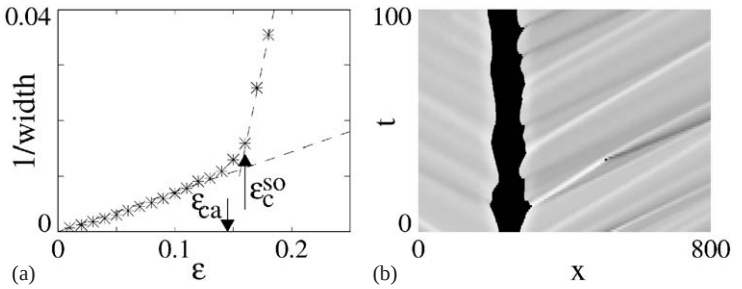

Fig. 41. Results of numerical simulations of the behavior or sources in the coupled CGL equations (140) and (141) in the absence of external noise. (a) Inverse average source width as a function of ε for the coupled equations with $s_0 = 1.5$, $c_1 = -1.7$, $c_2 = 0$, $c_3 = 0.5$, $g_2/g_0 = 2$, and $\xi_0 = \tau_0 = 1$. Note the crossover at ε_c^{so} just above $\varepsilon_{ca} = 0.14$, and the fact that the width diverges inversely proportional to ε for small ε. (b) Space–time plot of the local wavenumber of the fluctuating source for $\varepsilon = 0.11 < \varepsilon_{ca} = 0.14$, illustrating the fluctuations of the width and the incoherent dynamics it entails in the traveling wave domains away from it. In the black region the sum of the modulus of the two amplitudes have fallen below 10% of the saturated value; the light and dark streaks correspond to hole-like wavenumbers packets sent out by the source. From Pastur et al. [335].

to diverge at ε_{ca}. Just before ε_{ca}, however, the width becomes so large that the fluctuation effects from the region where both amplitudes A_R and A_L are small, take over. This happens at the point marked by ε_c^{so} in Fig. 41(a). For smaller values of ε sources are incoherent and their width scales as ε^{-1}. Fig. 41(b) shows a space–time plot of an incoherent source in this parameter range: the core (black region) fluctuates in time, and these fluctuations are reflected in the grey regions where the amplitudes are close to their saturation values.[74] As noted before, whether the incoherent source fluctuations arise from numerical noise in the simulations or from intrinsic dynamics in their center, is at present not completely clear. It is possible that there is no unique answer: when we generate source solutions starting from initial conditions with two widely separated fronts, it is conceivable that it depends on the initial separation of these fronts, which mechanism dominates.

Recent experiments on traveling waves near a heated wire[75] have confirmed these theoretical predictions [335,336]. In such experiments, a wire is suspended a few millimeters below the surface of a fluid, and heated with the aid of an electrical current [136,431,432]. Above some critical heating, the temperature pattern near the wire exhibits a bifurcation to waves which travel along the wire; by detecting the deformation of the surface, they can be detected with high precision. Measurements of this type not only confirm that the bifurcation is supercritical, and hence that the above coupled CGL equations are the appropriate amplitude equations, but also yield all parameters entering formula (139) for the crossover value [335,336]. The value obtained from such measurements is $\varepsilon_{ca} = 0.14 \pm 0.02$. In agreement with the results of the theoretical and numerical studies, a crossover in the inverse width of the sources is found precisely at this value, see Fig. 42(a) [335,336]. Furthermore,

[74] Not only is the phase of the amplitudes fluctuating in these regions, the source also sends out coherent structures at irregular intervals. These are visible as the light streaks, and appear to correspond to so-called homoclon solutions [416,418].

[75] In a related experiment on hydrothermal waves in a cell heated from the side, the transition from the convectively to absolutely unstable regime was recently also verified quantitatively [178].

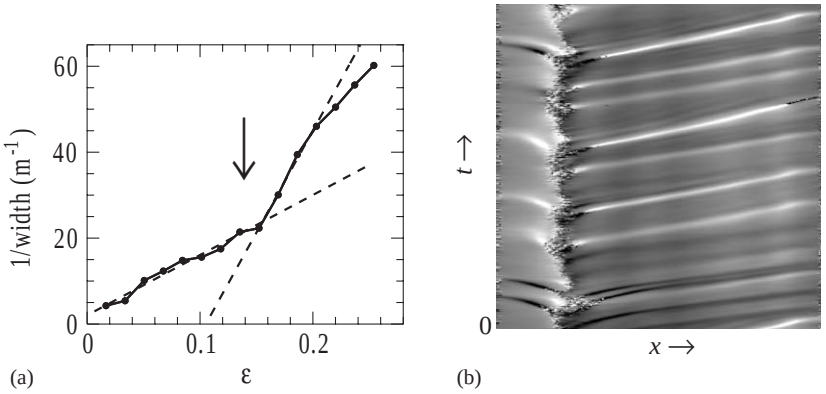

Fig. 42. (a) Dependence of the inverse of the average width of a source on the reduced control parameter ε which measures the distance from the threshold at which traveling waves appear in the heated wire experiment of Pastur et al. [335,336]. The value of ε_{ca} which was obtained independently from measurements of the group velocity s_0, the correlation length ξ_0 and the time scale τ_0, is indicated by an arrow. At this point, a crossover in the inverse source width as a function of ε is observed in the same way as in the numerical simulations, see Fig. 41(a). (b) Space–time diagram of the local wave number of a source in the experiments for $\varepsilon = 0.11$, i.e., in the incoherent source regime. The extent of the x-axis is 42 cm, the total time is 10485 s.

as Fig. 42(b) illustrates, space–time traces of the dynamics in the convectively unstable regime below ε_{ca} show that the sources are wildly fluctuating in this regime. Very much like what was found for the width of the frequency peak in the traveling Taylor patterns in Fig. 39(a), the peak in the spectrum rapidly broadens as ε is reduced below ε_{ca} [336].

We finally stress again that just above a supercritical transition, the situation is generally rather simple because the fronts are pulled: For this reason, the transition from convective to absolute instability is given by the linear criterion (the sign of $s_0 - v^*$). When a transition is subcritical (inverted), the fronts near the transition are usually pushed (see Section 2.7.5), and then the distinction between the two regimes is determined by the velocity of the pushed front, for which no general results are known. As an example of this, we may mention that a secondary bifurcation observed in a cell heated from the sides is subcritical, and that a pushed-front mediated transition from the convectively to absolutely unstable state was recently observed in such an experiment [179].

The discussion in this session clearly illustrates that fronts are important building blocks of the dynamics of traveling wave systems. Although this behavior has been mapped out sufficiently well that quantitative predictions can be made in realistic cases, on a more fundamental level many issues are poorly understood. We already mentioned that the origin of the fluctuating sources is not understood very well—is external noise necessary or is the deterministic interaction between the tails of the fronts sufficient to give the incoherent behavior? Can one understand some of the behavior from studying the (non)existence of coherent source solutions following the methods of [374]? Do sources send out homoclon solutions [418,419]? Why do sources seem to conform experimentally to those arising in amplitude equations, while sinks do not?

3.13. Chemical and bacterial growth fronts

The issue of front propagation into unstable states often plays a role indirectly in theoretical analysis of waves and fronts in coupled reaction–diffusion equations—e.g., fronts are an important building block of spirals. Nevertheless, clean examples of single fronts in realistic experimental situations do not appear to be abundant. In this section we will first briefly discuss few of the results of a series of experiments designed specifically to study fronts, and then briefly touch on the broader implications of the difference between pushed and pulled fronts for pattern dynamics in coupled reaction–diffusion systems.

In the last decade, experimentalists have been able to develop chemical reactors in which the Turing instability and other chemical reaction patterns could be probed [76,120,152,254,263,293,327]. The Turing instability is the stationary bifurcation to periodic patterns in coupled reaction diffusion systems, which may occur when the activator (the component with autocatalytic characteristics) has a diffusivity which is significantly smaller than that of the inhibitor [152,311,435]. The suppression of the activator diffusion coefficient is experimentally achieved by reversibly binding to an immobile species attached to an aerogel; this same gel also allows the continuous feeding of the reactants without inducing convection.

A few years ago, Horváth et al. [201,398] and De Kepper and coworkers [110,173] have introduced variants of such experiments that allow them to systematically produce and study fronts and the two-dimensional patterns they give rise to. The basic reaction is a chlorite oxidation of the $S_4O_6^{2-}$ ion. In this reaction, the hydrogen H^+ ion plays the role of the autocatalyst, and its diffusion is suppressed in a controlled way by incorporating carboxylate groups which reversibly bind it in the polymer gels (even an electric field may change the effective diffusion ratio [399]). Initially planar reaction fronts were created by cutting the polymer gel with the reactants into two, treating one of the parts so as to induce a reaction, and then putting the two parts carefully back together again in a sealed cell to prevent evaporation.

The dominant reactions in this system can to a good approximation be described by the following dimensionless coupled reaction–diffusion equations [110,201]

$$\partial_t \alpha = \nabla^2 \alpha - \alpha\beta^2(\kappa + 7\alpha) \ , \tag{142}$$

$$\partial_t \beta = \delta\sigma^{-1}\nabla^2 \beta + 6\sigma^{-1}\alpha\beta^2(\kappa + 7\alpha) \ , \tag{143}$$

where α is the dimensionless $S_4O_6^{2-}$ concentration and β the dimensionless H^+ concentration, δ is the ratio of diffusion coefficients of these two components in the absence of the binding of the H^+ to the carboxyl groups, and κ is a parameter which depends on the relative chlorite excess. The coefficient σ accounts for the reversible binding of the hydrogen: as σ increases, both the effective hydrogen diffusion and the effective reaction rate is suppressed.

Note that the state $\beta = 0$ (no hydrogen) in this system of equations is unstable: as soon as β becomes nonzero the autocatalytic reaction term in these equations makes β increase. However, since this reaction term is quadratic in β, to linear order in β there is no instability. Hence there is no nonzero linear spreading speed v^*, and fronts in this equation are always of the pushed type.

Theoretical studies [200,243,244] of fronts in such coupled reaction–diffusion models have shown that when the effective diffusion coefficient δ of the autocatalytic β component is sufficiently small, the fronts exhibit a long-wavelength instability of the type found for the Kuramoto–Sivashinsky

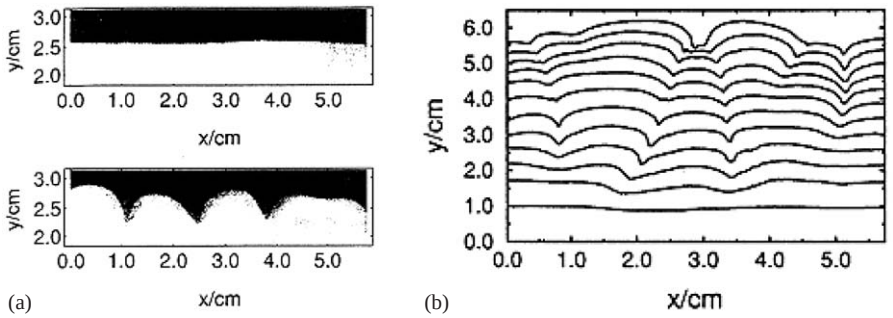

Fig. 43. (a) Front images in the experiments by Tóth and Horváth [398]. The upper image corresponds to the regime where the front is stable, while the lower one to the regime where the effective hydrogen diffusion coefficient is so small that the planar interface is unstable. The fronts are advancing upward. (b) Traces of the front positions in these experiments at time intervals of 120 min in the regime corresponding to the lower image of (a). The dynamics of the interfaces in this regime is very similar to that found in the Kuramoto–Sivashinsky equation, the generic lowest order equation just above threshold of a long-wavelength interface instability.

equation discussed in Section 2.11.4. In agreement with this, Tóth and Horváth [398] found that when the hydrogen ion diffusion was sufficiently suppressed, the fronts exhibited the lateral type of structures familiar from the Kuramoto–Sivashinsky equation [243,244,277,351,381,386], in agreement with the theoretical predictions. An example of some of their observations is shown in Fig. 43.

To what extent are these results of interest from a more general perspective? The answer lies in the deep connection with the issue discussed later in Section 5: because the fronts in this reaction–diffusion system are pushed, the spectrum of the linear stability operator of a planar front is gapped, and the dynamically important region for the stability modes is the front region itself. Because of this, in the thin interface limit the front behavior can be described by a moving boundary or effective interface approximation, in which the front is viewed as a line (in two dimensions) or a sheet (in three dimensions) of vanishing width. As we shall argue below, this immediately implies that for sufficiently small ratio of diffusion coefficients, the reaction front exhibits a long-wavelength instability, and this in turn means that just above the instability threshold, the interface dynamics maps onto that of the Kuramoto–Sivashinsky equation (96). [76]

The point now is the following. As we will discuss in Section 5 *pulled fronts cannot simply be viewed as a moving boundary or interface in the limit when their nonlinear transition zone is thin*, because their dynamically important region is the semi-infinite region ahead of the front. On the other hand, when a front is pushed, the situation is very different and actually much simpler: in the limit where their width is much smaller than the typical length scale of the pattern (e.g., the typical front radius of curvature), *pushed fronts are amenable to a moving boundary or effective*

[76] The prefactor of the linear terms in the Kuramoto–Sivashinsky equation are fixed by the coefficients in the dispersion relation of the weakly unstable interface mode. The prefactor of the nonlinear term is fixed by the fact that for an isotropic system, the projection of the velocity onto the overall propagation direction of a piece of interface of height h whose normal makes an angle θ with the propagation direction, is simply $v_{\rm planar}/\cos\theta = v_{\rm planar}(1 + \frac{1}{2}(\nabla h)^2 + \cdots)$. For a more explicit derivation of the Kuramoto–Sivashinsky equation and a study of the chaotic behavior in the context of the present type of reaction–diffusion equations, see, e.g., [277].

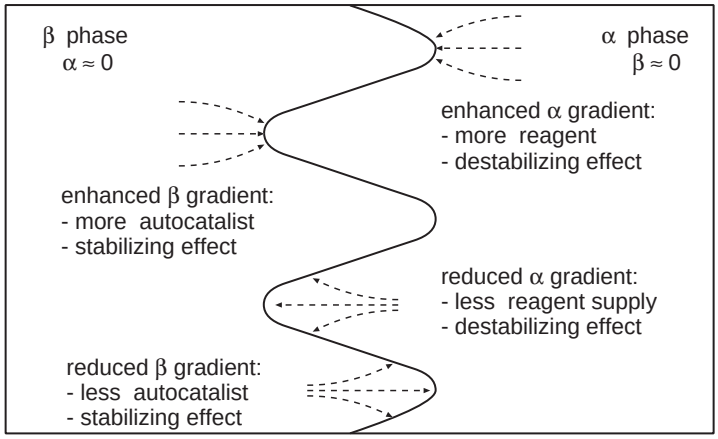

Fig. 44. Schematic illustration of the origin of long-wavelength lateral instabilities of a fronts in coupled reaction diffusion equations which describe the propagation of the domain of an "autocatalytic" substance β (e.g. bacteria in a bacterial growth model) into a region with abundant reactant α (nutrient in the bacterial case). The front is indicated by the solid line and is moving to the right. If it is a pushed front, its dynamics can be mapped onto an effective interface model or moving boundary problem for perturbations on length scales much larger than the interface width. For long-wavelength perturbations of this effective interface or boundary (drawn with a solid line), the supply of the reactant is enhanced at forward protrusions and decreased for the protrusions staying behind. This effect clearly tends to enhance the instability. On the back side, the situation is the opposite: the diffusion of β towards the interface is reduced behind the forward protrusions, and this tends to stabilize the interface. Which of the two effects dominates, depends the ratio of diffusion coefficients. If the diffusion coefficient of β is sufficiently large relative to that of the α reactant, then the stabilizing effect wins, while if the diffusion coefficient of β is small enough, the destabilizing effect dominates and the interface is unstable. For pulled fronts, the argument does not hold because they cannot be described in an effective interface approximation.

interface approximation in which the front is treated as a line or sheet of zero thickness at which the outer fields obey certain boundary conditions. As we illustrate in Fig. 44, a propagating reaction diffusion front which effectively leads to a replacement of one species ahead of it by another one on the back, *will generically exhibit a long-wavelength instability of the Kuramoto–Sivashinsky type in the limit in which the diffusion coefficient of the species behind the front* (*the autocatalyst in the language used above*) *is much smaller than that of the one in front* (*the reactant*).[77]

We need to stress that the above analysis does not give a prediction concerning the lateral instability of fronts which are pulled. Indeed, the discharge fronts discussed in Section 3.5 are examples of pulled fronts which *do* exhibit a long wavelength instability, while for the fronts in coupled chemical

[77] For moving fronts, the long-wavelength instability that arises for sufficiently small diffusion coefficients of the phase behind the front is intimately related to the Mullins–Sekerka instability discussed in Section 3.17. This may not be obvious at first sight, since the dispersion relation (158) is not analytic in k, while the actual dispersion relation near threshold of the long-wavelength instability of an interface has of course an expansion in k^2. The reason for the difference is that the usual Mullins–Sekerka dispersion relation is derived in the limit that the interface growth velocity is small enough that the diffusion equation of the outer phase ahead of the front can be approximated by the Laplace equation. Deep into the unstable region of the phase diagram, the dispersion relation of bacterial growth models like the one specified by Eqs. (146) and (147) becomes more like the Mullins–Sekerka form (158)—see e.g. [306].

reaction–diffusion equations of the form

$$\partial_t \alpha = \nabla^2 \alpha - \kappa\alpha\beta - \alpha\beta^2 \ , \tag{144}$$

$$\partial_t \beta = \delta\nabla^2 \beta + \kappa\alpha\beta + \alpha\beta^2 \ , \tag{145}$$

Horváth et al. [200] have found strong numerical indications that the fronts were always weakly stable in the pulled regime $\kappa > \frac{1}{2}$. As soon as they were pushed for $\kappa < \frac{1}{2}$, they were found to exhibit a long-wavelength instability, in accord with the above arguments. From a different angle, Kessler and Levine [228] have also found results which are consistent with our scenario: they pointed out that if a set of continuum reaction–diffusion equations with pulled fronts is simulated with a discrete lattice model, the resulting model does obey a long-wavelength lateral front instability of the type discussed above if the ratio of diffusion coefficients is sufficiently small. This is consistent with the observation, to be discussed in Section 7, that the effective cutoff provided by the particles makes the front (weakly) pushed, and hence that it should have a long-wavelength instability in the limits in which the diffusion coefficient of the phase on the back is much smaller than the one in the phase ahead of the front.

The general theme of this section is also of immediate relevance for biological growth models. E.g., bacterial colonies can exhibit growth patterns which are reminiscent of Diffusion Limited Aggregation clusters [292] and other growth patterns [39,40,107,183,288]. Various reaction diffusion models have been suggested to explain some of this behavior [41,107,183,298]. In particular, it has been argued [183,231,236] that in cases in which the bacteria secrete a fluid which acts like a lubricant for their motion, a model with a nonlinear diffusion coefficient of the type

$$\partial_t \alpha = \nabla^2 \alpha - \alpha\beta^m \ , \tag{146}$$

$$\partial_t \beta = \delta\vec{\nabla} \cdot (\beta^k \vec{\nabla}\beta) + \alpha\beta^m \ , \tag{147}$$

with $m = 1$ would be appropriate. In this case, β is the dimensionless bacterial density, and α plays the role of the nutrient field. As we already mentioned above, fronts in this model are pulled in the case $k = 0$, $m = 1$, and for any $m > 1$ the fronts are pushed and do have a long-wavelength lateral instability. Likewise, with nonlinear diffusion, $k > 0$ but bilinear kinetics ($m = 1$), fronts are pushed and have a long-wavelength lateral instability for small enough δ [306], again in accord with our general arguments.[78] Thus, these considerations are an important ingredient for chemical and biological model building: the above reaction–diffusion model (146), (147) with $m = 1$, $k = 0$ is a bit of a singular case,[79] as for any $m > 1$ or $k > 0$ the fronts are pushed and exhibit a long wavelength instability for small δ.

It is important to stress that although I believe the above scenario to be generally true on the basis of the strength of the arguments of Section 5 and those illustrated in Fig. 44, this powerful line of argument is, to my knowledge, relatively unexplored—I have not seen it discussed explicitly in

[78] Technically, the situation for the bacterial growth model (146), (147) with $m = 1$ is somewhat more complicated than we present it here: in the limit $\delta \downarrow 0$ the growth fronts have all the properties of an interfacial growth model with a Mullins–Sekerka like instability, but the moving boundary approximation is probably not rigorously correct, as it is not quite justified on all physically relevant length scales [306].

[79] Actually, to my knowledge, neither the singular behavior in the limit $k \downarrow 0$ nor the one in the limit $m \downarrow 1$ has been worked out; these limits appear to be interesting technical challenges [306].

the physics or mathematics [80] literature, and it should be considered as an interesting line of future research to investigate or (dis)prove this argument. The considerations are clearly an important ingredient for chemical or biological model building.

We finally note that the fronts we have discussed here connect domains where the system itself does not have a finite-wavelength instability. Fronts which generate a state which is unstable to a Turing or Hopf instability, or which propagate into a state with a pattern due to this instability, are discussed in [374].

3.14. Front or interface dynamics as a test of the order of a phase transition

When the thermodynamic phase transition between two phases is of first order, both individual phases are stable to small perturbations of the order parameter in the neighborhood of the transition. This immediately implies that there is then a nucleation barrier for the formation of a droplet or nucleus of one phase in the other. Since this nucleation barrier is large near the transition (as it proportional to a power of the ratio of the finite surface tension of the interface between the two phases and the difference in chemical potentials, which becomes arbitrarily small near the transition), the nucleation rate for such droplets of the other phase is small. On the other hand, once an interface exists, it can usually grow with a speed which is linear in the driving force, i.e., the difference in chemical potentials or free energy ΔF. [81]

$$v \sim \Delta F \sim T - T_c \ , \tag{148}$$

where T_c is the transition temperature. Here we used the fact that near first order transition the difference in free energy is linear in the temperature difference. The fact that the nucleation rate is exponentially small near the transition, while interfaces respond linearly to the driving force, is the reason for the ubiquity of interfacial growth phenomena in physics.

Near a second order transition, the situation is very different. For our purposes the important point is that the response is very asymmetric. If the system is rapidly heated up from below T_c where the system is ordered to above T_c, the driving force for the order to disappear is finite everywhere in the bulk of the system, so the order parameter relaxes homogeneously in the bulk of the system—one normally will not see a propagation of domains of the disordered phase into ordered domains: Instead, the order just dies away homogeneously. On the other hand, when the system is quenched from above to below T_c, the most common situation is that patches of the stable ordered phase grow out; usually the order parameter has a different sign (say magnetization up or down in the cases of systems with an Ising symmetry) or direction (in cases where the order parameter is a vector) in different patches, and so the initial phase is then followed by one where the domains coarsen in size or where defects anneal out. However, if the fluctuations are small it may happen that the ordering

[80] Apparently, in some cases which we would refer to as an example of a coupled reaction–diffusion problem with pulled fronts, it has been noted that standard analysis trying to prove convergence to a moving boundary description breaks down (D. Hilhorst, private communication), but the connection with the general scenario advanced here appears not to have been made.

[81] An exception are faceted crystals which in the absence of dislocations grow via the nucleation of new layers on top of the existing one. This nucleation rate is again small for small driving forces. If there are screw dislocations at the surface, these can act as sources for step motion, and the growth rate is quadratic in the chemical potential difference [42].

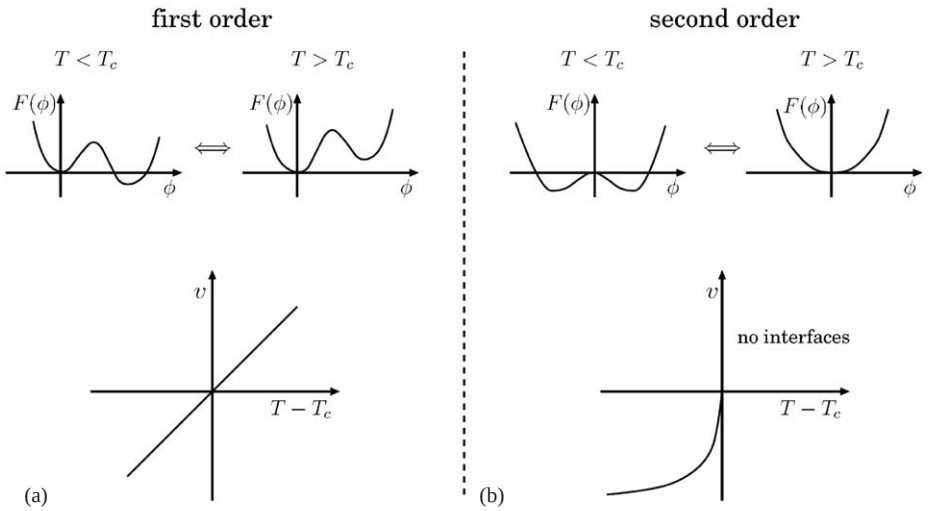

Fig. 45. Schematic sketch of the relation between the order of a phase transition and the behavior of the interface velocity near the critical point. The qualitative behavior is indicated within a Landau picture, but the behavior holds more generally for non-mean-field systems. (a) The case of a second order phase transition. The upper part indicates the behavior of the free energy density as a function of the order parameter below and above T_c, while the lower part illustrates that the interface velocity is linear in the deviation of the temperature at the interface from the critical value. (b) Similarly for the case of a second order phase transition. Note that the steady state propagation of an interface into a domain of the ordered state is not possible, as there is a finite driving force on the bulk order parameter to relax to zero. On the ordered side, the front velocity depends nonlinearly on the deviation from the critical point. In Landau theory this dependence is as $v \sim \sqrt{|T_c - T|}$.

in this case occurs mostly through the growth of domains of the stable phase into the disordered phase. The velocity of these interfaces will scale as ξ/τ where ξ is the correlation length which diverges as $|T - T_c|^{-\nu}$ at a second order transition, and τ is the characteristic correlation time which diverges as $|T - T_c|^{-\nu z}$ [199]. So we generally get a power-law scaling $v \sim |T - T_c|^{\nu(z-1)}$. In mean field theory, with $\nu = \frac{1}{2}$ and $z = 2$ for diffusive systems, this gives $v \sim |T - T_c|^{1/2}$.

These considerations can be illustrated simply in a Landau mean field picture for an order parameter ϕ described by the dynamical equation

$$\frac{\partial \phi}{\partial t} = -\frac{\delta \mathscr{F}}{\delta \phi}, \quad \text{with } \mathscr{F} = \int d\mathbf{r}[\tfrac{1}{2}(\vec{\nabla}\phi)^2 + F(\phi)] \ . \tag{149}$$

The dynamics implied by this equation is such that the free energy $\mathscr{F}$ is non-increasing in time ($\mathscr{F}$ acts like a Lyapunov function, see footnote 58), so it tends to drive ϕ to the value at which the free energy density $F(\phi)$ is minimal.

In the case of a first-order transition, the function $F(\phi)$ has the form sketched in Fig. 45(a): there are two local minima (or three if the order parameter is symmetric under a change of sign). At high temperatures, the one corresponding to the disordered phase ($\phi = 0$) is the absolute minimum, but as the temperature is lowered, the other one corresponding to the ordered phase comes down, and at $T = T_c$ the value of F at the two minima is the same. Below T_c, the latter one is the absolute minimum. If one consider a planar interface solution $\phi = \phi(\zeta)$ in a frame $\zeta = x - vt$ moving with

velocity v in this case, Eq. (148) reduces to

$$-v\frac{\partial\phi}{\partial\zeta}=-\frac{\delta\mathscr{F}}{\delta\phi}\ , \tag{150}$$

which upon multiplying with $\partial_\zeta\phi$ gives

$$v=\frac{\int_{-\infty}^{\infty}\mathrm{d}\zeta\,\partial_\zeta\delta\mathscr{F}/\delta\phi}{\int_{-\infty}^{\infty}\mathrm{d}\zeta(\partial_\zeta\phi)^2}=\frac{F(\phi(\infty))-F(\phi(-\infty))}{\int_{-\infty}^{\infty}\mathrm{d}\zeta(\partial_\zeta\phi)^2}\ . \tag{151}$$

The term in the numerator is a unique number for functions $F(\phi)$ like those sketched in Fig. 45(a). For stationary interfaces, when the minima of the free energy in the two phases is the same, this term is related to the excess energy associated with the presence of the interface [56,192,428]: we can then interpret it as the surface tension. Since this term is positive, the above expression confirms that the interface velocity is linear in the difference in the free energy densities of the two phases it separates, and hence linear in the temperature, as sketched in the figure and anticipated already in Eq. (148). Moreover, it propagates in such a direction that the domain with the lowest free energy density expands.

The function $F(\phi)$ corresponding to a second order transition is sketched in Fig. 45(b), and the prototypical dynamical equation for this case is of course the F-KPP equation (1) with $f(u)=\varepsilon u-u^3$ and $\varepsilon\sim T-T_c$. For $\varepsilon>0$, i.e., below T_c, we have indeed the possibility of fronts propagating into the unstable state $u=0$ with speed $v^*=2\sqrt{\varepsilon}$. As was already stated above, for $\varepsilon<0$, (above T_c), any nonzero initial condition for u is driven rapidly to zero, and hence no front propagation is possible. Thus, as illustrated in the lower part of Fig. 45(b), near a second order transition, propagation of fronts is very asymmetric relative to T_c, on one side fronts or interfaces are possible, but their growth velocity is a nontrivial power law of the distance from criticality, $T-T_c$, while on the other side interface motion does not occur.

Normally, one does not study the motion of an interface in order to determine the order of a phase transition, of course. However, these considerations have been of use in at least one case, the study of the so-called Halperin–Lubensky–Ma [194] effect near a nematic–smectic A transition. In the nematic phase, the orientation of the long liquid crystal molecules acquire a directional order: on average they all point in the same direction [114]. This directional order is the slow mode of a nematic phase that is responsible for much of the special behavior and applications of these materials. In the smectic phase, the molecules also obtain a layered ordering, and the smectic A phase is the one where the molecules point on average along the normal to these layers. In a classical Landau theory, the nematic to smectic-A transition can be both of first and of second order: if we think of ϕ in the discussion above as the smectic layering order parameter, then in a Landau theory, the free energy density $F(\phi)$ can have either of the forms sketched in Fig. 45. However, Halperin et al. [194] showed that when the coupling to the director fluctuations is taken into account, and when subsequently the director fluctuations are integrated out,[82] the Landau expression acquires a cubic term $|\phi|^3$ which renders the transition weakly first order in the regime where without this term it would be of second order. The Halperin–Lubensky–Ma effect is thus an example of a fluctuation-driven first order transition.

[82] The analysis of Halperin et al. [194] also applies to type I superconductors: the coupling to the gauge fluctuations can drive the normal to superconductor transition weakly first order in some regimes.

The first dynamical indications for the existence of this fluctuation effect came from a series of experiments near the nematic to smectic-A transition of Cladis et al. [87]. When the temperature was changed through T_c for a series of liquid crystals mixtures which before had been concluded to span a tricritical point where the transition changed from first order to second order, propagating interfaces were observed, both upon raising the temperature and upon lowering the temperature through T_c. As explained above, this might be taken as a sign that the transition was in fact always at least weakly first order for all compositions.[83] A more careful analysis by Anisimov et al. [8] later confirmed this and showed the consistency of these dynamical measurements with measurements of the latent heat and the correlation length near the transition [7]. These authors took the Landau free energy expression

$$\mathscr{F}(\phi) = \int \mathbf{dr}\,[\tfrac{1}{2}\,\xi_0^2(\vec{\nabla}\phi)^2 + a\phi^2 + b|\phi|^3 + c\phi^4 + d\phi^6]\ , \tag{152}$$

with the cubic term motivated by the analysis of Halperin et al. which as mentioned above always renders the transition first order. They then fitted the parameters a and c in this expression to both the latent heat data and the X-ray measurements of the correlation length of this series (for $b = 0$, the point where $c = 0$ marks the tricritical point). The other parameters were fixed once for the whole series of mixtures. The fit of the measurements of the cross-over function for the latent heat (which is always nonzero for $b \neq 0$) is shown in Fig. 46(a). Once these coefficients are determined, one can then calculate the slope $v/\varepsilon \sim v/|T - T_c$ of the interface response near the transition, apart from an overall factor that sets the scale. As Fig. 46(b) shows, the curve obtained this way from static measurements fits the experimental data for the interface mobility v/ε remarkably well for the 9CB–10CB mixtures. Taken as a whole, the dynamical measurements together with the theoretical analysis thus give quite strong evidence for the prediction by Halperin et al. [194] that the coupling to the director fluctuations drive the nematic to smectic-A transition weakly first order.

3.15. Switching fronts in smectic C* liquid crystals

In the previous section, we already encountered the smectic-A phase of a liquid crystal. In this phase the molecules form layers. Along the layers the molecules are fluid-like (no ordering), but the orientation of the molecules is aligned on average along the normal of the layer. In a smectic-C phase, the molecules again have a layered ordering, but on average they are tilted in each layer with a fixed angle relative to the normal. The projection of this tilt onto the layers forms an azimuthal angle, which is an important slow hydrodynamic variable for the smectic-C phases. In the smectic-C* phase, finally, this angle rotates over a small angle from layer to layer, so that it makes a full twist of 2π over a mesoscopic distance, the "pitch" of the liquid crystal. This situation is sketched in Fig. 47(a). In this figure, the local polarization (which is normal to the average orientation of the

[83] The tricky part experimentally is to rule out the possibility that there were no temperature gradients in the experiments which induced an effective interface—after all, if the temperature is above T_c on one side of the sample and below T_c on the other side, one will also create an interface if the transition at constant temperature is second order. Care was taken in the experiments [8,87] to rule out such gradients, but the strongest evidence for the fluctuation-induced weakly first order transition actually comes from the consistency of the dynamical measurements with the latent heat measurements and the X-ray measurements of the correlation length [8].

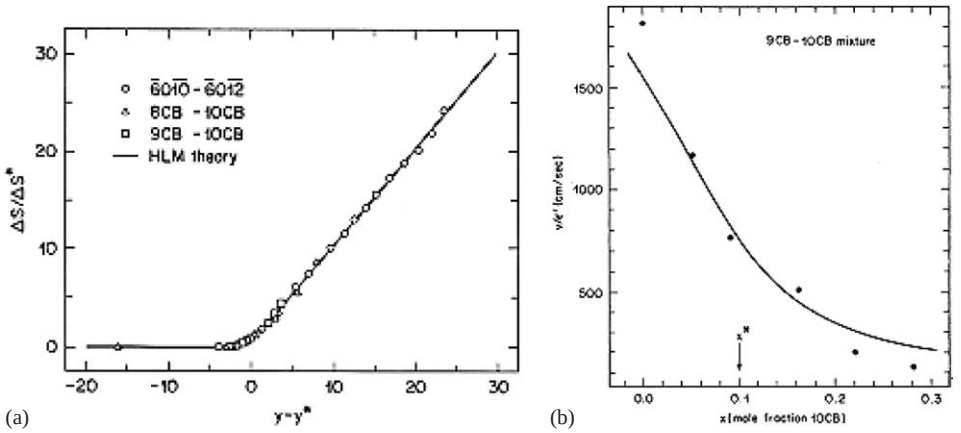

Fig. 46. (a) Normalized universal scaling form for the change of entropy ΔS at the transition (which is proportional to the latent heat) in a three series of liquid crystal mixtures. The full line is a fit to a scaling form obtained from the Landau free energy expression (152). The variable along the horizontal axis is a scaled composition variable. In the absence of the cubic term proportional to b in Eq. (152), the curve would vanish linearly at $y - y^* = 0$, and would be zero to the left of it: y^* marks the tricritical point in the scaled parameters and in the absence of the cubic term. From Anisimov et al. [8]. (b) The measured interface mobility v/ε plotted as a function of the concentration in the 9CB-10CB mixtures according to the analysis by Anisimov et al. [8]. The full line is obtained from the Landau expression obtained by fitting the parameters to latent heat data like in (a) and to measurements of the correlation length, apart from an overall factor that sets the scale.

molecules) is indicated with little arrows, and the angle this vector makes with the x-axis is denoted by ϕ; the z-axis is the coordinate along the normal of planes.

What makes the smectic-C* phase especially interesting from our perspective is that the angle ϕ can be oriented both with an electric field and with a magnetic field. Without a field, the twist of the director is uniform, i.e. $\phi = 2\pi z/p$, where p is the pitch length, which depending on the material can range from a few tenth of a micron to several microns. If we consider for simplicity the case that the angle ϕ is uniform within each layers, then in the presence of electric and magnetic fields perpendicular to the layers, the free energy per unit area can be written as [88,114,274]

$$\mathscr{F} = \int \mathrm{d}z \left[\frac{K}{2} \left(\frac{\partial \phi}{\partial z} - q_0 \right)^2 - PE \cos\phi + \left(\frac{\Delta\varepsilon E^2}{8\pi} + \frac{\Delta\chi H^2}{2} \right) \cos^2\phi \right] . \tag{153}$$

Here P is the ferroelectric polarization, which points normal to the direction in which the molecules are tilted. The second term describes the dielectric and diamagnetic coupling: $\Delta\varepsilon$ is the dielectric anisotropy and $\Delta\chi$ similarly the diamagnetic anisotropy [114]. Note that the electric and magnetic field enter the same way. In the theoretical analysis below, we therefore simply put $H = 0$ and consider the two cases in which $\Delta\varepsilon$ is positive or negative. Experimentally, however, the fact that there are two different contributions to this term is important. First of all, it allows one to shift the importance of this term relative to the polarization term. Secondly, if $\Delta\varepsilon$ and $\Delta\chi$ have opposite signs it opens up the possibility to change the *sign* of this term. As we shall see below, this has important implications for the front dynamics.

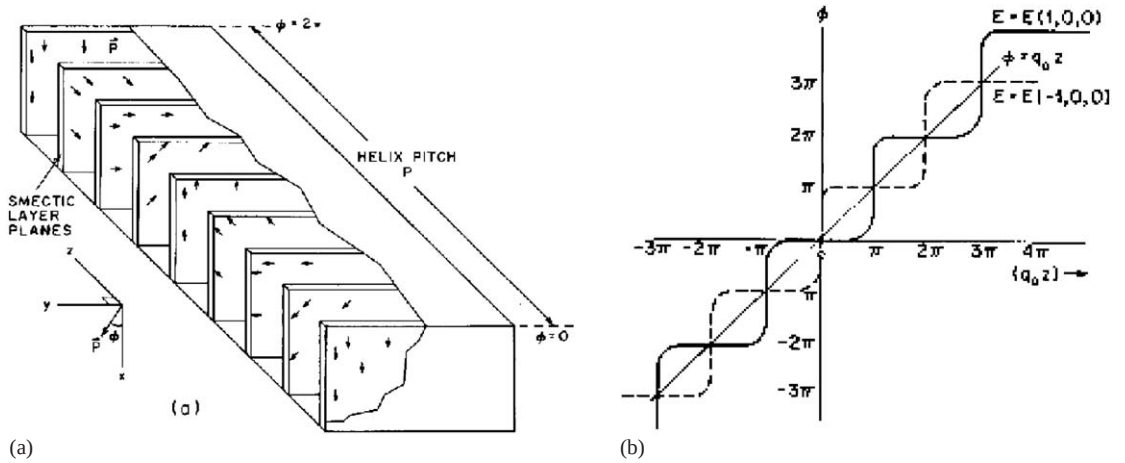

Fig. 47. (a) Sketch of a smectic-C* phase of a liquid crystal. In this phase the molecules are layered, but their average orientation is tilted relative to the normal to the planes. The local polarization P_s, which is normal to the c-director, is indicated with arrows in this figure. From layer to layer, this angle ϕ makes a small rotation, so that over a large distance the angle is wound over 2π. From Maclennan et al. [274]. (b) Schematic illustration of the stable angle solution $\phi(z)$ of a smectic-C* in a strong electric field E along pointing in the positive x-direction (full line) and in the negative x-direction (dashed line). Note that in the first case, there are wide plateaus at $0, \pm 2\pi, \pm 4\pi, \ldots$, while in the latter case these are at $\pm\pi, \pm 3\pi, \ldots$. Upon switching the field direction, each domain wall where ϕ changes rapidly before the switching splits into two fronts propagating into the two adjacent plateaus, which have been made unstable due to the reversal of the field. From [427].

Suppose we start from a case without any fields, so that the smectic is in the uniform helical state $\phi = 2\pi z/p$, and switch on the electric field to a large positive value. Then the free energy density is lowest for $\phi \approx 0, \pm 2\pi, \pm 4\pi$, etc. Because of the twist in the initial state, the smectic will form a series of domains of length close to the pitch length p, separated by thin domain walls where ϕ rapidly changes by 2π. This situation is sketched in Fig. 47(b) with the full line. If the field is now rapidly reversed, $E \to -E$, then the free energy density is lowest in the regions where $\phi = \pm\pi, \pm 3\pi$, etc. In the limit in which the fields are large so that the domain walls are thin, the original walls will then split into two fronts which propagate into the domains which have been made high energy domains by the field reversal.

In the absence of the dielectric and diamagnetic terms the situation is very simple: the switching of the fields makes the state in the domains unstable, since the prefactor of the $\sin\phi$ term in the free energy changes sign. Hence in the high field limit we have a clear case of pulled front propagation into unstable states. The general situation is more intricate as it depends on the sign of the dielectric and diamagnetic term; let us define for $H = 0$

$$\alpha = \frac{\Delta\varepsilon |E|}{4\pi P} \quad (H = 0) \ . \tag{154}$$

If α is negative, then the dielectric field contribution has extrema for the same angles where the polarization term is extremal, while when α is negative, it is minimal for $\phi = \pm\pi/2, 3\pi/2$, etc. The full behavior of the field contributions to the free energy density as a function of ϕ are sketched in Fig. 48(a) for various values α, both for field $E < 0$ (upper panel) and for field $E > 0$

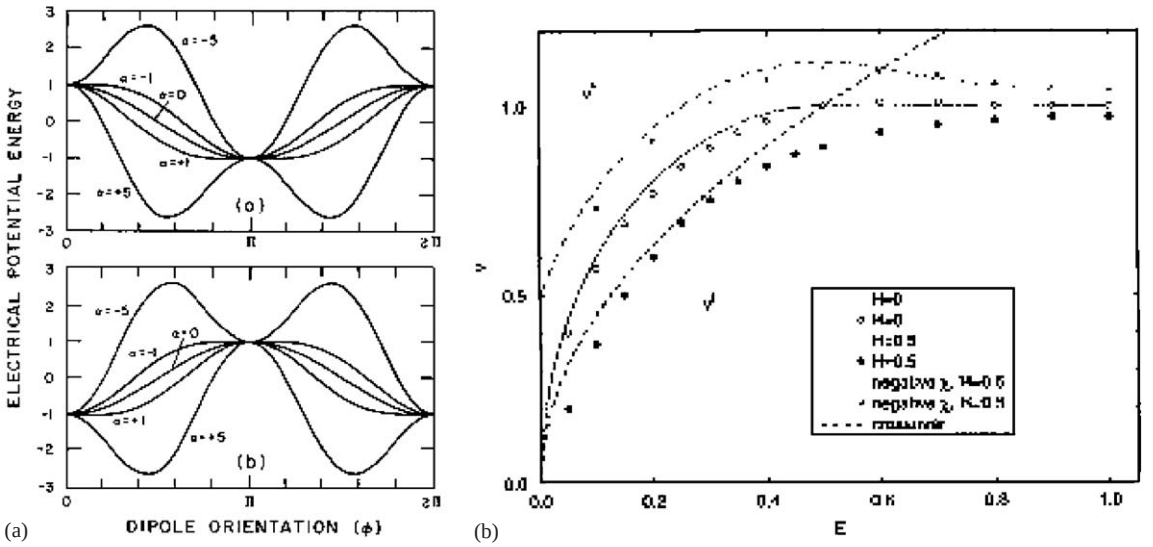

Fig. 48. (a) Electrical free energy density (153) of the smectic-C* as for various values of α. The upper panel corresponds to the case $E<0$ and the lower panel to the same field positive field strength. From Maclennan et al. [274]. (b) Front velocities for the generalization of Eq. (155) to the case $H=0$ for three values of the field. The full curve corresponds to the case $H=0$ discussed in the text. The crossover from pulled to pushed fronts occurs at $E=1/2$ in this case. Symbols indicate the velocity obtained numerically from simulations in runs of finite length. Note that the data points tend to lie slightly below the asymptotic velocities in the small field range, due to the slow power law convergence to the pulled front speed v^*. From [427].

(lower panel). Consider first the case $\alpha<0$, and take initially $E>0$. As the lower panel shows, the state with $\phi=0$ then has the lowest free energy, so in the domains we have $\phi\approx 0$ (modulus 2π). Now, upon switching the electric field, the free energy becomes the one of the upper panel. As the curves indicate, the state in the domains is then unstable for $-1<\alpha<0$ and metastable for $\alpha<-1$. Thus, by increasing the field one can continuously go from a case of front propagation into unstable states to a case of a front propagating into a metastable state, in this regime.

Clearly, the regime $\alpha>0$ is different, as Fig. 48(a) illustrates. While upon increasing the field E for negative values of α the free energy density sharpens at minima, upon increasing the field for $\alpha>0$ the minimum initially flattens and then turns into a local maximum. Moreover, upon switching the electric field for $\alpha>1$ the state which was stable before switching experiences a finite driving force to the new minimum. This implies that in this regime one will not observe front propagation.

For smectic-C* liquid crystals, the moment of inertia of the molecules is normally small enough that the inertial terms can be neglected in comparison with the viscous torque. In this regime, the dynamical equation for the angle ϕ then becomes $\eta\partial_t\phi=-\delta\mathcal{F}/\delta\phi$, where η is a twist viscosity. In appropriate dimensionless variables this gives for $\alpha<0$ and $E>0$ [88,114,274]

$$\partial_t\phi=\partial_z^2\phi+f(\phi)\quad\text{with}\quad f(\phi)=E\sin\phi-E^2\sin\phi\cos\phi\ , \tag{155}$$

which is nothing but the prototype equation for front propagation, the F-KPP equation (1); the only difference with the usual case is that the function $f(\phi)$ is now a periodic function of ϕ, which allows for stable arrays of kinks [84] like those sketched in Fig. 47(b).

For a full study of the dynamics exhibited by this equation upon reversal of the field direction we refer to the work by Maclennan, Clark and Handschy [274]; we focus our discussion here on the front dynamics which is relevant in the parameter range where the front width is much smaller than the pitch p.

The surprising feature in this case is that the selected front velocity can be obtained analytically both in the pulled and in the pushed regime, because it turns out that it is possible to solve for the pushed front solutions by making the Ansatz $h=E\sin(\phi)$ in the "reduction of order method" discussed briefly in the example at the end of Section 2.7.1. Indeed, for the case $H=0$ this yields pushed solutions for $E>1/2$ with velocity $v^\dagger=1$ of (155), whose analytic form is given by [88,387,427]

$$\phi^\dagger(\xi)=2\arctan[\exp(-\sqrt{|\alpha|}\xi)]\ . \tag{156}$$

Since $v^*=2\sqrt{E-E^2}$, one indeed immediately sees that $v^\dagger>v^*$ for $E>1/2$. As mentioned earlier, the results for $H\neq 0$ can all be obtained by appropriate transformations that translates this case back to the case $H=0$ summarized above. Nevertheless, from a practical point the possibility to play with both E and H may be quite important, since when $H\neq 0$ the front solutions are pushed both for small and for large fields E. Fig. 48(b) shows the selected front speed as a function of E for three values of the magnetic field H.

As is well known, liquid crystals are important for displays; if one would want to use the present switching effect in applications, the switching time is of course an important parameter, and this is inversely proportional to the front speed. For a discussion of the transient behavior as well as of the comparison with experiments, we refer to the review by Maclennan et al. [274].

3.16. Transient patterns in structural phase transitions in solids

One possible way in which a structural phase transition in a solid can occur is when certain atoms or ions which have two different competing sub-lattices available, order below some critical temperature. Often, such ordering phenomena in solids are strongly coupled to strain deformations and lower the symmetry of the crystal structure. About a decade ago, it was conjectured that certain transient metastable tweed patterns that are sometimes found near structural phase transitions might be due to the propagation of a pattern forming front into an unstable state [373].

For the transient patterns of interest—e.g. tweed patterns associated with vacancy ordering in YBCO superconductors or Al,Si ordering in Na feldspar—the equilibrium ordered state is to have a homogeneous phase in which the ions are (partially) ordered on one of two available sub-lattices. In practice, however, domains with alternating order are sometimes observed upon shock heating. Salje [373] has suggested that these pattern arise from a pattern forming front propagating into the structurally unstable homogeneous disordered phase. In particular, if ϕ denotes the dimensionless kinetic order parameter with $\phi=\pm 1$ indicating the two possible sub-lattice ordered states, and $\phi=0$ the disordered state in a coarse-grained description, Salje [373,406] arrived, on the basis of

[84] In the usual case, the equation also admits solutions which correspond to a periodic array of kinks where ϕ switches between the stable states of $f(\phi)$, but these multiple kink arrays are then unstable to pairing.

a treatment of the kinetics which approximately includes nonlocal strain effects, at the following dynamical equation for the order parameter:

$$\partial_t \phi = \partial_x^2 \phi - \gamma \partial_x^4 \phi + \delta_1 (\partial_x \phi)^2 + \delta_2 \phi^2 \partial_x^2 \phi \ . \tag{157}$$

Note that this equation can be viewed as an extension of the EFK equation discussed in Section 2.11.1. Like that one, the stable lowest energy states are clearly the homogeneously ordered states $\phi = \pm 1$. Moreover, since the terms linear in ϕ are exactly those of the EFK equation, it follows from the results of Section 2.11.1 that indeed for $\gamma > 1/12$ a pulled front propagating into the unstable disordered $\phi = 0$ state will give rise to transient patterns. Simulations in [373] also confirmed this. [85]

To our knowledge, there is at present no direct evidence in support of the intriguing conjecture that the transient modulated order patterns are caused by pattern forming pulled fronts—the difficulty with solid ordering phenomena is that it is often hard to rule out other possible mechanisms.

3.17. Spreading of the Mullins–Sekerka instability along a growing interface and the origin of side-branching

When the growth of an interface is limited mainly by how fast the material necessary for growth can be transported towards it from the phase into which it grows, or by how fast heat produced at the interface can be transported away through diffusion into the phase into which it grows, then a growing planar interface of this type is unstable: A small protrusion of the interface towards the phase into which it grows leads to an enhancement of the gradients in front of the interface. This enhanced gradient leads to an enhancement of the diffusion and hence to an enhanced growth: the protrusion will grow larger and larger, and render the interface unstable. This so-called Mullins–Sekerka instability [73,220,247,308,309], which we essentially already encountered in Section 3.13, underlies an enormous variety of diffusion-limited growth processes, ranging from crystal growth from the melt or electric discharge patterns like the streamers of Section 3.5, to fractal growth phenomena like Diffusion Limited Aggregation [22,292].

We focus our discussion on the Mullins–Sekerka instability of a planar crystal interface growing into an undercooled melt. In this case, the dispersion relation of small perturbation in the height h of the interface of the form $h \sim \mathrm{e}^{-\mathrm{i}\omega t + \mathrm{i}kx}$ is [73,247,308]

$$\omega = \mathrm{i} v_\mathrm{n} |k| (1 - d_0 \ell_\mathrm{D} k^2) \ . \tag{158}$$

Here v_n is the normal velocity of the planar interface, as sketched in Fig. 49, d_0 is the capillary length which is proportional to the surface tension of the interface, and ℓ_D is the diffusion length on the liquid side of the interface.

The linear spreading velocity associated with this dispersion relation is easy to determine; one simply finds

$$v^*_\mathrm{MS} = \sqrt{3} v_\mathrm{n} \ , \tag{159}$$

[85] Note that the term proportional to δ in (157) tends to enhance the growth rate, and that it is quadratic in the amplitude. We therefore would expect a transition to pushed fronts for sufficiently large δ; to our knowledge, this possibility has not been explored, however.

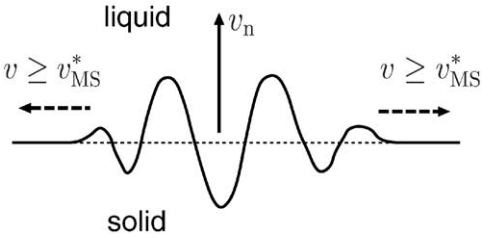

Fig. 49. Schematic illustration of the spreading of a localized perturbation along a growing crystal melt interface which is unstable as a result of the Mullins–Sekerka instability. The dashed line indicates the unperturbed planar interface, which is growing in the vertical direction with a normal velocity v_n. The dashed arrows indicate the propagation of the perturbation along the interface. In accord with the discussion of Section 2.6, the asymptotic Mullins–Sekerka front speed is larger than or equal to the linear spreading velocity v^*_{MS} given in Eq. (159).

with

$$\lambda^* \equiv k_i^* = \frac{1}{\sqrt{6 d_0 \ell_D}}, \quad k_r^* = \frac{1}{\sqrt{2 d_0 \ell_D}} , \tag{160}$$

where, as before, $k_r^* = \mathrm{Re}\, k^*$ and $k_i^* = \mathrm{Im}\, k^*$. To our knowledge, the spreading of the Mullins–Sekerka instability along the interface has not been studied directly, neither theoretically nor experimentally. [86] We therefore do not know whether the propagation of the Mullins–Sekerka along the interface corresponds to a pushed or pulled front, although since we know that dendritic growth is such a strong instability without saturation, we might intuitively expect it to be pushed in the case of a flat interface illustrated in Fig. 49. Thus, in line with the arguments of Section 2.6, we simply conclude that the front will propagate sideways with asymptotic velocity $v \geqslant v^*_{MS}$. Note that if the front would happen to be pulled, the relation (160) shows that the amplitude of the oscillations grows exponentially by a factor e^{r^*} over one wavelength $2\pi/k_r^*$, with

$$r^* \equiv \frac{2\pi k_i^*}{k_r^*} = \frac{2\pi}{\sqrt{3}} \approx 3.62 . \tag{161}$$

As was also discussed in Section 2.7.6, even if a front is pulled for sufficiently localized initial conditions, it can move faster than v^* if the initial conditions are falling off slower than $e^{-\lambda^* x}$ in space (this case was referred to as "leading edge dominated dynamics" in Section 2.7.6 and in [144]). For pattern forming fronts like these, it was argued in [421] that for a given spatial decay rate $\lambda = k_i < \lambda^*$, the wavenumber would be the one maximizing the growth rate $\mathrm{Im}\, \omega$, i.e., that k_r would be determined implicitly by the condition $\partial \omega_i(k)/\partial k_r = 0$. In the present case this gives

$$k_r^2 = k_i^2 + \frac{1}{3 d_0 \ell_D} , \tag{162}$$

[86] The experimental difficulty is that it is very hard to prepare an unstable interface in this case; if one starts with a stable interface and then tries to bring the interface to the unstable regime, the buildup of the diffusion boundary layer usually gives rise to long transients. Often, the instability already arises during this transient regime.

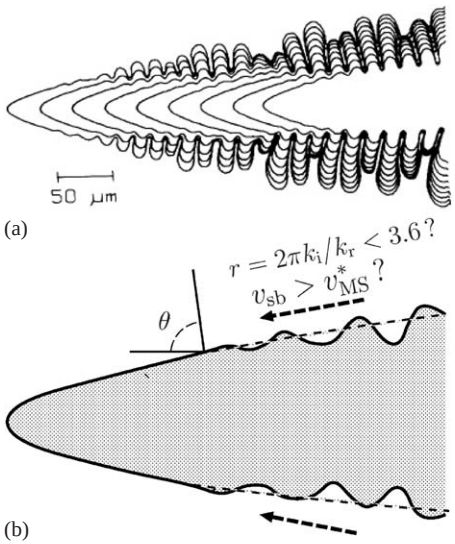

Fig. 50. (a) Snapshot of a NH_4Br dendrite in the experiments by Dougherty et al. [133,134]. (b) Sketch of a dendrite tip identifying the various quantities discussed in the text.

and for the velocity v of the leading edge of such profiles this gives

$$v \equiv \frac{\omega_i}{k_i} = v_n \frac{k_r}{k_i} \frac{2d_0\ell_D}{r} = v_n \frac{2\pi}{3r(1 - r^2/(4\pi^2))}$$

$$> v^*_{MS} = v_n\sqrt{3} \quad (\text{for } r \equiv 2\pi k_i/k_r < r^* = 2\pi/\sqrt{3}) \ . \tag{163}$$

Let us now explore a simple implication of this idea for dendrites. Dendrites are the tree-like growth structures of the type sketched in Fig. 50(a) which the Mullins–Sekerka instability gives rise to. Understanding the shape and velocity selection of a dendritic tip was one of the outstanding problems in the field of interfacial pattern selection in the 1980s. As discussed in various reviews [39,40,73,226,251,338,353], it is now accepted by most workers that the size and velocity of the near-parabolic tip are determined by the nonlinear eigenvalue problem for a uniformly growing near-parabolic tip, and that although surface tension effects are typically small, they act as a singular perturbation. The picture that has emerged is thus that the occurrence of "sidebranches" on these dendrite tips is not important for the dynamical mechanism that "selects" the tip shape and velocity.

The accepted view in the field is that the sidebranches occur due to selective amplification of noise from the tip: small perturbations and fluctuations occur at the tip of the dendrite; these grow out, while being convected away in a frame moving with the tip itself. These ideas have been put forward on the basis of WKB-type analysis of the spreading, growth and advection of side-branch "wave packets" which start near the tip [23,346,347]. Though there is some evidence for this behavior [359], experiments on this issue have turned out to be hard in general; moreover, it is not clear how realistic a WKB-type calculation is for the experimentally relevant regime where tip radius and sidebranch spacing are comparable. However, our analysis above gives us a very simple different way to verify this picture from the data, and in addition suggests a useful way to analyze experimental data on sidebranches. The discussion is a slight reformulation of [425].

The above picture that sidebranches arise from the amplification of noise near the tip is based on the idea that the flanks of the smooth needle solution underlying the dendritic tip region are unstable to the Mullins–Sekerka instability, but that the instability is convective there. Although the sidebranches do not form a coherent front due to the fluctuations, their envelope must propagate on average with a velocity whose projection $v_{sb||}$ along the growth direction is equal to the tip velocity v_{tip}. For a region on the side illustrated in Fig. 50(b) where the underlying tip profile makes an angle θ with the growth direction, this velocity can be expressed in terms of the velocity v_{sb} of the sidebranch front along the interface and the normal velocity:

$$v_{tip} = v_{sb||} = v_{sb} \sin\theta + v_n \cos\theta = v_{sb} \sin\theta + v_{tip} \cos^2\theta \ , \tag{164}$$

where we used the fact that $v_n = v_{tip} \cos\theta$. Equating the two sides gives simply

$$v_{sb} = v_{tip} \sin\theta \ . \tag{165}$$

This equation immediately allows us to compare measured quantities and infer the underlying dynamics from it. Indeed, if we take the interface on the sides as locally planar by ignoring the curvature of the underlying needle solution in this region and assume that the average wavenumber of the incoherent sidebranches can be associated with k_r above, v_{sb} is nothing but the velocity given in (163). If v_{sb} is indeed significantly bigger than v^*_{MS}, the sidebranch instability is indeed convective, and the selective amplification of noise scenario is corroborated by this analysis too. Since $v^* = \sqrt{3} v_n = \sqrt{3} v_{tip} \cos\theta$, in our lowest order approximation we may conclude:

$$\begin{array}{l} \text{sidebranch instability convective} \\ \text{sidebranches} = \text{amplified tip noise} \end{array} \Rightarrow \begin{cases} \theta > 60^o \ , \\ r < 3.62 \ , \\ v_{sb} > v^* \ [v_{sb} \text{ obeys (163)}] \ . \end{cases} \tag{166}$$

To illustrate this, let us apply the above line of argument to the dendrite shown in Fig. 50(a). First of all, the angle on the flanks of the tip region where the sidebranch amplitude is small, is bigger than 60^o. Furthermore, the amplitude of the sidebranch amplitude in this experiment was measured explicitly by Dougherty et al. [133,134]. As Fig. 51 shows, this amplitude initially does rise exponentially; the spatial exponential growth rate k_i is easily estimated to be about $1/(16\ \mu m)$ from these data. This is an indication that indeed in this case, nonlinearities lead to saturation of the sidebranch instability, and hence that if there were no fluctuations, the sidebranch front would correspond to a pulled front. Since the wavelength is about 13 μm in this experiment, we find $r \approx 0.8 < r^*$. In addition, the sidebranch velocity v_{sb} is also found to obey (163) to a good approximation, which indicates that the consistency of this line of argument. Hence, both the angle and the spatial growth rate confirm that the sidebranches in this experiment are consistent with the scenario [23,346] that they emerge from the amplification and convection of small fluctuations near the tip.

Many dendrites appear very much like the ones shown in Fig. 50(a) at first sight. It therefore does appear that in most cases the sidebranches are consistent with the above amplified tip-noise scenario. Unfortunately, the dimensionless growth rate r is hardly ever mentioned in experiments, but judging by the eye this quantity does appear to vary significantly from experiment to experiment.

An interesting question remains whether in some cases, the sidebranch instability might become absolute, in that the projection of the linear spreading velocity v^*_{MS} becomes comparable to the

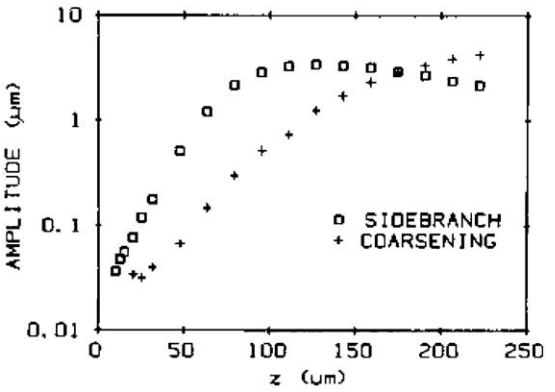

Fig. 51. Measured root mean square amplitude (squares) of the sidebranches of the dendrite shown in Fig. 50(a) as a function of the distance z from the tip, in the experiments by Dougherty et al. [133]. The crosses give a measure of the amount of coarsening of the sidebranches; they are based on the amount of spectral power at low frequencies [133].

tip velocity (such a scenario was also envisioned in [248,287]). One would expect that tip and sidebranches then become strongly coupled, and possibly that the tip region would show appreciable oscillations. That might happen in some parameter range was already suggested by simulations of the so-called Boundary Layer Model by Pieters [346]. Recently, Sakaguchi and Tokunaga [372] observed such behavior in phase field model calculations but the data were not correlated with the parameter r introduced above. A good way to classify sidebranch regimes experimentally and to search for this possibility is to measure the dimensionless growth factor r—if this value is found to increase towards $r^* \approx 3.6$ then the possibility of such a regime becomes more likely. Of course, for a realistic comparison with experiments, effects of interface kinetics and crystalline anisotropy may have to be included, but at the level of the approximations discussed here this poses no technical problems.

The above considerations concerning the absolute or convective nature of the sidebranch instability in my view help us understand how two competing theories might actually emerge as different limits within a more general framework. The usual "solvability theory" which focusses on the existence of featureless needle solutions, amounts, within a WKB approximation, to the requirement that a smooth tip solution without sidebranch-type modes on the flanks is stable [45]. In his "Interfacial Wave Theory", on the other hand, Xu [444] develops an approach in which he allows, essentially within the same WKB approximation, a tip mode to match to divergent sidebranch modes on the sides.[87] To my knowledge, the stability of these solutions, constructed this way, has not been fully investigated. Based on the above analysis, I would expect such dendrite-type solutions to be actually unstable in substantial parts of the parameter range—if so, they would presumably, in the parameter range where this happens, give way to needle-type solutions which are convectively stable in a deterministic approach. In other words, in the range where this happens the usual solvability

[87] The turning point in Xu's WKB analysis becomes, in some limit, the linear spreading point of our analysis, and in principle the "interfacial wave theory" predicts the value of the parameter r introduced above. Also note that the differences and similarities between Xu's approach and the usual solvability theory are brought out most clearly if one thinks of solvability theory in the spirit of the formulation of [45].

scenario would hold, both for the selection mechanism and for the amplification of noise. In other parts of parameter space (roughly identified by generalizations of the ideas presented in this section), needle solutions would be absolutely unstable to sidebranch modes. I would expect Xu's picture to emerge naturally in this regime.

Unfortunately, the dendrite problem is a hard one, and at present we have to consider the above scenario as speculative. In addition, the reader should keep in mind that the above view on the dendrite problem is a minority viewpoint—most workers consider the various theories as mutually exclusive, rather than as two extreme limits of a more general framework.

3.18. Combustion fronts and fronts in periodic or turbulent media

The classic work of Landau [245], who analyzed the stability of flame fronts in terms of a flame sheet of infinitesimal thickness, separating unburned and burned gases, provides a very early example of the clever use of a moving boundary approximation for a problem which more fundamentally is formulated in terms of continuity equations for the temperature and composition of a combustible mixture. The justification for this approximation was later shown to be that the activation energy of the relevant reactions is normally very high, so that the reaction rate is a very steep function of the temperature [67,90,209,439,449]. Inherently, realistic flame fronts are therefore in practice almost always examples of *pushed* fronts: the reaction rate is very strongly (essentially exponentially) suppressed ahead of the flame sheet. In other words, the linear spreading speed is essentially zero.

Although the minimal model for flames amounts to two coupled partial differential equations for the temperature and composition, simple model equations have always played an important role in combustion too. We mention two interesting examples coming from the combustion literature. In fact, an early example of the F-KPP equation (1) with a nonlinearity $f(u)$ which vanishes identically in a finite interval (e.g. $f(u)=0$ for $u<u_c$, $f(u)=(u-u_c)(1-u)$ for $u\geqslant u_c$) is due to Gel'fand [180]. This form was motivated by the above observation that the reaction rate drops so fast with decreasing temperature that it is virtually zero below some critical value.

Two other interesting classes of problems have also emerged from combustion theory: propagation of fronts in periodic media or turbulent media. We first discuss the case of fronts in periodic media. The simple model problem which has often been studied in this context is the following extension of the F-KPP equation [47,48]

$$\partial_t u=\partial_x^2 u+q(x)\partial_x u+f(u,x)\ , \tag{167}$$

and generalization to higher dimensions. In this equation, the advection rate $q(x)$ and nonlinear growth rate f are periodic functions of x with period L: $q(x+L)=q(x)$, $f(u,x+L)=f(u,x)$.

Two classes of growth functions f have been studied, those analogous to the one by Gel'fand mentioned above, and those which give rise to *pulled* fronts in the F-KPP equation [e.g. $f(u)=a(x)u(1-u)$]. The latter type of problem of a pulled front in a periodic medium is especially interesting from our perspective: It should be possible to obtain the asymptotic propagation speed v^* of such pulled fronts by extending our general approach using Floquet–Bloch theory for the linearized equation. To be specific, consider the linearized version of (167) with $f(u,x)$ given as above,

$$\partial_t u=\partial_x^2 u+q(x)\partial_x u+a(x)u\ , \tag{168}$$

where $q(x)$ and $a(x)$ are L-periodic,

$$q(x+L)=q(x), \quad a(x+L)=a(x)\ . \tag{169}$$

According to Bloch's theorem in the language of a physicist or Floquet theory in the more general setting, the generalization of the Fourier transform become the "Bloch waves"

$$\tilde{u}(k,t)=\mathrm{e}^{-\mathrm{i}\omega(k)t+\mathrm{i}kx}U(x)\ , \tag{170}$$

where $U(x)$ is a periodic function of x, $U(x+L)=U(x)$. Just as we did in Section 2.1 for the Fourier transform, once the dispersion relation $\omega(k)$ is obtained, one can analytically continue k into the complex plane. This immediately leads to the conclusion that the linear spreading velocity v^* is again given by the same saddle-point equations (12)—the periodicity of the medium is simply encoded in the dispersion equation $\omega(k)$. For solid state physicists this is no surprise: $\omega(k)$ is the analog of the band energy $\varepsilon(k)$ of Bloch electrons, and as they know, the behavior of free electrons in a solid is completely determined by the band structure.

To the best of my knowledge, the above line of analysis has unfortunately not been tried yet; we do hope such an approach will be explored in the near future, as it would probably be the most direct route to obtaining the asymptotic speed of pulled fronts and as interesting new phenomena might arise from the band structure. In particular, for the simple case $a(x)=1+a_0\cos(2\pi x/L)$ the linear equation reduces to the Mathieu equation, for which it should be possible to obtain a number of (semi-)analytic results.

Another class of front problems which has emerged from combustion theory is the propagation of a front in a spatially and/or temporally random medium as a model for turbulent combustion [225,241,341,443]. From an applied point of view, an important question is to understand the enhancement of the combustion rate due to turbulent advection. One way in which this issue has been approached recently within the context of model problems is to take the function f in Eq. (167) x-independent but the advection field q in this equation a space- and time-dependent random variable. This makes the field u into a stochastic variable as well, and recently several workers [1,2,153,171,172,225,400] have derived results for various probability distributions of the advected u variable. One reason that progress can be made on this complicated problem is that for a pulled front, the linear u-equation captures the essential elements of front propagation (more mathematically: bounds can be derived for the nonlinear equation, using the linearized advected dynamics). It was recently also found that if the q-variable is a stochastic Levy process, the front propagation can change drastically [281]—even an exponentially increasing speed is possible.[88]

There is one important issue concerning fronts in turbulent or random media that to our knowledge has not been discussed explicitly in the literature. Real combustion fronts are pushed fronts, because the combustion rate decreases very rapidly with decreasing temperature. In the limit of large activation energies, flame fronts are very thin and they can be analyzed with a moving boundary approximation [341,439]—this amounts to the approximation in which the flame sheet is treated as an interface of zero thickness. As we discuss in Section 5, for pushed fronts this approximation is indeed justified, but for a pulled fronts it is *not*: For these, the dynamically important region is the semi-infinite domain ahead of the nonlinear front region. It is therefore conceivable that simple

[88] We speculate that this may be related to the fact that an F-KPP equation with power law initial conditions can give rise to an infinite speed [256], and that the probability distribution function of a Levy process has power law tails.

models like (167), whose dynamically important fronts are pulled, are not necessarily good models for turbulent combustion. Probability distribution functions in simple combustion models might well be very different depending on whether fronts are pushed or pulled.

3.19. Biological invasion problems and time delay equations

As mentioned in the introduction, the first studies of front propagation into an unstable state were done in the context of population dynamics and biological invasion problems [163,234]. Not surprisingly, this has therefore remained an active field of research within mathematical biology. The main focus of a large fraction of the literature is still on proving existence, stability and uniqueness of traveling wave solutions in population dynamics models which can be considered as extensions of the F-KPP equation. We refer to Section 14 of the books by Britton [63] and Murray [311] or to the recent review of Metz et al. [296] for an introduction and overview of this subfield. The book by Shigesada and Kawasaki [385] not only gives a good review of the theory, but also discusses in detail a number of applications of the theory to practical invasion problems. Pulled front propagation into unstable states plays a dominant role in a recent model of infection in the Hantavirus epidemics [3].

Also in the bio-mathematical literature the slow power law convergence of pulled fronts to their asymptotic speed has been discussed [296], but I am not aware of examples in that field where this phenomenon has played a significant role. In real life, the fact that the entities in invasion problems are normally discrete may play a more important role—as we shall discuss in Section 7.1, the cutoff in the growth function that the discrete nature of the spreading population gives rise to, alters a pulled front in a continuum equation to a (weakly) pushed front in a model for discrete variables.

A recent development in this field, reviewed recently by Fort and Mendéz [165] has been to consider the effects of time-delay on a front [157,166,174,175]. The motivation for such terms in the case of the spreading of viruses into an uninfected population is that the time which elapses between the moment a cell gets infected and the moment a cell gets infected and the moment a cell dies and the virus begins to spread is an inherent part of the dynamics which cannot be neglected. Within the context of an F-KPP type equation, these effects would seem to lead naturally to equations with a memory kernel, like [89]

$$\partial_t u = \partial_x^2 u + \int^t \mathrm{d}t'\, K(t-t')u(t') - u^n \tag{171}$$

or equations with a finite delay time τ which are obtained when $K(t-t') = \delta(t-t'-\tau)$. However, in practice most work has concentrated on second order equations of the type [165,174,175]

$$\tau\partial_t^2 u + \partial_t u = \partial_x^2 u + u - u^n \tag{172}$$

[89] In cases in which the growth term is most naturally modeled by delay kernel, it would of course make more sense to also take a delay-type term for the nonlinear term describing saturation [295,296]. Of course, as long as the fronts remained pulled, this does not affect our conclusions.

which after appropriate rescalings are obtained by assuming that the time delay is sufficiently short that the memory kernel K can be expanded for short times as

$$\int^t \mathrm{d}t' K(t-t')u(t') = \tau_0 u(t) + \tau_1 \partial_t u(t) + \tau_2 \partial_t^2 u(t) \cdots \ , \tag{173}$$

$$\tau_m = \frac{1}{m!} \int_0^\infty \mathrm{d}\tau\, \tau^m K(\tau) \ . \tag{174}$$

Of course, the transition from a parabolic (first order in time) partial differential equation to a hyperbolic partial differential equation like (172) poses new mathematical challenges concerning existence, uniqueness and convergence [165,174,175]. However, from our pragmatic more "applied" point of view, we want to stress the following. In practice most of the cases that are considered in the literature on delay effects on front propagation into an unstable state, are pulled. Furthermore, the front velocity is the most important property one needs to know in practice. In view of this, it is important to realize there is absolutely no reason to approximate a true time delay equation like (172) by a hyperbolic equation by expanding the delay kernel as in (173). After all, as explained in Section 2.4, the spreading velocity v^* and the associated parameters λ^* and D which govern the shape and convergence of a pulled front, can straightforwardly be determined from the more general class of models as well. An example was given at the end of Section 2.4.

3.20. *Wound healing as a front propagation problem*

In the previous sections we already mentioned that front propagation into an unstable state features in various models that have been studied in the context of biological growth and invasion problems, as well as in the context of pulse propagation in nerves. Since there have, to our knowledge, been few *experiments* in the life sciences which are directly aimed at testing some of the specific front propagation predictions, we want to draw attention to a very nice recent experiment [275] on the healing of epidermal wounds, i.e., wounds on the outer layer of the skin. In the experiments, a 4 mm scrape wound was made; after removal of the displaced cells, the remaining cells were bathed in a fresh culture medium and the position of the invading healing front was measured. Fig. 52 shows a photograph of the wound while it is healing: clearly a rather well-defined front is seen to propagate upward into the space made by the scrape. The data for the position of the cell front as a function of time, extracted from such visual observations, are shown in Fig. 53 with large solid circles. As one can see from these data, the cell front initially moves ahead fast, and then slows down (around a time of order 40–60 h), before it finally settles to a more or less constant speed.

As discussed in [275] several mechanisms of wound healing have been discussed in the literature. Mathematically, most approaches are formulated as a system of nonlinear partial differential equations for cells, whose dynamics is usually taken diffusive, and whose growth responds to various chemical signals via chemokinesis and chemotaxis, or to mechanical signals. In the most simple-minded approach, one then arrives again at a F-KPP type equation, which then incorporates the diffusion, but lumps all the coupling to chemical and mechanical signals into a simple growth term. For this reason, the results of the experiment on the healing of wounds were compared with numerical results for the front dynamics in the F-KPP equation, obtained by tracking the front position at various levels of the dynamical variable u in Eq. (1) (symbols in Fig. 53); indeed, as the figure illustrates, the velocity data for fronts in the F-KPP equation have some similarities with those found

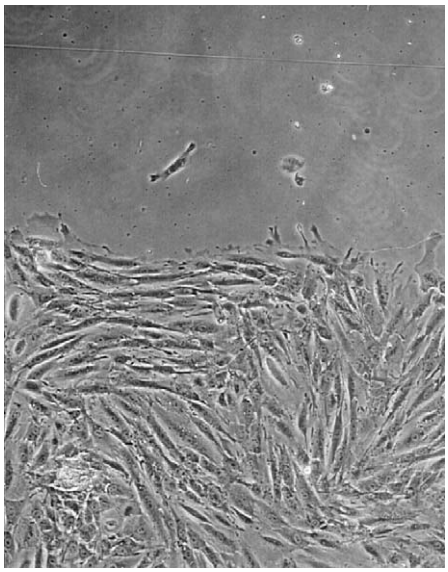

Fig. 52. Photograph of a typical human cell front 10 h after wounding. The cells are mesothelial cells from the peritoneum, the cells that form the superficial layer of the membrane that covers the abdominal cavity and its organs. From Maini et al. [275,276], courtesy of S. McElwain and B. MacGillavray.

experimentally: initially the velocity is relatively high, then there is a transient regime where it is relatively low, and then it gradually approaches the asymptotic speed from below (more detailed examples of such transient behavior and of the dependence on the level curve which is tracked, can be found in [144]). However, the behavior in the simulations appears to be more gradual then the rather sharp crossover seen experimentally after 40–50 h.

It is important to keep in mind that the time-dependent velocity of pulled fronts behaves this way quite generally—in fact, we already encountered the same behavior in the discussion of fronts in the Taylor–Couette and Rayleigh–Bénard systems, see Fig. 22(a) of Section 3.1. As we mentioned already there, and as will be discussed in more detail again in Section 4, for any pulled front emerging from sufficiently localized initial conditions, the asymptotic speed is approached from below. The precise behavior at small and intermediate times does not only depend on the model, but also on the initial conditions. In particular, when the initial conditions have large gradients (e.g., when they show step-function like behavior), the initial front speed at almost all levels of u is initially large, and then undershoots v^*—see Fig. 6 of [144].

If the sharp dip in the velocity of the wound healing is a reproducible effect, then my own guess is that this is a sign of the importance of other effects not included in the model, rather than a transient behavior of an F-KPP-type model with which the data have been compared so far.

3.21. Fronts in mean field approximations of growth models

In the last two decades it has become clear that many stochastic interfacial growth processes exhibit scale invariant behavior on long time and length scales: many growth processes are characterized

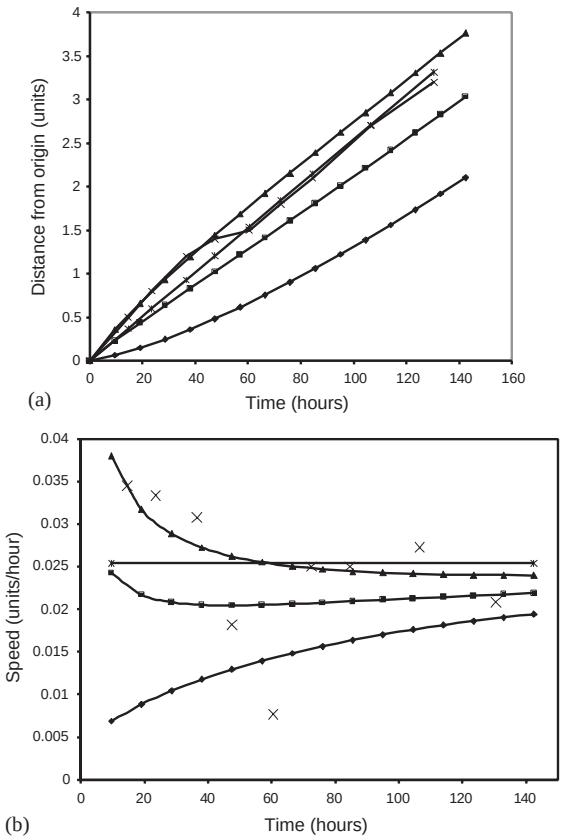

Fig. 53. (a) Crosses: typical plots from experimental data for the position of the invading cell front over different substrates. The distance units are 0.25 mm; the origin is taken as the position at 9.5 h and time is measured from that moment on. The other symbols denote results from simulations of the F-KPP equation with a quadratic nonlinearity, in which the front position is tracked at 1% (triangles), 10% (squares), and 50% (diamonds) of the asymptotic value. (b) Crosses: velocity extracted from the front position data of figure (a). From Maini et al. [275,276], courtesy of S. McElwain and B. MacGillavray.

by nontrivial dynamical critical exponents for the growth of the interface roughness (the root mean square interface fluctuations) with time and system size. There are various types of approaches that have been used to uncover the various universality classes that govern the long-wavelength long-time scaling, ranging from analytical mappings and solution of lattice models, to field-theoretic renormalization group calculations and extensive numerical simulations. The common denominator of almost all of these approaches is that one starts from an appropriate coarse-grained interfacial model. Provided such an interfacial description is appropriate, the topics that concern us in this paper are not directly relevant for this issue, for a discussion of which we therefore refer to the reader to the various reviews of this field [22,195,239,292]. However, if the universal scaling properties are not the main focus for a given growth problem, but if instead one wants to analyze the overall growth shape or a growth pattern or the possibility of a morphological transition, then a mean-field

approximation is often an indispensable tool. In this approximation, the analysis of fronts often does play an important role. We illustrate this general observation with an old example of a deposition model which at the same time is a nice example of a pulled front in a very nontrivial difference equation [238]. The discussion will also prepare us for an issue to which we will return later and which is at present not completely resolved: quite often, in a mean-field description one arises at pulled fronts. As we shall discuss in more detail in Sections 5 and 7, deterministic pulled fronts do not converge to the standard type of interfacial description and as a result a standard type mean-field analysis may miss some of the essential ingredients of the underlying stochastic model, or even exhibit pathological behavior that the underlying model does not have.

In ballistic deposition, particles rain down ballistically but at random positions onto a cluster and stick to it with a given probability as soon as they come to a site neighboring the cluster. Consider the special case of a two-dimensional square lattice with the depositing particles coming straight from above at discrete times (for simplicity we summarize a special case of the analysis of Krug and Meakin [238], who consider more general dimensions and deposition under and angle). Then a particle coming down in the ith column can stick with probability p at the first site in that column which is a nearest neighbor of the highest occupied site in that column or in the two neighboring columns. In a mean-field approximation, one ignores all correlations and formulates this growth process in terms of the probability $\rho_t(x,z)$ that a site at x,z is part of the deposit at time t. In this approximation and for one-dimensional profiles, the appropriate dynamical equation is [238]

$$\rho_{t+1}(z) - \rho_t(z) = p[1-\rho_t(z)]\{1-[1-\rho_t(z-1)][1-\rho_t(z)]^2\}\prod_{z'=z+1}^{\infty}[1-\rho(z')]^3 \ . \tag{175}$$

The term on the left describes the change in the probability at a site at height z that is part of the cluster; it changes when a particle is deposited at that site, and the terms on the right-hand side model this effect in a mean field approximation. The first term on the right-hand side is the probability that that site at height z is empty, the terms between parentheses is the probability that at least one of the neighboring sites (at height $z-1$ in that column or at height z in the neighboring columns) is occupied, and the product term is the probability that none of the sites in the column or its two neighbors is occupied.

Eq. (175) is a difference equation in both the discrete space and time variables; its form is unusual, in that the change at height z depends on all the probabilities at higher sites.[90] A rather complete study of the general form of this equation was given by Krug and Meakin [238]; their numerical solutions showed that at long times, the dynamics leads to front type solutions. Moreover the asymptotic velocity of these fronts turned out to be v^*: empirically, the fronts are found to be pulled.[91] Indeed, although as we discussed in Section 2.4 it is now clear that the linear spreading velocity v^* is given by the same equations for any equation which upon Fourier–Laplace transform leads to a linear equation of the form (41), this appears to be one of the earliest examples where the pulled velocity was calculated for a nontrivial difference equation, and where the power law convergence to v^* was also tested. Indeed, by linearizing the equation in ρ and substituting

[90] A continuum version appropriate in the limit $p \to 0$ can be found in [43].

[91] Intuitively, this can be understood from the observation that the nonlinearities in the dynamical equation express the suppression of the growth due to screening.

$\rho \sim e^{\sigma t - \lambda z}$, one finds the dispersion relation [238]

$$\sigma(\lambda) = \ln\{1 + p[e^{\lambda} + 2]\} \tag{176}$$

from which λ^* and v^* can easily be obtained by calculating the minimum of $\sigma(\lambda)/\lambda$. As mentioned above, Krug and Meakin also verified that the front velocity converged to v^* as $1/t$, with a prefactor which was consistent with (78) to within 15% (presumably, this small discrepancy is due to the higher order $1/t^{3/2}$ correction, which was not known at the time). This slow convergence in time in this case actually entails a very slow $1/z$ correction of the frozen-in density profile!

A common feature of mean field approximations of growth models that (175) also exhibits is that the growth is nonzero for arbitrarily small particle density ρ. This makes the state $\rho = 0$ really a linearly unstable state and gives rise to the existence of a finite linear spreading speed. In reality however, lattice models have an intrinsic cutoff for growth: there has to be at least one particle for a cluster to be able to grow. As we shall see in Section 7, the fact that the particle occupation number is "quantized" has important consequences for growth fronts: they are effectively always pushed rather than pulled.

3.22. Error propagation in extended chaotic systems

In almost all examples we have considered so far, the unstable state into which a front propagates is a well-defined state which is homogeneous in the appropriate variables.[92] An exception to this which deserves to be mentioned is the work by Kaneko [213] and Torcini et al. [396] on fronts propagating into extended chaotic systems. The unstable state in this chase is itself a chaotic state which is characterized by positive Lyapunov exponents. Specifically, the authors consider the Coupled Map Lattice

$$x_i^{n+1} = f([1-\varepsilon]x_i^n + \tfrac{1}{2}\varepsilon[x_{i-1}^n + x_{i+1}^n]) \ , \tag{177}$$

where i and n are the discrete space and time variables. Note that the terms in the argument of f proportional to ε have the form of a discretized version of the diffusion term. The function f maps the interval onto itself, as is usual in studies of maps.

In general, a Lyapunov exponent of a chaotic system measures how two infinitesimally close initial states grow apart. In this sense a chaotic state is an unstable state, since any small perturbation away from it grows out in time. The notion of a front introduced for such a system is illustrated in Fig. 54 from [396]. One considers two realizations of extended chaotic states x_i^0 and y_i^0 which differ on one side of the system (say $i \leqslant 0$) but not on the other. The front in this case is thus an "error propagation front" in the difference variable $x_i^n - y_i^n$—while each individual state is chaotic everywhere, the "error" between them spreads more and more to the right.

In the early work of Kaneko [213], the Lyapunov exponent was studied in a frame moving with fixed speed. The natural speed of the front was then found to be the speed at which this velocity-dependent Lyapunov exponent was equal to zero. In our words, this means that for the nonlinearities studied by Kaneko, the "error fronts" were pulled and that the speed v^* was given in terms of the Lyapunov exponent. Here we follow the formulation of Torcini et al. [396], who

[92] The unstable phase-winding state into which the fronts discussed in Section 2.11.5 propagate are homogeneous in the amplitude a and wavenumber k.

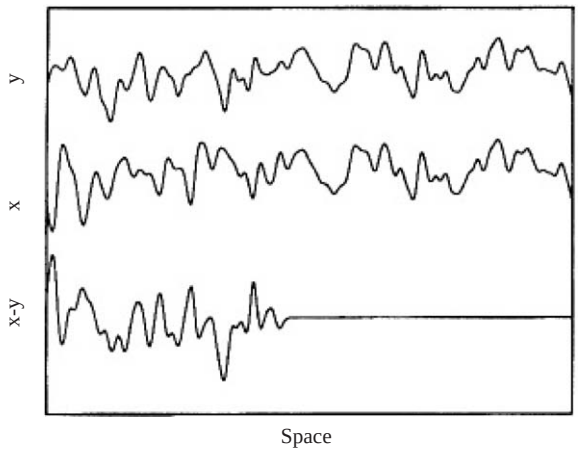

Fig. 54. Two initial realizations x and y of states of the coupled map lattice considered by Torcini et al. [396], together with the difference $x-y$. Note that while each state is chaotic, the difference variable vanished on the right. The propagation of the "error" $x-y$ into this state is then an example of a front propagating into an unstable chaotic state. Both pulled and pushed fronts can occur, depending on the form of the function f.

also studied the transition from pulled to pushed incoherent error fronts (see also [182]). One can indeed extend the notion of a pulled front to this case by analyzing the Lyapunov exponents $\Lambda(\lambda)$ for infinitesimal perturbations u_i^n of x_i^n of the form

$$u_i^n \sim \mathrm{e}^{\Lambda n-\lambda i}\ , \tag{178}$$

where the evolution of the u_i^n is governed by the linearized tangent map

$$u_i^{n+1} = f'([1-\varepsilon]x_i^n + \tfrac{1}{2}\varepsilon[x_{i-1}^n + x_{i+1}^n])([1-\varepsilon]u_i^n + \tfrac{1}{2}\varepsilon[u_{i-1}^n + u_{i+1}^n])\ . \tag{179}$$

Clearly, $\Lambda(\lambda)$ is the analogue for an extended chaotic system of the dispersion relation $-\mathrm{i}\omega(k)$, and the analogue of expression (12) for the linear spreading speed v^* is

$$v^*_{\mathrm{CML}} = \frac{\Lambda(\lambda^*)}{\lambda^*} = \left.\frac{\mathrm{d}\Lambda(\lambda)}{\mathrm{d}\lambda}\right|_{\lambda^*}\ . \tag{180}$$

Although the precise justification of this expression has not been studied, it is intuitively clear that the basis for it is that the Lyapunov exponent defines a finite time scale $\Lambda^{-1}(\lambda^*)$. Thus, after averaging over times sufficiently longer than $\Lambda^{-1}(\lambda^*)$, one obtains a linear problem characterized by an effective dispersion relation $\Lambda(\lambda)$, in terms of which the asymptotic ($t\to\infty$) spreading problem is well-defined.

In the numerical studies, it was found that for various functions f (corresponding to the logistic map, the cubic map and the tent map), the error propagation fronts were pulled (in the average sense) while in other cases (e.g., $f(x) = rx \bmod 1$ with $r > 1$), the fronts were pushed in that their average asymptotic speed was larger than v^*. Clearly, these error propagation fronts are examples of incoherent fronts, and as we noted in Section 2.7.3 we have at present no sharp mathematical characterization of a pushed incoherent front solution—intuitively we expect that enhancement of the growth by the nonlinearities will tend to give rise to a pushed front and that, like a coherent pushed front solution, it falls off spatially faster than the pulled front. But how to identify a pushed

front other than by the empirical observation that it moves faster than v^* I do not know. Indeed, Torcini and co-workers [396,77] have been able to provide a reasonable guidance into what type of maps give pushed error fronts, building on the insight from the nonlinear diffusion equation that pushed fronts are generally associated with growth functions f which increase faster than linear for increasing u. Possibly, further study of the pushed to pulled transition in these fronts might help to develop a sharp definition of pushed incoherent fronts. For recent extensions of such chaotic front studies, including the effective diffusion of such fronts, the reader is referred to [397].

We note in passing that Politi and coworkers [181,348] have argued that upon coarse-graining the effective equation for the dynamics of the difference variable $d_i = x_i - y_i$ of the lower graph of Fig. 54 becomes a diffusion-type equation with multiplicative noise, $\partial_t d = \nabla^2 d + \eta d$ where η is a stochastic noise term. With the Cole–Hopf transformation $d = e^h$ this equation is equivalent to the KPZ equation [22,195,218,239]. It is amusing to realize that the arguments of Section 7.3 indicate that therefore the scaling properties of such fluctuating error-propagation fronts are equivalent to those of the KPZ equation, but in one dimension higher than one would naively expect: As explained in that section, for pulled fronts the fluctuations in the direction of propagation continue to contribute to the scaling behavior, instead of being integrated out.

3.23. A clock model for the largest Lyapunov exponent of the particle trajectories in a dilute gas

One present line of research in kinetic theory touching on the foundations of statistical physics is the study of the Lyapunov exponents of the trajectories of the constituent particles or atoms in a dilute gas (the largest Lyapunov exponent gives the rate with which two nearby initial conditions grow apart under the dynamics, see Section 3.22 above). A few years ago van Zon et al. [430] were able to calculate the largest Lyapunov exponent exactly in a low density hard sphere gas by expressing it in terms of the speed of a pulled front in a differential-difference equation. The model is actually very closely related to a computationally very efficient lattice model introduced by Brunet and Derrida [64,66] in the context of the connection with phase transitions in disorder models discussed in Section 3.25.

For calculating the Lyapunov exponents, one has to analyze how the original trajectories of a typical hard sphere grow apart from a shadow one obtained from an infinitesimally different initial condition. For the largest Lyapunov exponent, the following picture becomes appropriate in the dilute gas limit. When a sphere collides with another one, the difference after the collision between the original trajectory of each sphere and its shadowing trajectory is, on average, equal to the largest of the two before the collision, multiplied by a constant factor that accounts for the enlargement due to the collision. This implies that the largest Lyapunov exponent is, in appropriate units, given by the front speed of a "clock model", in which every particle carries a clock with a discrete time k which is advanced at every collision [430]. This happens according to the following rule: when two particles collide, they *both* reset their respective clock values, say k and ℓ, to either $k+1$ or $\ell+1$, whichever is the largest. Thus, if we denote the number of particles with clock value k by N_k, we obtain the following dynamical equation:

$$\frac{dN_k}{dt} = -\sum_{\ell=-\infty;\ell\neq k}^{\infty} R_{k,\ell} - 2R_{k,k} + 2\sum_{\ell=-\infty}^{k-1} R_{k-1,\ell}\ , \tag{181}$$

where $R_{k,\ell}$ denotes the rate by which collisions occur between particles with clock values k and ℓ. In the dilute gas limit correlation effects become negligible; then $R_{k,\ell}$ is simply proportional to $N_k N_\ell/N^2$ when $k \neq \ell$ and to $N_k^2/(2N^2)$ when two particles with equal clock value k collide. Then, upon writing $f_k = N_k/N$ and scaling the time appropriately, we obtain

$$\frac{\mathrm{d}f_k}{\mathrm{d}t} = -f_k + f_{k-1}^2 + 2f_{k-1}C_{k-2} \ ,$$
$$= -f_k + C_{k-1}^2 - C_{k-2}^2 \ , \tag{182}$$

where we have set

$$C_k = \sum_{\ell=-\infty}^{k} f_\ell \ . \tag{183}$$

Adding the equations for f_ℓ for all values of $\ell \leqslant k$ then yields

$$\mathrm{d}C_j(t)/\mathrm{d}t = -C_j(t) + C_{j-1}^2(t) \ . \tag{184}$$

Eq. (184) has two spatially and temporally constant solutions: $C_j = 0$ and $C_j = 1$. The first one is stable and describes the state where all clocks are set to a value larger than j; the second one is unstable and corresponds to the case where all clocks are set to values less than j. As time proceeds, all clock values are continuously increased, and hence in the context of this model it is natural to consider the invasion of the unstable state $C_j = 1$ by the state $C_j = 0$—as indicated above, the front speed then determines the largest Lyapunov exponent of the dilute hard sphere gas.

Numerical solutions have shown that the fronts propagating into the unstable state $C_j = 1$ are pulled fronts [430]. This in itself is maybe not so much of a surprise, as it is easy to convince oneself that the nonlinearity on the right-hand side tends to reduce the growth relative to that of the terms linearized about the unstable state (very much like in the F-KPP equation with a nonlinearity of the form $f(u) = u - u^2$). However, the equation does illustrate nicely a number of general points concerning pulled fronts:

(i) The dynamical equation (184) is a difference-differential equation. Nevertheless, as we already pointed out so often, the same equations for v^* and for the rate of approach to v^* (Eq. (78) of Section 2.9) hold. The convergence of the front speed to its asymptotic value according to this result was checked explicitly with high precision numerical simulations in [144,146].

(ii) Although the dynamics is very different from that of the F-KPP equation—note the very asymmetric dynamics: the dynamics of C_j is unaffected by that of C_k with $k > j$—the equation is simple enough that several of the methods that play an important role in proving the existence and convergence of fronts for the F-KPP equation (like comparison theorems) can be extended to this equation [146].

(iii) As we will discuss in Section 7, when a mean field equation is simulated with a stochastic equation with a finite number of particles N, the convergence as a function of N to the asymptotic pulled v^* of the $N \to \infty$ mean-field equation is very slow, logarithmically slow. This slow convergence was also found when the present clock model was simulated with a finite number of particles [430].

(iv) In the context of the clock model the C_j's are non-decreasing functions of j: $C_j \leqslant C_{j+1}$ for any j. However, if we just take Eq. (184) as a general dynamical equation in which the C_j's are

allowed to decrease with increasing j, then we find that the state $C_j = 1$ is also convectively unstable to a front where the C_j decrease for increasing j! This turns out to be a retracting pulled front, a front which moves to the right in accord with the fact that any perturbation or coherent structure solution of (184) can only move towards increasing j. Such a retracting front corresponds to a negative value of v^* in our equations,[93] and has an amusing property: whereas the speed of a front which genuinely propagates *into* the unstable state approaches the positive asymptotic speed from *below* due to the negative $1/t$ correction in (78), the *absolute value* of the speed of a retracting front is larger than $|v^*|$ for large times, since v^* itself is negative!

(v) It is easy to modify the equation according to the general rules of thumb of Section 2.7.5 so that the fronts become pushed; an explicit example is discussed in [146].

3.24. Propagation of a front into an unstable ferromagnetic state

Although it may not be of great practical relevance, we briefly mention an amusing example whose front dynamics is governed by two pulled fronts separated by a phase slip region, the dynamical equations for an anisotropic ferromagnet [150,151]. The width of domain walls and the wavelength of spin-wave states in ferromagnets is often large enough that a continuum approximation is justified. For a ferromagnet with an easy-plane anisotropy the free energy in dimensionless units reads [246]

$$\mathscr{F} = \frac{1}{2}\int \mathrm{d}x\,[(\partial_x\theta)^2 + \sin^2\theta(\partial_x\phi)^2 + \cos^2\theta]\ . \tag{185}$$

Here θ and ϕ denote the direction of the magnetization M in polar coordinates, and we have assumed that the magnetization only varies in the spatial x-direction. The last term in the expression shows that the energy of states with polar angle $\theta = \pi/2$ is lowest, so indeed the free energy density describes a situation with an easy-plane direction.

The dynamics of a ferromagnet is governed by the so-called Landau–Lifshits equations

$$\frac{\mathrm{d}\mathbf{M}}{\mathrm{d}t} = \gamma\mathbf{M}\times\frac{\mathrm{d}\mathscr{F}}{\mathrm{d}\mathbf{M}} + \lambda\mathbf{M}\times\left(\mathbf{M}\times\frac{\mathrm{d}\mathscr{F}}{\mathrm{d}\mathbf{M}}\right)\ . \tag{186}$$

In the high damping limit, the first term which describes the torque can be neglected; in appropriate time units the equations then become

$$\partial_t\theta = \partial_x^2\theta + [1-(\partial_x\phi)^2]\sin\theta\cos\theta\ , \tag{187}$$

$$\partial_t\phi = \partial_x^2\phi + 2(\partial_x\phi)(\partial_x\theta)\operatorname{cotg}\theta\ . \tag{188}$$

Note that if we could consider $\partial_x\phi$ to be fixed, the first equation would be nothing but the F-KPP equation for θ, with the state $\theta = \pi/2$ stable if $(\partial_x\phi)^2 < 1$ and unstable if $(\partial_x\phi)^2 > 1$. Thus a phase-winding solution of the form $\theta = \pi/2, \phi = kx$ is unstable for $k > 1$. Elmer et al. [150,151] considered front propagating into this unstable state; because of the similarity of the first equation with the F-KPP equation, it is no surprise that these fronts are pulled, but the new feature is the

[93] Of course, there is only one dispersion relation for Fourier modes of the dynamical equation linearized about the unstable state. The fronts discussed above and analyzed in [430,146] fall off as $\exp(-\lambda^* j)$ with $\lambda^* = 0.768$ and $v^* = 4.311$. The retracting fronts correspond to the solutions of (78) which have negative $\lambda^* = -1.609$ and negative $v^* = -0.373$.

coupling to the ϕ-variable.[94] This front leaves behind a state with $\theta \approx 0$ but with the phase gradient $\partial_x\phi$ essentially unaltered. Because of the strong coupling between phase and polar angle due to the cotangent term in the ϕ-equation, this phase-winding state is unstable. As a result, the first front is followed by a region where phase slips occurs. The state which emerges from here has no appreciable phase gradient: The nonlinear term in the θ-equation then flips sign and this makes the $\theta \approx 0$ state unstable. As a result, this region is in turn invaded by a second pulled F-KPP-like front. The propagation speed of the phase slip region can even be calculated from a conservation-type argument for the phase winding, as all the properties of the back side of the first front and of the leading edge of the trailing front are known [150,151].

When the dynamical equations are written in terms of a complex amplitude $A = \sin\theta e^{i\phi}$, A is found to obey a Ginzburg–Landau type equation with an unusual nonlinearity [151]. From this perspective, the problem has some similarity with the problem of front propagation into an Eckhaus-unstable phase winding solution in the real Ginzburg–Landau equation that was mentioned briefly in Section 2.11.5.

3.25. Relation with phase transitions in disorder models

In hardly any of the situations that we have discussed so far do the front solutions which become relevant when the initial conditions are not sufficiently localized, play a role. There is one remarkable exception to this: it was discovered by Derrida and Spohn [122] that there are some statistical physical disorder models which can be shown to have phase transitions by mapping their generating function onto the F-KPP equation. The two regimes of pulled fronts emerging from localized initial conditions and of leading edge dominated dynamics associated with not sufficiently localized initial conditions then translate into two different phases of the disorder model! An amusing aspect is also that in the first regime, the $1/t$ power law relaxation and the associated crossover behavior of the front solutions translates back into detailed knowledge of the scaling behavior of the statistical model. More recently, the same type of mapping was applied to the renormalization group analysis of disordered XY models [74]—see Section 3.26.1.

Let us sketch the essence of the argument for the case of polymers on a Cayley tree with a random potential [122]. A Cayley tree is a graph which has branches but no loops, as sketched in Fig. 55(a). The hierarchical structure of Cayley trees makes the statistical physical models defined on them amenable to detailed analysis—phase transitions in such models are usually of mean field type, due to the absence of loops, but apart from this they often catch the essence of a transition in higher dimensions. We now consider "polymers" on such Cayley trees—we can think of them in terms of self-avoiding random walks which step one level down in every "time" step—in the presence of a random potential V at the bonds. These values of the potential are uncorrelated random variables distributed according to some distribution $\mathscr{P}(V)$. The statistical problem for a given realization of potentials is then defined as follows in terms of the so-called partition function

$$\mathscr{Z} = \sum_{\text{walks}} \exp[-\beta(V_{1i_1} + V_{2i_2} + \cdots)] \ , \tag{189}$$

[94] It is amusing to note that the nonlinearity of the θ-equation for fixed phase gradient $\partial_x\phi$ is a special case of the dynamical equations for the director angle in the smectic C^* problem discussed in Section 3.15.

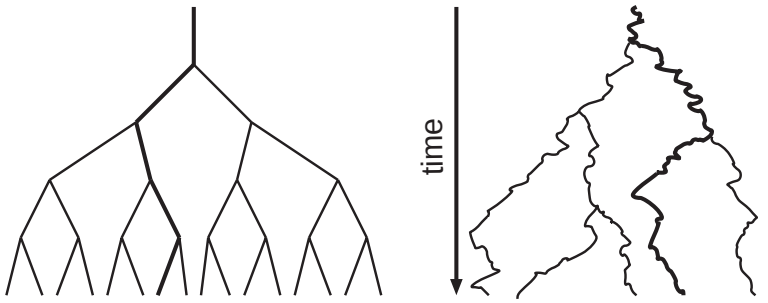

Fig. 55. (a) A "polymer" (thick lines) or self-avoiding walk on a Cayley tree. On each bond an independent random potential is defined. (b) Illustration of the statistical problem of a polymer on a Cayley tree with a random potential in the continuum limit. After Derrida and Spohn [122].

where β is the inverse temperature. The term in the exponents is the sum of all the potentials in level 1, level 2, etc. It is convenient to consider the vertical direction as a time coordinate t and to take the time-continuous limit. The potentials V on a branch of length $\mathrm{d}t$ are then taken as independent Gaussian variables with distribution

$$\mathscr{P}(V) = \frac{1}{(4\pi\,\mathrm{d}t)^{1/2}} \exp\left(-\frac{V^2}{4\,\mathrm{d}t}\right) \ . \tag{190}$$

Because of the branching structure of the Cayley tree, the partition function obeys a simple recursion relation,

$$\mathscr{Z}(t+\mathrm{d}t) = \begin{cases} \mathrm{e}^{-\beta V}\mathscr{Z}(t) & \text{with probability } 1-\mathrm{d}t \ , \\ \mathrm{e}^{-\beta V}[\mathscr{Z}^{1}(t)+\mathscr{Z}^{(2)}(t)] & \text{with probability } \mathrm{d}t \ , \end{cases} \tag{191}$$

which expresses that in the first small timespan $\mathrm{d}t$, the walk could remain a single walk with probability $1-\mathrm{d}t$, or have split into two with probability $\mathrm{d}t$ (the generalization to Cayley trees where every branch splits into $n>2$ is obvious). $\mathscr{Z}^{(1)}$ and $\mathscr{Z}^{(2)}$ are the two partition functions on these two branches.

Because the potentials are random variables, one actually has to study the distribution of partition functions. Instead of doing this, it is more convenient [122] to study the so-called generating function $G_t(x)$ which encodes the average and all moments of $\mathscr{Z}$,

$$G_t(x) \equiv \langle \exp[-\mathrm{e}^{-\beta x}\mathscr{Z}(t)]\rangle \ , \tag{192}$$

where the brackets indicate an average over the disorder. From this definition, one finds immediately that for small $\mathrm{d}t$

$$G_{t+\mathrm{d}t}(x) = (1-\mathrm{d}t)\int \mathrm{d}V\, \frac{1}{(4\pi\,\mathrm{d}t)^{1/2}} \exp\left(-\frac{V^2}{4\,\mathrm{d}t}\right) G_t(x+V) + \mathrm{d}t\, G_t^2(x) \ . \tag{193}$$

That the branching process simply leads to a term proportional to G^2 relies on the fact that the partition functions $\mathscr{Z}^{(1)}$ and $\mathscr{Z}^{(2)}$ in (191) are independent, because on a Cayley tree two branches

do not intersect below their common branch point. In the limit $dt \to 0$ the above equation for G becomes simply

$$\partial_t G = \partial_x^2 G + G(G-1) \ , \tag{194}$$

which is nothing but the F-KPP equation (1) with quadratic nonlinearity, if we put $G = 1 - u$.

The remarkable finding is that the dynamical equation for G does not depend on the temperature β^{-1} explicitly: the temperature only enters indirectly through the initial conditions which Derrida and Spohn considered,

$$G_0(x) = \exp(-e^{-\beta x}) \ \Leftrightarrow \ u \simeq e^{-\beta x} \quad (x \to \infty) \ . \tag{195}$$

As we know from our discussion of fronts in the F-KPP equation, when $\beta > 1$, this corresponds to localized initial conditions, and the long-time behavior of $G_t(x)$ is then simply given by the pulled front solution whose speed approaches v^* according to the asymptotic formula (78). This means that the "long-time" asymptotic average properties of the polymers are completely independent of temperature, and that they approach an asymptotic scaling behavior independently of temperature as well. Furthermore, when $\beta < 1$, the fronts correspond to fronts whose dynamics is "leading edge dominated" and whose velocity is determined by the initial condition, i.e., the temperature. This is the high-temperature regime. The low-temperature ($\beta > 1$) regime can be associated with a frozen phase: roughly speaking the fact that the front speed is independent of initial conditions translates into the free energy sticking at a constant temperature-independent value—we refer for a detailed discussion of this and of the translation of the various front results to those for the random polymer problem to [122]. Below in Section 3.26.1 the connection to renormalization treatments of disorder models is discussed.

We finally note that a lattice model version [64,66] of the statistical–physical disorder problem discussed here is closely related to the clock model discussed in Section 3.23.

3.26. Other examples

We finally draw attention to a number of issues related to front propagation which we do not review in detail.

3.26.1. Renormalization of disorder models via traveling waves

In the previous Section 3.25 we briefly reviewed how the generating function of a disorder model on a Cayley tree obeys the F-KPP equation. This connection between traveling waves and disorder models is actually more general and powerful, as was discovered by Carpentier and Le Doussal [74,75]. Very much like (194) is the evolution equation for the generating function in the "time-wise" direction down the Cayley tree, they found that the renormalization group equation for the distribution function of the local fugacity variables of defects in a disordered XY model takes the form of an F-KPP equation, with the length scale ℓ playing the role time. Like we saw in Section 3.25, the universal behavior of this distribution function comes from the independence of v^* on the details of the model. Moreover, the results for the universal rate of approach to the asymptotic pulled front speed v^* in the case of localized initial conditions (corresponding to temperatures below the glass transition) translate into nontrivial predictions for the scaling at the transition. We refer to these papers for an in-depth discussion of this.

3.26.2. Singularities and "fronts" in cascade models for turbulence

As is well known, fully developed turbulence is characterized by an energy cascade: energy flows from small wave numbers to larger wave numbers, till it is dissipated in the viscous range. In a shell model for this energy flow [408], this energy flow down the cascade shows similarities with front propagation. However, the essential dynamics is more properly analyzed in terms of a similarity analysis like that for the porous medium equation [17,184,339] than in terms of fronts. If interpreted in terms of front dynamics, these fronts have a nonlinear diffusion equation reminiscent of the one in the bacterial growth model (147) and are pushed.

In fact, as stressed in particular by Barenblatt [24,25], there is a formal connection between similarity analysis and front propagation, since if one write x and t of a propagating front solution $u(x-vt)$ in terms of logarithmic variables, $x=\ln X$, $t=\ln T$, a uniformly translating front solution $u(x-vt)$ looks like a similarity solution $\tilde{u}(X/T^v)$. In this formulation the propagation velocity of the front plays the role of a similarity exponent. This reformulation illustrates that in principle a sharp distinction between front propagation and similarity analysis [24,25] is difficult to make. In practice, however, it is often quite clear what the most natural type of analysis is for a given problem: especially if the system admits a linearly unstable state with a well-defined dispersion relation for the unstable branch of Fourier modes, the linear spreading analysis and the associated front formulation are the methods of choice.

3.26.3. Other biological problems

Although the clearest biological examples of front propagation into an unstable state appear to be the population spreading phenomena mentioned in Section 3.19 and the bacterial growth patterns discussed in Section 3.13, it is important to realize that there are many problems in biology and biophysics which are closely related. E.g., much work on pulse propagation in bistable systems or excitable media traces back to the study of the propagation of pulses in nerves [229,379]. Since these are not examples of front propagation into unstable states proper, and since excellent books in which these problems are treated have appeared recently [222,311], we will not explore the differences and similarities here.

3.26.4. Solar and stellar activity cycles

There is an extensive literature—see e.g. [28] for a brief introduction and entry into the literature—associating the sunspot cycle to the occurrence of so-called dynamo waves. The coupled equations for the azimuthal and radial magnetic fields take the form of two reaction–diffusion type equations, and an important ingredient of the relevant dynamics is associated with the problem of front propagation into unstable states [28,395,441]. Of course, for waves on a spherical rotating object like the sun, there are many complicating aspects: not only is there the question whether the instability is locally convective or absolute, but also the fact that the geometry is intrinsically finite and that the background of the waves is spatially varying plays a role. These latter type of issues are related to the question of the emergence of so-called "global modes" which we will discuss briefly in Section 6. For a detailed discussion of the dynamo waves themselves we refer to the literature cited above.

3.26.5. Digital search trees

After acceptance of this article, we learnt of a very new exciting line of research: traveling fronts play an important role in computer science in digital search trees and data compression. Moreover,

such types of problems are related to directed DLA on a Caley tree. See [452,453] and references therein.

4. The mechanism underlying the universal convergence towards v^*

In Section 2.9 we saw that pulled fronts converge to their asymptotic speed and shape[95] with a universal power law behavior—e.g., for the velocity we have according to (82)

$$v(t) = v^* - \frac{3}{2\lambda^* t} + \frac{3\sqrt{\pi}}{2(\lambda^*)^2 t^{3/2}} \operatorname{Re} \frac{1}{\sqrt{\mathscr{D}}} + \mathcal{O}\left(\frac{1}{t^2}\right) . \tag{196}$$

For uniformly translating fronts, for which $\mathscr{D}$ is real, this expression reduces to the simpler version (78).

In the above expression v^*, λ^* and $\mathscr{D}$ are given explicitly by Eq. (12) in terms of the dispersion relation $\omega(k)$ of the linearized dynamical equation. This and other remarkable features of this general expression were discussed extensively in Section 2.9.3 but we did not justify or derive the result itself. It is the aim of this section to review the underlying mechanism and derivation [144] in some detail. The importance of the derivation does not lie in the technicalities themselves, but in the fact that the pulled front picture that we have advanced can be made into a fully explicit and predictive formalism.

4.1. Two important features of the linear problem

Several of the most important insights on which the full derivation of (196) is based [144] come from our understanding of the fully linear problem discussed in Sections 2.1–2.4. In Section 2.1 we saw that according to the saddle point analysis of the fully linear spreading problem a "steep" initial condition gives rise to the following long-time expression for a generic dynamical field ϕ,

$$\phi(\xi,t) \sim \mathrm{e}^{-\lambda^*\xi + \mathrm{i}k_r^*\xi - \mathrm{i}(\omega_r^* - k_r^* v^*)t} \frac{\mathrm{e}^{-\xi^2/(4\mathscr{D}t)}}{\sqrt{t}} , \tag{197}$$

where $\xi = x - v^* t$, and where λ^*, k_r^*, v^* and $\mathscr{D}$ are given by the linear spreading point equations (12). The first exponential factor is the asymptotic exponential fall-of with steepness λ^* in the frame moving with velocity v^*. The second exponential factor, together with the $t^{-1/2}$ term, is the first correction term to the asymptotic behavior—it arises simply from the Gaussian saddle point integral. Of course, in this Gaussian term we also recognize the fundamental similarity solution of the diffusion equation. Thus, if we define a new field ψ through the transformation

$$\phi(\xi,t) \equiv \mathrm{e}^{-\lambda^*\xi + \mathrm{i}k_r^*\xi - \mathrm{i}(\omega_r^* - k_r^* v^*)t} \psi(\xi,t) , \tag{198}$$

[95] The shape convergence only holds for uniformly translating fronts and coherent pattern forming pulled fronts, of course. Nevertheless, the incoherent dynamics of an incoherent pulled front arises from the intrinsic chaotic behavior of the nonlinear state behind the front (as, e.g., in panels (a) of Figs. 16–19) or from the fact that the spreading point dynamics does not match on to a fully coherent front profile in the nonlinear region (as, e.g., in Fig. 18(b)). In the leading edge the dynamics of incoherent pulled fronts is still smooth and coherent, as close inspection of these figures and Fig. 58 below shows quite clearly. This dynamics is governed by the extension of Eq. (210) below to pattern forming fronts.

then we expect that the long-time dynamics of ψ is governed by the equation

$$\frac{\partial\psi}{\partial t} = \mathscr{D}\,\frac{\partial^2\psi}{\partial\xi^2} + \text{corrections}\ , \tag{199}$$

since its fundamental similarity solution is the Gaussian form $\psi = t^{-1/2}\mathrm{e}^{-\xi^2/4\mathscr{D}t}$ of (197). Note that the transformation (198), which was called the "*leading edge transformation*" in [144], acts like a mathematical magnifying glass: it allows us to focus on the dynamics of the correction to the dominant exponential behavior. Moreover, do realize that since the saddle point analysis is quite general (see Section 2.4) the long-time dynamics of the leading edge variable ψ is effectively governed in dominant order by this diffusion equation *even if the underlying dynamical equation is of higher order*, *a set of equations*, *a difference equation*, *etc.* The reason that ψ obeys a differential equation even when the original dynamical equation is a difference equation is that for long times ψ becomes arbitrarily smooth in space and time.

The above line of reasoning is intuitive and based on working backward from the general expression (197). The diffusion-type form of the equation—first order in time and second order in space—is actually an immediate consequence of the fact that two roots k coincide at the linear spreading point k^*. After all, Eqs. (9) and (12) imply that in the neighborhood of the spreading point we have in the co-moving frame ξ

$$\omega - \omega^* = -\mathrm{i}\mathscr{D}(k-k^*)^2 + \cdots\ , \tag{200}$$

and upon inverse Fourier–Laplace transformation this gives (199) for long times. In fact, the full generalization of (199) for ψ is easy to derive [144]: by expanding about the linear spreading point and taking an inverse Fourier–Laplace transform, we immediately obtain [144]

$$\frac{\partial\psi}{\partial t} = \mathscr{D}\,\frac{\partial^2\psi}{\partial\xi^2} + \mathscr{D}_3\,\frac{\partial^3\psi}{\partial\xi^3} + w\,\frac{\partial^2\psi}{\partial t\,\partial\xi} + \tau_2\,\frac{\partial^2\psi}{\partial t^2} + \cdots\ , \tag{201}$$

where the expansion coefficients $\mathscr{D}_3, w, \tau_2$, etc. can all be expressed in terms of the characteristic equation of the branch corresponding to the relevant spreading point—see Eq. (5.64) of [144]. E.g., we simply have $\mathscr{D}_3 = (1/3!)\,\mathrm{d}^3\omega/\mathrm{d}k^3|_{k^*}$.

Since we already know from the saddle point analysis that the relevant long-time dynamics of the leading edge variable ψ is a diffusion-type dynamics on slow spatial and temporal scales, the crucial conclusion from these considerations is that[96]

> *the dynamical equation of the leading edge variable ψ that governs the convergence to the linear spreading behavior in the leading edge is a diffusion equation, with subdominant terms which are determined explicitly in terms of the dispersion relation $\omega(k)$ of the linear dynamical equation of the original problem. The appropriate similarity variable for the long-time expansion of ψ is the similarity variable $\xi/\sqrt{t}$ of the diffusion equation.*

[96] There *is* actually a surprise here: A priori, one would expect that the second and third terms of (201) would affect the subdominant $t^{-3/2}$ correction term in the expression (196) for $v(t)$. Actually, they do affect the shape scaling function but *not* the velocity correction—see Eq. (5.70) of [144]. I do not have a real intuitive understanding of this remarkable finding which comes out of the explicit calculation.

Our second important observation concerning the fully linear problem is the following. One may well wonder "how can the leading edge dynamics ever determine the dominant convergence dynamics of the *full* nonlinear profile?" To understand this, let us return to (197) and write it as

$$|\phi(\xi,t)| \sim \mathrm{e}^{-\lambda^*\xi}\left|\frac{\mathrm{e}^{-\xi^2/(4\mathscr{D}t)}}{\sqrt{t}}\right| = \mathrm{e}^{-\lambda^*\xi-\frac{1}{2}\ln t-\xi^2/(4Dt)}\ , \tag{202}$$

where, as in (13), $D^{-1}=\mathrm{Re}\,\mathscr{D}^{-1}$. If we follow the position ξ_C of the level line $\phi(\xi_C,t)=C$, then according to the above expression for the linear dynamics we have in dominant order

$$\xi_C = -\frac{1}{2\lambda^*}\ln t + \cdots \ \Leftrightarrow\ \dot{\xi}_C = -\frac{1}{2\lambda^* t} + \cdots\ . \tag{203}$$

We already drew attention to this logarithmic shift in our discussion of the front relaxation in Section 2.9.1, but we now identify more clearly where this behavior originates from: The $1/t$ relaxation of the velocity of the level line corresponds to a logarithmic shift in the position, and this results from the Gaussian $t^{-1/2}$ prefactor in combination with the overall $\mathrm{e}^{-\lambda^*\xi}$ spatial decay of the leading edge variable. In other words, *the prefactor of the* $1/t$ *velocity relaxation is essentially the exponent of the appropriate similarity solution of the diffusion equation* (199).

So why then does the logarithmic shift carry over to the fully nonlinear profile? The important point to realize is simply that[97]

> *when we track the position of a front whose width of the nonlinear region is finite, the unbounded logarithmic shift imposed by the diffusive leading edge dynamics always dominates the large time behavior over the relaxation of the front shape itself.*

This observation was already illustrated in Fig. 12.

4.2. The matching analysis for uniformly translating fronts and coherent pattern forming fronts

So we know that the leading edge variable ψ, which measures the deviation from the asymptotic exponential profile $\mathrm{e}^{-\lambda^*\xi+\mathrm{i}k_r^*\xi-\mathrm{i}(\omega^*-k^*v^*)t}$ in the moving frame, obeys a diffusion-type equation with corrections. To construct the solution to the fully nonlinear font relaxation problem, we have to *match* the behavior in the leading edge (the region where the dynamical equation can be linearized about the unstable state) to the nonlinear front region, the region where the nonlinearities in the equation are important.

In order to understand the matching behavior, it is clearest to first consider the case of uniformly translating fronts or coherent pattern forming fronts: For these the arguments can be made most precise and for these the matching analysis has been worked out in detail. The case of incoherent pattern forming fronts will be discussed in the next section; the analysis given there will give

[97] The argument is obvious for the divergent logarithmic term. Actually, since the front shape relaxation is driven by the $1/t$ term in the velocity—see Eq. (211) below—any contribution from the leading edge which gives a time-dependent shift which decays slower than the $1/t$ intrinsic shape relaxation is universal. This is the reason that even the $1/t^{3/2}$ term in the velocity relaxation is universal: it corresponds to a shift proportional to $1/t^{1/2}$. Even incoherent fronts whose fluctuating width converges faster than $1/t$ to some average value, still exhibit the subdominant $1/t^{3/2}$ velocity relaxation term.

a more intuitive dynamical argument why the leading edge variable ψ approaches the behavior that we identify with matching arguments here.

At the linear spreading point k^* two roots coincide—this is illustrated both by Eq. (200) and the fact that v^* corresponds to the minimum of the curve $v_{\rm env}(\lambda)$ in Fig. 3. It is a general result [13,14] that in the presence of a double root the $\xi \to \infty$ asymptotic behavior of the uniformly translating pulled front solutions $\Phi_{v^*}(\xi)$ or the leading coherent pulled front solution $\Phi^1_{v^*}(\xi)$, is

$$\Phi_{v^*}(\xi) \sim (a_1\xi + a_2)\mathrm{e}^{-\lambda^*\xi}, \quad \Phi^1_{v^*}(\xi) \sim (A_1\xi + A_2)\mathrm{e}^{-\lambda^*\xi + \mathrm{i}(k_{\rm r}^*\xi - \omega_{\rm r}^* t)} \ , \tag{204}$$

as we already noted before in Eqs. (59) and (75). As $t \to \infty$, the leading edge dynamics should approach this behavior, so in dominant order the matching condition for the leading edge variable ψ is

$$\psi(\xi, t \to \infty) \sim \xi \ . \tag{205}$$

At this point, we can already understand the leading term of the convergence behavior of $v(t)$ in a very simply manner. For simplicity, we will from now on specialize to the case of uniformly translating fronts but the generalization to coherent pattern forming fronts is straightforward [147,383,388]. The similarity solution of the diffusion equation which for large times matches the above $\psi \sim \xi$ behavior is the "dipole solution"

$$\psi \sim \frac{\xi}{t^{3/2}}\mathrm{e}^{-\xi^2/(4Dt)} \ \Leftrightarrow \ \phi \sim \mathrm{e}^{-\lambda^*\xi - 3/2\ln t + \ln\xi - \xi^2/(4Dt)} \ . \tag{206}$$

Analogously to the discussion following Eq. (202), this result implies that to order $1/t$ the velocity relaxation is

$$v(t) = v^* - \frac{3}{2\lambda^* t} + \cdots \ , \tag{207}$$

which is indeed the leading order term of the full expression (196).

To go beyond the leading order term, we have to perform a full systematic matching calculation. To do so, it is crucial to describe the nonlinear front in the right frame: as we saw in the previous section, a $1/t$ relaxation of the velocity corresponds to an ever-increasing logarithmic shift in the position of a level line, when viewed in the frame ξ moving with the *asymptotic* speed v^*. Thus, as Fig. 12 illustrates so nicely, *if we would attempt to do perturbation theory about the asymptotic front solution* $\Phi_{v^*}(\xi)$, *the difference between the actual transient profile and this asymptotic profile would increase without bound.* Nevertheless, the *shape* of the transient profile is always close to Φ_{v^*} placed at an appropriate position. This suggests to perturb about the asymptotic front solution in a frame ξ_X which incorporates this shift,

$$\xi_X = \xi - X(t) = x - v^* t - X(t) \ , \tag{208}$$

where the shift $X(t)$ has the expansion

$$\dot{X}(t) = \frac{c_1}{t} + \frac{c_{3/2}}{t^{3/2}} + \frac{c_2}{t^2} + \cdots \ \Leftrightarrow \ X(t) = c_1 \ln t - \frac{2c_{3/2}}{t^{1/2}} + \cdots \ . \tag{209}$$

The expansion in powers of $1/\sqrt{t}$ results from the fact that the similarity variable governing the long-time dynamics of ψ is $\xi_X/t^{1/2}$, so powers of ξ_X generate powers of $1/t^{1/2}$.

From here on, the matching expansion is conceptually straightforward but technically nontrivial. In the leading edge we make a large-t expansion in terms of the similarity variable $\xi_X/t^{1/2}$,

$$\psi = \left[t^{1/2}\, g_{-1/2}(\xi_X/t^{1/2}) + g_0(\xi_X/t^{1/2}) + \frac{g_{1/2}(\xi_X/t^{1/2})}{t^{1/2}} + \cdots \right] \mathrm{e}^{-\xi_X^2/(4\mathscr{D}t)} \ , \tag{210}$$

where the matching condition (205) requires that $g_{-1/2}(\xi_X/t^{1/2}) \sim \xi_X/t^{1/2}$. In the nonlinear front region we expand the profile in the form dictated by the above observations, [98]

$$\phi(x,t) = \Phi_{v^*}(\xi_X) + \frac{\eta_1(\xi_X)}{t} + \frac{\eta_{3/2}(\xi_X)}{t^{3/2}} + \cdots \ . \tag{211}$$

These expansions generate hierarchies of equations which can be solved order by order; in first nontrivial order we straightforwardly recover the $1/t$ term along the same lines as above, and in the next order the nontrivial $t^{-3/2}$ term in the general expression (196) for $v(t)$ is found [144].

The explicit calculation also shows that the functions η_1 and $\eta_{3/2}$ are proportional to the "shape mode" $\delta\Phi_v/\delta v$ which gives the change in the shape of the profile under a change of the velocity v: one finds

$$\Phi_{v^*}(\xi) + \frac{\eta_1(\xi_X)}{t} + \frac{\eta_{3/2}(\xi_X)}{t^{3/2}} = \Phi_{v*}(\xi_X) + \left.\frac{\delta\Phi_v(\xi_X)}{\delta v}\right|_{v^*} \dot{X}(t) + \mathscr{O}(t^{-2}) \ . \tag{212}$$

Since $\dot{X}(t)$ is nothing but the deviation $v(t) - v^*$, this implies that to order t^{-2} the profile shape can be written in form (80), i.e.,

$$\phi(x,t) = \Phi_{v(t)}(\xi_X) + \mathscr{O}(t^{-2}) \ . \tag{213}$$

In other words, to order t^{-2} the shape of the profile follows the shape of a uniformly translating profile with velocity equal to the instantaneous value $v(t)$.

At first sight, it may appear surprising that such a result could hold, since on the one hand $v(t)$ always approaches v^* from below, and since on the other hand uniformly translating profiles Φ_v with $v < v^*$ approach the asymptotic state $\phi = 0$ in an oscillatory manner. There is no contradiction here, however. The above expression is only the asymptotic expression for ξ_X fixed, $t \to \infty$. The limits do not commute: For any *fixed* time, the profile crosses over to expression (210) for large enough ξ_X. As one might expect from the diffusive nature of the ψ-equation, this crossover region moves to the right diffusively, as $\sqrt{t}$ [144].

These analytical predictions for the relaxation of the profile shape have been confirmed in great detail numerically for the F-KPP equation (1) with a cubic nonlinearity [144]. Fig. 56 shows a plot of

$$\frac{\phi(\xi_X,t) - \Phi_{v^*}(\xi_X)}{\delta\Phi_v/\delta v|_{v^*}(v^* - v(t))} \ , \tag{214}$$

where the shape mode in the denominator was obtained by numerically solving the ordinary differential equation that it obeys. According to the analytical predictions, the ratio (214) should approach unity for long time; the numerical results clearly confirm this. Note that since the denominator

[98] Remember that we have written here the form for the case that the asymptotic front solution is uniformly translating. For coherent fronts the expansion is similar [147,383,388], we only have to add the upper indices and a phase relaxation term.

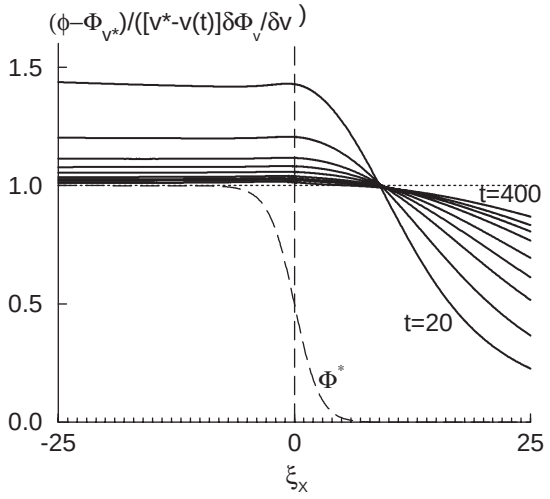

Fig. 56. Numerical confirmation of the analytical prediction for the shape relaxation of a transient front in the F-KPP equation (1) with cubic nonlinearity for various times ranging from $t = 20$ to $t = 400$. Plotted is the normalized deviation from the asymptotic profile Φ_{v^*} given by (214). As indicated by the dashed vertical line, the co-moving coordinate ξ_X is taken such that $\phi(\xi_X, t) = 1/2$. The fact that ratio (214) converges to 1 confirms that to order t^{-2} the shape of the profile follows $\Phi_{v(t)}(\xi_X)$ adiabatically. Note the diffusive-type crossover on the far right to the asymptotic behavior (210). Whether it is accidental or significant that all the lines roughly cross at one point near $\xi_X \approx 10$ is at present not understood. From Ebert et al. [144].

approaches zero for long times, plots like Fig. 56 are very accurate confirmations of the analytical expressions—in some cases the predictions have been verified to within six significant figures [144,146]!

As we already indicated, the matching calculation can be extended to the case of coherent pattern forming fronts [147,383,388]. We actually already illustrated in Fig. 19 how the results of numerical simulations of the Swift–Hohenberg equation (92) confirm the predicted relaxation behavior of the velocity and the wavenumber just behind the front. That the shape relaxation of the front also follows the velocity adiabatically has also been verified in these studies [147,383]. For coherent pattern forming fronts an explicit calculation of the shape modes $\delta\Phi_v''/\delta v$ is quite nontrivial, even numerically, since it in principle involves an infinite set of coupled ordinary differential equations. Therefore in these studies the quantity

$$\frac{\langle \phi(\xi_X, t) - \sum_{n=0,\pm1,\ldots} \mathrm{e}^{-\mathrm{i}n\Omega^* t} \langle \Phi_{v^*}^n(\xi_X) \rangle_T}{t^{-1}} \tag{215}$$

was studied. Here the brackets $\langle \cdot \rangle_T$ denote an average over one period $T \approx 2\pi/\Omega^*$ in the co-moving frame. According to the analytical predictions, the various plots of this ratio should all fall on top of each-other, and the resulting curve is nothing but the shape mode. As Fig. 57 shows, this expectation is borne out by the simulations. Given that for such a coherent pattern forming front obtaining the front profile involves extensive interpolation, it is remarkable how nicely the scaling works [147,383]! To our knowledge this is the only existing explicit demonstration of the universal shape relaxation of a coherent pattern forming pulled front.

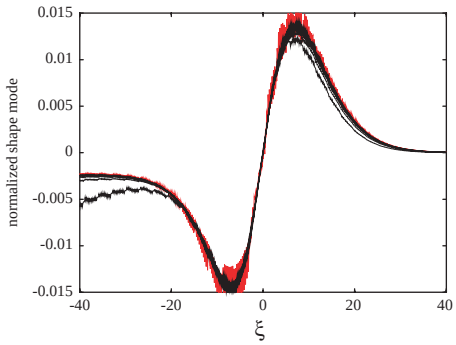

Fig. 57. Demonstration of the universal relaxation behavior of the shape of a front in the Swift–Hohenberg equation (92), according to Spruijt et al. [147,383]. Plotted is ratio (215) for times 20–160 in steps of 20 for fronts in numerical simulations of fronts in for $\varepsilon = 1/2$. The fact that the various curves fall almost on top of each other confirms that the shape of the fronts follows the relaxation of the velocity adiabatically. The curve which deviates somewhat on the left side is taken at the earliest time, $t = 20$. Up to an overall multiplicative constant, the resulting curve represents the shape mode of the pulled Swift–Hohenberg front. Note that since ε is not small, various harmonics contribute to the expansion of the asymptotic profile, and the front solution is *not* close to the front solution of the cubic amplitude equation that one can derive in the limit $0 < \varepsilon \ll 1$.

4.3. A dynamical argument that also holds for incoherent fronts

The matching arguments reviewed above were essentially based on the observation that the asymptotic uniformly translating and coherent front solutions have a $\xi e^{-\lambda^* \xi}$ behavior, and that the long-time dynamics in the leading edge should match this behavior. This essentially gave the requirement that $\psi \sim \xi$ in dominant order for long times. From there on the calculation is in essence a straightforward matching calculation.

The above argument does not give much insight into how this linear gradient in ψ builds up *dynamically*. Moreover, the argument hinges on the existence and behavior of a coherent pulled front profile. However, the *same* relaxation holds for *incoherent* fronts. Let us now clarify why this is so and how the linear gradient builds up dynamically [388].

The argument can be formulated quite generally, but let us for simplicity just consider the quintic CGL equation (103). If we make a transformation to the leading edge variable $\psi = e^{\lambda^* \xi - i k_r^* \xi + i(\omega_r^* - k_r^* v^*)t} A$ and write the equation for ψ in the frame ξ_X defined in (208), we obtain

$$\partial_t \psi = \mathscr{D} \partial_{\xi_X}^2 \psi + N(\psi) + \mathscr{O}(t^{-1}) \ , \tag{216}$$

where the terms of $\mathscr{O}(t^{-1})$ are proportional to $\dot{X}(t)$ and come from the transformation to the frame ξ_X, and where $N(\psi)$ denotes the nonlinear terms

$$N(\psi) = (1 + i c_3) e^{-2\lambda^* \xi_X} |\psi|^2 \psi - (1 - i c_5) e^{-4\lambda^* \xi_X} |\psi|^4 \psi \ . \tag{217}$$

We normally associate a front with a solution for which the physical field, the amplitude A in the present case, *saturates* behind the front. Because of the exponential term introduced in the leading edge transformation, this means that the leading edge variable should vanish exponentially $\sim \exp \lambda \xi_X$ as $\xi \to -\infty$. Thus, to the right, for large positive ξ_X, $|N|$ vanishes exponentially as $e^{-2\lambda \xi_X}$ due to the explicit exponential term in front of the cubic term in (217), while to the left $|N|$ vanishes exponentially as $e^{\lambda \xi_X}$ because of the exponential vanishing of the leading edge variable ψ. In other

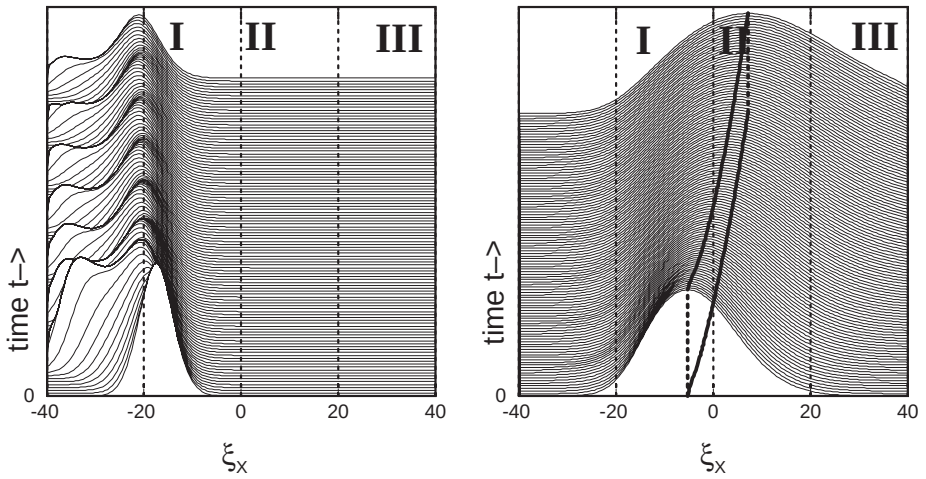

Fig. 58. Results from simulations by Storm et al. [388] of the quintic CGL equation for the same parameter values and run as in Fig. 19(a), shown from time 35 to 144. Panel (a) shows the nonlinear function $|N|$ defined in (217) as a function of ξ_X. Note that this function falls off exponentially to both sides. (b) The evolution of the leading edge variable $|\psi|$ for the same run as in panel (a). The region marked I in the figure is the region where a linear gradient builds up, II marks the crossover region which moves out as $\sqrt{t}$ and in region III ψ is falling of in dominant order as a diffusive Gaussian with width proportional to $\sqrt{t}$. The solid line indicates the position of the maximum. The regions I, II and III are also marked in panel (a). Note that the nonlinear function N essentially vanishes in these regions and that ψ builds up to the right of the region where N is non-vanishing. Intuitively, we can think of the nonlinearities as acting like an "absorbing wall" for the field ψ.

words, $|N|$ is actually nonzero only in some limited spatial range. This is illustrated in the space–time plot of Fig. 58(a), which shows $|N|$ for the same simulation of the quintic CGL as in Fig. 19(a). The exponential vanishing to the right is clear from the figure; the time-dependent behavior of $|N|$ on the left reflects the fact that the front is incoherent.

The leading edge of the front is essentially the region where $|N|$ is negligible. Hence it is the semi-infinite interval to the right of N, and this nonlinear term acts like a *boundary condition* for the dynamics of ψ in the leading edge! Moreover, since in leading order ψ obeys a diffusion equation, let us think of ψ as a density field obeying a diffusion equation. In this analogy, the nonlinear term N *acts like a localized sink term or an absorbing wall* which suppresses the density field (it must suppress it as behind the front ψ vanishes). Now, as is well known, when we have an absorbing wall at long times the density field will build up a linear gradient—from this analogy we see that the role of the nonlinearities in the equation is to make the dynamical field ψ build up a linear gradient, $\psi \sim \xi_X$, at long times! In other words, the long-time behavior (205) is not only a matching condition, but it also naturally emerges dynamically from the fact that the dynamics of the leading edge variable is essentially governed by a diffusion equation with an absorbing wall. Fig. 58(b) shows a space-time plot of $|\psi|$ from the simulations of the quintic CGL equation, which fully confirms the gradual buildup of a linear gradient to the right of the "absorbing wall" $|N|$, with a crossover to a diffusive Gaussian behavior to the right of it.

In conclusion, we finally understand the universal nature of the power law corrections to the asymptotic pulled front velocity: Only the fact that there is an absorbing wall matters, its internal

structure—i.e., the form of the nonlinearities in the equation, or the question whether the front is uniformly translating, coherent or incoherent—is unimportant [144,388]!

5. Breakdown of moving boundary approximations of pulled fronts

So far, we have focused our discussion on the dynamics of fronts in one dimension. Quite often, however, we are interested in the formation of patterns in two or three dimensions which naturally can be thought of as consisting of domains separated by domain walls or fronts. Usually—think of viscous fingering or dendritic growth [57,73,220,226,247,249,251,338,353], bacterial growth patterns [39–41], late stage coarsening [56,192], flames [67,90,209,449], chemical waves [160,292,294], thermal plumes [30,451] etc.—the state of the system inside each domain is asymptotically close to an intrinsically stable homogeneous state. But we have also encountered examples of such type of pattern formation in higher dimensions which are driven by the motion of a front into a linearly unstable state: streamer patterns of Section 3.5 are formed when an ionization front propagates into a non-ionized gas, the unstable normal state of a superconductor can give way to the superconducting state through the motion of a front (see Section 3.8), the chaotic dynamics of domains in the rotating Rayleigh–Bénard experiments discussed in Section 3.4 is in one regime driven by the propagation of fronts into linearly unstable states, and if fluctuation effects are sufficiently small, front propagation into an unstable state can be relevant to the early stage of spinodal decomposition as well (see Section 3.7).

When the width of the fronts or domain walls separating the domains is much smaller than the radius of curvature which is set by the typical scale of the pattern, then a natural way to analyze the pattern dynamics is in terms of a *moving boundary approximation* or *effective interface approximation*. This approximation amounts to treating these fronts or transition zones as a mathematically sharp interface or boundary. In other words, their width is taken to be zero on the outer scale of the pattern, and their internal degrees of freedom are eliminated using singular perturbation theory. We shall henceforth use the word *boundary* or *interface* to denote this zero width limit and use the word front when we look at a scale where its internal structure can be resolved.

Sometimes, it is numerically advantageous go in the opposite direction, i.e., to translate a model with sharp interfaces into what has become known as a *phase field model* in which the order parameter field varies continuously through the interfacial zone. Examples where this idea was exploited for a variety of physical problems can be found in [29,71,187,219,221,232,372]; for careful discussions of the derivation of a moving boundary problem for a variety of different physical systems, we refer to [30,67,132,160,219,306].

Is it true, as one might be tempted to think when looking at pictures like the streamer patterns of Fig. 30, that a moving boundary approximation or effective interface description can be derived whenever the fronts in the system under study are much thinner than the scale of the pattern? Or, to put it more clearly, *can one generally derive a moving boundary approximation for front propagation into unstable states in the limit that the width of the front is much less than its radius of curvature*? The answer to this question is a definite "*no*" for *pulled fronts* and "*yes*" for *pushed fronts* [145].

How come? The reason for this statement is that for a moving boundary approximation to hold, we need not only have separation of *spatial scales* but also separation of *time scales*: the main physical idea underlying the derivation of a moving boundary approximation is that the front itself can on large length and time scales be viewed as a well-defined coherent structure which responds on a "fast"

time scale—the internal front relaxation time—to the "slow" change in the local values of the outer dynamical fields that characterize the domains. *Both elements are missing for a pulled front.* Indeed, as we have seen in Section 2, the dynamics of a pulled one-dimensional front is essentially determined in the whole "semi-infinite" region ahead of the front, not in the nonlinear transition region itself. As a consequence, the velocity and shape of a pulled front relax very slowly, with a $1/t$ power law, to their asymptotic velocity and shape. For a pushed front, on the other hand, both conditions *are* fulfilled: in one dimension, a pushed front relaxes exponentially fast to its asymptotic velocity and shape, and its dynamics responds essentially only to changes in the nonlinear front region only.

We will clarify the above statements below. We first illustrate how in two and three dimensions the relaxation correction and the curvature correction are of the same order for a spherically symmetric expanding pulled front, and then trace the main steps of the derivation of a moving boundary approximation to discuss the breakdown of singular perturbation theory for pulled fronts.

5.1. A spherically expanding front

It is well known—see e.g. the classic work of Allen and Cahn [6] or the reviews [56,162]—that when the radius of curvature of a front which connects two stable states of an order parameter equation is much larger than the front width, the dominant correction to the front velocity is a curvature correction. Consider now a front expanding radially in two or three dimensions. For large times, the curvature correction to the front velocity will go as $1/R(t) \approx 1/(v_{\rm as}t)$, where $v_{\rm as}$ is the asymptotic front velocity. For a front connecting two stable states, or more generally for a pushed front, this is the *only* asymptotic correction. This is simply because such fronts reduce in this limit to an effective interface—the formal derivation is summarized in the next section—and because for a weakly curved interface separating two states of a single order parameter the curvature is the dominant correction.

For a pulled front, on the other hand, the universal power law relaxation term is according to (78) also of order $1/t$, i.e., *of the same order as the curvature correction in this case.* This illustrates that a weakly curved pulled front cannot simply be viewed as a weakly curved interface with velocity given uniquely in terms of its local curvature: A moving boundary approximation does not hold.

We can illustrate these considerations by considering the F-KPP equation in three dimensions in the case of spherical symmetry,

$$\partial_t u(r,t) = \partial_r^2 u(r,t) - (2/r)\partial_r u + f(u)\ . \tag{218}$$

For a front at a distance $R(t) \gg 1$ from the origin, the second term on the right-hand side which accounts for the curvature of the spherical front, serves as a small perturbation. When the front is pushed, the singular perturbation methods discussed below show that indeed it gives a correction $-2/R(t)$ to the front. Thus, starting from a localized initial condition $u(r, t = 0)$ (nonzero only in a ball around the origin), the velocity of the pushed front for large times is $v(t) \approx v^\dagger - 2/R(t) \approx v^\dagger - 2/(v^\dagger t) + \cdots$. For a pulled front with $f'(0) = 1$, on the other hand, one expects that for large times one can add the curvature correction and the asymptotic relaxation term given in (78) with $v^* = 2$ and $\lambda^* = 1$, to get[99] $v(t) \approx v^* - 2/R(t) - 3/(2t) \approx v^* - 5/2t + \cdots$. The numerical results shown in Fig. 59 are consistent with this asymptotic expression and hence confirm the fact that a moving boundary approximation can never hold for a pulled front—one cannot simply characterize

[99] This result was first pointed out to me by B. Derrida (private communication).

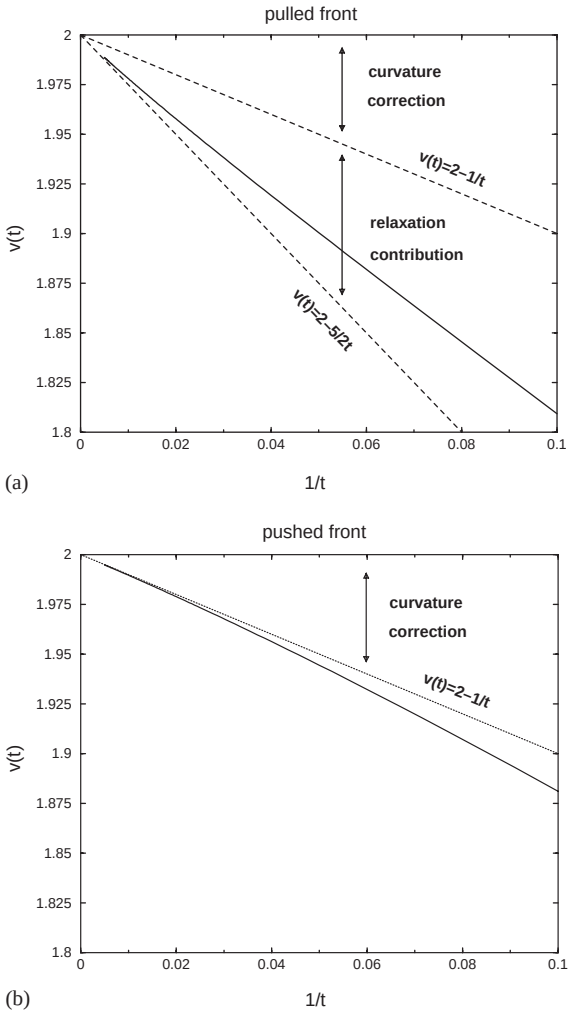

Fig. 59. Illustration of the fact that while a moving boundary approximation applies to a weakly curved pushed front, an interfacial description does not apply to weakly curved pulled fronts. In both graphs the full lines show the velocity as a function of time of a spherically expanding front in the F-KPP equation, starting from initial conditions $u(r,0)=1$ for $r<1$ and $u(r,0)=\exp[-(r-1)^2]$ for $r>1$. (a) In the pulled case, obtained with $f=u-u^3$, the long time relaxation asymptotically approaches the result $v(t)=2-5/2t$, illustrating that curvature and relaxation effects are of the same order. The upper dashed line indicates the relaxation that would result if only the curvature term would contribute, in other words if a moving boundary approximation would hold. The slow convergence to the line $v(t)=2-5/2t$ is due to the subdominant $t^{-3/2}$ term in the velocity relaxation expression (78). (b) Results for the pushed case, obtained with $f(u)=\varepsilon u+du^3-u^5$ with $\varepsilon=1/4$ and $d=(2+2/\sqrt{3})$. According to the exact result discussed in the example at the end of Section 2.7.1, the velocity of the pushed front for these parameters is $v^\dagger=2$ ($v^*=1$ in this case). Note the rapid convergence to the line $v(t)=2-2/R(t)=2-1/t$ which is the result given by the curvature correction to the velocity, in accord with the fact that a moving boundary approximation applies to a weakly curved pushed front.

the properties of the weakly curved pulled front in terms of its asymptotic behavior and curvature correction only.

5.2. Breakdown of singular perturbation theory for a weakly curved pulled front

Let us now trace the main steps of the derivation of solvability type expressions for a weakly curved or weakly perturbed front, to illustrate the breakdown of singular perturbation theory for pulled fronts. Our main goal is to discuss how the crucial differences in behavior of pulled and pushed fronts is reflected in the derivation and in the behavior of solvability expressions that underly the moving boundary approximation. Therefore, it suffices here to consider the simplest case, a weakly curved front in the F-KPP equation with a slowly varying external parameter, rather than a more general "phase field model" of the type referred to in the beginning of Section 5. More detailed discussions of the derivation of a moving boundary approximation can be found in virtually any of the references cited there. The general and more precise discussion of the breakdown of singular perturbation theory for pulled fronts is given by Ebert et al. [145].

Let us consider the F-KPP equation in two dimensions in the case that the nonlinear function f depends on a small and spatially slowly varying external field W,

$$\partial u/\partial t = \nabla^2 u + f(u, W) \ . \tag{219}$$

A moving boundary approximation consists of first matching an inner expansion of the problem on the scale where the fast variable (usually the order parameter variable in phase field models) varies rapidly to the outer problem on large scales, the scale of variation of the other variables like the temperature etc. In the present case, when W is a slowly varying external field, the outer problem is simple for the stable states of $f(u, W)$: u will to lowest order follow the stable stationary states of $f(u, W)$.

Let us imagine that the front is also curved on a large length scale, so that the curvature κ of the front is a small parameter. Since κ and W are expected to be small and slowly varying, the velocity and shape of the profile will differ only weakly from the velocity and shape of the straight (planar) front, and we expect them to vary only slowly in time and space. One therefore introduces a locally curvilinear coordinate system, with ζ measuring distances normal to the front, and s distances along the level lines of the front. In the adiabatic approximation we then perturb about the reference front solution in the absence of curvature and W, by writing in the front region

$$u(x, y, t) = U_0(\zeta) + U_1(\zeta, s, T) + \cdots \ , \tag{220}$$

where T denotes the slow outer time scale and where U_0 is the planar front profile for $W = 0$ which obeys the ordinary differential equation

$$\frac{\mathrm{d}^2 U_0}{\mathrm{d}\zeta^2} + v_0 \frac{\mathrm{d}U_0}{\mathrm{d}\zeta} + f(U_0, W) = 0 \ . \tag{221}$$

with v_0 the velocity of this profile. Since the strongest variation of the profile in the front region is in the ζ direction, in the weakly curved ζ, s coordinate system the Laplacian becomes to lowest order in the curvature

$$\nabla^2 = \frac{\partial^2}{\partial \zeta^2} + \kappa \frac{\partial}{\partial \zeta} + \cdots \ . \tag{222}$$

Upon substituting (220) with this result into the F-KPP equation (219), expanding in U_1 and W, and making the Ansatz that the velocity correction v_1 of the profile follows the change due to the curvature and potential *adiabatically*, we get

$$LU_1 = -(v_1 - \kappa)\frac{\mathrm{d}U_0}{\mathrm{d}\zeta} - \left.\frac{\partial f(U_0, W)}{\partial W}\right|_{W=0} W \ . \tag{223}$$

Here L is the linear operator

$$L \equiv \left(\frac{\mathrm{d}^2}{\mathrm{d}\zeta^2} + v_0\frac{\mathrm{d}}{\mathrm{d}\zeta} + \left.\frac{\partial f(U,0)}{\partial U}\right|_{U_0}\right) \ , \tag{224}$$

which results from linearizing about the profile about U_0 in the frame moving with v_0.

If we perform a stability analysis of a planar front profile in one dimension, the same operator L arises: for the profile U_0 to be stable, its eigenvalues have to be non-positive. However, since the F-KPP equation with $W = 0$ is translation invariant, L always has one eigenmode with eigenvalue zero: $\mathrm{d}U_0/\mathrm{d}\zeta$ gives the change in the uniformly translating profile U_0 if it is shifted over some small distance a, $U_0(\zeta + a) = U_0(\zeta) + a\,\mathrm{d}U_0(\zeta)/\mathrm{d}\zeta + \mathcal{O}(a^2)$, and hence it is a zero eigenmode of L,

$$L\frac{\mathrm{d}U_0(\zeta)}{\mathrm{d}\zeta} = 0 \ . \tag{225}$$

Since the unknown function U_1 in (223) is acted on by L, solvability theory (the "Fredholm alternative" in more mathematical terms) requires that the sum of the other terms in (223) are orthogonal to this zero mode. In more technical terms, they have to be orthogonal to the "left zero mode" χ_0 of L, the zero mode of the adjoint L^+

$$L^+ \equiv \left(\frac{\mathrm{d}^2}{\mathrm{d}\zeta^2} - v_0\frac{\mathrm{d}}{\mathrm{d}\zeta} + \left.\frac{\partial f(U,0)}{\partial U}\right|_{U_0}\right) \tag{226}$$

of L, which obeys $L^+\chi_0 = 0$. Normally, it is nontrivial to find the zero mode of the adjoint of a non-self-adjoint operator. In this particular case, L can transformed into the self-adjoint Schrödinger operator with a simple transformation, a trick that has often been exploited in the stability analysis [72,144,216,230,252,317,376]. Here it suffices to note the result of this analysis, which can be verified directly by substitution, namely that

$$\chi_0(\zeta) = \mathrm{e}^{v_0\zeta}\frac{\mathrm{d}U_0}{\mathrm{d}\zeta} \ . \tag{227}$$

The solvability condition obtained from taking the inner product of (223) with χ_0 simply reads

$$v_1 = -\kappa - \frac{\int_{-\infty}^{\infty}\mathrm{d}\zeta\,\mathrm{e}^{v_0\zeta}\,\frac{\mathrm{d}U_0}{\mathrm{d}\zeta}\,\frac{\partial f(U_0,W)}{\partial W}|_{W=0}}{\int_{-\infty}^{\infty}\mathrm{d}\zeta\,\mathrm{e}^{v_0\zeta}\left(\frac{\mathrm{d}U_0}{\mathrm{d}\zeta}\right)^2} W \ . \tag{228}$$

This equation explicitly gives the change in the velocity of the front due to the curvature and the variation of the parameter W. The first term is the one we already alluded to in the previous section on spherical fronts and gives the "motion by mean curvature" effect familiar from many models for coarsening [6,56,192]. The second one which gives the response to the changes in the parameter W is of the form that one typically encounters in a solvability type approach.

The above discussion has been based on the assumption that the curvature and front velocity change on a slow time scale. Underlying this idea is the assumption that the shape and velocity of the front relax exponentially on some time scale of order unity to the shape and velocity of the planar front we perturb about. One can show this more explicitly [145] by a more careful analysis in which the adiabatic assumption is not made immediately, and in which U_1 is expanded explicitly in terms of the eigenmodes of the stability operator L. The amplitude of these modes are than of order τ_i/T, where τ_i are the relaxation times of these modes and T the time scale of the change of v_1 and κ. Thus, if the spectrum of the stability operator L is "gapped", i.e., if the relaxation times τ_i associated with the stability operator are bounded, the separation-of-time-scales-condition underlying the derivation of the above expression is fulfilled.

There are two ways in which the difference between pushed and pulled fronts shows up in the context of the above analysis. First of all, for pushed fronts the results summarized in Section 2.8 do indeed show that the stability spectrum of a pushed front is gapped, and hence, pushed fronts obey the conditions underlying the derivation of a moving boundary approximation following the lines sketched above. For pulled fronts, however, the conditions are *not* fulfilled. That a separation of scales is not possible is immediately clear from the fact that the velocity and shape of a planar pulled front profile relax as $1/t$ to their asymptotic values; within the above analysis, this emerges from the fact that the spectrum of the stability operator L of a pulled front is not "gapped", i.e., the relaxation times τ_i of the eigenmodes are arbitrarily large.

Secondly, while for pushed fronts the solvability integrals in expressions like (228) are finite and well-defined, for pulled fronts they are infinite. For the F-KPP equation discussed above, one can see this as follows. As we discussed in Section 2.7.1, a pushed front falls off for large ζ as $\exp[-\lambda_2\zeta]$, where λ_2 is the second smallest spatial decay rate. According to results (28) for the F-KPP equation given in the example at the end of Section 2.2, for the F-KPP equation one has according to (60)

$$\text{pushed front:} \quad U_0(\zeta) \overset{\zeta\gg 1}{\sim} a_2 e^{-\lambda_2\zeta} \quad \text{with } \lambda_2 = \frac{v_0 + \sqrt{v_0^2 - 4}}{2} , \tag{229}$$

with $v_0 = v^\dagger > 2$. Hence the integrand of the term in the denominator of (228) converges as

$$e^{v_0\zeta}\left(\frac{dU_0(\zeta)}{d\zeta}\right)^2 \sim e^{(v_0-2\lambda_2)\zeta} \overset{\zeta\gg 1}{=} e^{-\sqrt{v_0^2-4}\,\zeta} \quad (v^\dagger = v_0 > 2) , \tag{230}$$

so that the solvability integral is finite. Likewise, if $\partial f(U_0, W)/\partial W \sim U_0$ as $\zeta \to \infty$, the integral in the numerator of the second term in (228) converges. Thus, for a pushed front, the conditions underlying the derivation of a moving boundary approximation are fulfilled, and the resulting expressions for the dependence of the velocity of the front on slowly varying parameters like W are finite, as it should.

It is easy to see that for pulled fronts, on the other hand, the integrand in the solvability integrals diverges for $\zeta \to \infty$: indeed, according to Eq. (59) for the asymptotic decay of the pulled profile U_0, we have

$$\text{pulled front:} \quad e^{v_0\zeta}\left(\frac{dU_0(\zeta)}{d\zeta}\right)^2 \overset{\zeta\gg 1}{\sim} \zeta^2 e^{(v_0-2\lambda^*)\zeta} = \zeta^2 , \tag{231}$$

with $v^* = v_0 = 2$. *The divergence of the solvability integrals reflects the fact that for pulled fronts the dynamically important region is the semi-infinite region ahead of the front*, while for pushed

fronts or fronts between two stable states the dynamically important region for the front dynamics is the nonlinear front region itself. At the same time, the divergence signals the inapplicability of singular perturbation theory for pulled fronts.[100]

In this section, we have simply illustrated the breakdown of the singular perturbation theory approach to deriving a moving boundary or effective interface approximation for pulled fronts by considering the simple cases of the F-KPP equation. But from our general result that pulled fronts always relax with the same slow power law to their asymptotic speed, it is clear that this conclusion holds more generally. Indeed, even the divergence of the solvability integrals for pulled fronts can be derived quite generally [145].

5.3. So what about patterns generated by pulled fronts?

So far, we have focused our discussion on the fact that a moving boundary approximation does not hold for a pulled front. What then are the implications? To my knowledge, there is at present no clear answer to this question. Clearly, the fact that moving pulled fronts in higher dimensions can strictly speaking never be viewed as moving interfaces, reflects that the important dynamics of a pulled front takes place ahead of the front itself! This makes these fronts especially sensitive to changes in the initial conditions or even to slight changes in the dynamics[101] (see Section 7). Although there are some indications for this for the streamer patterns discussed in Section 3.5, this issue has to my knowledge not been explored systematically. More fundamentally, the question is whether in most cases making a moving boundary approximation in patterns dominated by propagating pulled fronts is "almost right" in the sense that it captures all the gross qualitative features, or whether there are new effects which are fundamentally due to the pulled nature of the fronts. To put it concretely: are there qualitative or quantitative differences in the chaotic domain dynamics of the rotating Rayleigh–Bénard patterns of Section 3.4 between the regime where the fronts are pulled and when they are pulled? Could it be that the behavior of the domain correlation function, or the behavior of the correlation length and time shown in Fig. 29 for the amplitude model, is fundamentally different in the pulled and pushed regimes? Likewise, does the pulled nature of a discharge front show up in any fundamental way in the shape and dynamics of a propagating streamer front, or does the difference between the superconductor patterns of Figs. 33(a) and (b) reflect in a fundamental way the fact that in the first figure the front is pushed, while in the second one it might be pulled? To my knowledge, these basic questions have not been studied at all.

One interesting example of a qualitative change in the front behavior, which is related to this issue, is the work of Kessler and Levine [228], who show that the finite particle cutoff effects discussed in Section 7.1 may render a stable pulled front unstable. Likewise, the behavior of the average occupation density of an ensemble of DLA fingers hinges on the fact that the fronts are pushed rather then pulled, as one finds in a mean field approximation—see the introduction of Section 7.

---

[100] It has been proposed [83,333] to regularize the integrals by introducing a cutoff ζ_c which is taken to infinity at the end of the calculation. Since then only the most divergent terms survive, this procedure reproduces trivially the change in v^* upon changing the linear term in f, but it does not cure the inapplicability of a moving boundary approximation for pulled fronts [145].

[101] Pulled fronts are therefore also very sensitive numerically to the scheme and grid size in the region ahead of the front. Adaptive grid size methods that tend to put a dense grid in the nonlinear front region may not converge to the right result. This was pointed out to me by U. Ebert (private communication).

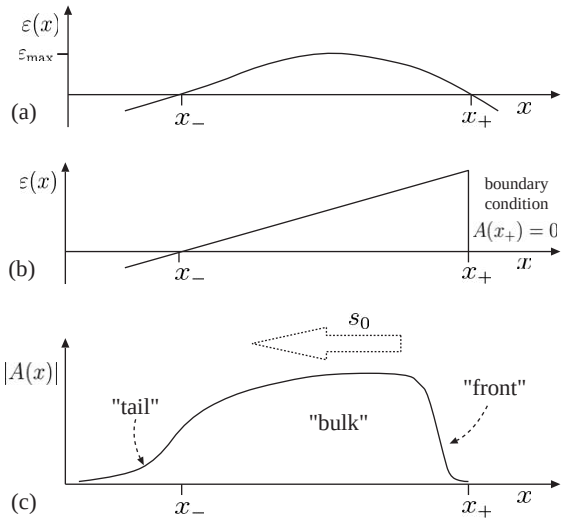

Fig. 60. (a, b) Examples of a control parameter $\varepsilon(x)$ which varies in space, and for which the system is locally unstable only in some finite interval $[x_-, x_+]$. Case (b) is supplemented with a boundary condition $A(x_+)=0$. (c) Qualitative sketch of a "nonlinear global mode" in the regime where $\varepsilon(x)$ varies as sketched in (b) and in which the interval $[x_-, x_+]$ is large enough that different scaling regimes exist. The steep region on the right is close to a front solution in a spatially uniform system.

6. Fronts and emergence of "global modes"

Throughout most of this paper, we have focused our analysis on systems which were infinite and homogeneous, so that their dynamical equations were spatially invariant. Especially in fluid dynamics systems in which there is an overall convective flow, a crucial feature is often the fact that the system is finite and that there is a well-defined inlet—think of the Taylor–Couette cells with throughflow discussed in Section 3.11—or the fact that there is a well-defined obstacle behind which the effective parameters are slowly varying in space—think of the wake of the fluid flow behind a body in the stream-wise direction, where as we discussed in Section 3.10 an instability can give rise to a vortex street. Investigations of these issues in the field of fluid dynamics have given rise to the concept of "global mode" [84,203,206,257].

The idea of a "global mode" is essentially the following. Suppose we consider a system whose properties are slowly varying as a function of the spatial coordinate x (in the case of the flow behind the cylinder of Section 3.10 this would be coordinate in the stream-wise direction). As a result of this, the dimensionless control parameter $\varepsilon(x)$ is then a slowly varying function of x. The dimensionless control parameter ε is defined as the parameter which marks that when the system is *spatially homogeneous*, the basic state of the system exhibits an instability for $\varepsilon > 0$, while it is stable for $\varepsilon < 0$. For pattern forming instabilities in homogeneous systems, the control parameter ε appears as the prefactor of the linear term in an amplitude description, see Eqs. (97) and (103). When $\varepsilon(x)$ is a slowly spatially varying function which, as sketched in Figs. 60(a) and (b), is only positive in some finite range of coordinates x, then we can think of the system as being locally unstable. Nevertheless, the system only turns globally unstable once the interval $[x_-, x_+]$ where

$\varepsilon(x) > 0$ is large enough: it is clearly not sufficient that the system is locally unstable ($\varepsilon(x) > 0$ for some x)—instability only sets in when a *global mode* goes unstable. While for the translationally invariant system the unstable modes are Fourier modes, the modes which have been termed "global modes" and which govern the instability of inhomogeneous systems are essentially localized to the spatial range $[x_-, x_+]$ where $\varepsilon(x) > 0$. The global modes that govern the linear instability problem in spatially varying systems have been studied in particular for the cubic CGL equation (97) for general $\varepsilon(x)$ in the limit that the range over which $\varepsilon(x)$ varies is much larger than the wavelength of the pattern, so that a WKB analysis can be employed [84,203,206,257]. In the case sketched in Fig. 60(b), which might be a reasonable model for the instability in the wake of a cylinder of Section 3.10, the linear eigenmodes can be calculated explicitly. The nonlinear behavior of such global modes has in recent years also been studied [99,100,342–344,358]. We will only highlight here those aspects of global modes that connect immediately with the general theme of this paper.

6.1. A front in the presence of an overall convective term and a zero boundary condition at a fixed position

As a model problem to investigate the influence of a fixed boundary in a system with a convective instability, Couairon and Chomaz [99] have analyzed the F-KPP equation (or Ginzburg–Landau equation for a real variable)

$$\partial_t u(x,t) - s_0 \partial_x u = \partial_x^2 u(x,t) + f(u), \quad f(u) = \varepsilon u + u^3 - u^5 \ , \tag{232}$$

in the semi-infinite axis $(-\infty, L]$, with the boundary condition

$$u(L,t) = 0 \ . \tag{233}$$

Note that the second term on the left-hand side models an overall convection with velocity s_0 *to the left*.[102] As we already discussed in the example at the end of Section 2.5, for an infinite system this term can simply be transformed away by going to a frame moving with velocity s_0 to the left; here, however, the boundary condition at the fixed position $x = L$ does not allow us to do so. The specific choice for the function $f(u)$ in (232) has the advantage that explicit calculations can be done, since in the pushed regime $\varepsilon < 3/4$ the pushed front solutions are known explicitly (see the discussion of the "reduction of order method" at the end of Section 2.7.1), but is not needed for the general scaling arguments below.

Let $v_{\rm sel}$ be the selected front speed in the infinite system for $s_0 = 0$. If the advection velocity s_0 is larger than the selected front speed, $s_0 > v_{\rm sel}$, a front naturally retracts to the left and the system is nonlinearly convectively unstable, as discussed in Section 2.10. We then expect that the asymptotic state is simply $u = 0$; the explicit analysis [99] confirms this. Of course, as we already saw in Section 3.11, in this regime $s_0 > v_{\rm sel}$, the system remains very sensitive to perturbations. For example, a finite forcing at $x = L$ gives rise to a finite u front-type profile [99], while a small amount of noise at $x = L$ gives rise to incoherent front-type patterns. The phase diagram of convective systems with noise has been worked out in particular by Proctor et al. [358].

If $s_0 < v_{\rm sel}$ the infinite system is nonlinearly absolutely unstable: virtually any initial perturbation of the state $u = 0$ for $x < L$ will evolve into a front that propagates to the right, till the boundary

[102] Like in our earlier sections, we use the notation s_0 instead of U_0 of [99] to denote the overall group velocity; moreover, unlike in [99] the overall convection is to the left rather than to the right.

condition at $x = L$ makes itself felt. A full analysis in this regime confirms our intuitive expectation that the long-time asymptotic state is a stationary front-type profile locked near the right boundary.

When the advection speed is just slightly less than the selected front speed in the infinite system, for $0 < v_{\rm sel} - s_0 \ll 1$, we expect that the final stationary front profile remains very close to the profile with speed s_0 just below $v_{\rm sel}$ for essentially all $u > 0$, until a crossover behavior occurs for very small u of $\mathcal{O}(\delta) \ll 1$.

Let us first make this more precise for the pushed regime, i.e., when $v_{\rm sel} = v^\dagger$. The line of analysis we will present below generalizes many of the results of [99,100] for the specific case considered there. As we noted in Section 2.7.1, the pushed front profile is precisely the one for which the coefficient a_1 in the asymptotic expression (58) vanishes: $a_1(v^\dagger) = 0$. Since a_1 will generally go through zero linearly in v, the uniformly translating front profile $U_{s_0}(\zeta)$ with velocity s_0 in the infinite system will to a good approximation in the leading edge be given by

$$\begin{aligned} U_{s_0}(\zeta \gg 1) &\approx a_1'(-\Delta v)\mathrm{e}^{-\lambda_1\zeta} + a_2(v^\dagger)\mathrm{e}^{-\lambda_2\zeta}, \\ &= a_2(v^\dagger)\mathrm{e}^{-\lambda_2\zeta}\left(1 + \frac{|a_1'|\Delta v}{a_2(v^\dagger)}\,\mathrm{e}^{-(\lambda_1-\lambda_2)\zeta}\right) , \end{aligned} \tag{234}$$

where $a_1' = \mathrm{d}a_1/\mathrm{d}v$ and where

$$\Delta v \equiv v_{\rm sel} - s_0 = v^\dagger - s_0 \tag{235}$$

is assumed to be positive but small. As we explained above, the stationary front solution in the presence of the boundary condition $u = 0$ at $x = L$ and the convective term $-s_0\partial_x u$ in the dynamical equation (232) will be the one given by (234) on the outer scale till it crosses over to different behavior when u becomes of order δ. In this crossover range, clearly the overall term $a_2\mathrm{e}^{-\lambda_2\zeta}$ must be of order δ, while the perturbative correction term will be comparable to the dominant one. The latter implies that the exponential term between parentheses in the second line must be of order unity in the crossover region. Upon eliminating ζ from the two expressions obtained from these requirements, we obtain the scaling relation

$$\delta \sim (\Delta v)^\beta \quad \text{with } \beta = \frac{\lambda_2}{\lambda_2 - \lambda_1} . \tag{236}$$

According to this expression the scaling exponent β depends on the properties of the pushed front through the spatial decay rates $\lambda_1(v^\dagger)$ and $\lambda_2(v^\dagger)$. Since outside the crossover region we can to a good approximation use the term proportional to $\mathrm{e}^{-\lambda_2\zeta}$ for the front profile, the distance between the point, where the front reaches a finite value, and the point, where it is pinned by the boundary condition $u = 0$, will for $\Delta v \to 0$ scale as

$$\frac{1}{\lambda_2}\ln\delta \simeq \frac{\beta}{\lambda_2}\ln\Delta v . \tag{237}$$

The above scaling behaviour (236) has also been obtained by Kessler et al. [227], and as they point out this formula gives the scaling of the effect of a finite particle cutoff on the front speed in the pushed regime (see Section 7).

The scaling behavior of a pulled front is very different. In fact, as it turns out the perturbation theory about a uniformly translating pulled front in the case that the front is "cut off" at a small value δ of the field by a boundary condition that makes the dynamical variable vanish, was also developed

by Brunet and Derrida [64] in the context of the stochastic fronts. We will discuss the rather peculiar logarithmic scaling dependence in more detail in Section 7.1; the final result for the relation between $\Delta v = v^* - s_0$ and δ obtained from Eq. (246) below is

$$\Delta v \simeq \frac{\pi^2 D\lambda^*}{\ln^2 \delta} \quad \Leftrightarrow \quad \delta \simeq \exp\left(-\pi\sqrt{\frac{D\lambda^*}{\Delta v}}\right) , \tag{238}$$

where as before in this paper D is the effective diffusion coefficient which is given in terms of the linear dispersion relation by Eq. (13) and which according to (24) is related to the curvature of $v_{\rm env}(\lambda)$ at the minimum v^*. Since the front profile rises approximately as $\delta e^{-\lambda^*(\zeta - L)}$ away from the boundary in the outer region, the distance between the right boundary and a point where u is finite will to dominant order diverge as $|\ln\delta|/\lambda^*$, i.e., as

$$\pi\sqrt{\frac{D}{\lambda^* \Delta v}} . \tag{239}$$

The detailed matching analysis in [99] and in [100] is fully consistent with the above scaling relations and also yields the prefactors for the specific nonlinearity $f(u)$ used in (232). On the other hand, our arguments show that these scaling results hold more generally for uniformly translating pulled and pushed fronts which are pinned by a zero boundary condition. In fact, the arguments apply to coherent pattern forming fronts too; indeed the result of [100] for pulled fronts in the quintic CGL equation (103) are consistent with the above dominant scaling behavior as well.

6.2. *Fronts in nonlinear global modes with slowly varying $\varepsilon(x)$*

Just above the threshold to instability of a global mode, a weakly nonlinear description in terms of the single most unstable mode suffices. However, as soon as the interval $[x_-, x_+]$ and $\varepsilon(x)$ are sufficiently large, it is more natural to think of the nonlinear structures as being decomposed into various regions, as sketched in Fig. 60(c): a front region where the amplitude rises quickly, a bulk region where a well-developed pattern exists whose properties follow the local variation of $\varepsilon(x)$ and a tail region where the pattern amplitude decays back to zero. Most of the analysis of such type of structures has been done in terms of a cubic or quintic CGL equation with a slowly spatially varying ε. To emphasize the separation of scales, let us denote the slow scale on which ε is varying by X. Since the CGL equation is of second order in its spatial partial derivatives, there are always two roots q corresponding with a given amplitude a of a phase winding solution of the form $A = a e^{iqx - i\Omega t}$ of the homogeneous (translationally invariant) CGL equation—see Sections 2.11.5 and 2.11.6 and in particular Eq. (99). Hence, when ε varies on a slow scales X much larger than q^{-1}, it becomes possible to treat the two roots $q_\pm$ as slow variables $q_\pm(X)$ whose variation can be treated by a nonlinear WKB type analysis—as is well known [105,155,193,413], the phase is the slow variable of the translation invariant CGL equation, while the amplitude is slaved adiabatically to the phase dynamics.

Intuitively, we expect that when we consider structures of the type sketched in Fig. 60(c), the region on the right should be close to a front-type solution of the type we have discussed in this paper for translationally invariant systems, and that depending on the dynamical equation under investigation these front-like regions could be either pulled-like or pushed-like. How does this emerge in the above type of WKB analysis? Very simply: if the translation invariant equation admits pulled front solutions, the existence of a front type region is signaled by the two roots $q_\pm(X)$ both

approaching the linear spreading point values k^* in some region [342–344], while if the translation invariant equation admits pushed fronts [101] there is a region where the profile is dominated by one of the roots which is locally close to the mode k_2 of the underlying pushed front in accord with the defining property (76) of a pushed coherent front solution.

For further discussion of these scenarios and of the detailed scaling analysis of the width of the various regions we refer to the literature. In closing it is also useful to point out that while the idea of a global mode has emerged mostly in the fluid dynamics literature in recent years, the problem of pattern selection through a slowly varying control parameter—often called a "ramp"—was already considered in the 1980s both from a more general perspective and for various specific problems [140,237,280,299,362,368]. Not surprisingly, there are strong similarities between these approaches and those mentioned above.

7. Elements of stochastic fronts

We have so far limited the theoretical analysis of front propagation into unstable states to the case in which the front dynamics is governed by deterministic dynamical equations. In this last section on special topics we finally briefly address some elements of the propagation of stochastic fronts into an unstable state.

We do want to stress that we will only touch on a few selected topics that tie in with this review's main emphasis on deterministic fronts. First of all, in reading this section, one should keep in mind that the study of stochastic fronts is a vast field in itself, to which we cannot do full justice. Our choice will be to focus on those issues that are connected with the question of how the deterministic limit can be approached, and on how the front velocity and front diffusion coefficient behave in that limit. Secondly, as is well known, the critical scaling properties of fluctuating growing interfaces are an active research subject in itself [22,195,239]. We will not directly touch on these interesting issues, except for a brief discussion at the end of this section of the question whether fluctuating pulled fronts are in a different universality class from the normal type of fluctuating interfaces.

In Section 5.2 we have seen that while singular perturbation theory works fine for weakly curved pushed fronts or for one-dimensional fronts in a slowly spatially varying external field, it breaks down for pulled fronts. We saw that this implied that while the motion of a weakly curved pushed front can be mapped onto an effective sharp interface model, such an interfacial description does not apply to fluctuating pulled fronts. These findings carry over to fluctuating fronts propagating into an unstable state: when these are pushed, their asymptotic scaling properties are simply those of an appropriate interface model. For pulled fronts, on the other hand, the situation is more complicated: as we shall discuss, fluctuating variants of fronts which in the mean field limit are pulled are very sensitive to noise or to the cutoff effects introduced inherently in simulations with discrete particles executing stochastic jumps. We will focus our discussion on these effects which are special to fluctuating fronts propagating into a linearly unstable state. A more detailed review of several of these issues is given by Panja [332].

It is amusing to note that on hindsight, it is fair to say that the first clear evidence of the strong finite-particle cutoff effects on fluctuating fronts already surfaced in 1991 [58] in the context of a mean-field analysis of diffusion limited aggregation (DLA) fingers. It had been found empirically that when one grows many DLA fingers in a channel, the level lines of the average occupation density of these fingers is very close to the shape of viscous fingers. When researchers made attempts to

study this issue with the aid of the mean-field equations for this density, they ran into the problem that the naive theory, which was based on the existence of pulled fronts in these equations [313], leads to divergences in two dimensions. Brener et al. [58] then showed that if the nonlinear growth term is modified, the fronts behaved properly and the theory reproduced the observed behavior. The broader implications of this empirical trick seem not to have been realized at the time. In hindsight, this was the first sign that in a finite-particle model like DLA, the fact that there is no growth if there is no particle at all makes the front intrinsically pushed and that this is crucial for the model to be well-behaved. This will be a recurrent theme in our discussion.

In the next section, we will first discuss the slow convergence to the asymptotic spreading speed v^* as a function of N, the average number of particles in the saturated state behind the front in a stochastic discrete particle model. Then we briefly review some of the field-theoretic formulations of stochastic fronts, and we close with a short discussion of the implications or our findings for the asymptotic scaling properties of fluctuating fronts in more than one dimension.

7.1. Pulled fronts as limiting fronts in diffusing particle models: strong cutoff effects

The most natural deterministic dynamical equation that arises in the mean field limit from a stochastic model is the F-KPP equation. After all, this equation embodies the two essential ingredients of a lattice model with discrete particles A which make diffusive hops to neighboring sites, and which have some reaction of the type $A \rightleftharpoons 2A$. The latter type of reaction would after a proper scaling lead to a nonlinearity of the type $f(u)=u-u^2$ in the F-KPP equation (1). In line with the literature on this subject we will in this section take the F-KPP equation as our reference deterministic front equation, but one should keep in mind that all our conclusions hold more generally.

One can arrive at the full continuum F-KPP equation from a stochastic lattice model with discrete particles by taking the limit in which the length ℓ_D which a particle diffuses before giving birth to another particle, becomes much larger than the mean inter-particle spacing. A very nice pedagogical discussion of this limit can be found in [304]. Note that while the convergence to a F-KPP type equation in such limits is rather obvious, the precise way in which the front diffusion coefficient $D_{\rm front}$ vanishes is less trivial—stochastic particle models generally give rise to fronts which themselves exhibit a stochastic wandering around the average front displacement, but $D_{\rm front}$ generally depends in an intricate way on the total front structure (see also below). We will not review the details of such type of scaling limits here as they essentially rely on advanced methods of probability theory, and refer to the literature [31,55,121,127,128,223,224,304] for details.

The approach to the mean field limit that will interest us here in particular is the case in which we allow an arbitrary number of particles per lattice site, but in which N, the average number of particles per lattice site (or correlation length) in the region behind the front, becomes large. Again, as N increases, fluctuation effects are suppressed and we expect a mean field front equation to emerge from the underlying stochastic model as $N \to \infty$. Note that in this case we keep $D_{\rm part}$ fixed (and often of order unity), so we *cannot* expect the limit to be governed by a continuum F-KPP equation: The mean field limit will be an equation for a *continuum* density variable u on a *discrete* lattice. Luckily, this is no problem for our discussion as the concepts of pulled and pushed fronts are equally well defined for difference equations, as we discussed in Section 2.4.

Even though earlier simulations [59] had already given hints of a very slow convergence of the speed with N to its asymptotic value, Brunet and Derrida [64] were the first to clearly identify this

issue and to recognize that the $N \to \infty$ convergence to the mean field limit is very different depending on whether the limiting front is pulled or pushed. For pushed fronts, the nonlinear front region where the particle density u is finite determines essentially the front speed. This is also reflected in the fact that the integrands of the solvability integrals that arise in the singular perturbation theory of Section 5.2 converge exponentially. In this finite-density region the relative importance of fluctuations decreases rapidly with N, typically as $N^{-1/2}$. Hence the convergence to the mean field limit is power law fast if the asymptotic front is pushed. For pulled fronts, on the other hand, the situation is different: The fact that they are pulled by the growth and spreading of arbitrarily small perturbations about the unstable state implies that they are very sensitive to small changes in the dynamics in the region of very small particle densities. *At the very tip of any such front is always a region where there are very few particles per lattice site or correlation length, and where the mean field approximation breaks down: Pulled fronts are very sensitive to the unavoidable existence of this tip region where the particle density is of order* $1/N$.

Following Brunet and Derrida [64], we can understand the effect of this on the front speed as follows. For F-KPP type equations, the asymptotic front profiles are uniformly translating, i.e., of the type $u(\zeta) = u(x - vt)$.[103] This is true even for pulled fronts on a lattice. As we have discussed in Section 2.2, following Eq. (25), the uniformly translating fronts with velocity $v > v^*$ are monotonic and fall off simply as $e^{-\lambda\zeta}$ (in other words, $k_r = 0$), but for $v < v^*$ the solutions in the leading edge are of the form

$$u_{v_N} \approx \mathrm{Re}\, c e^{-\lambda\zeta + ik_r\zeta} = c_1 e^{-\lambda\zeta} \sin(k_r\zeta + c_2) \ , \tag{240}$$

where c_1 and c_2 are real coefficients.

Let us now consider the case in which as $N \to \infty$ the front is pulled, and normalize the density field u such that $u \approx 1$ in the region behind the front. Let us furthermore assume that the stochastic model we consider is such that in the very tip region of the fluctuating front—we refer to the region where there are only very few particles per site so that the density field u is of $\mathcal{O}(1/N)$ at the *tip* of the front—the stochastic rules are such that the growth is significantly suppressed. This is what one typically expects intuitively, as there needs to be at least one particle in order to have any growth at all. In the case of suppression of the growth, one expects that the asymptotic average front velocity v_N approaches v^* from below as $N \to \infty$, and hence that for finite but large N the profile in most of the leading edge is given to good approximation by Eq. (240) above.

For uniformly translating profiles, we already saw in Section 2.2 that by expanding about the linear spreading point we can for $v_N < v^*$ express k_r as a function of the velocity as

$$k_r \approx \sqrt{\frac{\lambda^*(v^* - v_N)}{D}} \ , \tag{241}$$

where we have used Eqs. (27) and (24) to write the result in terms of the effective diffusion coefficient D associated with the linear spreading point. The variation of the steepness λ is of higher order in $v^* - v_N$ and to obtain the leading behavior we can therefore take $\lambda \approx \lambda^*$; likewise we can in the analysis below replace the co-moving coordinate ζ by $\xi = x - v^*t$.

[103] Remember that as in Section 2.7, we use the co-moving coordinate $\zeta = x - vt$ for arbitrary velocities, while $\xi = x - v^*t$.

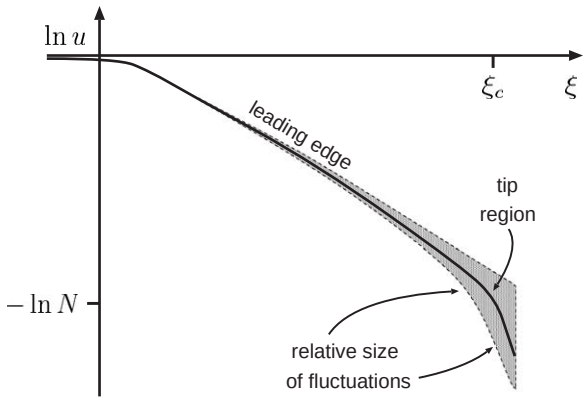

Fig. 61. Schematic sketch of the front profile for a stochastic particle model for very large N. Along the vertical axis, we plot the logarithm of the density u as a function of the co-moving spatial coordinate ξ plotted along the horizontal axis. The leading edge of the front, where $u \gg 1$, corresponds to the behavior on the right for positive ξ. The mean field profile given by (243) is plotted as a full line, while the dotted area gives a qualitative idea of the importance of fluctuation effects. For very large N, the fluctuation effects are small and can be treated perturbatively throughout most of the leading edge, except near the tip where $\xi_c \simeq (\lambda^*)^{-1} \ln N$. As the increase in slope of the full line in this region indicates, the finite particle effects suppress the growth.

Let us position this coordinate system ξ suitably so that the nonlinear front region is roughly near $\xi \approx 0$. As N becomes large, the overall exponential behavior $e^{-\lambda^* \xi}$ of the density field u then implies that the crossover region where $u = \mathcal{O}(1/N)$ is located at

$$\xi_c \simeq \frac{1}{\lambda^*} \ln N \ . \tag{242}$$

Moreover, as Fig. 61 illustrates, upon increasing N the leading edge of the asymptotic profile increases logarithmically in size, as it spans the region from ξ small to ξ_c defined above. On the other hand, the region where fluctuations are important is roughly *confined to a range of finite size near the tip*. E.g., a distance of order $5/\lambda^*$ behind the tip the typical number of particles per lattice site or correlation length is already of order 100, so their effect is already relatively small. Stated more clearly, for any finite N the leading edge exhibits a crossover at $\xi_c \simeq (\lambda^*)^{-1} \ln N$ to a fluctuation-dominated regime but as $N \to \infty$ the fraction of the leading edge where the fluctuating front profile is accurately approximated by the mean field expression (240) approaches 100%!

The asymptotic large-N correction to the velocity now follows directly from simple matching arguments [64]. For ξ positive but small, at the left side of the leading edge, we know that the profile should converge to the $\xi e^{-\lambda^* \xi}$ behavior as $v_N \uparrow v^*$ and hence $k_r \to 0$. This implies $c_2 = 0$ and $c_1 \simeq 1/k_r$, so that

$$u_{v_N} \simeq \frac{1}{k_r} \sin(k_r \xi) e^{-\lambda^* \xi} \quad (k_r \to 0) \ . \tag{243}$$

Let us now look at the crossover region at ξ_c; Eq. (243) immediately implies

$$\left. \frac{du_{v_N}/d\xi}{u_{v_N}} \right|_{\xi_c} \simeq k_r \operatorname{cotg}(k_r \xi_c) - \lambda^* \ . \tag{244}$$

As we stated above, near and beyond the crossover scale ξ_c the deviations from the mean field expressions are significant, say of order unity. In order that the above expression in the leading edge is consistent with this, *the matching condition we have to impose* is that the right-hand side of the above expression (244) deviates more than infinitesimally from the value $1/\xi_c - \lambda^*$ it has in the limit $k_r \to 0$, ξ_c fixed. This is only possible if the argument of the cotangent approaches π in this limit,[104] hence if in dominant order

$$k_r \simeq \frac{\pi\lambda^*}{\ln N} , \tag{245}$$

so that according to (241) we finally have

$$v_N \simeq v^* - \frac{\pi^2\lambda^* D}{\ln^2 N} + \cdots . \tag{246}$$

This is the central result for the dominant large-N correction that was first obtained by Brunet and Derrida [64].[105] As our discussion shows, this expression holds generally for fluctuating pulled fronts which converge to a pulled front as $N \to \infty$ and for which the fluctuation-dominated region is in the large-N limit confined to a finite range near the tip.[106] Just like the power law convergence to v^* of a deterministic front is universal and independent of the details of the model (see Sections 2.9 and 4), so is this large-N convergence: like the expressions for the temporal convergence it only depends on λ^* and D, quantities which are completely determined by the linearized equations of the deterministic (mean field) limit! Note also that the universality is intimately related to the logarithmic N-dependence: the *only input condition* for the derivation is the fact that the region where the strength of the fluctuations is non-vanishing *remains finite* in the limit $N \to \infty$. Since $\ln N/a \simeq \ln N$ in dominant order, this implies that the asymptotic behavior is independent of the precise behavior in the fluctuation region—it does not matter whether the cutoff is effectively at $100/N$ or at $1/N$—the only thing that matters is that it scales as N^{-1}!

The above logarithmic correction to the front velocity contrasts with the power law dependence of the correction in the pushed regime. This was first pointed out by Kessler et al. [227]; the exponent of the power law dependence is given by Eq. (236) above.

To perform an explicit calculation, one of course needs an explicit model. In their paper [64], Brunet and Derrida did the detailed matching analysis for the deterministic F-KPP equation (1) with a cutoff for the nonlinear growth function f of the form sketched in Fig. 62(a), i.e., $f(u,\varepsilon) = \Theta(|u| - \varepsilon)u(1 - u^n)$, where $\varepsilon = 1/N$.

This deterministic front model has the advantage that many aspects can be calculated explicitly, and that it helps one to get intuitive insight into the behavior. For instance, since there is no growth for $|u| < \varepsilon$ *arbitrarily small* perturbations about the state $u = 0$ *do not grow*: a Gaussian initial condition with maximum less than $\varepsilon = 1/N$ just spreads out diffusively, without growing in amplitude. *Strictly speaking*, therefore, the state $u = 0$ in this model is *not linearly unstable* in the

[104] This is the smallest value of k_r satisfying this constraint. Higher values are associated with profiles which have oscillations in the leading edge itself, and therefore rejected.

[105] It is amusing to note that from a technical point of view the same result emerged the same year in the work of Chomaz and Couairon [99] on global modes from a very different perspective—see Eq. (238).

[106] We shall see in Section 7.3 below that when the strength of fluctuations scales with the density field itself (rather than with the square root of it), then the fluctuations throughout the whole leading edge contribute. The fluctuation behavior of such fronts is in a different universality class.

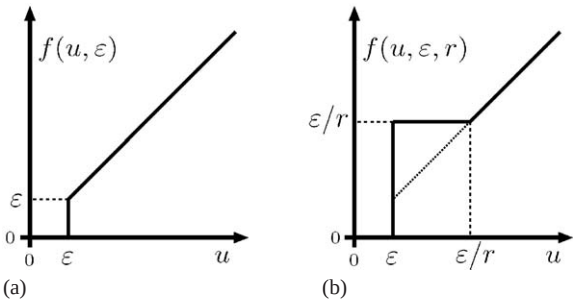

Fig. 62. (a) The nonlinear function $f(u,\varepsilon)$ used by Brunet and Derrida [64] in the F-KPP equation to study the effect of a cutoff on the growth function at $\varepsilon = 1/N$. Since $\varepsilon \ll 1$, the nonlinear behavior of f for values of u of $\mathcal{O}(1)$ is not visible on this scale. (b) The nonlinear function $f(u,\varepsilon,r)$ analyzed by Panja et al. [330] (thick line). In a small interval of u of order ε the growth is enhanced. For $r < r_c = 0.283833$ the fronts are pushed in the limit $\varepsilon \to 0$. Stochastic simulations confirm this effect.

sense we have defined it. An immediate consequence of this is that for $\varepsilon \neq 0$ fronts in this equation cannot be of the pulled type [107] —they are pushed! In line with the fact that the stability spectrum of a pulled front is generally continuous, while it is discrete for a pushed front, one can calculate the relaxation times τ_m of the slowest relaxation modes of the fronts in the above model to find [227,328]

$$\frac{1}{\tau_m} \simeq \frac{\pi^2[(m+1)^2 - 1]}{\ln^2 N} \quad (m \geqslant 1)\ . \tag{247}$$

The modes associated with this slow relaxation extend throughout the whole leading edge; that they are also relevant for fluctuating fronts is for the same reason that for $N \to \infty$ the dominant velocity correction is determined by the matching of the mean field front profile to a finite cross-over region where fluctuations are important. Even though the relaxation times diverge as $N \to \infty$ the logarithmic divergence is so slow that for many practical values of N the relaxation time is still relatively short. If so, convergence to the asymptotic speed v_N is relatively fast [227], and for all practical purposes the front behaves like a pushed front.

Prediction (246) for the asymptotic large-N velocity correction of fluctuating fronts has been corroborated [108] by simulations of a variety of stochastic lattice models [59,64–66,227,329,430]; also field-theoretic arguments are in agreement with this prediction [337] for reasons we shall come to below in the next section.

For any finite N, a front in a stochastic model also shows a stochastic wandering about the average position. This diffusive wandering, which for the type of models we are interested in can be studied by tracking, e.g., the position of the point where the particle density reaches a certain fraction of

[107] Keep in mind that this is only true for this particular model. If one takes instead a modified models in which $f(u) = \mu u$ for $|u| < \varepsilon$ and with $\mu < 1$, then the state $u = 0$ is linearly unstable, but strictly speaking the linear spreading speed is then equal to $2\sqrt{\mu}$. Since this is less than the spreading speed to which the model converges in the limit $\varepsilon \to 0$, the velocity correction is than still given by (246). Also from this point of view we conclude that the dynamically relevant front is a pushed one. The details of the matching analysis and of the calculation of the relaxation spectrum are different in this case, but the final conclusions are the unchanged.

[108] Kessler et al. [227] have reported a discrepancy of a factor of 2 in the prefactor of the $1/\ln^2 N$ correction, but the simulations by Panja [329] do not find evidence for such a large deviation.

the average particle density behind the front,[109] can be characterized by a *front diffusion coefficient* $D_{\rm front}$. The large-N asymptotic scaling of $D_{\rm front}$ is very difficult to study by simulations since one needs reliable data over several decades while $D_{\rm front}$ rapidly becomes very small. Nevertheless, Brunet and Derrida have been able to study the scaling in simulations of a stochastic model which is closely related to the clock model of Section 3.23, by using a clever trick which allowed them to go up to values of N of order 10^{150}. They obtained a scaling

$$D_{\rm front} \sim 1/\ln^3 N \quad (N \to \infty) \,, \tag{248}$$

and empirically found that this asymptotic scaling originates from fluctuations in the tip region: In a simplified version of their model in which only the very first lattice site of the front shows stochastic fluctuations, they observed the same asymptotic behavior for $D_{\rm front}$ as in their full model. It appears that the behavior is associated with the fluctuation behavior of the low-lying modes of the stability operator of the deterministic equation, whose relaxation time τ_m is given in (247) above.[110]

The analysis we have sketched above only identifies the leading order finite-N velocity correction. This term is remarkably universal; it appears that if one wants to go beyond this term, one is forced to perform a detailed analysis of the fluctuations in the tip region, and to match the behavior there to the front profile in the rest of the leading edge. This is a complicated problem, because the number densities in the tip region are small so that standard perturbation methods do not apply. Although a first-principles theory is still lacking, quite a bit of insight is obtained from an approximate analysis [329] in the tip region, which focuses on the stochastic behavior of the foremost occupied lattice site (an idea that has also played a role in earlier stochastic lattice models for small values of N [31,223,224,331]). This analysis shows that corrections beyond the leading velocity correction term depend on virtually all the details of the microscopic model, including the precise mean-field behavior in the region behind the front. In fact, in the tip region the lattice and finite-particle effects are so important that the profile is not truly a uniformly translating profile anymore [328].

Finally, it is good to stress once more that the analysis summarized above is based on the assumption that the fluctuation effects in the tip region *suppress* the growth. Obviously, if the growth rate for u of order $1/N$ is *enhanced*, the very tip region can move faster than v^* of the unperturbed case, and this will lead to a pushed front with asymptotic velocity *larger than* v^*. It easy to show this explicitly following the lines of [64] by using the growth function shown in Fig. 62(b). The explicit analysis shows that for $r < r_{\rm c} = 0.283833$ the asymptotic front speed in the limit $\varepsilon = 1/N \to 0$ is indeed larger than v^*. Simulations of a stochastic particle model in which growth rates for particle occupancies of 3 or less are enhanced in the same way as suggested by the function $f(u, \varepsilon, r)$ of

[109] In models in which the total number of particles remains fixed, like in the clock model of Section 3.23 or the model studied by Brunet and Derrida [64], one can equivalently track the center of mass of the particles. However, in models where the particle density behind the front region is finite, one has to be careful not to include the fluctuations from this region—the total mass fluctuations in this region will grow proportionally to $\sqrt{NL}$ where L is the size of this region. Since L grows linearly in time, this will look like a diffusive behavior, but it has nothing to do with the *diffusive wandering* of the *front position* that is of interest here and in the stochastic Langevin models discussed in the next section.

[110] If one follows the arguments of [365] by expanding the fluctuation behavior of the fronts in terms of the eigenmodes of the stability operator, one finds that for large N the coefficients in this expansion obey Langevin-equations with noise which is exponentially dominated by fluctuations at the tip. Moreover, the noise that drives the different coefficients is correlated. It is easy to convince oneself that the resulting expressions (and Eq. (251) below) lead to logarithmic scaling of $D_{\rm front}$ but whether such arguments lead to behavior (248) is at present unclear to me. It is also possible that non-perturbative effects like those discussed in the next section are important.

Fig. 62(b) already show this enhancement of the average front speed. Note that these results clearly illustrate that the limits do not commute: if we take the limit $\varepsilon \to 0$ in the function f, we arrive at the classic F-KPP equation with asymptotic velocity $v^* = 2$, while if we consider fronts with $\varepsilon > 0$ and $r < r_c$ and then take the limit $\varepsilon \to 0$, we get a pushed front with speed $v^\dagger$ larger than v^*!

Since the main conclusions of this section affect the gross features of fluctuating fronts in more than one dimension, we summarize them below:

Fronts in stochastic particle models which in the mean field limit $N \to \infty$ converge to a pulled front solution, are generically pushed fronts for any finite N. Their speed relaxes exponentially in time to an asymptotic speed v_N which for models in which the growth at small particle occupancies is suppressed relative to the mean field value, is given for large N by (246). Different growth rules at very small particle numbers can give pushed fronts for finite N with speed $v^\dagger$ larger than the spreading speed v^* of the mean field limit.

For a fixed N one has to consider such fluctuating fronts as being "pushed" as far as their long-time large-size scaling properties is concerned (see Section 7.3 below). On the other hand, all the special scaling properties as $N \to \infty$ originate from the fact that in this limit one approaches a pulled front solution. To remind us of their special character, we have therefore sometimes referred to such fronts as fluctuating "pulled" fronts [328]. However, as we will see below, even this name does not do full justice to the fact that in particle models, the fluctuation properties of the fronts are essentially like those of pushed fronts, not like those of pulled fronts.

A remarkable consequence of the effects discussed in this section has been demonstrated by Kessler and Levine [228]. As we discussed in Section 3.13, there are deterministic pulled fronts which do now show a long-wavelength instability for any value of the parameters, but which do so for suitable diffusion ratios as soon as they are pushed. As we have just seen, finite particle effects are sufficient to induce this crossover, and as was shown in [228] in this way finite particle effects can induce a long-wavelength interfacial instability.

7.2. Related aspects of fluctuating fronts in stochastic Langevin equations

The previous discussion has already mentally prepared us for another surprise concerning fluctuating fronts in field-theoretic approaches to the study of fronts propagating into an unstable state. In a field theoretic formulation, the natural starting point to study propagating fronts in the presence of noise [10,11,129,130,177,176,259,260,289,297,337,377,409] is to start with a stochastic version of the F-KPP equation (1),

$$\partial_t u(x,t) = \partial_x^2 u(x,t) + f(u(x,t)) + g(u(x,t))\eta(x,t) \ . \tag{249}$$

In this Langevin-type equation η is a stochastic noise term which is delta-correlated in space and time with strength 2μ,

$$\langle \eta(x,t)\eta(x',t')\rangle = 2\mu\delta(x-x')\delta(t-t') \ , \tag{250}$$

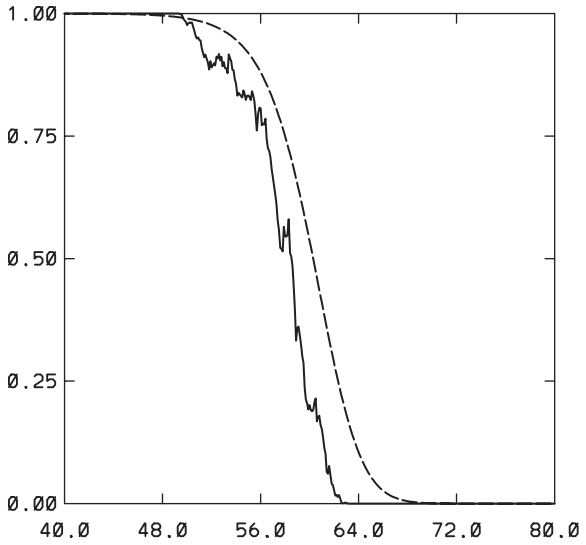

Fig. 63. Snapshot of a stochastic front in a simulation by Doering et al. [129] of the stochastic F-KPP equation (249) with $f(u)=u(1-u)$ and $g(u)=\sqrt{u(1-u)}$ (full line). With this function $g(u)$ there are no fluctuations in the stable state $u=1$ behind the front. The dashed line is a plot of a uniformly translating front profile of the deterministic F-KPP equation (1). Note that the stochastic front solution has compact support: the dynamical variable is *identically zero* beyond some point. The deterministic front solution, on the other hand, is nonzero at every position.

where the brackets denote an average over the noise. Since η is multiplied by some function $g(u)$ of the fluctuating field u in (249), the noise term is "multiplicative" rather than additive.[111]

The form of the function g in (249) that gives the noise strength as a function of the dynamical variable u, depends on the physical model for the noise. When the origin of the noise lies in the fluctuations in the number of particles per correlated volume or per lattice site, then it is customary to take $g(u) \propto \sqrt{u}$. The rationale behind this is that quite generally the fluctuations in the number of stochastic moves of n independent particles in some correlated volume or at some lattice site is of order $\sqrt{n}$; after normalization this gives fluctuations of order $\sqrt{u}$ in the particle density. In simulations, it is often advantageous to take the function $g(u)$ to vanish too in the saturated state behind the front, so that fluctuations in the trivial state behind the front are suppressed (compare footnote 109).

If the noise originates from independent random fluctuations in one of the parameters of the function $f(u)$, it is natural to take the noise strength $g(u) \propto u$ for small u (see [366] and references therein). We shall come back to this case in the next section.

Let us return to the case in which $g(u) \propto \sqrt{u}$ for small u. The remarkable finding [129,130,307] is that these stochastic fronts have *compact support*! In other words, these stochastic fronts are identically zero beyond some finite value of x [307]. This is illustrated in Fig. 63. Since for any finite time front solutions in the deterministic F-KPP equation are nonzero *for all* x, this implies that

[111] As is well known, for a stochastic differential equation with multiplicative noise, one faces the question whether the noise is interpreted in the Itô or in the Stratonovich sense. The issues we address here are unaffected by the particular choice one makes, so we refer to the literature [12,176,177] for further discussion.

this type of noise has a *non-perturbative effect* on fronts—we cannot think of the noise as being a small stochastic perturbation on top of an underlying smooth front profile that obeys a mean-field like deterministic equation!

The fact that fronts in stochastic front equations with multiplicative noise with $g \propto \sqrt{u}$ for small u have compact support has as a remarkable consequence that they show the same surprising $1/\ln^2 N$ scaling of the correction to the front velocity in the small noise limit ($\mu \to 0$ in (250)) [337]. The reason for this is clear from the discussion of the previous section: as long as the non-perturbative effects of the noise is limited to a finite region near the tip of the front, then as we saw the $1/\ln^2 N$ scaling of the velocity correction results from the matching analysis of the part of the leading edge of the front where the noise effect becomes arbitrarily small in the limit $N \to \infty$.

There are many intriguing and open questions regarding such stochastic fronts, but we refer to the two recent papers by Doering et al. [129,130] for further discussion of such issues. To my knowledge, an open question is a proper understanding of scaling (248) of the front diffusion coefficient $D_{\rm front}$, e.g., by exploiting the fact that in some limits the behavior of such Langevin equations can be mapped onto finite particle models using a duality transformation [129,130,337].

We stress once more that these considerations are in practice essentially only of importance for fronts which are pulled in the mean-field limit. As we mentioned earlier, the discussion of Section 5.2 showed that singular perturbation theory does apply to pushed fronts, and this means that in the weak noise limit one can study the effect of noise on the motion of pushed fronts perturbatively. As an example, we note that for small noise strength the diffusion coefficient $D_{\rm front}$ of pushed fronts is given by

$$D_{\rm front} = \mu \frac{\int_{-\infty}^{\infty} {\rm d}\zeta\, {\rm e}^{2v_{\rm as}\zeta} ({\rm d}U_0/{\rm d}\zeta)^2 g^2(U_0)}{\left[\int_{-\infty}^{\infty} {\rm d}\zeta\, {\rm e}^{v_{\rm as}\zeta} ({\rm d}U_0/{\rm d}\zeta)^2\right]^2} \ . \tag{251}$$

Here g is the multiplicative noise strength in (249) and $U_0(\zeta) = U_0(x - v_{\rm as}t)$ is the pushed front solution of the deterministic limit of this stochastic differential equation [11,297,365]. This expression has the typical structure discussed in Section 5.2, a ratio of two solvability-type integrals with the perturbing term in the numerator—compare, e.g., Eq. (228). For pushed fronts the integrands vanish exponentially for large positive ζ and hence pushed fronts are quite insensitive to the non-perturbative effects in the tip region when the stochastic noise is turned on. But, as we already discussed in Section 5.2, for pulled deterministic fronts the integrals do not converge; the anomalous scaling properties of fluctuating pulled fronts that we will discuss in the section below are a result of this. Armero et al. [11] have compared the above expression for $D_{\rm front}$ with extensive numerical simulations of pushed fronts with noise, and found that the formula works quite well, even at appreciable values of the noise strength μ.

7.3. The universality class of the scaling properties of fluctuating fronts

Now that we understand some of the important features of the behavior of stochastic fronts in one dimension, let us close with considering the implications for the universality class of the scaling properties of these propagating fronts in more than one dimension.

As we noted in the very beginning of this section on stochastic fronts, the scaling properties of fluctuating front and interfaces is usually studied in terms of interface models like the KPZ equation

[22,195,218,239]. Now, even though in the limit $N \to \infty$ some stochastic fronts can become pulled, for any fixed N or noise strength μ the stochastic fronts we have examined all are pushed fronts. Therefore, in view of the conclusion of Section 5.2 that pushed fronts do map onto an effective interface model for their long-wavelength and long-time dynamics, these models should all effectively map onto one of the familiar type of interface models that have been studied so extensively in the literature [22,195,218,239]. Or, to put it differently:

the particle lattice models or the stochastic differential equations with multiplicative noise and $g(u) \propto \sqrt{u}$ which in the mean field limit map onto dynamical equations with pulled fronts, are in practice in the same universality classes as the usual interface models that one would naively write down for them.

As a historical note, it is only fair to admit that I got this issue wrong initially [402]. When we started to wonder about the question whether fluctuating pulled fronts might be in a different universality class, we were motivated by several observations: (i) the fact that deterministic pulled fronts do not map onto an effective interface model; (ii) the fact that their dynamics is driven by the dynamics in the semi-infinite region ahead of the front itself rather than the dynamics in the front region itself; and (iii) the fact that there were simulations of stochastic versions of the F-KPP equation [363] which appeared to suggest that in two and higher dimensions such fronts are in a different universality class than the KPZ equation. This made us argue [402] that stochastic lattice model realizations of the F-KPP equation with pulled fronts would exhibit non-KPZ scaling. The insight summarized above that both lattice model realizations and Langevin-type versions with multiplicative noise strength proportional to $\sqrt{u}$ make the fronts always pushed invalidates this conjecture. In fact, soon after our proposal, Moro [303] demonstrated this and presented numerical simulation results in support of this.

There is actually one rather special case where fluctuating fronts deserve to be viewed as genuinely pulled, and for these the scaling properties seem to be anomalous indeed [364,403]: if one has a medium in which the parameters entering the nonlinear growth function $f(u)$ are fluctuating (see, e.g., [366]), a natural model is to take $g(u) \approx u$ for small u in (249). Let us consider the case that the growth function $f(u)$ is such that the fronts are pulled, and that $f'(0) = 1$. In the presence of noise the leading edge equation for a front in d bulk dimensions then reads [112]

$$\partial_t u = \nabla_x^2 u + (1 + \eta)u \ . \tag{252}$$

If the front propagates on average in the x direction, then upon transforming to the co-moving frame $\xi = x - v^* t = x - 2t$ the equation for the leading edge variable $\psi = \mathrm{e}^{\xi} u$, which already played an important role in the analysis of the universal relaxation of pulled fronts in Section 4.1, reads

$$\partial_t \psi = \nabla^2 \psi + \psi\, \eta \ . \tag{253}$$

As is well known, with a Cole–Hopf transformation $\psi = \mathrm{e}^h$ this equation reduces to the standard KPZ equation [22,195,218,239] for h,

$$\partial_t h = \nabla^2 h + (\vec{\nabla} h)^2 + \eta \ . \tag{254}$$

[112] We immediately focus on the analysis in the leading edge, where nonlinear terms in u can be ignored. In Section 4.3 we showed that the nonlinear terms play the role of a boundary condition for the leading edge dynamics.

The point to note about this simple argument is that one arrives at the KPZ equation *in the dimension of the system in which the front propagates*: h and the noise η are functions of both the ξ coordinate perpendicular to the front and the coordinates parallel to the front. This implies that the universality class of such genuinely pulled fluctuating fronts is that of the KPZ equation, but in one dimension higher than one would naively guess if one would think of the front as a moving interface [364,403]. One implication of this is that such fronts in one dimension show sub-diffusive behavior, an observation that is corroborated by numerical simulations [364].

We emphasize again that this anomalous scaling—KPZ-type scaling but in one dimension higher than one would naively expect—is only expected if the effective equation is of form (252), i.e., if the strength $g(u)$ of the noise is linear in the dynamical field u. As we discussed above, intrinsic fluctuations like those that arise naturally in any particle model correspond naturally to fluctuations of strength proportional to $\sqrt{u}$ and in such models one indeed never sees signs of anomalous diffusion or scaling behavior. I believe that this is due to the following. Whatever the precise model, the relative strength $g(u)/u$ of intrinsic fluctuations is stronger the smaller u, i.e., the stronger the smaller the number of particles. Now, it is easily seen from (251) that whenever $g(u)/u$ behaves as $u^{-\gamma}$ with $\gamma > 0$ for small u, the integrand in the numerator is *exponentially dominated* by the contributions at the tip of the front. This means that fronts with intrinsic fluctuations behave like objects with fluctuations in a *finite* region and hence with normal scaling behavior. In other words, only if fluctuations throughout the whole leading edge contribute equally to the fluctuating behavior ($\gamma = 0$), as they do when they are driven by fluctuations in an external parameter (or possibly for error propagating fronts—see the last paragraph of Section 3.22), will one see anomalous (transient) scaling. In realistic particle models, one won't.

These observations illustrate that the behavior of a fluctuating front is subtle. Because they operate close to a bifurcation point, whether or not we should think of them as being close to being pulled depends on the quantity under consideration. Indeed, regarding their velocity, we can consider such fronts as being "weakly pulled" for large N in the sense that their velocity approaches v^* for $N \to \infty$, but when we consider the fluctuation properties of a front with intrinsic fluctuations we should not think of them as being weakly pushed.[113] Hopefully future research will clarify these subtleties and the scaling behavior (248) of $D_{\rm front}$.

8. Outlook

In this article we have aimed to introduce the subject of front propagation into linearly unstable states from a unifying perspective, that allows us to bring together essentially all important developments in this field. The concept of linear spreading speed v^* not only aids in developing an intuitive understanding and in sharply defining pulled and pushed fronts, but it also lies at the basis of the formalism that allows one to derive the universal relaxation towards the pulled front speed, using matched asymptotic expansions. In addition, "global modes", the breakdown of an effective interface formulation of pulled fronts or the universal large-N velocity corrections of stochastic fronts can all be naturally approached from this perspective. The many examples that we have discussed show

[113] This was stressed in particular to me by E. Moro.

the ubiquity of the problem of front propagation into unstable states, and illustrate how one can understand an enormous variety of systems with a few simple tools.

There are several open issues. Concerning deterministic fronts, the most pressing one is a sharp definition, using an appropriate averaging procedure, of an incoherent pushed front. In what sense are incoherent fronts which arise from the nonexistence of coherent pattern forming fronts different from incoherent fronts which originate from the instability of coherent fronts? Furthermore, while our definition of coherent pattern forming pushed fronts is consistent with what is know for the quintic CGL equation or extensions of the Swift–Hohenberg equation, such types of fronts remain relatively unexplored. For pulled fronts in periodic media, we have conjectured that their asymptotic speed can be calculated using Floquet analysis, but this proposal remains to be explored. Also our understanding of stochastic fronts, especially when they are close to the mean field limit, is still incomplete. In addition, I have the impression that the difference between pulled and pushed fronts may be underestimated in the fields of turbulent combustion and wave propagation in periodic media. Finally, even though we have argued that there are hints of slow convergence to the asymptotic speed in experiments specifically aimed at probing pulled fronts, only very accurate new experiments can settle this issue.

Of a different nature are the challenges posed by pushed fronts. Even though the mechanism of pushed front propagation for uniformly translating and coherent pattern forming fronts can be considered known, making concrete predictions for a given problem requires the explicit construction of the nonlinear pushed front solution. Even for nonlinearly translating fronts, this is a highly nontrivial problem for any equation beyond the F-KPP equation. Moreover, I do not think there is much hope that there will ever be a general framework that allows one to calculate pushed front solutions for large classes of equations, as every detail counts. Guessing how one can add a term to a dynamical equation to make the front propagation become pushed is often trivial, but any serious analysis of pushed fronts is often virtually impossible—the fact that the pushed front solutions of the quintic CGL equation can be obtained analytically is an exceptional miracle.

For those mathematicians who only accept rigorous proofs, almost everything in this paper can be considered an open issue. The route we have chosen to follow here is quite different from the usual one favored in the mathematics literature. I believe the approach we have advanced here is ready to be put on rigorous footing. If this will be done, it will undoubtedly allow one to approach large classes of equations at one fell swoop.

Acknowledgements

I would like to take this opportunity to express my thanks to Ute Ebert for intense collaborations and discussion on front propagation issues in the last few years. Much of the presentation in this article is shaped by the interaction with her. In addition I want to acknowledge all the other collaborators, colleagues and friends with whom I have worked on or discussed front propagation and related issues in the past decade: Mischa Anisimov, Chiara Baggio, Markus Bär, David Bensimon, Henri Berestycki, Tomas Bohr, Daniel Bonn, Haim Brezis, Christiane Caroli, Jaume Casademunt, Hugues Chaté, Pat Cladis, Elaine Crooks, Mike Cross, Greg Dee, Patrick De Kepper, Bernard Derrida, Arjen Doelman, George Gilmer, Ray Goldstein, Henry Greenside, Tim Halpin-Healy, Danielle Hilhorst, Pierre Hohenberg, Robert Hołyst, Deszö Horváth, Martin Howard, Joost Hulshof, Reijer

Jochemsen, Tasso Kaper, Julien Kockelkoren, Lorenz Kramer, Joachim Krug, Philip Maini, Hiroshi Matano, Mayan Mimura, Chaouqi Misbah, Esteban Moro, Judith Müller, Alan Newell, Yasumasa Nishiura, Alexander Morozov, Peter Palffy-Muhoray, Debabrata Panja, Bert Peletier, Mark Peletier, Werner Pesch, Zoltan Racz, Andrea Rocco, Vivi Rottschäfer, Bjorn Sandstede, Boris Shraiman, Willem Spruijt, Kees Storm, Alessandro Torcini, Goutam Tripathy, Henk van Beijeren, Jan-Bouwe van den Berg, Martin van Hecke, Willem van de Water, Ramses van Zon, John Weeks and Rinke Wijngaarden. Finally, I also want to thank Kees Storm for detailed comments on an earlier version of the manuscript, Deb Panja and Alexander Morozov for help with some of the figures, and Yolande van der Deijl for her perspective.

Appendix A. Comparison of the two ways of evaluating the asymptotic linear spreading problem

There are two ways to extract the long-time asymptotics of the general equation (44),

$$\underline{\hat{\phi}}(k,\omega) = \underline{\underline{\hat{G}}}(k,\omega)\cdot\underline{\underline{\hat{H}}}(k,\omega)\cdot\underline{\bar{\phi}}(k,t=0)\ , \tag{A.1}$$

depending on whether one first evaluates the ω-integral of the inverse Laplace transform, or the inverse k-integral of the Fourier transform. The first route most closely parallels our earlier discussion of Section 2.1. Indeed, if we first evaluate the ω-integral—which runs along a line in the upper half ω-plane, as (42) converges for sufficiently large ω_i, so the functions are analytic sufficiently far up in the upper half ω-plane—then the poles where $|\underline{\underline{\hat{S}}}| = 0$ determine the dispersion relations $\omega_\alpha(k)$ of the various branches which we label by α. The remaining spatial Fourier inversion then has a form similar to (8), except that there is an additional sum over the branch index α, and that associated with each branch α and wavenumber k there is an eigenvector $\underline{\hat{U}}$ of the linear dynamical matrix (see Section 5.5 of [144] further details). From there on, the analysis is essentially similar to the one given for a single field in Section 2.1 for each branch. If it so happens that there is more than one branch where modes are unstable, then it is possible that there is more than one linear spreading velocity v^*_α. *Since we are considering a fully linear problem, it is clear that the largest value of* v^*_α *is the relevant linear spreading velocity* for generic initial conditions which have nonzero overlap with the associated eigenvector $\underline{\hat{U}}$. We refer to the largest velocity of these as *the* linear associated with each of these branches spreading velocity v^* and likewise associate k^*, λ^* and D with the values at the corresponding linear spreading point.[114]

The advantage of this line of analysis (first evaluating the ω-integral by contour integration) is that the importance of initial conditions is immediately clear. In complete analogy with (37) and the earlier discussion, so-called steep initial conditions, for which the amplitudes of the components $\phi_m(x,t=0)$ decay faster than $\exp(-\lambda^* x)$, lead to profiles which asymptotically spread with velocity v^*.

The second route to extract the long time asymptotics is the one which was developed since the late 1950s in plasma physics. We only summarize the essentials here and refer to [49,62,204,264] for details. The main idea of the analysis is the following. For each ω, there are poles of the integrand in the complex k-plane, so when ω varies along the ω-integration path in the upper half of the

[114] Since the discussion of Section 2.2 implies that each velocity v^*_α corresponds to the minimum of a curve $v_{\alpha,\mathrm{env}}$, it is sometimes said that the selected speed is the maximum of the minimum velocities. An example where this was checked for fronts can be found in [334].

complex ω-plane which runs parallel to the real axis, the poles trace out curves in the k-plane. Imagine now that we lower the ω-integration path; then these lines of poles in the k-plane will shift. If one of these lines of poles tends to cross the k-axis, we just deform the k-integration path, so as to avoid the lines traced out by the poles. Now, we can continue to deform the k-integration path so as to avoid the lines of poles, until at some point, upon lowering the ω-path, two lines of poles in the k-plane come together from opposite sides of the integration path and "pinch off" this path [49,62,204,264]. Where will this "pinch point" be? Not surprisingly, it is the same as the saddle point in the previous formulation. Indeed, since close to the point ω_α^*, k_α^*

$$\omega - \omega_\alpha^* \approx \frac{1}{2}\left.\frac{\mathrm{d}^2\omega}{\mathrm{d}k^2}\right|_{k_\alpha^*} (k-k_\alpha^*)^2 = -\mathrm{i}\mathscr{D}(k-k_\alpha^*)^2\,, \tag{A.2}$$

we have

$$k - k_\alpha^* \approx \pm\sqrt{\mathrm{i}(\omega-\omega_\alpha^*)/\mathscr{D}}\ . \tag{A.3}$$

Hence as the ω-integration path is lowered towards ω_α^*, two poles in the k-plane merge together to "pinch off" the k-contour. In this analysis, which is often referred to as the "pinch point analysis", one thus evaluates the k-integral first and then performs the ω-integration. In view of (A.3), after performing the k-integration there is a branch cut in the ω-plane. Evaluation of the ω-integration around the branch cut then gives the same expressions as those we found before.

The above discussion of the pinch point analysis gives the long-time asymptotic behavior of the Green's function. This implicitly means that delta-function like initial conditions are assumed; the possibility of exponentially decaying initial conditions is usually not discussed in the literature, but these do lead to the same conclusions as before: steep initial conditions lead to profiles spreading asymptotically with velocity v^*. In fact, since the k-integral is closed first in the pinch-point analysis, poles in the complex k-plane arising from exponentially decaying initial conditions give rise to additional terms in the ω-integral which compete with the contribution from the pinch point in a way similar to the one we discussed before in Section 2.2.

One final caveat is important. While the linear spreading point k^* is determined by a local condition, the relevance of this point for the dynamics is subject to some (mild) conditions on the analytic structure in the k-plane. In the first formulation, where we focus on the k-integral evaluation given the dispersion relation $\omega(k)$, the underlying assumption is that the k-integration path can be deformed continuously to go through the saddle point. In other words, there should be no branch cuts or non-analyticities to prevent us from reaching this point. Furthermore, the condition that at the spreading point $D > 0$ is important. For, if this condition is not fulfilled, then if we would write $\phi(\xi,t) = \mathrm{e}^{-\lambda^*\xi}\psi$, the equation for ψ is governed by a negative diffusion coefficient [see Section 4.1, Eq. (199)]. This means that convergence to a smooth asymptotic exponential behavior is not possible for $D < 0$.

Likewise, there are conditions on the analytic behavior in the pinch point formulation: the "pinching off" of the deformed k-integration path by the two lines of poles in the complex k-plane means that these two lines have to be analytical continuations of branches which are below and above the k-integration path when it was running along the real k-axis. It actually appears to me that the precise status of such conditions and of the relation between the conditions in the two formulations is not

fully understood. E.g., the condition $D > 0$ is not generally found in the pinch point literature.[115] Nevertheless, our pragmatic point of view in this paper is that once can proceed with the general analysis laid out in this paper, keeping in mind that for any given problem, one can explicitly check whether the conditions underlying the general derivation are satisfied.

Appendix B. Additional observations and conjectures concerning front selection

It turns out that the exact pushed front solutions of the F-KPP equation obtained by the "reduction of order method" discussed briefly at the end of Section 2.7.1, do have some special properties in the complex ζ-plane [188]. This has led to the speculation that these properties hold more generally [188]—if true, this would allow one to obtain the pushed front speed $v^\dagger$ without explicitly constructing the strongly heteroclinic front profile itself. However, the fact that pushed front solutions are sensitive to every change in the equations indicate that such a remarkable property is very unlikely; detailed investigations and the construction of an explicit counterexample have indeed confirmed that the idea is untenable [82].

Another observation which has been proposed as a possible road to understanding the selection problem of uniformly translating fronts is to look for front solutions which monotonically connect the *exact* unstable state $\phi = 0$ and the stable state in a *finite* but large interval $[0, L]$ of the co-moving coordinate ζ [391,392]. It is clear that this requirement does reproduce the selected speed for uniformly translating fronts. After all, this requirement amounts to searching for front solutions which go trough zero at L when a larger interval is considered. Now, in the uniformly translating regime the selected front is always the only front solution which is close to a front solution $\Phi_v(\zeta)$ which will just go through zero when the velocity is lowered. Indeed, the pushed front solution $\Phi_{v^\dagger}(\zeta)$ has $a_1 = 0$ and so in its neighborhood are the first solutions (58) which have $a \neq 0$ and which go through zero, while in the pulled case the first solutions which go through zero appear just below $v = v^*$, because the $k_r \neq 0$. Thus this approach is consistent with known results for uniformly translating fronts, but it gives no insight into the underlying dynamical mechanism and it does not apply to pattern forming fronts. The convergence of the velocity obtained this way to the selected one can be analyzed using the methods discussed in Section 6.1.

Recently, there has been interest in reformulating the front propagation problem in terms of Hamilton–Jacobi theory (see, e.g., [156]). At present such methods appear to be limited to the obtaining the asymptotic front speed, not the convergence to it. Since these results are already contained within those discussed here, we will not discuss it further.

We finally note that the renormalization group approach developed for partial differential equations [184] has also been used in the context of front propagation [61,83,333,334]. Viewed as a reformulation of singular perturbation theory, the renormalization group method is very useful in reinterpreting the basis of amplitude equations and similar methods [60,184]; however, as we discuss in

[115] In view of (A.3) this condition implies a statement about the local orientation of the two lines of poles in the complex k-plane: if the ω-contour grazes just over ω^* in the horizontal direction the condition $D > 0$ implies that one of the lines of poles always lies in the upper half Δk-plane and the other one in the lower Δk-plane. The example give in [49] of two poles which merge but which do not form a pinch point, is actually an example of a point where $D < 0$, but whether this is accidental I do not know. See also Appendix M of [144] for further discussion of the difference between the two methods.

Section 5 singular perturbation methods do not apply when one wants to go beyond the asymptotic speed of pulled fronts, so here its use for the front propagation problem appear to be limited. In addition, renormalization group methods can be used to study contraction to the asymptotic speed or front stability [61]. Whether the universal convergence towards the asymptotic speed can be analyzed or proved with this method, is to my knowledge an open question.

Appendix C. Index

Several colleagues have asked me to supply an index for this paper. Unfortunately, the paper format of Physics Reports does not allow for an index with references to the page numbers. We therefore provide an index to section numbers.

References

[1] M. Abel, A. Celani, D. Vergni, A. Vulpiani, Front propagation in laminar flows, Phys. Rev. E 64 (2001) 046307.
[2] M. Abel, M. Cencini, D. Vergni, A. Vulpiani, Front speed enhancement in cellular flows, Chaos 12 (2002) 481.
[3] G. Abramson, V.M. Kenkre, T.L. Yates, R.R. Parmenter, Traveling waves of infection in the Hantavirus epidemics, Bull. Math. Biol. 65 (2003) 519.
[4] G. Ahlers, D.S. Cannell, Vortex front propagation in rotating Couette–Taylor flow, Phys. Rev. Lett. 50 (1983) 1583.
[5] P. Albarède, M. Provansal, Quasi-periodic cylinder wakes and the Ginzburg–Landau model, J. Fluid. Mech. 291 (1995) 191.
[6] S.M. Allen, J.W. Cahn, A microscopic theory for antiphase boundary motion and its application to antiphase domain coarsening, Acta Metall. 27 (1979) 1085.
[7] M.A. Anisimov, V.P. Voronov, E.E. Gorodetskii, V.E. Prodneks, F.F. Kholmodorov, Observation of the Halperin–Lubensky–Ma effect in a liquid crystal, Pis'ma Zh. Exp. Teor. Fiz. 45 (1987) 336 [JETP Lett. 45 (1987) 425].
[8] M.A. Anisimov, P.E. Cladis, E.E. Gorodetskii, D.A. Huse, V.E. Podneks, V.G. Taratuta, W. van Saarloos, V.P. Voronov, Experimental test of fluctuation induced first order transition: the Nematic–Smectic a transition, Phys. Rev. A 41 (1990) 6749.
[9] I.S. Aranson, L. Kramer, The world of the complex Ginzburg–Landau equation, Rev. Mod. Phys. 74 (2002) 99.
[10] J. Armero, J.M. Sancho, J. Casademunt, A.M. Lacasta, L. Ramirez-Piscina, F. Sagues, External fluctuations in front propagation, Phys. Rev. Lett. 76 (1996) 3045.
[11] J. Armero, J. Casademunt, L. Ramirez-Piscina, J.M. Sancho, Ballistic and diffusive corrections to front propagation in the presence of multiplicative noise, Phys. Rev. E 58 (1998) 5494.
[12] L. Arnold, Stochastic Differential Equations: Theory and Applications, Wiley, New York, 1974.
[13] V.I. Arnold, Ordinary Differential Equations, MIT Press, Cambridge, 1978.
[14] V.I. Arnold, Geometrical Methods in the Theory of Ordinary Differential Equations, Springer, New York, 1983.
[15] D.G. Aronson, H.F. Weinberger, Nonlinear diffusion in population genetics, combustion, and nerve propagation, in: J.A. Goldstein (Ed.), Partial Differential Equations and Related Topics, Springer, Heidelberg, 1975.
[16] D.G. Aronson, H.F. Weinberger, Multidimensional nonlinear diffusion arising in population dynamics, Adv. Math. 30 (1978) 33.
[17] D.G. Aronson, The porous medium equation, in: A. Fasano, M. Primicario (Eds.), Nonlinear Diffusion Problems, Springer, Berlin, 1986.
[18] M. Arrayás, U. Ebert, W. Hundsdorfer, Spontaneous branching of anode-directed streamers between planar electrodes, Phys. Rev. Lett. 88 (2002) 174502.
[19] K.L. Babcock, G. Ahlers, D.S. Cannell, Noise-sustained structure in Taylor–Couettee flow with through flow, Phys. Rev. Lett. 67 (1991) 3388.
[20] K.L. Babcock, G. Ahlers, D.S. Cannell, Stability and noise in Taylor–Couette with through-flow, Physica D 61 (1992) 40.
[21] R.C. Ball, R.L.H. Essery, Spinodal decomposition and pattern formation near surfaces, J. Phys.: Condens. Matter 2 (1990) 10303.
[22] A.-L. Barabási, H.E. Stanley, Fractal Concepts in Surface Growth, Cambridge University Press, Cambridge, 1995.
[23] M.N. Barber, A. Barbieri, J.S. Langer, Dynamics of dendritic sidebranching in the two-dimensional symmetric model of solidification, Phys. Rev. A 36 (1987) 3340.
[24] G.I. Barenblatt, Similarity, Self-Similarity and Intermediate Asymptotics, Consultants Bureau, New York, 1979.
[25] G.I. Barenblatt, Scaling, Self-Similarity and Intermediate Asymptotics, Cambridge University Press, Cambridge, 1996.
[26] R. Bar-Ziv, E. Moses, Instability and pearling states produced in tubular membranes by competition of curvature and tension, Phys. Rev. Lett. 73 (1994) 1392.
[27] R. Bar-Ziv, T. Tlusty, E. Moses, Critical dynamics in the pearling instability of membranes, Phys. Rev. Lett. 79 (1997) 1158.
[28] A.P. Bassom, K.M. Kuanyan, A.M. Soward, A nonlinear dynamo wave riding on a spatially varying background, Proc. R. Soc. London A 455 (1999) 1443.

[29] P.W. Bates, P.C. Fife, R.A. Gardner, C.K.R.T. Jones, Phase field models for hypercooled solidification, Physica D 104 (1997) 1.
[30] M. Ben Amar, Plumes in Hele–Shaw cells, Phys. Fluids A 4 (1992) 2641.
[31] D. ben-Avraham, Fisher waves in the diffusion-limited coalescence process A+A $\rightleftharpoons$ A, Phys. Lett. A 247 (1998) 53.
[32] C.M. Bender, S.A. Orszag, Advanced Mathematical Methods for Scientists and Engineers, McGraw-Hill, New York, 1978.
[33] R.D. Benguria, M.C. Depassier, Validity of the linear speed selection mechanism for fronts of the nonlinear diffusion equation, Phys. Rev. Lett. 73 (1994) 2272.
[34] R.D. Benguria, M.C. Depassier, Exact fronts for the nonlinear diffusion equation with quintic nonlinearities, Phys. Rev. E 50 (1994) 3701.
[35] R.D. Benguria, M.C. Depassier, Speed of fronts of the reaction diffusion equation, Phys. Rev. Lett. 77 (1996) 1171.
[36] R.D. Benguria, M.C. Depassier, Variational characterization of the speed of propagation of fronts for the nonlinear diffusion equation, Commun. Math. Phys. 175 (1996) 221.
[37] R.D. Benguria, M.C. Depassier, Speed of fronts of generalized reaction–diffusion equations, Phys. Rev. E 57 (1998) 6493.
[38] E. Ben-Jacob, H.R. Brand, G. Dee, L. Kramer, J.S. Langer, Pattern propagation in non-linear dissipative systems, Physica D 14 (1985) 348.
[39] E. Ben-Jacob, From snowflake formation to growth of bacterial colonies. 1. Diffusive patterning in azoic systems, Contemp. Phys. 34 (1993) 247.
[40] E. Ben-Jacob, From snowflake formation to growth of bacterial colonies. 2. Cooperative formation of complex colonial patterns, Contemp. Phys. 38 (1997) 205.
[41] E. Ben-Jacob, I. Cohen, H. Levine, Cooperative self-organization of microorganisms, Adv. Phys. 49 (2000) 395.
[42] P. Bennema, G.H. Gilmer, in: P. Hartman (Ed.), Crystal Growth: An Introduction, North-Holland, Amsterdam, 1973.
[43] D. Bensimon, B. Shraiman, L.P. Kadanoff, in: F. Family, D.P. Landau (Eds.), Kinetics of Aggregation and Gelation, Elsevier, Amsterdam, 1984.
[44] D. Bensimon, L.P. Kadanoff, S. Liang, B.I. Shraiman, C. Tang, Viscous flow in two dimensions, Rev. Mod. Phys. 58 (1986) 977.
[45] D. Bensimon, P. Pelcé, B.I. Shraiman, Dynamics of curved fronts and pattern selection, J. Phys. (France) 48 (1987) 2081.
[46] D. Bensimon, B.I. Shraiman, V. Croquette, Nonadiabatic effects in convection, Phys. Rev. A 38 (1988) 5461.
[47] H. Berestycki, Some nonlinear PDE's in the theory of flame propagation, preprint.
[48] H. Berestycki, F. Hamel, Front propagation in periodic excitable media, Commun. Pure Appl. Math. 55 (2002) 949.
[49] A.N. Bers, Space–time evolution of plasma instabilities—absolute and convective, in: M.N. Rosenbluth, R.Z. Sagdeev (Eds.), Handbook of Plasma Physics, North-Holland, Amsterdam, 1983.
[50] G. Blatter, M.V. Feigel'man, V.B. Geshkenbein, A.I. Larkin, V.M. Vinokur, Vortics in high-temperature superconductors, Rev. Mod. Phys. 66 (1994) 1125.
[51] E. Bodenschatz, D.S. Cannell, R. Ecke, Y. Hu, K. Lerman, G. Ahlers, Experiments on three systems with nonvariational aspects, Physica D 61 (1992) 77.
[52] T. Bohr, G. Grinstein, C. Jayaprakash, M.H. Jensen, J. Krug, Turbulence, power laws, and Galilean invariance, Physica 59D (1992) 177.
[53] M.R. Booty, R. Haberman, A.A. Minzoni, The accommodation of traveling waves of Fisher's type to the dynamics of the leading tail, SIAM J. Appl. Math. 53 (1993) 1009.
[54] M. Bramson, Convergence of solutions of the Kolmogorov equation to traveling waves, Mem. Am. Math. Soc. 44 (1983) 285.
[55] M. Bramson, P. Calderoni, A. De Masi, P.A. Ferrari, J.L. Lebowitz, R.H. Schonmann, Microscopic selection principle for a diffusion–reaction equation, J. Stat. Phys. 45 (1986) 905.
[56] A.J. Bray, Theory of phase ordering kinetics, Adv. Phys. 43 (1994) 357.
[57] E.A. Brener, V.I. Mel'nikov, Pattern selection in two-dimensional dendritic growth, Adv. Phys. 40 (1991) 53.

[58] E. Brener, H. Levine, Y. Tu, Mean-field theory for diffusion-limited aggregation in low dimensions, Phys. Rev. Lett. 66 (1991) 1978.
[59] H. Breuer, W. Huber, F. Petruccione, Fluctuation effects on wave propagation in a reaction–diffusion process, Physica D 73 (1994) 259.
[60] J. Bricmont, A. Kupiainen, Renormalization group and the Ginzburg–Landau equation, Commun. Math. Phys. 150 (1992) 193.
[61] J. Bricmont, A. Kupiainen, Stability of moving fronts in the Ginzburg–Landau equation, Commun. Math. Phys. 159 (1994) 287.
[62] R.J. Briggs, Electron-stream Interaction with Plasmas, MIT Press, Cambridge, 1964.
[63] N.F. Britton, Reaction–diffusion Equations and their Applications to Biology, Academic, New York, 1986.
[64] E. Brunet, B. Derrida, Shift of the velocity of a front due to a cutoff, Phys. Rev. E 56 (1997) 2597.
[65] E. Brunet, B. Derrida, Microscopic models of traveling wave equations, Comput. Phys. Commun. 122 (1999) 376.
[66] E. Brunet, B. Derrida, Effect of microscopic noise on front propagation, J. Stat. Phys. 103 (2001) 269.
[67] J.D. Buckmaster, G.S.S. Lundford, Theory of Laminar Flames, Cambridge University Press, Cambridge, 1982.
[68] P. Büchel, M. Lücke, D. Roth, R. Schmitz, Pattern selection in the absolutely unstable regime as a nonlinear eigenvalue problem: Taylor vortices in axial flow, Phys. Rev. E 53 (1996) 4764.
[69] P. Büchel, M. Lucke, Pattern selection as a nonlinear eigenvalue problem, in: J. Parisi, S.C. Müller, W. Zimmermann (Eds.), Nonlinear Physics of Complex Systems, Springer, Berlin, 1996.
[70] P. Büchel, M. Lücke, Localized perturbations in binary fluid convection with and without throughflow, Phys. Rev. E 63 (2000) 016307.
[71] G. Caginalp, P. Fife, Higher order phase field models and detailed anisotropy, Phys. Rev. B 34 (1986) 4940.
[72] J. Canosa, On a nonlinear diffusion equation describing population growth, IBM J. Res. Dev. 17 (1973) 307.
[73] B. Caroli, C. Caroli, B. Roulet, in: C. Godrèche (Ed.), Solids Far from Equilibrium, Cambridge University Press, Cambridge, 1992.
[74] D. Carpentier, P. Le Doussal, Disordered XY models and Coulomb gases: renormalization via traveling waves, Phys. Rev. Lett. 81 (1998) 2558.
[75] D. Carpentier, P. Le Doussal, Topolocal transitions and freezing in XY models and Coulomb gases with quenched disorder: renormalization via traveling waves, Nucl. Phys. B 588 [FS] (2000) 565.
[76] V. Castets, E. Dulos, J. Boissonade, P. De Kepper, Experimental evidence of a sustained standing turing-type nonequilibrium chemical pattern, Phys. Rev. Lett. 64 (1990) 2953.
[77] M. Cencini, A. Torcini, Linear and nonlinear information flow in spatially extended systems, Phys. Rev. E 63 (2001) 056201.
[78] S. Chandrasekhar, Hydrodynamics and Hydrodynamic Stability, Clarendon Press, Oxford, 1961.
[79] H.-C. Chang, E.A. Demekhin, D.I. Kopelevich, Stability of solitary pulse against wave packet disturbances in an active medium, Phys. Rev. Lett. 75 (1995) 1747.
[80] S.J. Chapman, Subcritical transition in channel flow, J. Fluid Mech. 451 (2002) 35.
[81] H. Chaté, Spatiotemporal intermittency regimes of the one-dimensional complex Ginzburg–Landau equation, Nonlinearity 7 (1994) 185.
[82] J. Cisternas, M.C. Depassier, Counterexample to a conjecture of Goriely for the speed of fronts of the reaction–diffusion equation, Phys. Rev. E 55 (1997) 3701.
[83] L.-Y. Chen, N. Goldenfeld, Y. Oono, G. Paquette, Selection, stability and renormalization, Physica A 204 (1994) 111.
[84] J.M. Chomaz, P. Huerre, L.G. Redekopp, Bifurcations to local and global modes in spatially developing flows, Phys. Rev. Lett. 60 (1988) 25.
[85] J.M. Chomaz, Absolute and convective instabilities in nonlinear systems, Phys. Rev. Lett. 69 (1992) 1931.
[86] J.-M. Chomaz, A. Couairon, Propagating pattern selection and causality reconsidered, Phys. Rev. Lett. 84 (2000) 1910.
[87] P.E. Cladis, W. van Saarloos, D.A. Huse, J.S. Patel, J.W. Goodby, P.L. Finn, A dynamical test of phase transition order, Phys. Rev. Lett. 62 (1989) 1764.
[88] P. Cladis, W. van Saarloos, Some non-linear problems in anisotropic systems, in: L. Lam (Ed.), Solitons in Liquid Crystals, Springer, Berlin, 1991.

[89] P.A. Clarkson, E.A. Mansfield, Symmetry reductions and exact-solutions of a class of nonlinear heat-equations, Physica D 70 (1993) 250.
[90] P. Clavin, Diffuse interfaces, in: J.E. Wesfreid, H.R. Brand, P. Manneville, G. Albinet, N. Boccara (Eds.), Propagation in Systems Far from Equilibrium, Springer, New York, 1988.
[91] P. Collet, J.P. Eckmann, The stability of modulated fronts, Helv. Phys. Acta 60 (1987) 969.
[92] P. Collet, J.P. Eckmann, Instabilities and Fronts in Extended Systems, Princeton University Press, Princeton, 1990.
[93] P. Collet, J.P. Eckmann, A rigorous upper bound on the propagation speed for the Swift–Hohenberg and related equations, J. Stat. Phys. 108 (2002) 1107.
[94] C.V. Conrado, T. Bohr, Singular growth shapes in turbulent field theories, Phys. Rev. Lett. 72 (1994) 3522.
[95] R. Conte, M. Musette, Linearity inside nonlinearity—exact-solutions to the complex Ginzburg Landau equation, Physica D 69 (1993) 1.
[96] R. Conte, Exact solutions of nonlinear partial differential equations by singularity analysis, in: A. Greco (Ed.), Direct and Inverse Methods in Nonlinear Evolution Equations, Springer, Berlin, 2002.
[97] D. Coombs, G. Huber, J.O. Kessler, R.E. Goldstein, Periodic chirality transformations propagating on bacterial flagella, Phys. Rev. Lett. 89 (2002) 118102.
[98] A. Couairon, J.M. Chomaz, Pattern selection in the presence of cross flow, Phys. Rev. Lett. 79 (1997) 2666.
[99] A. Couairon, J.M. Chomaz, Absolute and convective instabilities, front velocities and global mode in nonlinear systems, Physica D 108 (1997) 236.
[100] A. Couairon, J.M. Chomaz, Primary and secondary nonlinear global instability, Physica D 132 (1999) 428.
[101] A. Couairon, J.M. Chomaz, Pushed global modes in weakly inhomogeneous subcritical flows, Physica D 158 (2001) 129.
[102] P. Coullet, T. Frisch, F. Plaza, Sources and sinks of wave patterns, Physica D 62 (1993) 75.
[103] P. Coullet, L. Kramer, Retracting fronts induce spatio-temporal intermittency, Chaos (2003), to appear [nlin.PS/0202054].
[104] M.C. Cross, Structure of nonlinear traveling-wave states in finite geometries, Phys. Rev. A 38 (1988) 3593.
[105] M.C. Cross, P.C. Hohenberg, Pattern formation outside of equilibrium, Rev. Mod. Phys. 65 (1992) 851.
[106] Z. Csahok, C. Misbah, On the invasion of an unstable structureless state by a stable hexagonal pattern, Europhys. Lett. 47 (1999) 331.
[107] A. Czirók, Bacterial colonies, in: T. Vicsek (Ed.), Fluctuations and Scaling in Biology, Oxford University Press, Oxford, 2001.
[108] O. Dauchot, F. Daviaud, Finite amplitude perturbation in plane Couette flow, Europhys. Lett. 28 (1994) 225.
[109] F. Daviaud, J. Hegseth, P. Bergé, Subcritical transition to turbulence in plane Couette flow, Phys. Rev. Lett. 69 (1992) 2511.
[110] P.W. Davies, P. Blanchedeau, E. Dulos, P. De Kepper, Dividing blobs, chemical flowers, and patterned islands in reaction–diffusion systems, J. Phys. Chem. A 102 (1998) 8236.
[111] G. Dee and J.S. Langer, Propagating pattern selection, Phys. Rev. Lett. 50 (1983) 383.
[112] G. Dee, Propagation into an unstable state, J. Stat. Phys. 39 (1985) 705.
[113] G. Dee, W. van Saarloos, Bistable systems with propagating fronts leading to pattern formation, Phys. Rev. Lett. 60 (1988) 2641.
[114] P.G. de Gennes, J. Prost, The Physics of Liquid Crystals, Clarendon Press, Oxford, 1993.
[115] R.J. Deissler, Turbulent bursts, spots and slugs in a generalized Ginzburg–Landau equation, Phys. Lett. A 120 (1987) 334.
[116] R.J. Deissler, The convective nature of instability in plane Poiseuille flow, Phys. Fluids 30 (1987) 2303.
[117] R.J. Deissler, Spatially growing waves, intermittency, and convective chaos in an open-flow system, Physica D 25 (1987) 233.
[118] R.J. Deissler, K. Kaneko, Velocity-dependent Lyapunov exponents as a measure of chaos for open-flow systems, Phys. Lett. 119 (1987) 397.
[119] R.J. Deissler, External noise and the origin of dynamics of structure in convectively unstable systems, J. Stat. Phys. 54 (1989) 1459.
[120] P. De Kepper, J.J. Perraud, B. Rudovic, E. Dulos, Experimental study of stationary turing patterns and their interaction with traveling waves in a chemical system, Int. J. Bifurc. Chaos 4 (1994) 1215.

[121] A. De Masi, P.A. Ferrari, J.L. Lebowitz, Reaction diffusion equations for interacting particle systems, J. Stat. Phys. 44 (1986) 589.
[122] B. Derrida, H. Spohn, Polymers on disordered trees, spin glasses, and traveling waves, J. Stat. Phys. 51 (1988) 817.
[123] S.J. Di Bartolo, A.T. Dorsey, Velocity selection for propagating fronts in superconductors, Phys. Rev. Lett. 77 (1996) 4442.
[124] O. Diekmann, Run for your life: a note on the asymptotic speed of propagation of an epidemic, J. Differential Equations 33 (1979) 58.
[125] R.C. Di Prima, H.L. Swinney, Instabilities and transition in flow between concentric rotating cylinders, in: H.L. Swinney, J.P. Gollub (Eds.), Hydrodynamic Instabilities and the Transition to Turbulence, Springer, Berlin, 1981.
[126] A. Doelman, B. Sandstede, A. Scheel, G. Schneider, Propagation of hexagonal patterns near onset, Eur. J. Appl. Math. 14 (2003) 85.
[127] C.R. Doering, M.A. Burschka, W. Horsthemke, Fluctuations and correlations in a diffusion–reaction system—exact hydrodynamics, J. Stat. Phys. 65 (1991) 953.
[128] C.R. Doering, Microscopic spatial correlations induced by external noise in a reaction–diffusion system, Physica A 188 (1992) 386.
[129] C.R. Doering, C. Mueller and P. Smereka, Noisy wavefront propagation in the Fisher–Kolmogorov–Petrovsky–Piscounov equation, in: Proceedings of the UPoN 2002 Conference, American Institute of Physics Press, New York, to appear.
[130] C.R. Doering, C. Mueller, P. Smereka, Interacting particles, the stochastic Fisher–Kolmogorov–Petrovsky–Piscounov equation, and duality, Physica A 325 (2003) 243.
[131] A.J. Doelman, T.J. Kaper, P. Zegeling, Pattern formation in the one-dimensional Gray–Scott model, Nonlinearity 10 (1997) 523.
[132] A.T. Dorsey, Dynamics of interfaces in superconductors, Ann. Phys. 233 (1994) 248.
[133] A. Dougherty, P.D. Kaplan, J.P. Gollub, Development of side branching in dendritic crystal growth, Phys. Rev. Lett. 58 (1987) 1652.
[134] A. Dougherty, J.P. Gollub, Steady-state dendritic growth of NH_4Br from solution, Phys. Rev. A 38 (1988) 3043.
[135] P.G. Drazin, W.H. Reid, Hydrodynamic Stability, Cambridge University Press, Cambridge, 1981.
[136] M. Dubois, F. Daviaud, O. Ronsin, P. Bergé, Traveling waves in pure fluids locally heated along wires, Physica D 61 (1992) 140.
[137] C.A. Durán, P.L. Gammel, R.E. Miller, D.J. Bishop, Observation of magnetic-field penetration via dendritic growth in superconducting niobium films, Phys. Rev. B 52 (1995) 75.
[138] R. Durrett, Maxima of branching random walks versus independent random walks, Stochastic Process. Appl. 9 (1979) 117.
[139] R. Durrett, An infinite particle system with additive interactions, Adv. Appl. Probab. 11 (1979) 353.
[140] P.M. Eagles, Benard convection problem with a perturbed lower wall, Proc. R. Soc. London A 371 (1980) 569.
[141] U. Ebert, W. van Saarloos, C. Caroli, Streamer propagation as a pattern formation problem, Phys. Rev. Lett. 77 (1996) 4178.
[142] U. Ebert, W. van Saarloos, C. Caroli, Propagation and structure of planar streamer fronts, Phys. Rev. E 55 (1997) 1530.
[143] U. Ebert, W. van Saarloos, Universal algebraic relaxation of fronts propagating into unstable state and implications for moving boundary approximations, Phys. Rev. Lett. 80 (1998) 1650.
[144] U. Ebert W. van Saarloos, Front propagation into unstable states: universal algebraic convergence towards uniformly pulled fronts, Physica D 146 (2000) 1.
[145] U. Ebert, W. van Saarloos, Breakdown of the standard perturbation theory and moving boundary approximation for "pulled" fronts, Phys. Rep. 337 (2000) 139.
[146] U. Ebert, W. van Saarloos, L.A. Peletier, Universal algebraic convergence in time of pulled fronts: the common mechanism for difference-differential and partial differential equations, Eur. J. Appl. Math. 13 (2002) 53.
[147] U. Ebert, W. Spruijt and W. van Saarloos, Physica D, submitted.
[148] R.E. Ecke, F. Zhong, E. Knobloch, Hopf bifurcation with broken reflection symmetry in rotating Rayleigh–Bénard convection, Europhys. Lett. 19 (1992) 177.

[149] J.-P. Eckmann, C.E. Wayne, Propagating fronts and the center manifold theorem, Commun. Math. Phys. 161 (1994) 323.
[150] F.J. Elmer, J. Burns, H. Suhl, Front propagation into an unstable ferromagnetic state, Europhys. Lett. 22 (1993) 399.
[151] F.J. Elmer, J.-P. Eckmann, G. Hartsleben, Dual fronts propagating into an unstable state, Nonlinearity 7 (1994) 1261.
[152] I.R. Epstein, J.A. Pojman, An Introduction to Nonlinear Chemical Dynamics, Oxford University Press, Oxford, 1998.
[153] G. Eyink, J. Xin, Statistical analysis of a semilinear hyperbolic system advected by a time random velocity field, Nonlinearity 15 (2002) 551.
[154] G. Fáth, Propagation failure of traveling waves in a discrete bistable medium, Physica D 116 (1998) 176.
[155] S. Fauve, Pattern forming instabilities, in: C. Godrèche, P. Manneville (Eds.), Hydrodynamics and Nonlinear Instabilities, Cambridge University Press, Cambridge, 1998.
[156] S. Fedotov, Wave front for a reaction–diffusion system and relativistic Hamilton–Jacobi dynamics, Phys. Rev. E 59 (1999) 5040.
[157] S. Fedotov, Front propagation into an unstable state of reaction-transport systems, Phys. Rev. Lett. 86 (2001) 926.
[158] M. Fermigier, P. Jennfer, L. Limat, J.E. Wesfreid, Fluid–fluid interaction instabilities induced by gravity, in: Proceedings VIIIth European Symposium on Materials and Fluid Sciences in Microgravity, ESA, 1992.
[159] M. Fermigier, L. Limat, J.E. Wesfreid, P. Boudinet, C. Quillet, Two-dimensional patterns in Rayleigh–Taylor instability of a thin layer, J. Fluid Mech. 236 (1992) 349.
[160] P.C. Fife, Dynamics of Internal Layers and Diffusive Interfaces, SIAM, Philadelphia, 1988.
[161] J. Fineberg, V. Steinberg, Vortex front propagation in Rayleigh–Bénard convection, Phys. Rev. Lett. 58 (1987) 1332.
[162] J. Fineberg, V. Steinberg, P. Kolodner, Weakly nonlinear states as propagating fronts in convecting binary mixtures, Phys. Rev. A 41 (1990) 5743.
[163] R.A. Fisher, The wave of advance of advantageous genes, Ann. Eugenics 7 (1937) 355.
[164] A.S. Fokas, A new transform method for evolution partial differential equations, IMA J. Appl. Math. 67 (2002) 559.
[165] J. Fort, V. Méndez, Wavefronts in time-delayed reaction–diffusion systems. Theory and comparison to experiment, Rep. Prog. Phys. 65 (2002) 895.
[166] J. Fort, V. Méndez, Time-delayed spread of virusses in growing plaques, Phys. Rev. Lett. 89 (2002) 178101.
[167] H. Frahm, S. Ullah, A.T. Dorsey, Flux dynamics and the growth of the superconducting phase, Phys. Lett. 66 (1991) 3067.
[168] F.C. Frank, in: R. Doremus, B. Roberts, D. Turnbull (Eds.), Growth and Perfection of Crystals, Wiley, New York, 1958.
[169] M.R. Freeman, Picosecond studies of nonequilibrium flux dynamics in a superconductor, Phys. Rev. Lett. 69 (1992) 1691.
[170] M.I. Freidlin, Wave front propagation for FKPP-type equations in: J.B. Keller, D.W. McLaughlin, G.C. Papanicalaou (Eds.), Surveys in Applied Mathematics, Vol. 2, Plenum, New York, 1995.
[171] M.I. Freidlin, T.-Y. Lee, Wave front propagation and large deviations for diffusion–transmutation process, Probab. Theory Relat. Fields 106 (1996) 39.
[172] M. Freidlin, Reaction–diffusion in incompressible fluid: asymptotic problems, J. Differential Equations 179 (2002) 44.
[173] M. Fuentes, M.N. Kuperman, P. De Kepper, Propagation and interaction of cellular fronts in a closed system, J. Phys. Chem. A 105 (2001) 6769.
[174] Th. Gallay, G. Raugel, Stability of propagating fronts in damped hyperbolic equations, in: W. Jäger, J. Neăs, O. John, K. Najzar, J. Satá (Eds.), Partial Differential Equations: Theory and Numerical Solutions, Chapman & Hall, London, 2000.
[175] Th. Gallay, G. Raugel, Scaling variables and stability of hyperbolic fronts, SIAM J. Math. Anal. 32 (2000) 1.
[176] García-Ojalvo, J.M. Sancho, Noise in Spatially Extended Systems, Springer, Berlin, 1999.
[177] C.W. Gardiner, Handbook of Stochastic Methods for Physics, Chemistry and the Natural Sciences, Springer, Berlin, 1985.

[178] N. Garnier, A. Chiffaudel, Nonlinear transition to a global mode for traveling-wave instability in a finite box, Phys. Rev. Lett. 86 (2001) 75.
[179] N. Garnier, A. Chiffaudel, F. Daviaud, Convective and absolute Eckhaus instability leading to modulated waves in a finite box, Phys. Rev. Lett. 88 (2002) 134501.
[180] I.M. Gel'fand, Some problems in the theory of quasilinear equations, Usp. Mat. Nauk 14 No. 2 (86) (1959) 87 [Am. Math. Soc. Transl. Ser. 2, 29 (1963) 295].
[181] G. Giacomelli, A. Politi, Spatiotemporal chaos and localization, Europhys. Lett. 15 (1991) 387.
[182] G. Giacomelli, R. Hegger, A. Politi, M. Vassalli, Convective Lyapunov exponents and propagation of correlations, Phys. Rev. Lett. 85 (2000) 3616.
[183] I. Golding, Y. Kozlovsky, I. Cohen, E. Ben-Jacob, Studies of bacterial branching growth using reaction–diffusion models for colonial development, Phys. Rev. E 59 (1999) 7025.
[184] N. Goldenfeld, Lectures on Phase Transitions and the Renormalization Group, Addison-Wesley, Reading, MA, 1992.
[185] R. Goldstein, P. Nelson, T. Powers, U. Seifert, Front propagation in the pearling instability of tubular vesicles, J. Phys. II France 6 (1996) 767.
[186] P. Gondret, P. Ern, L. Meignin, M. Rabaud, Experimental evidence of a nonlinear transition from convective to absolute instability, Phys. Rev. Lett. 82 (1999) 1442.
[187] R. González-Cinca, L. Rámirez-Piscina, J. Casademunt, A. Hernández-Machado, L. Kramer, T. Tóth-Katona, T. Börzsönyi, Á. Buka, Phase-field simulations and experiments of faceted growth in liquid crystals, Physica D 99 (1996) 359.
[188] A. Goriely, Simple solution to the nonlinear front problem, Phys. Rev. Lett. 75 (1995) 2047.
[189] H.S. Greenside, M.C. Cross, Pattern Formation and Dynamics of Nonequilibrium Systems, Cambridge University Press, Cambridge, 2003.
[190] S. Grossmann, The onset of shear flow turbulence, Rev. Mod. Phys. 72 (2000) 603.
[191] J. Guckenheimer, P. Holmes, Nonlinear Oscillations, Dynamical Systems, and Bifurcations of Vector Fields, Springer, New York, 1983.
[192] J.D. Gunton, M. San Miguel, P.S. Sahni, in: C. Domb, J.L. Lebowitz (Eds.), Phase Transitions and Critical Phenomena, Vol. 8, Academic, New York, 1983.
[193] V. Hakim, Asymptotic techniques in nonlinear problems: some illustrative examples, in: C. Godrèche, P. Manneville (Eds.), Hydrodynamics and Nonlinear Instabilities, Cambridge University Press, Cambridge, 1998.
[194] B.I. Halperin, T.C. Lubensky, S.K. Ma, First-order transitions in superconductors and smectic-A liquid crystals, Phys. Rev. Lett. 32 (1974) 292.
[195] T. Halpin-Healy, Y.C. Zhang, Kinetic roughening, stochastic growth, directed polymers and all that, Phys. Rep. 254 (1995) 215.
[196] J.L. Hansen, T. Bohr, Comment on "Stability of solitary pulse against wave packet disturbances in an active medium", Phys. Rev. Lett. 77 (1996) 5441.
[197] D.S. Henningson, Wave growth and spreading of a turbulent spot in plane Poiseuille flow, Phys. Fluids A 1 (1989) 1876.
[198] W. Hereman, M. Takaoka, Solitary wave solutions of nonlinear evolution and wave-equations using a direct method and Macsyma, J. Phys. A. 23 (1990) 4805.
[199] P.C. Hohenberg, B.I. Halperin, Theory of dynamical critical phenomena, Rev. Mod. Phys. 49 (1977) 435.
[200] D. Horváth, V. Petrov, S.K. Scott, K. Showalter, Instabilities in propagating reaction–diffusion fronts, J. Chem. Phys. 98 (1993) 6332.
[201] D. Horváth, A. Tóth, Diffusion-driven front instabilities in the chlorite-tetrathionate reaction, J. Chem. Phys. 108 (1998) 1447.
[202] R.P. Huebener, Magnetic Flux Structures in Superconductors, Springer, Berlin, 2001.
[203] P. Huerre, P.A. Monkewitz, Local and global instabilities in spatially developing flows, Annu. Rev. Fluid Mech. 22 (1990) 473.
[204] P. Huerre, in: J.E. Wesfreid, H.R. Brand, P. Manneville, G. Albinet, N. Boccara (Eds.), Propagation in Systems Far from Equilibrium, Springer, New York, 1988.
[205] P. Huerre, M. Rossi, Hydrodynamic instabilities in open flows, in: C. Godrèche, P. Manneville (Eds.), Hydrodynamics and Nonlinear Instabilities, Cambridge University Press, Cambridge, 1998.

[206] R.E. Hunt, D.G. Crighton, Instability of flows in spatially developing media, Proc. R. Soc. London A 435 (1991) 109.
[207] N. Israeli, D. Kandel, M.F. Schatz, A. Zangwill, Convective instability of strained layers step flow, Surf. Sci. 494 (2001) L735.
[208] R.A.L. Jones, L.J. Norton, E.J. Kramer, F.S. Bates, P. Wiltzius, Surface-directed spinodal decomposition, Phys. Rev. Lett. 66 (1991) 1326.
[209] G. Joulin, P. Vidal, An introduction to the instability of flames, shocks and detonations, in: C. Godrèche, P. Manneville (Eds.), Hydrodynamics and Nonlinear Instabilities, Cambridge University Press, Cambridge, 1998.
[210] Ch. Jung, M. Lücke, P. Büchel, Influence of through-flow on linear pattern formation properties in binary mixture convection, Phys. Rev. E 54 (1996) 1510.
[211] M. Kaern, M. Menziger, Pulsating wave propagation in reactive flows: flow distributed oscillations, Phys. Rev. E 61 (2000) 3334.
[212] P. Kaliappan, An exact solution for traveling waves of $u_t = Du_{xx} + u - u^k$, Physica D 11 (1984) 368.
[213] K. Kaneko, Lyapunov analysis and information flow in coupled map lattices, Physica 23D (1986) 436.
[214] D. Kandel, J.D. Weeks, Step bunching as a chaotic pattern formation process, Phys. Rev. Lett. 69 (1992) 3758.
[215] D. Kandel, J.D. Weeks, Simultaneous bunching and debunching of surface steps: theory and relation to experiments, Phys. Rev. Lett. 74 (1995) 3632.
[216] T. Kapitula, On the stability of traveling waves in weighted L^∞ spaces, J. Differential Equations 112 (1994) 179.
[217] E. Kaplan, V. Steinberg, Phase slippage, nonadiabatic effect, and dynamics of source of traveling waves, Phys. Rev. Lett. 71 (1993) 3291.
[218] M. Kardar, G. Parisi, Y.C. Zhang, Dynamics scaling of growing interfaces, Phys. Rev. Lett. 56 (1986) 889.
[219] A. Karma, W.-J. Rappel, Quantitative phase field modeling of dendritic growth in two and three dimensions, Phys. Rev. E 57 (1998) 4323.
[220] K. Kassner, Pattern Formation in Diffusion-Limited Crystal Growth, World Scientific, Singapore, 1996.
[221] K. Kassner, C. Misbah, J. Müller, J. Kappey, P. Kohlert, Phase-field modeling of stress-induced instabilities, Phys. Rev. E 63 (2001) 036117.
[222] J. Keener, J. Sneyd, A Mathematical Introduction to Medical Physiology, Springer, New York, 1998.
[223] A.R. Kerstein, Computational study of propagating fronts in a lattice gas model, J. Stat. Phys. 45 (1986) 921.
[224] A.R. Kerstein, A 2-particle representation of front propagation in diffusion–reaction systems, J. Stat. Phys. 53 (1988) 703.
[225] A.R. Kerstein, W.T. Ashurst, F.A. Williams, Field equation for interface propagation in an unsteady homogeneous flow field, Phys. Rev. A 37 (1998) 2728.
[226] D.A. Kessler, J. Koplik, H. Levine, Pattern selection in fingered growth phenomena, Adv. Phys. 37 (1988) 255.
[227] D.A. Kessler, Z. Ner, L.M. Sander, Front propagation: precursors, cutoffs, and structural stability, Phys. Rev. E 58 (1998) 107.
[228] D.A. Kessler, H. Levine, Fluctuation-induced diffusive instabilities, Nature 394 (1999) 556.
[229] J. Kinzel, J.B. Keller, Traveling wave solutions of a nerve conduction equation, Biophys. J. 13 (1973) 1313.
[230] K. Kirchgässner, On the nonlinear dynamics of traveling fronts, J. Differential Equations 96 (1992) 256.
[231] S. Kitsunezaki, Interface dynamics for bacterial colony formation, J. Phys. Soc. Japan 66 (1997) 1544.
[232] R. Kobayashi, Modeling and numerical simulations of dendritic crystal growth, Physica 63D (1993) 410.
[233] J. Kockelkoren, C. Storm, W. van Saarloos, Evidence for slow velocity relaxation in front propagation in Rayleigh–Bénard convection, Physica D 174 (2003) 168.
[234] A. Kolmogoroff, I. Petrovsky, N. Piscounoff, Study of the diffusion equation with growth of the quantity of matter and its application to a biology problem, Bulletin de l'université d'état à Moscou, Ser. int., Section A, Vol. 1 (1937); translated and reprinted in [338].
[235] P. Kolodner, Stable, unstable and defected confined states of traveling wave convection, Phys. Rev. E 50 (1994) 2731.
[236] Y. Kozlovsky, I. Cohen, I. Golding, E. Ben-Jacob, Lubricating bacteria model for branching growth of bacterial colonies, Phys. Rev. E 59 (1999) 7025.
[237] L. Kramer, E. Ben-Jacob, H. Brand, M.C. Cross, Wavelength selection in systems far from equilibrium, Phys. Rev. Lett. 49 (1982) 1891.

[238] J. Krug, P. Meakin, Columnar growth in oblique incidence ballistic deposition: faceting, noise reduction, and mean-field theory, Phys. Rev. A 43 (1991) 900.
[239] J. Krug, Origin of scale invariance in growth processes, Adv. Phys. 46 (1997) 139.
[240] E.Y. Kuo, M.C. Cross, Traveling-wave wall states in rotating Rayleigh–Bénard convection, Phys. Rev. E 47 (1993) R2245.
[241] O. Kupervasser, Z. Olami, I. Procaccia, Stability analysis of flame fronts: dynamical systems approach in the complex plane (nlin.PS/0302020).
[242] G. Kuppers, D. Lorz, Transition from laminar convection to thermal turbulence in a rotating fluid layer, J. Fluid Mech. 35 (1969) 609.
[243] Y. Kuramoto, T. Tsuzuki, Persistent propagation of concentration waves in dissipative media far from thermal equilibrium, Prog. Theor. Phys. 55 (1976) 356.
[244] Y. Kuramoto, Chemical Oscillations, Waves, and Turbulence, Springer, Berlin, 1984.
[245] L.D. Landau, On the theory of slow combustion, Zh. Eksp. Teor. Fiz. 14 (1944) 240.
[246] L.D. Landau, E.M. Lifshitz, Electrodynamics of Continuous Media, in: Course of Theoretical Physics, Vol. 8, Pergamon, New York, 1975.
[247] J.S. Langer, Instabilities and pattern formation in crystal growth, Rev. Mod. Phys. 52 (1980) 1.
[248] J.S. Langer, H. Müller-Krumbhaar, Mode selection in a dendritelike nonlinear system, Phys. Rev. A 27 (1983) 499.
[249] J.S. Langer, in: G. Grinstein, G. Mazenko (Eds.), Directions in Condensed Matter Physics, World Scientific, Singapore, 1986.
[250] J.S. Langer, in: J. Souletie (Ed.), Chance and Matter, North-Holland, Amsterdam, 1987.
[251] J.S. Langer, in: C. Godreche (Ed.), Solids Far from equilibrium, Cambridge University Press, Cambridge, 1992.
[252] D.A. Larson, Transient bounds and time asymptotic behavior of solutions of nonlinear equations of Fisher type, SIAM J. Appl. Math. 34 (1978) 93.
[253] A.V. Latyshev, A.B. Krasilnikov, A.L. Aseev, UHV REM study of the anti-band structure on the vicinal Si(111) surface under heating by a direct electric current, Surf. Sci. 311 (1994) 395.
[254] I. Lengyel, S. Kádár, I.R. Epstein, Transient turing structures in a gradient-free closed system, Science 259 (1993) 493.
[255] J.A. Leach, D.J. Needham, The evolution of traveling waves in generalized Fisher equations via matched asymptotic expansions: algebraic corrections, Q. J. Mech. Appl. Math. 54 (2001) 157.
[256] J.A. Leach, D.J. Needham, A.L. Kay, The evolution of reaction–diffusion waves in a class of scalar reaction–diffusion equations: algebraic decay rates, Physica D 167 (2002) 153.
[257] S. Le Dizès, P. Huerre, J.M. Chomaz, P.A. Monkewitz, Linear global modes in spatially developing media, Phil. Trans. R. Soc. London A 454 (1996) 169.
[258] J. Lega, J.V. Moloney, A.C. Newell, Swift–Hohenberg equation for lasers, Phys. Rev. Lett. 73 (1994) 2978.
[259] A. Lemarchand, A. Lesne, A. Perera, M. Moreau, M. Mareschal, Chemical wave front in two dimensions, Phys. Rev. E. 48 (1993) 1568.
[260] A. Lemarchand, A. Lesne, M. Mareschal, Langevin approach to a chemical wave-front—selection of the propagation velocity in the presence of internal noise, Phys. Rev. E 51 (1995) 4457.
[261] T. Leweke, M. Provansal, Model for the transition in bluff body wakes, Phys. Rev. Lett. 72 (1994) 3174.
[262] T. Leweke, M. Provansal, G.D. Miller, C.H.K. Williamson, Cell formation in cylindrical wakes at low Reynolds numbers, Phys. Rev. Lett. 78 (1997) 1259.
[263] G. Li, Q. Ouyang, H.L. Swinney, Transitions in two-dimensional patterns in a ferrocyanide–iodate–sulfite reaction, J. Chem. Phys. 105 (1996) 10830.
[264] E.M. Lifshitz, L.P. Pitaevskii, Physical kinetics, Course of Theoretical Physics, Vol. 10, Pergamon, New York, 1981.
[265] L. Limat, P. Jenffer, B. Dagens, E. Touron, M. Fermigier, J.E. Wesfreid, Gravitational instabilities of thin liquid layers: dynamics of pattern selection, Physica D 61 (1992) 166.
[266] F. Liu, N. Goldenfeld, Dynamics of phase separation in block co-polymer melts, Phys. Rev. A 39 (1989) 4805.
[267] F. Liu, M. Mondello, N. Goldenfeld, Kinetics of the superconducting transition, Phys. Rev. Lett. 66 (1991) 3071.
[268] J.D. Logan, An Introduction to Nonlinear Partial Differential Equations, Wiley, New York, 1994.
[269] M. Lücke, M. Mihelcic, B. Kowalski, Propagation of Taylor vortex fronts into unstable circular Couette flow, Phys. Rev. Lett. 52 (1984) 625.

[270] M. Lücke, M. Mihelcic, B. Kowalski, Front propagation and pattern formation of Taylor vortices growing into unstable circular Couette flow, Phys. Rev. A 31 (1985) 399.
[271] M. Lücke, M. Mihelcic, B. Kowalski, Propagating convection fronts, Phys. Rev. A 35 (1987) 4001.
[272] M. Lücke, A. Szprynger, Noise sustained pattern growth: bulk versus boundary effects, Phys. Rev. E 55 (1997) 5509.
[273] V. L'vov, V.V. Lebedev, M. Paton, I. Procaccia, Proof of scale-invariant solutions in the Kardar–Parisi–Zhang and Kuramoto–Sivashinsky equations in 1+1 dimensions—analytical and numerical results, Nonlinearity 6 (1993) 25.
[274] J.E. Maclennan, N.A. Clark, T. Carlsson, in: L. Lam (Ed.), Solitons in liquid Crystals, Springer, Berlin, 1991.
[275] P.K. Maini, S. McElwain, D. Leavesley, Traveling Waves in a Wound Healing Assay, Appl. Math. Lett., 2002, submitted.
[276] P.K. Maini, S. McElwain, D. Leavesley, A traveling wave model to interpret a wound healing cell migration assay for human peritoneal mesothelial cells, unpublished.
[277] A. Malevanets, A. Careta, R. Kapral, Biscale chaos in propagating fronts, Phys. Rev. E 52 (1995) 4724.
[278] B. Malomed, Nonlinear waves in nonequilibrium systems of the oscillatory type, part I, Z. Phys. B 55 (1984) 241.
[279] B. Malomed, Nonlinear waves in nonequilibrium systems of the oscillatory type, part II, Z. Phys. B 55 (1984) 249.
[280] B.A. Malomed, A.A. Nepomnyashchy, Two-dimensional stability of convection rolls in the presence of a ramp, Europhys. Lett. 21 (1993) 195.
[281] R. Mancinelli, D. Vergni, A. Vulpiani, Superfast front propagation in reactive systems with anomalous diffusion, Europhys. Lett. 60 (2002) 532.
[282] P. Manneville, Dissipative Structures and Weak Turbulence, Academic Press, Boston, 1990.
[283] P. Manneville, O. Dauchot, Patterning and transition to turbulence in subcritical systems: the plane Couette flow, in: M. Rubi (Ed.), Coherent Structures in Classical Systems, Springer, Berlin, 2000.
[284] G. Marees, R.F. Mudde, H. van Beelen, On the motion of plugs of turbulence in the flow of helium II, Physica B 144 (1987) 292.
[285] M. Marchevsky, L.A. Gurevich, P.H. Kes, J. Aarts, Flux droplet formation in $NbSe_2$ single crystals observed by decoration, Phys. Rev. Lett. 75 (1995) 2400.
[286] C. Mathis, M. Provansal, L. Boyer, The Bénard–Von Karman instability: an experimental study near threshold, J. Phys. Lett. 45 (1984) L483.
[287] O. Martin, N.D. Goldenfeld, Origin of sidebranching in dendritic growth, Phys. Rev. A 35 (1987) 1382.
[288] M. Matsushita, in: J.A. Shapiro, M. Dworkin (Eds.), Bacteria as Multicellular Organisms, Oxford University Press, Oxford, 1997.
[289] G.F. Mazenko, O.T. Valls, P. Ruggiero, Front propagation into an unstable state in the presence of noise, Phys. Rev. B 40 (1989) 384.
[290] P.N. McGraw, M. Menziger, Towards a general theory of nonlinear flow-distributed oscillations, preprint nlin.PS/030372.
[291] H.P. McKean, Application of Brownian motion to the equation of Kolmogorov–Petrovskii–Pikunov, Commun. Pure Appl. Math. 28 (1975) 323.
[292] P. Meakin, Fractals, Scaling and Growth Far from Equilibrium, Cambridge University Press, Cambridge, 1998.
[293] E. Meron, Pattern formation in excitable media, Phys. Rep. 218 (1992) 1.
[294] A. Hagberg, E. Meron, Domain walls in nonequilibrium systems and the emergence of persistent patterns, Phys. Rev. E 48 (1993) 705.
[295] J.A.J. Metz, in: D. Mollison (Ed.), Epidemic Models, their Structure and Relation to Data, Cambridge University Press, Cambridge, 1995.
[296] J.A.J. Metz, D. Mollison, F. van den Bosch, The dynamics of invasion waves, in: U. Dieckmann, R. Law, J.A.J. Metz (Eds.), The Geometry of Ecological Interactions: Simplifying Spatial Complexity, Cambridge University Press, Cambridge, 2000.
[297] A.S. Mikhailov, L. Schiemansky-Geier, W. Ebeling, Stochastic motion of the propagating front in bistable media, Phys. Lett. A 46 (1983) 453.
[298] M. Mimura, H. Sakaguchi, M. Matsushita, Reaction–diffusion modelling of bacterial colony patterns, Physica A 282 (2000) 283.
[299] C. Misbah, Wavelength selection in rotating solidification of binary mixtures, J. Phys. France 50 (1989) 971.

[300] P.A. Monkewitz, The absolute and convective nature of instability in two-dimensional wakes at low Reynolds numbers, Phys. Fluids 31 (1988) 999.
[301] P.A. Monkewitz, P. Huerre, J.M. Chomaz, Global instability analysis of weakly non-parallel shear flows, J. Fluid Mech. 251 (1993) 1.
[302] P.A. Monkewitz, C.K.H. Williams, G.D. Miller, Phase dynamics of Karman vortices in cylindrical wakes, Phys. Fluids 8 (1996) 91.
[303] E. Moro, Internal fluctuation effects on Fisher waves, Phys. Rev. Lett. 87 (2001) 238303.
[304] E. Moro, Emergence of pulled fronts in fermionic microscopic particle models, Phys. Rev. E 68 (2003) 025102.
[305] H.W. Müller, M. Lücke, M. Kamps, Transversal convection pattern in horizontal shear flow, Phys. Rev. A 45 (1992) 314.
[306] J. Müller, W. van Saarloos, Morphological instability of bacterial growth fronts, Phys. Rev. E 65 (2002) 061111.
[307] C. Mueller, R.B. Sowers, Random traveling waves for the KPP equation with noise, J. Funct. Anal. 128 (1995) 439.
[308] W.W. Mullins, R.F. Sekerka, Morphological stability of a particle growing by diffusion or heat flow, J. Appl. Phys. 34 (1963) 323.
[309] W.W. Mullins, R.F. Sekerka, Stability of a planar interface during solidification of a dilute binary alloy, J. Appl. Phys. 35 (1964) 444.
[310] C.B. Muratov, A global variational structure and propagation of disturbances in reaction–diffusion systems of gradient type, Discrete Continuous Dyn. Systems, series B, to appear.
[311] J.D. Murray, Mathematical Biology, Springer, Berlin, 1989.
[312] M. Musette, R. Conte, Analytic solitary waves of nonintegrable equations, Physica D 181 (2003) 70.
[313] M. Nauenberg, Critical growth velocity in diffusion-controlled aggregation, Phys. Rev. B 28 (1983) 449.
[314] D.J. Needham, A.N. Barnes, Reaction–diffusion and phase waves occurring in a class of scalar reaction–diffusion equations, Nonlinearity 12 (1999) 41.
[315] A.C. Newell, Envelope equation, in: Lectures in Applied Mathematics, American Mathematical Society, Providence, RI, 1974.
[316] A.C. Newell, T. Passot, J. Lega, Order parameter equations for patterns, Annu. Rev. Fluid Mech. 25 (1993) 399.
[317] W.I. Newman, The long-time behavior of solutions to a nonlinear diffusion problem in population genetics and combustion, J. Theor. Biol. 104 (1983) 473.
[318] M. Niklas, M. Lücke, H. Müller-Krumbhaar, Propagating front of a propagating pattern: influence of group velocity, Europhys. Lett. 9 (1989) 237.
[319] M. Niklas, M. Lücke, H. Müller-Krumbhaar, Velocity of a propagating Taylor-vortex front, Phys. Rev. A 40 (1989) 493.
[320] Y. Nishiura, Far-From-Equilibrium Dynamics, American Mathematical Society, Providence, RI, 2002.
[321] K. Nozaki, N. Bekki, Pattern selection and spatio-temporal transition to chaos in the Ginzburg–Landau equation, Phys. Rev. Lett. 51 (1983) 2171.
[322] K. Nozaki, N. Bekki, Exact solutions of the generalized Ginzburg–Landau equation, J. Phys. Soc. Japan 53 (1984) 1581.
[323] T. Ogiwara, H. Matano, Monotonicity and convergence results in order-preserving systems in the presence of symmetry, Discrete Continuous Dyn. Systems 5 (1999) 1.
[324] A. Oras, S.H. Davis, S.G. Bankoff, Long-scale evolution of thin liquid films, Rev. Mod. Phys. 69 (1997) 931.
[325] A. Oron, P. Rosenau, Some symmetries of the nonlinear heat and wave equations, Phys. Lett. A 118 (1986) 172.
[326] M. Otwinowski, R. Paul, W.G. Laidlaw, Exact traveling wave solutions of a class of nonlinear diffusion equations by reduction to quadrature, Phys. Lett. A 128 (1988) 483.
[327] Q. Ouyang, H.L. Swinney, Transition from a uniform state to hexagonal and striped turing patterns, Nature 352 (1991) 610.
[328] D. Panja, W. van Saarloos, The weakly pushed nature of "pulled" fronts with a cutoff, Phys. Rev. E 65 (2002) 057202.
[329] D. Panja, W. van Saarloos, Fluctuating pulled fronts: the origin and the effects of a finite particle cutoff, Phys. Rev. E 66 (2002) 036206.
[330] D. Panja, W. van Saarloos, Fronts with a growth cutoff but speed higher than v^*, Phys. Rev. E 66 (2002) 015206(R).

[331] D. Panja, G. Tripathy, W. van Saarloos, Front propagation and diffusion in the A to 2A hard-core reaction on a chain, Phys. Rev. E 67 (2003) 046206.
[332] D. Panja, Effects of fluctuations on propagating fronts (cond-mat/0307363).
[333] G.C. Paquette, L.-Y. Chen, N. Goldenfeld, Y. Oono, Structural stability and renormalization group for propagating fronts, Phys. Rev. Lett. 72 (1994) 76.
[334] G.C. Paquette, Y. Oono, Structural stability and selection of propagating fronts in semi-linear parabolic partial differential equations, Phys. Rev. E 49 (1994) 2368.
[335] L. Pastur, M.-T. Westra, W. van de Water, M. van Hecke, C. Storm, W. van Saarloos, Sources and holes in a one-dimensional traveling wave experiment, Phys. Rev. E 67 (2003) 036305.
[336] L. Pastur, M.-T. Westra, W. van de Water, Sources and sinks in 1D traveling waves, Physica D 174 (2003) 71.
[337] L. Pechenik, H. Levine, Interfacial velocity correction due to multiplicative noise, Phys. Rev. E 59 (1999) 3893.
[338] P. Pelcé, Dynamics of Curved Fronts, Academic Press, San Diego, 1988.
[339] L.A. Peletier, The porous media equation, in: H. Amman, N. Bazley, K. Kirchgaessner (Eds.), Application of Nonlinear Analysis in the Physical Sciences, Pitman, London, 1981.
[340] L.A. Peletier, W.C. Troy, Spatial Patterns: Higher Order Models in Physics and Mechanics, Birkäuser, Boston, 2001.
[341] N. Peters, Turbulent Combustion, Cambridge University Press, Cambridge, 2000.
[342] B. Pier, P. Huerre, J.-M. Chomaz, A. Couairon, Steep nonlinear global modes in spatially developing media, Phys. Fluids 10 (1998) 2433.
[343] B. Pier, P. Huerre, J.M. Chomaz, Bifurcations to fully nonlinear synchronized structures in slowly varying media, Physica D 148 (2001) 49.
[344] B. Pier, P. Huerre, Fully nonlinear global modes in spatially developing media, J. Fluid Mech. 435 (2001) 145.
[345] B. Pier, On the frequency selection of finite-amplitude vortex shedding in the cylindrical wake, J. Fluid. Mech. 458 (2002) 407.
[346] R. Pieters, J.S. Langer, Noise-driven sidebranching in the boundary-layer model of dendritic solidification, Phys. Rev. Lett. 56 (1986) 1948.
[347] R. Pieters, Noise-induced sidebranching in the boundary-layer model of dendritic solidification, Phys. Rev. A 37 (1988) 3126.
[348] A. Pikovsky, A. Politi, Dynamic localization of Lyapunov vectors in space–time chaos, Nonlinearity 11 (1998) 1049.
[349] A. Pinter, M. Lücke, Ch. Hoffmann, Spiral and Taylor vortex fronts and pulses in axial through flow, Phys. Rev. E 67 (2003) 026318.
[350] L.M. Pismen, A.A. Nepomnyashchy, Propagation of the hexagonal pattern, Europhys. Lett. 27 (1994) 433.
[351] Y. Pomeau, A. Pumir, P. Pelcé, Intrinsic stochasticity with many degrees of freedom, J. Stat. Phys. 37 (1984) 39.
[352] Y. Pomeau, Front motion, metastability and subcritical bifurcations in hydrodynamics, Physica 23D (1986) 3.
[353] Y. Pomea, M. Ben-Amar, Dendritic growth and related topics, in: C. Godrèche (Ed.), Solids Far from Equilibrium, Cambridge University Press, Cambridge, 1992.
[354] J.A. Powell, A.C. Newell, C.K.R.T. Jones, Competition between generic and nongeneric fronts in envelope equations, Phys. Rev. A 44 (1991) 3636.
[355] J.A. Powell, M. Tabor, Nongeneric connections corresponding to front solutions, J. Phys. A 25 (1992) 3773.
[356] T.R. Powers, R.E. Goldstein, Pearling and pinching: propagation of Rayleigh instabilities, Phys. Rev. Lett. 78 (1997) 2555.
[357] T.R. Powers, D. Zhang, R.E. Goldstein, H.A. Stone, Propagation of a topological transition: the Rayleigh instability, Phys. Fluids 10 (1998) 1052.
[358] M.R.E. Proctor, S. Tobias, E. Knobloch, Noise-sustained structures due to convective instability in finite domains, Physica D 145 (2000) 191.
[359] X.W. Qian, H.Z. Cummins, Dendritic sidebranching initiation by a localized heat pulse, Phys. Rev. Lett. 64 (1990) 3038.
[360] A. Ramani, B. Grammaticos, T. Bountis, The Painlevé property and singularity analysis of integrable and nonintegrable systems, Phys. Rep. 180 (1989) 159.
[361] A. Recktenwald, M. Lücke, H.W. Müller, Taylor vortex formation in axial through-flow: linear and weakly nonlinear analysis, Phys. Rev. E 48 (1993) 4444.

[362] H. Riecke, Imperfect wave-number selection by ramps in a model for Taylor vortex flow, Phys. Rev. A 37 (1988) 636.
[363] J. Riordan, C.R. Doering, D. ben-Avraham, Fluctuations and stability of Fisher waves, Phys. Rev. Lett. 75 (1995) 565.
[364] A. Rocco, U. Ebert, W. van Saarloos, Subdiffusive fluctuations of pulled fronts with multiplicative noise, Phys. Rev. E 62 (2000) R13.
[365] A. Rocco, J. Casademunt, U. Ebert, W. van Saarloos, The diffusion coefficient of propagating fronts with multiplicative noise, Phys. Rev. E 65 (2002) 012102.
[366] A. Rocco, L. Ramirez-Piscina, J. Casademunt, Kinematic reduction of reaction–diffusion fronts with multiplicative noise: derivation of stochastic sharp-interface equations, Phys. Rev. E 65 (2002) 056116.
[367] M. Rost, J. Krug, A particle model for the Kuramoto–Sivashinksky equation, Physica D 88 (1995) 1.
[368] D. Roth, M. Lcke, M. Kamps, R. Schmitz, Phase dynamics of patterns: the effect of boundary induced amplitude variations, Phys. Rev. E 50 (1994) 2756.
[369] V. Rottschäfer, Co-dimension 2 phenomena in pattern formation, Thesis, Utrecht, 1998.
[370] V. Rottschäfer, A. Doelman, On the transition from the Ginzburg–Landau equation to the extended Fisher–Kolmogorov equation, Physica D 118 (1998) 261.
[371] V. Rottschäfer, C.A. Wayne, Existence and stability of traveling fronts in the extended Fisher–Kolmogorov equation, J. Differential Equations 176 (2001) 532.
[372] H. Sakaguchi, S. Tokunaga, Tip oscillation of dendritic patterns in a phase field model, Prog. Theor. Phys. 109 (2003) 43.
[373] E.K.H. Salje, On the kinetics of partially conserved order parameters: a possible mechanism for pattern formation, J. Phys.: Condens. Matter 5 (1993) 4775.
[374] B. Sandstede, A. Scheel, Essential instabilities of fronts: bifurcation, and bifurcation failure, Dyn. Systems 16 (2001) 1.
[375] B. Sandstede, A. Scheel, Defects in oscillatory media—towards a classification (preprint May 2003).
[376] D.H. Sattinger, Weighted norms of the stability of traveling waves, J. Differential Equations 25 (1977) 130.
[377] L. Schimansky-Geier, Ch. Zülicke, Kink propagation induced by multiplicative noise, Z. Phys. B 82 (1991) 157.
[378] J. Schumacher, B. Eckhardt, Evolution of turbulent spots in an parallel shear flow, Phys. Rev. E. 63 (2001) 046307.
[379] A.C. Scott, The electrophysics of a nerve fiber, Rev. Mod. Phys. 47 (1975) 487.
[380] B. Shraiman, D. Bensimon, On the dynamical mechanism of velocity selection, Phys. Scr. T9 (1985) 123.
[381] B.I. Shraiman, Order, disorder, and phase turbulence, Phys. Rev. Lett. 57 (1986) 325.
[382] B.I. Shraiman, A. Pumir, W. van Saarloos, P.C. Hohenberg, H. Chaté, M. Holen, Spatiotemporal chaos in the one-dimensional complex Ginzburg–Landau equation, Physica D 57 (1992) 241.
[383] W. Spruijt, Master's thesis, Leiden University 1998 (available from the author).
[384] A.N. Stokes, On two types of moving fronts in quasilinear diffusion, Math. Biosci. 31 (1976) 307.
[385] N. Shigesada, K. Kawasaki, Biological Invasions: Theory and Practice, Oxford University Press, Oxford, 1997.
[386] G.I. Sivashinsky, Nonlinear analysis of hydrodynamic instability in laminar flames—I. Derivation of basic equations, Acta Astronaut. 4 (1977) 1177.
[387] I.W. Stewart, T. Carlsson, F.M. Leslie, Chaotic instabilities in smectic-C liquid crystals, Phys. Rev. E 49 (1994) 2130.
[388] C. Storm, W. Spruijt, U. Ebert, W. van Saarloos, Universal algebraic relaxation of velocity and phase in pulled fronts generating periodic or chaotic states, Phys. Rev. E 61 (2000) R6063.
[389] J. Swift, P.C. Hohenberg, Hydrodynamic fluctuations at the convective instability, Phys. Rev. A 15 (1977) 319.
[390] A. Szprynger, M. Lücke, Noise sensitivity of sub- and supercritically bifurcating patterns with group velocity close to the convective-absolute instability, Phys. Rev. E 67 (2003) 046301.
[391] S. Theodorakis, E. Leontides, Emergence of approximate translation invariance in finite intervals as a speed selection mechanism for propagating fronts, Phys. Rev. E 62 (2000) 7802.
[392] S. Theodorakis, E. Leontides, Speed selection mechanism for propagating fronts in reaction diffusion systems with multiple fields, Phys. Rev. E 65 (2002) 026122.
[393] K. Thürmer, D.J. Liu, E.D. Williams, J.D. Weeks, Onset of stepa anitbanding instability due to surface electromigration, Phys. Rev. Lett. 83 (1999) 5531.
[394] M. Tinkham, Introduction to Superconductivity, McGraw-Hill, New York, 1975.

[395] S. Tobias, M.R.E. Proctor, E. Knobloch, Convective and absolute instabilities of fluid flows in finite geometry, Physica D 113 (1998) 43.
[396] A. Torcini, P. Grassberger, A. Politi, Error propagation in extended chaotic systems, J. Phys. A 28 (1995) 4533.
[397] A. Torcini, A. Vulpiani, A. Rocco, Front propagation in chaotic and noisy reaction–diffusion systems: a discrete-time map approach, Eur. J. Phys. B 25 (2002) 333.
[398] A. Tóth, I. Lagzi, D. Horváth, Pattern formation in reaction–diffusion systems: cellular acidity fronts, J. Phys. Chem. 100 (1996) 14837.
[399] A. Tóth, D. Horváth, W. van Saarloos, Lateral instabilities of cubic autocatalytic reaction fronts in constant electric field, J. Chem. Phys. 111 (1999) 10964.
[400] M.V. Tretyakov, S. Fedotov, On the FKPP equation with Gaussian shear advection, Physica D 159 (2001) 190.
[401] G.S. Triantafyllou, K. Kupfer, A. Bers, Absolute instabilities and self-sustained oscillations in the wakes of circular cylinders, Phys. Rev. Lett. 59 (1987) 1914.
[402] G. Tripathy, W. van Saarloos, Fluctuation and relaxation properties of pulled fronts: a possible scenario for non-KPZ behavior, Phys. Rev. Lett. 85 (2000) 3556; Erratum: 87 (2001) 049902.
[403] G. Tripathy, A. Rocco, J. Casademunt, W. van Saarloos, The universality class of fluctuating pulled fronts, Phys. Rev. Lett. 86 (2001) 5215.
[404] A. Tsameret, V. Steinberg, Noise-modulated propagating pattern in a convectively unstable system, Phys. Rev. Lett. 67 (1991) 3392.
[405] A. Tsameret, V. Steinberg, Absolute and convective instabilities and noise-sustained structures in the Couette–Taylor system with axial flow, Phys. Rev. E 49 (1994) 1291.
[406] I. Tsatskis, E.K.H. Salje, V. Heine, Pattern formation during phase transitions: kinetics of partially conserved order parameters and the role of gradient energies, J. Phys.: Condens. Matter 6 (1994) 11027.
[407] Y. Tu, M.C. Cross, Chaotic domain structure in rotating convection, Phys. Rev. Lett. 69 (1992) 2515.
[408] C. Uhlig, J. Eggers, Singularities in cascade models of the Euler equation, Z. Phys. B 103 (1997) 69.
[409] O.T. Valls, L.M. Lust, Effect of noise on front propagation, Phys. Rev. B 44 (1991) 4326.
[410] G.J. van den Berg, Dynamics and equilibria of fourth order differential equations, Thesis, Leiden, 2000.
[411] J.P. van der Eerden, H. Müller-Krumbhaar, Dynamics coarsening of crystal surfaces by formation of macrosteps, Phys. Rev. Lett. 57 (1986) 2431.
[412] M. van Hecke, W. van Saarloos, P.C. Hohenberg, Comment on "absolute and convective instabilities in nonlinear systems", Phys. Rev. Lett. 71 (1993) 2162.
[413] M. van Hecke, P.C. Hohenberg, W. van Saarloos, Amplitude equations for pattern forming systems, in: H. van Beijeren, M.H. Ernst (Eds.), Fundamental Problems in Statistical Mechanics VIII, North-Holland, Amsterdam, 1994.
[414] M. van Hecke, E. de Wit, W. van Saarloos, Coherent and incoherent drifting pulse dynamics in a complex Ginzburg–Landau equation, Phys. Rev. Lett. 75 (1995) 3830.
[415] M. van Hecke, W. van Saarloos, Convection in rotating annuli: Ginzburg–Landau equations with tunable coefficients, Phys. Rev. E 55 (1997) R1259.
[416] M. van Hecke, Building blocks of spatiotemporal intermittency, Phys. Rev. Lett. 80 (1998) 1896.
[417] M. van Hecke, C. Storm, W. van Saarloos, Sources, sinks and wavenumber selection in coupled CGL equations and experimental implications for counter-propagating wave systems, Physica D 134 (1999) 1.
[418] M. van Hecke, M. Howard, Ordered and self-disordered dynamics of holes and defects in the one-dimensional complex Ginzburg–Landau equation, Phys. Rev. Lett. 86 (2001) 2018.
[419] M. van Hecke, M. Howard, Ordered and self-disordered dynamics of holes and defects in the one-dimensional complex Ginzburg–Landau equation, Phys. Rev. Lett. 86 (2001) 2018.
[420] W. van Saarloos, Front propagation into unstable states: marginal stability as a dynamical mechanism for velocity selection, Phys. Rev. A 37 (1988) 211–229.
[421] W. van Saarloos, Front propagation into unstable states II: linear versus nonlinear marginal stability and rate of convergence, Phys. Rev. A 39 (1989) 6367.
[422] W. van Saarloos, in: F.H. Busse, L. Kramer (Eds.), Nonlinear Evolution of Spatio-Temporal Structures in Continuous Media, Plenum, New York, 1990.
[423] W. van Saarloos, P.C. Hohenberg, Pulses and fronts in the complex Ginzburg–Landau equation near a subcritical bifurcation, Phys. Rev. Lett. 64 (1990) 749.

[424] W. van Saarloos, P.C. Hohenberg, Fronts, pulses, sources and sinks in generalized complex Ginzburg–Landau equations, Physica D 56 (1992) 303 [Errata: Physica D 61 (1993) 209].
[425] W. van Saarloos, B. Caroli, C. Caroli, On the stability of low-anisotropy dendrites, J. Phys. I 3 (1993) 26.
[426] W. van Saarloos, The complex Ginzburg–Landau equation for beginners, in: P.E. Cladis, P. Palffy-Muhoray (Eds.), Proceedings of the Santa Fe Workshop on "Spatio-Temporal Patterns in Nonequilibrium Complex Systems", Addison-Wesley, Chicago, 1994.
[427] W. van Saarloos, M. van Hecke, R. Hołyst, Front propagation into unstable and metastable states in smectic C^* liquid crystals: linear and nonlinear marginal stability analysis, Phys. Rev. E 52 (1995) 1773.
[428] W. van Saarloos, Three basic issues concerning interface dynamics in nonequilibrium pattern formation, Phys. Rep. 301 (1998) 9.
[429] W. van Saarloos, unpublished.
[430] R. van Zon, H. van Beijeren, Ch. Dellago, Largest Lyapunov exponent for many-particle systems at low densities, Phys. Rev. Lett. 80 (1998) 2035.
[431] J.M. Vince, M. Dubois, Hot-wire below the free surface of a liquid—structural and dynamic properties of a secondary instability, Europhys. Lett. 20 (1992) 505.
[432] J.M. Vince, M. Dubois, Critical properties of convective waves in a one-dimensional system, Physica D 102 (1997) 93.
[433] P.A. Vitello, B.M. Penetrante, J.N. Bardsley, Simulation of negative-streamer dynamics in nitrogen, Phys. Rev. E 49 (1994) 5574.
[434] A.I. Volpert, V.A. Volpert, V.A. Volpert, Traveling Wave Solutions of Parabolic Systems, American Mathematical Society, Providence, RI, 1994.
[435] D. Walgraef, Spatio-Temporal Pattern Formation, with Examples in Physics, Chemistry and Materials Science, Springer, New York, 1996.
[436] X.Y. Wang, S. Fan, T. Kyu, Complete and exact solutions of a class of nonlinear diffusion equations and problem of velocity selection, Phys. Rev. E 56 (1997) R4931.
[437] R.J. Wijngaarden, K. Heeck, M. Welling, R. Limburg, M. Pannetier, K. van Zetten, V.L.G. Roorda, A.R. Voorwinden, Fast imaging polarimeter for magneto-optical investigations, Rev. Sci. Instrum. 72 (2001) 2661.
[438] E.D. Williams, E. Fu, Y.-N. Yang, D. Kandel, J.D. Weeks, Measurement of the anisotropy ratio during current-induced step bunching, Surf. Sci. 336 (1995) L746.
[439] F.A. Williams, Combustion Theory, Benjamin/Cummings, Menlo Park, 1985.
[440] P. Wiltzius, F.S. Bates, W.R. Heffner, Spinodal decomposition in isotropic polymer mixtures, Phys. Rev. Lett. 60 (1988) 1538.
[441] D. Worledge, E. Knowloch, S. Tobias, M.R.E. Procoto, Dynamo waves in semi-infinite and finite domains, P. R. Soc. London A 119 (1997).
[442] J. Xin, Front propagation in heterogeneous media, SIAM Rev. 42 (2000) 161.
[443] J. Xin, KPP front speeds in random shears and the parabolic Anderson problem, Methods Appl. Anal. (2003), to appear.
[444] J.J. Xu, Interfacial Wave Theory of Pattern Formation, Springer, Berlin, 1998.
[445] V. Yakhot, Large-scale properties of unstable systems governed by the Kuramoto–Sivashinsky equation, Phys. Rev. A 24 (1981) 642.
[446] X. Yang, A. Zebib, Absolute and convective instability of a cylindrical wake, Phys. Fluids A 1 (1989) 689.
[447] Z.J. Yang, Traveling-wave solutions to nonlinear evolution and wave-equations, J. Phys. A 27 (1994) 2837.
[448] S. Zaleski, Wavelength selection in one-dimensional cellular structures, Physica D 34 (1989) 427.
[449] Ya.B. Zeldovich, G.I. Barenblatt, V.B. Librovich, G.M. Makhviladze, The Mathematical Theory of Combustion and Explosions, Consultants Bureau, New York, 1985.
[450] W. Zimmermann, Propagating fronts near a Lifshitz point, Phys. Rev. Lett. 66 (1991) 1546.
[451] G. Zocchi, P. Tabeling, M. Ben Amar, Saffman–Taylor plumes, Phys. Rev. Lett. 69 (1992) 601.
[452] S.N. Majumdar, P.L. Kaprivsky, Extreme value statistics and traveling fronts: Application to computer science, Phys. Rev. E 65 (2002) 036127.
[453] S.N. Majumdar, Traveling front solutions to directed diffusion-limited aggregation, digital search trees, and the Lempel-Ziv data compression algorithm, Phys. Rev. E 68 (2003) 026103.